

# **Microwave Synthesis and Mechanistic Examination of the Transition Metal Carbides**

A thesis submitted to the University of Nottingham for the degree of  
Doctor of Philosophy

by

**Simon Richard Vallance Msci.(Hons)**

School of Chemistry,  
University of Nottingham.

July 2008



The University of  
**Nottingham**

## **Declaration**

Except where specific reference is made to other sources, the work presented in this thesis is the original work of the author. It has not been submitted, in whole or in part, for any other degree.

Signed:

Simon R. Vallance

Date: July 2008

For Jane

## ABSTRACT

This thesis aims to describe the ultra-rapid synthesis of a number of important transition metal carbides as well as investigating their reaction mechanisms. 4 binary systems are discussed; Nb-C, Mo-C, Ta-C and W-C, and work carried out on the ternary system, Nb-Ta-C, is also evaluated. Carbide production was investigated from both the oxide and elemental precursors.

Ultra-rapid synthesis has been achieved through the development of a reproducible experimental technique and the investigation into a plethora of reaction variables as well as microwave applicators and powers. This resulted in, specifically within the single mode cavity, the completion of the majority of reactions within 20 s. Further development was then built upon the direct relationship observed between phase fraction results (obtained from Powder X-ray Diffraction (PXD) data), *in-situ* temperature and *ex-situ* dielectric property measurements; allowing reaction profiles of the various carbides to be mapped, as well as a crucial understanding of the effects of microwave energy on materials at various temperatures.

Powder Neutron Diffraction (PND) was also used to evaluate product purity and the C occupancy of the final products, revealing non-stoichiometry which relates directly to the  $T_c$  onset observed for the superconducting transition metal carbides. This, in turn, allowed the trends observed for the ternary carbides to be explained, a linear trend does not exist between  $T_c$  and C occupancy.

In an effort to develop on the understanding of solid state microwave heating, in-situ reaction monitoring techniques were investigated. Through the use of thermal imaging and high speed photography, the W-C system was observed during the crucial initial stages of the reaction process. The information obtained both corroborated previously collected data and allowed a possible reaction mechanism to be alluded to. The observation of localised heating, prior to the beginning of carbide formation, suggests possible high temperatures far exceeding those observed by optical pyrometry. This could well explain the rapid reaction times as well as suggest an interaction mechanism between carbon, an efficient microwave absorber, and tungsten, a low dielectric loss metal.

## **ACKNOWLEDGEMENTS**

I would like to take this opportunity to thank the University of Nottingham for funding and my three supervisors for all their assistance during my PhD: Professor Duncan H. Gregory, Dr. Eddie Cussen and Professor Sam Kingman. Duncan, Eddie and Sam have given me many years of support and advice and it is thanks to them that I am able to write this thesis. I feel privileged to have worked with them. I would also like to thank all those in both my chemistry and engineering groups who have helped me over the years, particularly Dr. Mike Brogan, Dr. Charlie Dunnill, Dr. Katie Jewell, Mr. Nicolas Pinguet, Mr. Michael O'Callaghan, Dr. Chris Dodds and Dr. Aled Jones.

Of course I would not have gotten this far without the support of all my friends and family, many who have been a big part of my life for many years and others who I have only known during my years in Nottingham. My heartfelt thanks go out to my parents, Lynn and Richard, my sister Emily and finally my fiancée Jane, who has been understanding, loving and patient throughout my studies.

# CONTENTS

## **1 Introduction**

- 1.1 Transition metal carbides
  - 1.1.1 Bonding and structure
  - 1.1.2 Synthesis and preparation
  - 1.1.3 Applications
- 1.2 Transition metal carbide summary
- 1.3 History of microwave heating and solid state microwave materials synthesis
- 1.4 Microwave solid state synthesis: A review
  - 1.4.1 Borides
  - 1.4.2 Carbides
  - 1.4.3 Nitrides
  - 1.4.4 Oxides
- 1.5 Review summary
- 1.6 Scope of this work
- 1.7 References

## **2 Experimental**

- 2.1 Microwave radiation
  - 2.1.1 Microwave heating mechanisms
  - 2.1.2 Microwave applicators
    - 2.1.2.1 Multimode cavities
    - 2.1.2.2 Single mode cavities
    - 2.1.2.3 Travelling wave applicators
- 2.2 Synthesis and processing
  - 2.2.1 Synthesis using a Domestic Microwave Oven (DMO)

- 2.2.2 Synthesis using a single mode microwave cavity
- 2.3 Characterisation techniques
  - 2.3.1 Powder X-ray Diffraction (PXD)
    - 2.3.1.1 Powder X-ray diffraction sample preparation, data collection and analysis
  - 2.3.2 Powder Neutron Diffraction (PND)
    - 2.3.2.1 D1A at ILL
    - 2.3.2.2 POLARIS at ISIS (RAL)
  - 2.3.3 Rietveld refinement
  - 2.3.4 Dielectric properties
    - 2.3.4.1 Cavity perturbation technique
  - 2.3.5 Magnetism
    - 2.3.5.1 Superconductivity
    - 2.3.5.2 Magnetic measurements
  - 2.3.6 Scanning Electron Microscopy (SEM)
    - 2.3.6.1 Energy Dispersive X-ray spectroscopy (EDX)
  - 2.3.7 X-ray Photoelectron Spectroscopy (XPS)
  - 2.3.8 X-ray Fluorescence (XRF) and CHN analysis
  - 2.3.9 Thermal Analysis, evolved gas analysis and Mass Spectrometry (MS)
- 2.4 References

### **3 Tungsten carbide investigations**

- 3.1 Introduction
- 3.2 Experimental: Synthesis of W-C
  - Results and discussion: W-C synthesis and experimental development using a Domestic Microwave Oven (DMO)
- 3.3 Results and discussion: WC synthesis using a single mode cavity
- 3.4
  - 3.4.1 W-C reaction profile

- 3.4.1.1 PND study of WC
- 3.4.2 Effect of excess graphite on WC formation
- 3.4.3 Sample volume variation: Experimental scale up
- 3.4.4 *In-situ* analysis
  - 3.4.4.1 High speed photography
  - 3.4.4.2 Thermal imaging
- 3.4.5 WC synthesis from tungsten oxide,  $\text{WO}_3$
- 3.5 Summary
- 3.6 References

## **4 Molybdenum carbide investigations**

- 4.1 Introduction
- 4.2 Experimental: Synthesis of Mo-C
  - 4.3 Results and discussion: Mo-C synthesis and experimental development using a Domestic Microwave Oven (DMO)
    - 4.3.1  $\text{Mo}_2\text{C}$  synthesis
    - 4.3.2  $\text{Mo}_2\text{C}$  Powder Neutron Diffraction (PND) study
    - 4.3.3 MoC and  $\text{Mo}_3\text{C}_2$  synthesis
  - 4.4 Results and discussion:  $\text{Mo}_2\text{C}$  synthesis using a single mode cavity
    - 4.4.1  $\text{Mo}_2\text{C}$  synthesis and investigation
      - 4.4.1.1 Powder Neutron Diffraction (PND) structural investigation
      - 4.4.1.2  $\text{Mo}_2\text{C}$  reaction profile study
    - 4.4.2  $\text{Mo}_2\text{C}$  synthesis: Variations in applied power
    - 4.4.3 Sealed reaction investigation
  - 4.5 Results and discussion:  $\text{Mo}_2\text{C}$  synthesis from the oxide,  $\text{MoO}_3$ 
    - 4.5.1  $\text{Mo}_2\text{C}$  synthesis in a Domestic Microwave Oven (DMO)
      - 4.5.1.1 1<sup>st</sup> approach: Two-step synthesis

- 4.5.1.2 2<sup>nd</sup> approach: One-step synthesis
- 4.5.2 Mo<sub>2</sub>C synthesis in a single mode cavity
  - 4.5.2.1 Further reaction study;  $2\text{MoO}_3 + 7\text{C} \rightarrow \text{Mo}_2\text{C} + 6\text{CO}$
  - 4.5.2.2 Mo<sub>2</sub>C synthesis using Magnetronics 0 - 1.5 kW single mode microwave applicator
- 4.6 Summary
- 4.7 References

## **5 Group V carbide investigations**

- 5.1 Introduction
  - 5.1.1 Ternary carbides, Nb-Ta-C
- 5.2 Experimental: Synthesis of Nb-C, Ta-C and Nb-Ta-C
- 5.3 Results and discussion: Synthesis using a Domestic Microwave Oven (DMO)
  - 5.3.1 NbC synthesis
  - 5.3.2 TaC synthesis
- 5.4 Results and discussion: Synthesis using a single mode cavity
  - 5.4.1 Reaction profile investigations for NbC and TaC
    - 5.4.1.1 Reactant mixing study; Nb + C
  - 5.4.2 Nb-Ta-C solid solution series investigation through PND and magnetic measurements
- 5.5 Summary
- 5.6 References

## **6 General Summary**

## **7 Appendices**

# 1: INTRODUCTION

## 1.1 TRANSITION METAL CARBIDES

The name “transition metal carbides” covers specifically the carbides of groups IV, V and VI. These carbides are often referred to as the refractory carbides due to their very high melting points (2000 – 4000 °C) and form the basis of the “cemented carbides” which are prevalent in industry.<sup>1</sup> Their main use is in tools and wear-resistant parts due to their extreme hardness, excellent high temperature strength and good resistance to corrosion.<sup>1</sup> However, recently they have found applications in very different areas such as catalysis.<sup>2, 3</sup>

Among groups IV to VI, all elements in the first three rows of the transition series are capable of forming refractory carbides. However, the complexity increases with group number; group IV only exhibiting one known structure, group V containing two and three in group VI (Table 1- 1).

<b>Group IV</b>	<b>Group V</b>	<b>Group VI</b>
TiC	V <sub>2</sub> C VC	Cr <sub>23</sub> C <sub>6</sub> Cr <sub>7</sub> C <sub>3</sub> Cr <sub>3</sub> C <sub>2</sub>
ZrC	Nb <sub>2</sub> C NbC	Mo <sub>2</sub> C Mo <sub>3</sub> C <sub>2</sub> MoC
HfC	Ta <sub>2</sub> C TaC	W <sub>2</sub> C W <sub>3</sub> C <sub>2</sub> WC

**Table 1- 1: Known carbides within groups IV, V and VI.**

Although these structures (Table 1- 1) look relatively simple from the outset, it is widely understood that carbides are not primarily stoichiometric phases. In fact the compositional range for each binary phase varies significantly with all properties being dependent on the metal to non-metal ratio. Even small changes in vacancy concentration can result in drastic changes in certain properties, for example the superconducting transition temperature.<sup>4, 5</sup>

All the transition metal carbides, except VC which is slowly oxidised in air, are chemically stable at room temperature and are attacked slowly only by very concentrated acid solutions to form oxides.<sup>1</sup> Other properties, such as electrical conductivity and magnetic characteristics, follow the trends for metallic compounds, but, like many other properties, are extremely sensitive to structural vacancies.

Some of these properties and structural changes are discussed in greater depth in later chapters, specific to the relevant carbide (Chapters 3, 4 and 5).

### **1.1.1 Bonding and structure**

Three strongly related factors contribute to bonding in the refractory carbides: electronegativity, atomic radius and the nature of the bond between the metal and non-metal. All three of these factors contribute to the resultant structure and the alternative name given for this group of carbides, “interstitial carbides”.

Electronegativity can be defined as the tendency of an element to gain electrons and form negative ions.<sup>6</sup> Although the Electronegativity of an element is not a fixed value, but depends on its valence state, values can still be assigned to specific elements.<sup>7</sup> Pauling observed that the bond energy,  $E(AB)$  (measured in  $\text{KJ mol}^{-1}$ ), in a molecule  $AB$  is always greater than the mean of the bond energies  $E(AA) + E(BB)$ .<sup>8</sup> He argued that for an “ideal” covalent bond,  $E(AB)$  should equal the mean and so any “excess” bond energy is caused by electrostatic attraction between the partially charged atoms in the  $AB$  species. This excess can also be described as an ionic contribution to the bond and resulted in the following equation where  $\chi_A - \chi_B$  represents the difference in electronegativity between the two elements,  $A$  and  $B$ :

$$E(AB) = [E(AA) \cdot E(BB)]^{1/2} + 96.48(\chi_A - \chi_B)^2$$

Pauling found  $F$  to have the largest electronegativity of all the elements and so set this to a value of 4.0, giving a scale in which all other elements are less, but still positive. Table 1- 2 shows the calculated Pauling electronegativity values for  $C$  and the transition metals in question with an apparent large difference in electronegativity observed between them. The same applies to atomic radii (Table 1- 2) with respect to their absolute value. No atom has a precise radius and so again these are only approximations, with the reported values changing depending on their role in the structure.<sup>9</sup> However, it can be clearly seen that a carbon atom is much smaller than any one transition metal atom.

Element	<i>C</i>	<i>Nb</i>	<i>Mo</i>	<i>Ta</i>	<i>W</i>
Atomic Number, <i>Z</i>	6	41	42	73	74
Electronegativity	2.5	1.6	1.8	1.5	1.7
Atomic Radius / Å	0.78	1.456	1.386	1.457	1.394

**Table 1- 2: Electronegativity and atomic radii of elements discussed in this thesis.<sup>6</sup>**

Finally the nature of the bonds between the metals and non-metals present in the carbide must be discussed due to their importance in the structure of the transition metal carbides. Bonds between atoms relate directly to electronegativity and atomic size and are the function of the electronic configuration of the constituent elements, the orbitals available and the bond polarity.<sup>6</sup> It is also true that in the majority of cases, short bonds are stronger than long bonds.<sup>10</sup> Three types of bonding exist: Ionic, Covalent and Metallic:<sup>11</sup>

- An ionic bond is formed by the transfer of valence electrons between two atoms, resulting in a positive and negative ion and consequently an electrostatic interaction between these atoms. Due to the nature of this bond it is favoured by atoms with large differences in electronegativity.
- A covalent bond is formed by the sharing of a pair of electrons between two atoms and, unlike ionic bonds, is favoured by atoms with similar electronegativity.

- In a metallic bond the atoms are considered to be ionised, with the positive ions arranged in lattice positions. The electrons are delocalised within the structure and can essentially move freely throughout the lattice. The bonding occurs as an electrostatic interaction between these metal ions and the delocalised electron field.

Examination of the three factors, electronegativity, atomic size and bonding, leads to the resultant bonding and structure observed in the interstitial carbides. Due to the contribution from the difference in electronegativity and atomic size between carbon and the Group IV, V or VI metal present, the carbon nests in the interstices of the metal lattice, hence the name interstitial carbides. The resultant bonding is primarily metallic, due to the metal lattice present throughout the structure, however, degrees of ionic and covalent bonding also exist due to the carbon present. For this reason the interstitial carbides closely resemble metals and, like metallic alloys, their composition is often indeterminate and their electrical and thermal properties, melting points and hardness are high as well as them being chemically inert.<sup>12</sup> The structure itself contains a host metal, generally arranged in a close-packed structure, and carbon, which occupies specific interstitial sites. The population of these sites directly relates to the stoichiometry of the carbide. However, in order to understand it fully one must first examine the electronic structure of the atoms involved, which ultimately leads to the bonding within the structure.

Electrons within an atom exist in regions known as orbitals where each orbital is a mathematical function that describes the wave-like behaviour of the

electrons. Specifically, atomic orbitals are the possible quantum states of an individual electron in the electron cloud around a single atom.<sup>13</sup> They can be defined as quantum numbers which describe the electron configuration within the atom. For a neutral carbon atom this is  $1s^2 2s^2 2p^2$  and results in the atomic configuration seen in Figure 1- 1.

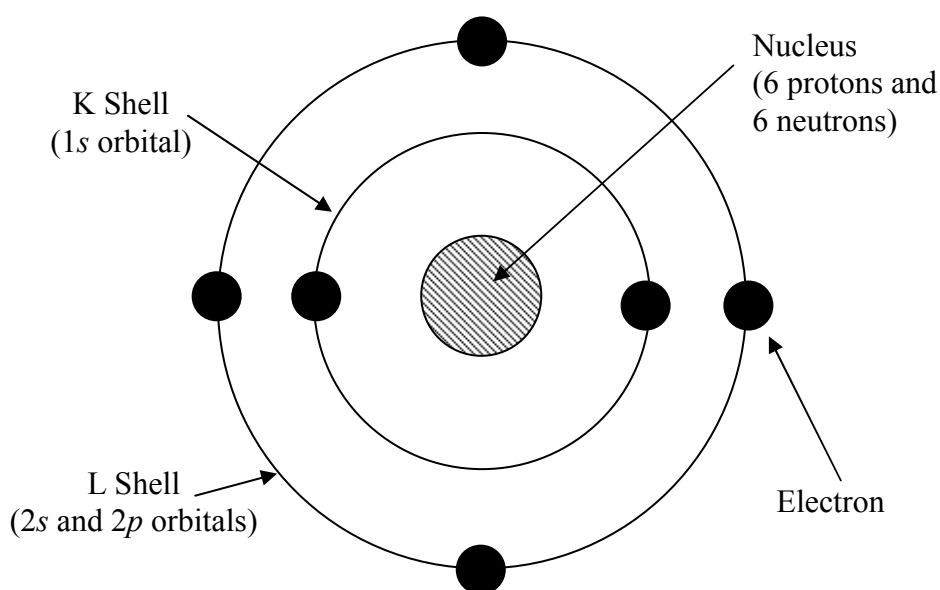


**Figure 1- 1: Schematic representation of the electronic structure of the carbon atom.**

The filled K shell is stable and so does not take part in any bonding. The L shell on the other hand contains 4 of a possible 8 electrons, in the *s* and *p* subshells (Table 1- 3), and are known as the valence electrons due to their existence in the outer orbitals. This electron configuration is known as the ground state; defined as the state where electrons are in their minimum orbits, as close to the nucleus as possible, with their lowest energy level.<sup>6</sup> Currently only 2 electrons exist in the outer *p* orbitals and so are the only electrons available for bonding. However, it is common knowledge that carbon does not

usually bond in a divalent manner, therefore one must account for the bonding observed in the majority of carbon compounds.<sup>6</sup> To achieve this, the ground state configuration observed for carbon must be altered so that 4 valence electrons exist in 4 separate orbitals, thus allowing the atom to bond covalently to 4 other atoms in a tetrahedral symmetry. For this to occur, hybridisation of atomic orbitals must take place resulting in the most common configuration,  $sp^3$ . This label results from the promotion of one L shell electron from the  $s$  to a  $p$  orbital, which combines the  $2s$  and  $2p$  orbitals into a hybrid (Table 1- 3).

Electron Shell	$K$	$L$			
Orbital	1s	2s	2px	2py	2pz
Electron Spin (Ground State)	↓↑	↓↑	↓	↓	
Electron Spin ( $sp^3$ hybrid state)	↓↑	↓	↓	↓	↓

**Table 1- 3: Electron configuration of the carbon atom in both the ground state and  $sp^3$  hybrid state. Arrows indicate direction of electron spin.**

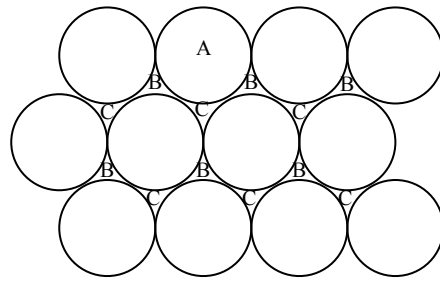
The transition metals have a special electron arrangement. Unlike other elements, which fill their electronic shells systematically from the inside out, transition metals are able to have partially filled inner shells due to the existence of a  $d$  subshell. This plays an important role in the formation of interstitial carbides.<sup>12</sup> These  $d$  shells, which provide valence electrons, are only ever partially filled with the  $s$  orbital in the outermost shell also providing valence electrons for bonding (Table 1- 4). Despite the outermost  $d$  shell being part of an inner shell, it is still capable of providing these valence electrons as the  $d$  orbitals extend outward to the periphery of the atom and are strongly influenced by other atoms, such as carbon, and vice versa.

Element	Z	Shells and subshells															
		K			L			M			N			O			P
		<i>1s</i>	<i>2s</i>	<i>2p</i>	<i>3s</i>	<i>3p</i>	<i>3d</i>	<i>4s</i>	<i>4p</i>	<i>4d</i>	<i>4f</i>	<i>5s</i>	<i>5p</i>	<i>5d</i>	<i>5f</i>	<i>5g</i>	<i>6s</i>
Nb	41	2	2	6	2	6	10	2	6	4	-	1	-	-	-	-	-
Mo	42	2	2	6	2	6	10	2	6	5	-	1	-	-	-	-	-
Ta	73	2	2	6	2	6	10	2	6	10	14	2	6	3	-	-	2
W	74	2	2	6	2	6	10	2	6	10	14	2	6	4	-	-	2

**Table 1- 4: Electronic configuration of selected transition metals.<sup>12</sup>**

The total number of valence electrons, as well as their location, influences the structure and characteristics of the respective carbides.<sup>14</sup> A number of crystalline structures are possible for the carbides of groups IV, V and VI: Close-packed, which comprise hexagonal and face-centred cubic structures, body-centred cubic and simple hexagonal structures.

Within a close-packed structure the atoms of the planes fit into the depressions of the adjacent planes (Figure 1- 2), with each atom surrounded by 6 close neighbours. These atoms can either be hexagonal close-packed (*hcp*) or face-centred cubic close-packed (*fcc*).<sup>7</sup> In the former structure, the first plane of atoms lies directly over the third plane and can be expressed as ABAB (Figure 1- 3). This results in a hexagonal symmetry. In the latter structure each plane mirrors the one 3 planes adjacent to it resulting in an ABCABC sequence (Figure 1- 3). In both cases each atom is equidistant from 12 other atoms, leading to the co-ordination number of 12.



A = atoms  
 B = interstices pointing upwards  
 C = Interstices pointing downwards

**Figure 1- 2: Schematic of close packing of atoms.**

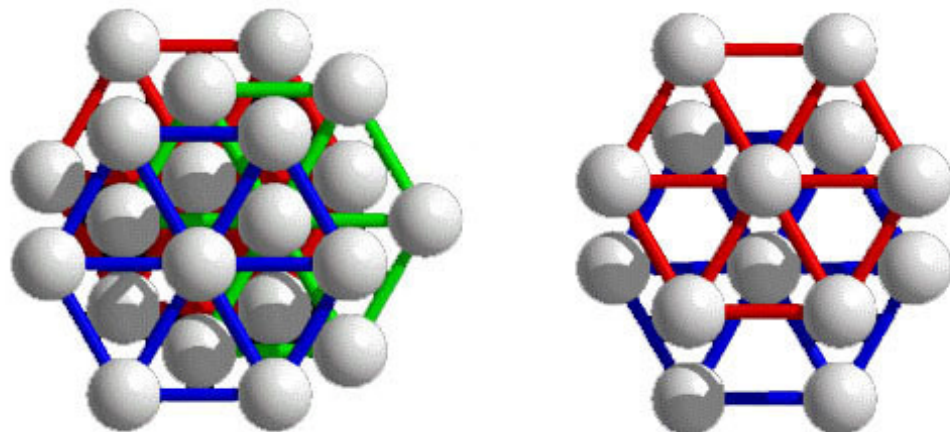
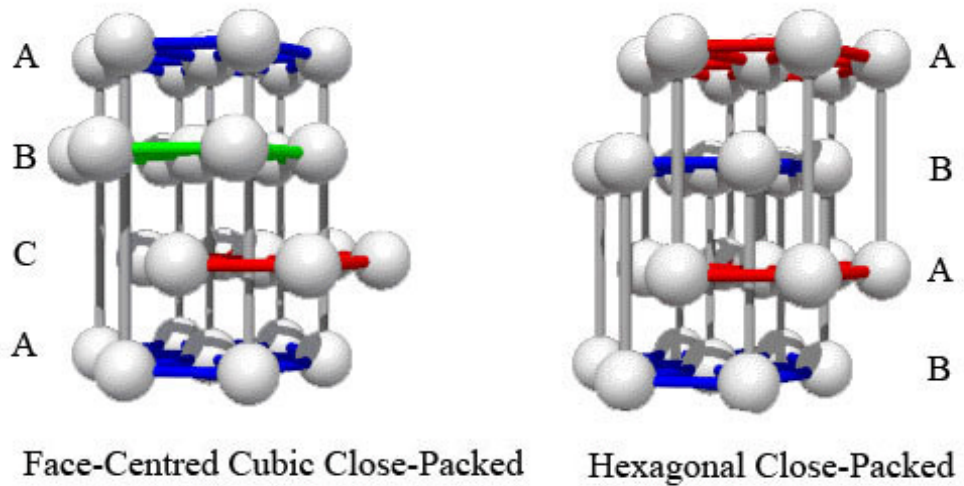


**Figure 1- 3: Schematic of hexagonal close-packed (*hcp*) and face-centred cubic close-packed (*fcc*) structures.**

Body-centred cubic (*bcc*) and primitive hexagonal structures are not close-packed and both have a co-ordination number of 8 resulting in a lower structural density (Figure 1- 4).<sup>7</sup> Tungsten carbide is an example of a typical simple hexagonal carbide.

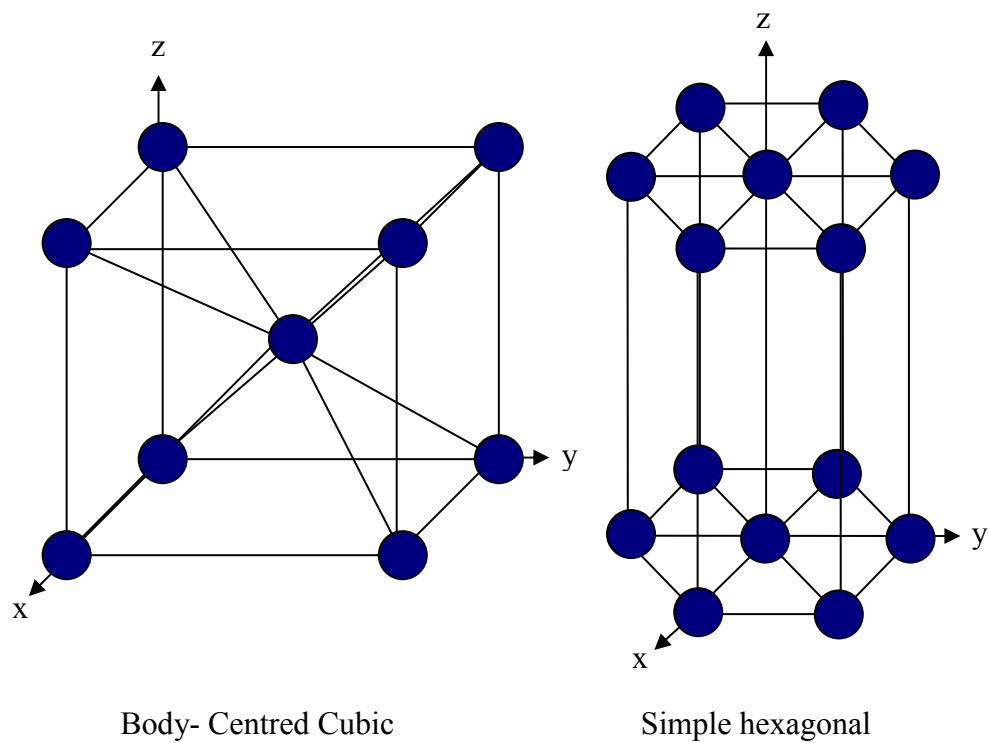


**Figure 1- 4: Schematic of the unit cell of a body-centred cubic and a simple hexagonal crystal structure.**

Despite the metal atoms in close-packed structures sitting as close as possible to one another within the structure, due to the atoms being treated as solid spheres, voids exist between the atoms. This can be observed in Figure 1- 2 and these voids are known as interstitial sites. Each site forms a polyhedron with neighbouring atoms, with the void at the centre, resulting in either an octahedral or tetrahedral polyhedron. A tetrahedral polyhedron has 4 plane faces while an octahedral one has 8.

In a close-packed structure both tetrahedral and octahedral sites exist, with the former being much smaller than the latter. In fact the tetrahedral site is far too small to be occupied by carbon atoms without causing distortion of the metal lattice. For this reason carbon exclusively occupies the octahedral voids, co-ordinating with 6 metal atoms, to achieve the highest possible co-ordination number. Since only one octahedral site exists per metal atom the highest stoichiometry possible is a 1:1 ratio of metal atoms to carbon resulting in a monocarbide.

Within simple hexagonal structures, such as WC, the carbon atom exists in trigonal prismatic interstitial sites due to the metal atom layer stacking observed. The metal planes are stacked on top of each other, which can be expressed as AA (observed in Figure 1- 4), resulting in much less efficient packing of the metal atoms compared to close-packed structures. The carbon then occupies the interstitial sites which exist between metal layers (Figure 1- 5). This carbide structure predominates with metals from group VI.

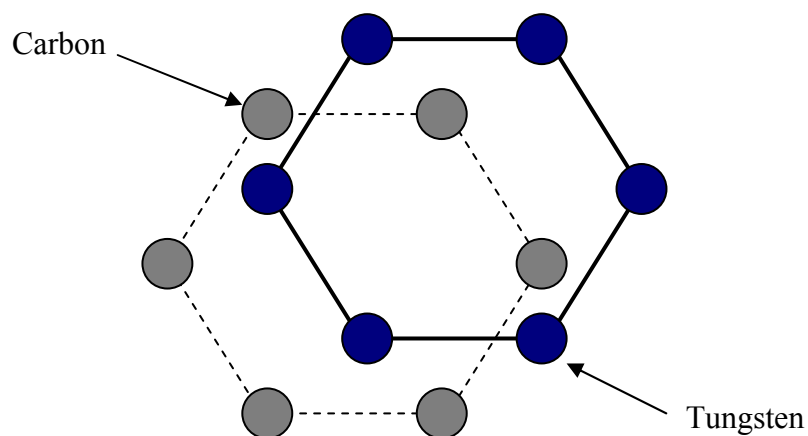


**Figure 1- 5: Schematic representing the interstitial sites occupied by carbon within the simple hexagonal structure adopted by tungsten carbide.**

At the beginning of section 1.1, the compositions of the transition metal carbides of groups IV, V and VI were discussed (Table 1- 1). Despite the increased complexity with group number, similarities exist between the groups. Monocarbides from groups IV and V have an *fcc* structure, with the group VI carbide WC having a simple hexagonal structure. In all cases  $M_2C$  carbides, where M is the metal, form *hcp* crystal structures. These structures, and the resultant arrangement of metal and carbon atoms, are well understood, however, the specifics underpinning the bonding within the structure are still an area of controversy.<sup>6</sup> This is apparent in a broad review of the properties of carbides and the host metals. Carbides are hard, brittle and have high melting points whereas the metals, relatively speaking, are softer, malleable and have lower melting points.<sup>15</sup> These property changes indicate that the interstitial carbides are held together by much stronger bonds than just the metallic ones observed in the parent metal structure. Using the evidence discussed throughout this section one can therefore conclude the following:

- Ionic bonding occurs due to the difference in electronegativity between the metal and carbon atom, resulting in electrostatic bonding existing due to a transfer of electrons from the metal to the carbon atom.
- Metallic bonding exists between the host metal atoms, as observed in the metal structure pre-formation of the carbide. This allows the carbide to maintain much of its “metallic character” and properties, such as good electrical conductivity.

- Covalent bonding is the result of an interaction between the metal *d*-shell and the carbon *p*-shell. This bonding is very strong and no doubt contributes to the property changes observed when the carbide is compared to the host metal.

Finally, the importance of structural composition must be remarked upon. This topic is often overlooked, many believing that stoichiometric carbides are easily achieved, but in truth stoichiometry within the structure is rarely reached with structures being stable over a wide range of compositions. Atomic vacancies, almost always due to carbon, result in widely varying lattice parameters depending on atomic occupancy, which link directly to the properties of the material. When the concentration of carbon is high within the structure, a long-range order is often observed, however this effect, along with the important physical properties of the carbide, change significantly with variations in stoichiometry, often to an unsatisfactory conclusion.

## 1.1.2 Synthesis and Preparation

There are a number of conventional synthetic approaches used to manufacture polycrystalline carbides. Although specific synthetic routes to carbides will be discussed in the relevant results chapters (chapters 3, 4 and 5), the general synthetic routes are worth discussion here.

Figure 1- 6 shows the five possible conventional routes available for the synthesis of the transition metal carbides. Traditionally, many were obtained by melting the elements in an electric arc furnace, however, the most common synthesis method is to heat a mixture of the metal and carbon at temperatures below the metal melting point.<sup>16</sup> This is possible due to reactivity of metals with carbon under these conditions and is often carried out in a reducing gas, such as H<sub>2</sub>, with carbon usually sourced from carbon powder (amorphous or graphite). Alternatively, due to the expense of some of the transition metal powders, the carbide can be synthesised in a two-step process by first reducing the corresponding metal oxide (Figure 1- 6). This is possible due to the lower affinity for oxygen compared to carbon for the metals in question, thus allowing the reduction of the metal oxide to take place.<sup>16</sup> However, despite the obvious economic advantages of using the oxide in carbide synthesis, it seldom results in a purity sufficient for industrial applications let alone laboratory analysis. Almost always arc melting or high vacuum annealing is required to purify the carbide.<sup>17</sup> Carbides can dissolve a considerable amount of oxygen, affecting their properties, however, oxygen content can be reduced with rapid synthesis times, high-vacuum reactions and high-content carbon carbides.<sup>17</sup>

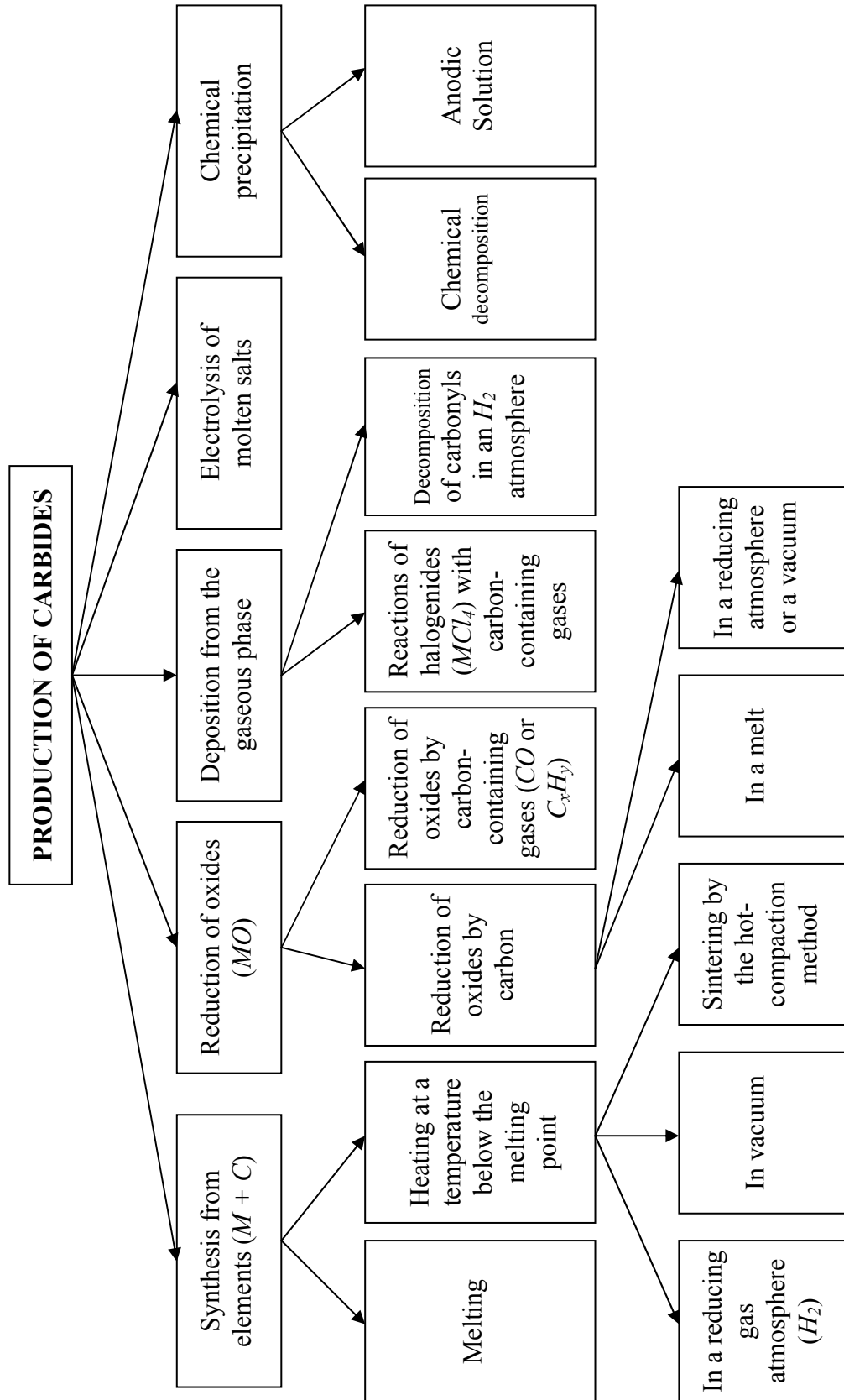


Figure 1- 6: Summary of synthetic methods used to obtain carbides ( $M$  represents the metal). Based on a diagram by Pierson.<sup>6</sup>

For the majority of the synthesis methods, high temperatures are required. For the more common method (direct synthesis from the elements) temperatures in excess of 1000 °C are necessary. Temperatures in this region are also required for synthesis from the metal oxides, although it has been shown, for both synthetic processes, that static pressurisation of the reaction significantly reduces the temperatures required for successful carbide formation.<sup>18</sup> An alternative method of reducing the synthesis temperature is to use carbon-containing gases at sufficiently high partial pressures to afford the required amount of carbon for carbide formation, but to prevent precipitation of free carbon.<sup>16</sup> The gases used include carbon monoxide, CO, and methane, CH<sub>4</sub>, and their reaction with metals has been thoroughly investigated.<sup>16</sup> Comparisons of reaction temperatures required in both the synthesis of the carbide from the elements/oxide and using a carbon-containing gas can be seen in Table 1- 5.

	<b>Reaction</b>	<b>Temperature / °C</b>
Synthesis from the elements	$\text{Nb} + \text{C} \rightarrow \text{NbC}$	1300 – 1400
	$\text{Mo} + \text{C} \rightarrow \text{Mo}_2\text{C}$	1200 – 1400
	$\text{Ta} + \text{C} \rightarrow \text{TaC}$	1300 – 1500
	$\text{W} + \text{C} \rightarrow \text{WC}$	1400 – 1600
Synthesis using a carbon-containing gas	$\text{Nb} + \text{H}_2 + \text{C}_x\text{H}_y \rightarrow \text{NbC} + \text{H}_2 + (\text{CH})$	1300
	$\text{Mo} + \text{H}_2 + \text{CH}_4 \rightarrow \text{Mo}_2\text{C} + \text{H}_2 + (\text{CH})$	800
	$\text{Ta} + \text{H}_2 + \text{C}_x\text{H}_y \rightarrow \text{TaC} + \text{H}_2 + (\text{CH})$	1300 – 2900
	$\text{W} + \text{N}_2 + \text{H}_2 + \text{C}_x\text{H}_y \rightarrow \text{NbC} + \text{H}_2 + \text{N}_2 (\text{CH})$	1000 – 2200

**Table 1- 5: Temperatures required for successful carbide synthesis from the reported reactants.<sup>16</sup>**

Successful bulk synthesis of relatively pure carbides is achieved through the techniques reported in Figure 1- 6, however, high-purity homogeneous carbides are difficult to manufacture in this way.<sup>1</sup> In recent years alternative methods have been pursued to rectify this problem, however, these produce only powders and require further pressing/sintering to achieve bulk carbides. These methods include conventional grinding,<sup>1</sup> vapour-phase reactions,<sup>16</sup> RF plasma torch,<sup>6</sup> Self-propagating High-temperature Synthesis (SHS)<sup>6</sup> and sol-gel processing<sup>6</sup>.

Conventional grinding can be used to obtain smaller, more uniform particles, usually through the use of a ball mill. The ball material is often the same as the materials being ground to avoid contamination and the resulting ground powder is a mixture of coarse and fine particles. This technique is relatively inexpensive, although time consuming, but results in limited purity and homogeneity. An example of this technique is in the successful room temperature ball mill synthesis of WC.<sup>19, 20</sup>

In a Chemical-Vapour phase Deposition (CVD) reaction, if the temperature and supersaturation are sufficiently high, powder is primarily precipitated from the gas phase. This resultant powder has very few impurities, small particle diameter and good particle size uniformity. In addition, the temperatures required for synthesis are lower than for conventional carbide formation (Table 1- 5). Although the successful synthesis of submicron SiC has been reported,<sup>21</sup> this technique has yet to show any promise in a commercial process. It is not possible either to produce bulk carbides on a large scale with

this method due to processing expense and timescales; however, it has shown great promise for use in carbide coating of other materials.

Similar to CVD, production of carbides using RF plasma torch results in only small quantities of the carbide material, however it does enable the synthesis of ultrafine powders. It has been successfully demonstrated in the synthesis of SiC.<sup>22</sup>

Self-propagating High-temperature Synthesis (SHS) is another method which has shown promise for carbide production. Under the right conditions, highly exothermic reactions, once initiated, will spread as a combustion wave throughout the reactants.<sup>23</sup> This technique has been used successfully in the synthesis of a number of carbides from group IV, V and VI.<sup>6</sup>

Finally the sol-gel method has been used in the successful synthesis of SiC.<sup>24</sup> This technique uses a liquid reactive precursor material that is converted to the final product by chemical and thermal means. This precursor is prepared to form a colloidal suspension or solution (sol) which goes through a gelling stage (gel) followed by drying and consolidation.<sup>6</sup> The process often requires temperatures less than half of those required conventionally and permits close control of the composition and structure of the final carbide.<sup>25</sup> Despite most work being concentrated on silicon carbide synthesis, carbides, such as tungsten carbide, have shown promise from the precursors tungsten carbonyl and dimethyl acetylene dicarboxylate.<sup>6</sup>

Many of these novel synthesis techniques however, do not facilitate mass production and have so far been investigated for only a small number of carbides. In terms of conventional synthesis methods, reliability and simplicity are definite positive factors, however, high temperatures and long reaction times are often required with the processes not always resulting in carbides which are commercially or laboratory applicable. It seems among these techniques there is certainly room for a method which may offer the tonnage required conventionally alongside the control of properties and structure obtained with the more recent synthetic methods.

### **1.1.3 Applications**

The refractory carbides lend themselves to a number of applications due to their specific properties. As discussed previously, these include high melting points, high hardness, good resistance to wear and corrosion and a number of properties usually associated with metals such as good electrical conductivity. The application of specific carbides is discussed in detail in the relevant results chapters (chapter 3, 4 and 5), but a general discussion for these materials is appropriate. These properties highlighted above allow the carbide materials to be used in a number of different applications, including the following:<sup>16</sup>

- As corrosion-resistant materials in the chemical industry
- Materials for use in nuclear energy production
- Materials for the manufacture of aircraft and rockets
- Materials for electrical and radio purposes
- Hard and wear resistant materials for use in demanding applications such as tools and drills

Depending on the nature of the application the carbide can take many forms such as powders, bulk shapes, coatings, fibres and whiskers, often depending on the specific properties being utilised, for example hardness in wear applications. Table 1- 6 reports a summary of applications, but it should be noted this does not contain all applications or details on all the carbides.<sup>6</sup>

<b>Application</b>	<b>Typical Form</b>	<b>Typical Property</b>	<b>Typical Material</b>	<b>Industrial Category</b>
Structural	Bulk Fibres	Strength Hardness	SiC B <sub>4</sub> C WC	Automotive Aerospace Chemicals Armour
Wear and Erosion	Bulk Coating Powder	Hardness Chemical resistance	TiC SiC WC	Machinery Cutting tools Aerospace Abrasives
Nuclear	Bulk Coatings	Neutron resistance	B <sub>4</sub> C TiC	Nuclear power
Semiconductor and optical	Coatings	Electron conductivity Thermal conductivity	SiC	Semiconductor Optics Electronic

**Table 1- 6: Applications of refractory carbides.**

It is apparent that a number of synthetic routes and refractory carbides exist, all with their own merits and flaws. The assessment of the importance of specific refractory carbides and their synthetic processes is difficult due to the plethora of applications. For example, one cannot compare the vast quantity of SiC manufactured per annum as an inexpensive abrasive, and the small, but important, amount of B<sub>4</sub>C produced as a coating for armour applications.<sup>6</sup> In other words, one must not just look at the quantity a particular synthetic route produces, but also the quality of the product and the applications for that material. For this reason, a number of synthetic routes to a given material are viable depending on the targeted application for the carbide in question.

## 1.2 TRANSITION METAL CARBIDE SUMMARY

The transition metal carbides have been shown to be far more complex in terms of their synthesis, structure and bonding than they appear. Even the binary structures, which have been well researched, are still not fully understood in terms of the bonding between metal and non-metal atoms. It appears that this bonding, comprising ionic, covalent and metallic, explains a number of the properties observed for the refractory carbides. The ionic bonding likely exists due to the difference in electronegativity between metal and carbon, while the covalent bonding is a result of electron sharing between the *d*-state of the metal and *p*-state of the hybridised carbon atom. This bond is very strong and allows the structure to have a high hardness which is not observed in the pure-metal structure. The metallic bonding, observed between metal atoms, results in the “metallic properties” observed for the carbides, such as good electrical conductivity.

The synthesis of the transition metal carbides has also been discussed showing a number of approaches to the manufacture of these materials. Conventionally a number of routes are available, with ultimately the synthesis carried out from the oxide or elements in the majority of cases. This is due to the relative ease of production, although these routes do not allow for the formation of high quality carbides, particular in the case of synthesis from the metal oxide where oxygen impurities are difficult to remove. Alternative, synthetic routes include CVD, sol-gel and SHS, which allow for better control over carbide synthesis and the applied power, resulting in possible targeting of specific carbon stoichiometries and carbide structures.

### 1.3 HISTORY OF MICROWAVE HEATING AND SOLID STATE MICROWAVE MATERIALS SYNTHESIS

Microwaves (MW) are high frequency (0.3 to 300 GHz) electromagnetic waves which are situated between infrared and radio wavelengths in the electromagnetic spectrum. The first real world applications for microwaves began in 1920 with the development of the magnetron by Hull.<sup>26</sup> However it was not until decades later when applications of microwaves in communications were realised.<sup>27</sup> Then with the advancements in technology and the onset of the 2<sup>nd</sup> World War and the development of effective radar<sup>28</sup> and communications saw huge potential for microwave applications. During this time the potential for drying of materials and cooking of food was also realised. However it was not until the 1960's when the first domestic microwave ovens were manufactured.<sup>29</sup> It was then a decade later when the first report of microwave heating used in chemical research was published.<sup>30</sup> This sparked off further research into this novel technique with more papers being published in the early 1980's, but it was not until the early 1990's when interest flourished in this area thanks to the first successful reactions in conventional Domestic Microwave Ovens (DMOs).<sup>31, 32</sup> Over the next two decades a number of scientists contributed to the development of microwaves for materials synthesis. These include the groups of Sutton,<sup>33</sup> Katz,<sup>34</sup> Gerdes and Willert-Porada,<sup>35</sup> and Agrawal,<sup>36</sup> who all published work on the processing and sintering of ceramics. In addition Clark and Sutton produced a seminal review in 1996 on microwave processing of materials.<sup>37</sup> The role of microwaves specifically for "chemical synthesis" was steered by

Clark et al. with work on combustion synthesis<sup>38</sup> and Whittaker and Mingos with work on microwave-assisted solid state reactions.<sup>39</sup> Now, research into microwave heating is more extensive than ever, covering a plethora of material families, and offering a genuine alternative to more conventional heating methods. However, it is still not well understood with many issues still remaining with the process, including reproducibility and a fundamental understanding of why these reactions often occur so rapidly compared to conventional process techniques. This latter topic is a subject of much discussion and the literature proposes two principal models to explain the microwave activation process.<sup>40</sup> The first model, as proposed by Galema,<sup>41</sup> discusses a non-thermal interaction of the material with microwaves, indicating that microwaves decrease the activation energy of the chemical reaction through either storage of energy as vibrational energy or by the alignment of molecules. The second model, favoured by many, attributes the activation process to purely a thermal effect. Certainly, within materials synthesis, the latter model seems more plausible, however incomplete descriptions of experimental setups and limitations of *in-situ* measurement techniques have meant that until now it has been difficult to reproduce results and not easy to elucidate the mechanism of activation. Further discussion of microwave heating and microwave reactor engineering can be found in chapter 2 (sections 2.1 and 2.1.2).

## 1.4 MICROWAVE SOLID STATE SYNTHESSES: A REVIEW

The diversity of solid state materials synthesised using microwave heating is vast, ranging from multinary oxides to simple binary, yet industrially relevant, carbides and nitrides. A highly cited review from 1999 by Rao et al,<sup>42</sup> covers much of the work in the later part of the 20<sup>th</sup> century, however, since its publication rapid growth in this field of research has embraced many new material systems and has seen significant technical and experimental advances. The following section aims to cover, with a specific look at novel and innovative research, some of the relevant major families of materials represented in the literature, i.e. families in which the literature directly affects work discussed in this thesis. The importance of these families, not just the carbide, should not be underestimated. A number of techniques which have been investigated for a sole material can be applied across the range of solid state compounds. For this reason one must discuss the plethora of materials in an effort to correlate similarities, differences and discrepancies with a view to building on specific experiments and the overall understanding of microwave solid state heating. This is an important step as much can be assimilated and applied to work discussed in this thesis.

This section focuses purely on the reactivity of solids in a microwave field, avoiding discussion of plasma reactions and the use of organic liquids in solid state synthesis. These are rapidly emerging areas in their own right, but are not relevant to this thesis. For accounts of some of the leading work the

following references apply: microwave plasmas<sup>43,44,45,46,47,48</sup>, zeolites and aluminium phosphates<sup>49,50,51,52</sup> and glasses.<sup>53,54,55</sup>

### 1.4.1 Borides

The discovery of a superconducting transition of 39 K in  $\text{MgB}_2$ <sup>56</sup> led to the attempted, and ultimately successful synthesis of this material (from Mg + B) in 30 minutes using a domestic microwave oven set at 900 W.<sup>57</sup> Reaction temperature was probed with an optical pyrometer and never exceeded 900 °C; noticeably lower than that employed by conventional methods (>1000 °C). However, this temperature difference can be contested due to the inaccuracy of temperature measurements within microwave cavities. This is discussed further in chapter 3 (section 3.4.1) due to its specific relevance in the experimental procedure design, but here it should be noted that, unless optical pyrometers have their emissivity calibrated correctly, their readings can be erroneous. Regardless of this temperature argument, this synthesis led to smaller and more uniform grain sizes (14(3)  $\mu\text{m}$ ) that appeared to enhance mechanical properties (increased hardness for example), but with no change in lattice parameters. The methodology also described the use of carbon as a reaction susceptor by exploiting its high loss tangent which is discussed in more detail in a previous publication by the same group.<sup>58</sup> In this earlier work Agostino discusses the importance of avoiding contamination from the necessary carbon susceptor. Susceptors are used repeatedly within the literature as a reliable method for initiating a reaction where reactants present generally have low loss tangents or equipment design is poor. By elevating the reaction temperature, in most cases,

the reactants loss tangents increase allowing a reaction to take place.<sup>42, 59</sup> SiC is another such susceptor which has been reported in the MW synthesis of MgB<sub>2</sub>.<sup>60</sup> In these experiments Dong et al. achieved a complete synthesis in 11 minutes at only 560 W in an un-modified DMO. They noted a temperature of approximately 800 °C, while acknowledging that the use of a thermocouple post reaction is only a crude measurement technique. They also report grain sizes of between 0.1 and 0.5 μm, much smaller than Agostino et al.<sup>57</sup>, and claim to be able to control particle size through the adjustment of the grain sizes of the starting materials. This obvious difference is mirrored in the vast difference in reaction time reported in both cases. However, a comparison of the two synthetic strategies is difficult as Agostino does not provide enough experimental information for a comprehensive argument. Dong explains the use of the turntable present in the DMO, which could increase the efficiency of heating as multiple modes will be encountered (see DMO description, section 2.1.2.1).

## 1.4.2 Carbides

The subject of this thesis, refractory carbides, are extremely important materials in modern industry. They have a number of advantageous properties,<sup>16</sup> but their synthesis is long and arduous as discussed in section 1.1.2.<sup>17</sup> For this reason, as for many other materials, microwave heating has been recognised as a viable alternative to conventional heating and has led to the successful synthesis of a number of carbides. In fact this area is second only to oxide material synthesis, in terms of current research, with synthesis generally concentrated on the more industrially relevant materials such as

tungsten, silicon and titanium carbide, but many other compounds have also been investigated. Some selected materials recently synthesised/sintered by microwave methods are shown in Table 1- 7. For a more detailed discussion of microwave synthesis of carbides specific to this thesis, see chapters 3, 4 and 5.

Si	Ca	Ti	Fe	Co	Ni	Mo	Ta	W
SiC <sup>61, 62,</sup> MoSi <sub>2</sub> -SiC <sup>63,</sup> ZrC-SiC <sup>64,</sup>	CaC <sub>2</sub> <sup>65</sup>	TiC <sup>66, 67,</sup> Al <sub>2</sub> O <sub>3</sub> -TiC <sup>68</sup>	Fe-Cu-C <sup>69,</sup> Fe-Ni-C <sup>69</sup>				TaC <sup>66</sup>	WC <sup>70,71,72,73,</sup> WC-Co <sup>74,75,36</sup>
						Mo <sub>2</sub> C <sup>76</sup>		
				MgCo <sub>3</sub> C <sub>x</sub> <sup>65</sup>	Ca <sub>4</sub> Ni <sub>3</sub> C <sub>5</sub> <sup>65,</sup> MgNi <sub>3</sub> C <sub>x</sub> <sup>65,77,</sup> MgCNi <sub>3</sub> <sup>77</sup>			

**Table 1- 7: Binary and ternary carbides successfully synthesised (red references)/sintered (blue references) in the last decade.**

The dominant theme in the publications referenced in Table 1- 7 is the advantages microwave heating brings to the synthesis of the desired material. In all cases the carbide is synthesised faster and often seemingly at a lower temperature than that required in the conventional heating process. Another feature of the MW processing appears to be improved mechanical properties and finer grain sizes. For example, for the sintering of WC-Co, Cheng et al. report a sintering time of less than 30 minutes compared to hours required conventionally with a reaction temperature of only 1250 °C; 250 °C lower than that used in the commercial process.<sup>75</sup> Unfortunately, they do not discuss the method for which the temperature data were collected. In addition, they report enhanced densification of the product as well as a fine grain size (~1 µm). Cheng et al. also report the development of a continuous flow process in this article. Utilising a single mode cavity reactor it is shown how one can successfully sinter up to 1 metre long ceramics. This is an important step in the

development of commercial microwave heating apparatus and is one of a few notable developments in microwave reactor design within the last decade. Complementing this work Rodiger et al. published work examining the penetration depth in various materials, including metals, while investigating WC-Co sintering.<sup>70</sup> This is an important factor in the development from batch towards continuous processing.

Although numerous papers report successful rapid sintering/synthesis of carbides, comparatively little work has been carried out on determination of the reaction mechanism or to attempt to explain experimental observations. Aguilar et al. observed a temperature plateau, indicating a self terminating reaction, in the synthesis of SiC from  $\text{SiO}_2 + \text{C}$ .<sup>62</sup> During the 25 min synthesis time, temperatures up to 1900 °C were observed with an optical pyrometer with the plateau appearing at about 500 s. Unfortunately the article does not indicate phase fractions at any given points during the reaction so it is impossible to infer any more from these results. Similar comparisons between temperature and phase purity were carried out in the synthesis of ZrC-SiC (from  $\text{ZrO}_2 + \text{SiO}_2 + \text{C}$ ) composites.<sup>64</sup> In this case Das et al. evaluated the kinetics of the reaction by examining the change in phase composition with temperature over a 30 min time period during the course of the reaction. A detailed study is shown of the influence of phase formation on each other, highlighting the exothermic SiC formation reaction (beginning above 1000 °C) and how this local heating initiates the ZrC formation. It was also noted that a slow increase in the microwave power up to 700 W was required initially to avoid pellet disintegration. This was likely due to the gas evolved from the pellet as the oxide starting materials are reduced.

Synthesis of carbides from the metal oxides often requires a susceptor depending on the dielectric properties (discussed in section 2.1.2) of the starting materials. Hassine et al. used metal oxides in the synthesis of TiC (from  $\text{TiO}_2 + \text{C}$ ,  $< 1550\text{ }^\circ\text{C}$ ) and TaC (from  $\text{Ta}_2\text{O}_5 + \text{C}$ ,  $< 1500\text{ }^\circ\text{C}$ ).<sup>66</sup> In both cases the power was slowly ramped from 500 W to 5 kW to avoid the thermal shock of the reaction crucible and both were completed in 1 h. This is much shorter compared to the 6 h at  $1750\text{ }^\circ\text{C}$  required conventionally.<sup>66</sup> Interestingly the carbothermal reduction passed through  $\text{Ti}_4\text{O}_7$  on its way to Ti, but the more common intermediate (seen conventionally),  $\text{Ti}_2\text{O}_3$ , was never observed. This could be due to a lower reaction temperature in MW synthesis, but is most likely due to the rapid reaction rate. Unfortunately, commercial grade TiC could not be produced due to excessive grain growth as the temperature increased. Interestingly this is very different to the situation observed by Satapathy et al. in the synthesis of SiC, where they see no change in grain size at different reaction temperatures ( $900\text{ }^\circ\text{C}$  to  $1300\text{ }^\circ\text{C}$ ).<sup>61</sup>

### **1.4.3 Nitrides**

The synthesis of nitrides saw a surge in research in the mid-late 1990's. DMOs, modified to operate under a variety of atmospheres, were used to supply flowing nitrogen or ammonia gas (often essential for nitride synthesis) to the solid sample. Table 1- 8 displays a number of recent successfully synthesised binary and ternary nitrides.

<b>B</b>	<b>Al</b>	<b>Si</b>	<b>Ti</b>	<b>V</b>	<b>Fe</b>	<b>Ga</b>	<b>Nb</b>	<b>Ta</b>
BN <sup>78</sup> , Li <sub>3</sub> BN <sub>2</sub> <sup>78</sup>	AlN <sup>78,79</sup> , Li <sub>3</sub> AlN <sub>2</sub> <sup>78</sup>	LiSi <sub>2</sub> N <sub>3</sub> <sup>78</sup> , Li <sub>2</sub> SiN <sub>2</sub> <sup>78,80</sup>	TiN <sup>78,81,82,83</sup> , Li <sub>5</sub> TiN <sub>3</sub> <sup>78</sup> , Li <sub>5</sub> TiN <sub>3</sub> <sup>78</sup>	VN <sup>78,82</sup>	Li <sub>3</sub> FeN <sub>2</sub> <sup>78</sup>	GaN <sup>82</sup>	NbN <sup>78</sup>	
							Nb <sub>2</sub> N <sup>78</sup>	Ta <sub>2</sub> N <sup>84</sup>
		Si <sub>3</sub> N <sub>4</sub> <sup>78,85</sup>					Nb <sub>3</sub> N <sub>4</sub> <sup>78</sup>	

**Table 1- 8: Binary and ternary nitrides successfully synthesised in the last decade.**

The majority of publications report the employment of multimode cavities for nitride synthesis, however, single mode cavities have been used, for example in the synthesis of AlN,<sup>78</sup> obtained after only 30 min with temperatures observed as high as 1900 °C and a reaction time much shorter than the 8-12 h required in the commercial process.<sup>78</sup> These same trends in processing are observed in the synthesis of the much studied TiN. Synthesis was achieved from TiO<sub>2</sub> by Liu et al,<sup>81</sup> with sphere-like particles present in the microwave heated sample and, importantly, no large agglomerates were observed. Using the same starting materials, Peeladmedu reported successful synthesis of TiN and investigated the effect of excess carbon on the reaction, revealing the reaction time to drop to only 1 min. However, difficulty was found in removing the carbon post-reaction.<sup>83</sup> In addition it was observed that no formation of the intermediate Ti<sub>3</sub>O<sub>5</sub> occurs, which is present in the conventional synthesis. Vaidhyanathan also reports successful synthesis of TiN in a modified DMO (to cater for different atmospheres), along with numerous other binary nitrides.<sup>82</sup> However, discrepancies arise when comparing these publications on the successful synthesis of this material. In each of the above, examples of TiN synthesis, the microwave reactor design differs resulting in the observed reaction time decreasing with increasing power as one might

expect. It is also known that the use of a single mode cavity commonly decreases reaction time over a multimode equivalent.<sup>71</sup> Yet in this case, the single mode cavity used at 1.5 kW by Liu et al. leads to a synthesis time of 1 h for TiN<sup>81</sup>, which is almost twice as long as Vaidhyanathan reports using a DMO at 980 W.<sup>82</sup> Even quicker than both (20 min) is Peelamedu's reports of work using a modified multimode microwave furnace at 1.4 kW.<sup>83</sup> Although many of the parameters required to make an informed comparison are not reported, what is known is that Peelamedu reported a reaction temperature of ~1400 °C (monitored using an optical pyrometer). This is higher than that reported by Liu (1200 °C). The latter paper reports that the reaction rate at this temperature is slow due to the low free energy of reaction which goes some way to explaining these discrepancies in TiN synthesis. It is also possible that poor temperature measurements could be to blame. One thing is clear, the importance of detailed reporting of observations and experimental procedures is paramount to avoid these conflicting results so that, ultimately, further understanding of microwave heating in solid state systems can be obtained.

#### 1.4.4 Oxides

The vast majority of microwave materials synthesis concentrates on oxide materials. This is no doubt due to their wide variety of applications as well as their relative ease of synthesis as no specialised reactive or inert atmospheres are required. These include materials such as Na<sub>x</sub>Co<sub>1-y</sub>Mn<sub>y</sub>O<sub>2</sub> as a thermoelectric conversion material<sup>86</sup>; NaZr<sub>2</sub>(PO<sub>4</sub>)<sub>3</sub>: part of a series of inorganic phosphates<sup>87</sup>, garnets: Y<sub>3</sub>(Al, Fe)<sub>5</sub>O<sub>12</sub><sup>88</sup>, Bi<sub>4</sub>Ti<sub>3</sub>O<sub>12</sub><sup>89</sup>, the high temperature

superconductor  $\text{YBa}_2\text{Cu}_3\text{O}_{7-x}$ <sup>90,91</sup>, and numerous lithium, copper, cobalt and nickel ferrites.<sup>92</sup> However the synthesis of perovskites far exceeds other oxide materials resulting in the publication of numerous articles.<sup>36,67,93,94,95,96,97,98,99,100</sup>

In common with non-oxide reduced reaction times, lower reaction temperatures and enhanced properties are observed in the microwave synthesis of oxides, however, a number of articles also mention key observations which could help explain microwave heating and mechanisms. For example Iwasaki et al., on the synthesis of  $\text{Na}_x\text{Co}_{1-y}\text{Mn}_y\text{O}_2$  (1 kW multimode furnace taking 2 h at 900 °C), discuss the observation, using SEM, of accelerated grain growth in a specific direction leading them to conclude that selective heating of grains was occurring.<sup>86</sup> This is not unexpected in microwave heating due to the different dielectric properties of materials such that some are more susceptible than others to microwave irradiation. Microwave heating has also been shown to offer alternative methods in desired materials. In the synthesis of the perovskite lead zirconium titanate (PZT), the depression of the reaction temperature (< 750 °C) resulted in no vapourisation of the PbO starting material leading to a more reproducible and cost effective reaction.<sup>96</sup>

The majority of microwave oxide synthesis is performed in a multimode microwave furnace, however, a number of examples exist in which a single mode cavity is used. The synthesis of  $\text{La}_{0.8}\text{Sr}_{0.2}\text{MnO}_3$  (LSMO) by Grossin et al. clearly shows the effect on temperature and reaction rate with change in power.<sup>93</sup> For a fixed time of 10 min the power was varied between 700 and 1000 W for a number of samples and it is clearly shown how the

temperature rises, at a much faster rate, as the power increases due to the power density being proportional to electric field strength squared (discussed further in chapter 2, section 2.1.2). Directly related to this is the phase purity of the product which improves with temperature. Another example is the sintering of BaTiO<sub>3</sub> at 1 kW.<sup>95</sup> In a ground breaking study Harrison et al. used *in-situ* neutron diffraction to follow the structure of the titanate during microwave irradiation. Due to the rapid nature of microwave reactions and the nature of the setup it is very difficult to find *in-situ* techniques that (a) accurately probe samples on a rapid timescale, (b) can be directed into the microwave cavity and (c) do not interact with the microwave irradiation. In this instance the authors used a pyrometer to monitor the sample surface temperature and collected data at specific temperatures resulting in some unexpected structural observations compared to a sample heated conventionally. A larger cubic cell parameter, but smaller anisotropic displacement parameters (ADPs) were observed in the MW heated sample. It was suggested that the increased cell volume was due to higher temperatures within the sample than are recorded at the surface. However the low ADPs, which contradict this, arise from damping of certain forms of ion motion by the microwave field. The data also suggested that due to a significant increase in fitted peak width parameters, the existence of hot spots or at least thermal gradients within the sample. These are effects that are often hypothesised as phenomena directly associated with microwave heating.

## 1.5 REVIEW SUMMARY

It is apparent from this review that microwave heating shows great promise in the area of solid state synthesis. Specifically, within the last decade, much has been published on the microwave synthesis/sintering of boride, nitride, carbide and oxide powders. Fundamentally the reactions are similar, relying on the dielectric properties of the compounds present to drive the reaction and where this is not initially possible, a susceptor is used. However, a number of authors have sought different results from their experiments and have approached the challenge of microwave solid state synthesis from different directions. This allows much to be gleaned from the results published which, ultimately, has the potential to both aid in the design of experiments and explain the results published in this thesis. These results warrant a brief discussion to assist coherency and highlight some key points which have been lifted from the literature.

Firstly, microwave solid state heating, in the majority of cases, has been shown to exhibit a number of advantages over conventional furnace heating:

- Lower reaction temperatures.<sup>57, 60, 75, 96</sup>
- Faster reaction times.<sup>60, 62, 66, 75, 78, 93</sup>
- Smaller and more uniform product particle (grain) size.<sup>57, 60, 81, 86</sup>
- Enhanced mechanical properties.<sup>57</sup>

Reactions have also been shown to proceed through different routes to obtain the product. Suspected to be due to the rapid reaction times and lower temperatures, intermediates are often not observed. For example, no intermediate oxide in the reduction of  $\text{TiO}_2$  to ultimately afford TiC. These lower reaction temperatures have also allowed unique approaches to the synthesis of certain materials; for example in the synthesis of PZT, no vapourisation of the starting material PbO occurs due to the reaction temperature being less than  $750\text{ }^\circ\text{C}$ . This allows for a more reproducible and cost effective (no loss of starting materials) reaction. In fact cost effectiveness is a key advantage of microwave heating which is frequently referred to in the literature, no doubt due to a number of advantages, such as fast reaction times, which have already been mentioned.

Despite numerous researchers seeking purely the synthesis of materials, many have also investigated the heating process, revealing a number of key statements:

- Penetration depth plays an important role in solid state experiments and should always be taken into account when designing procedures.<sup>70</sup>
- Temperature measurements in microwave fields are notoriously difficult with no method offering a perfect solution (further discussion of temperature measurements is presented in section 3.4.1).<sup>60</sup>
- Product phase fraction is directly related to reaction temperature.<sup>93</sup>
- Reaction temperature rises more rapidly with increasing applied microwave power.<sup>93</sup>

- Often ramping of the applied microwave power is required to avoid thermal shock of the reaction vessel or to control gas evolution in the reduction of oxides.<sup>66</sup>
- When multiple compounds are present, selective heating can occur of individual phases. PND has been used to indicate the presence of “hot spots” in samples.<sup>95</sup>
- The comparison between single mode and multimode cavities and the noted variations in reaction time and reproducibility.<sup>75, 78, 93</sup>

Despite much being learnt however, the literature contains a number of discrepancies and contradictions. One example of this is in the synthesis of TiN. It is clear from the examination of the papers published on this material that, (a) not enough information is available on the experimental procedure and how the results were obtained and (b) much is still not understood as to how the reaction proceeds, leading to limited control of variables such as temperature which is often measured inaccurately or not monitored at all.

## **1.6 SCOPE OF THIS WORK**

It is apparent from the discussion of current research that much of the understanding surrounding microwave solid state synthesis has yet to be obtained. Although much of the theory on microwave interaction with materials is known, no one has yet clarified the reason for the rapid reaction times, let alone define a solid state heating mechanism. This is arguably the key to furthering this area of study, but one should not forget the importance of rapid materials synthesis and the development of microwave applicators.

The following chapters aim to describe the ultra-rapid synthesis of a number of important transition metal carbides as well as investigating their reaction mechanisms and properties. Four binary systems are discussed, Nb-C, Mo-C, Ta-C and W-C, and work carried out on the ternary system, Nb-Ta-C, is also evaluated. Carbide production was investigated from both the oxide and elemental precursors.

To achieve these goals described above, two approaches needed to be taken; first the successful development of a reproducible experimental procedure, reinforced by investigations into various microwave cavity types and microwave powers; and secondly, the investigation into the reaction mechanism through an in depth study of samples collected throughout the reaction process. By evaluating the structure of phases present and their dielectric properties, alongside temperature data collected during the reaction, it was hoped a reaction profile could be established. Through this, further understanding could then be gained on the microwave synthesis of carbides. In addition, a number of *in-situ* techniques were attempted, including high speed photography, in an attempt to build on this knowledge and to perhaps infer a mechanism.

## 1.7 REFERENCES

---

- <sup>1</sup> L. E. Toth, *Transition Metal Carbides and Nitrides*, 1<sup>st</sup> edition, Academic Press, New York and London, 1971.
- <sup>2</sup> T. Xiao, A. Hanif, A. P. E. York, J. Sloan and M. L. H. Green, *Phys. Chem. Chem. Phys.*, 2002, **4**, 3522.
- <sup>3</sup> M. J. Ledoux, C. H. Pham, J. Guille and H. Dunlop, *J. Catalysis*, 1992, **134**, 383.
- <sup>4</sup> A. L. Giorgi, E. G. Szklarz, E. K. Storms, A. L. Bowman and B. T. Matthias, *Phys. Rev.*, 1962, **125**, 837.
- <sup>5</sup> K. Schwarz, and N. Rösch, *J. Phys. C: Solid State Phys.*, 1976, **9**, 433.
- <sup>6</sup> H. O. Pierson, *Handbook of Refractory Carbides and Nitrides*, 1<sup>st</sup> Edition, Noyes, Park Ridge NJ, 1960.
- <sup>7</sup> R. C. Evans, *An introduction to crystal chemistry*, Cambridge Univ. Press, Cambridge, 1979.
- <sup>8</sup> A. R. West, *Basic Solid State Chem.*, 2<sup>nd</sup> Edition, John Wiley & Sons Ltd, Chichester, 1999.
- <sup>9</sup> J. March, *Adv. Inorg. Chem.*, John Wiley & Sons, New York, 1985.
- <sup>10</sup> L. H. Van Vlack, *Elements of Materials Science and Engineering*, 4<sup>th</sup> Edition, Addison-Wesley Publishing Co., Reading, MA, 1980.
- <sup>11</sup> P. Atkins and L. Jones, *Chemical Principles*, 2<sup>nd</sup> Edition, W. H. Freeman & Co., New York, 2000.
- <sup>12</sup> F. A. Cotton and G. Wilkinson, *Adv. Inorg. Chem.*, Interscience Publishers, New York, 1972.

- 
- <sup>13</sup> J. Daintith, *Oxford Dictionary of Chemistry*. Oxford University Press New York, 2004.
- <sup>14</sup> D. M. Adams, *Inorg. Solids*, John Wiley & Sons, New York, 1981.
- <sup>15</sup> I. E. Campbell and E. M. Sherwood, *High-Temperature Materials and Technology*, John Wiley & Sons, New York, 1967.
- <sup>16</sup> T. Ya. Kosolapova, *Carbides: Properties, Production and Applications*, 1<sup>st</sup> Edition, Plenum Press, New York, 1971.
- <sup>17</sup> E. K. Storms, *The Refractory Carbides*, 1<sup>st</sup> Edition, Academic Press, New York, 1967.
- <sup>18</sup> W J Kroll, *Trans. electrochemical soc.*, 1945, **87**, 571.
- <sup>19</sup> M. S. El-Eskandarany, A. A. Mahday, H. A. Ahmed and A. H. Amer, *J. Alloy and Compounds*, 2000, **312**, 315.
- <sup>20</sup> G. M. Wang, S. J. Campbell, A. Calka and W. A. Kaczmarek, *J. Mater. Sci.*, 1997, **32**, 1461.
- <sup>21</sup> H. D. Wu and D. W. Ready, *Ceram. Trans.*, 1987, **2**, 35.
- <sup>22</sup> C. M. Hollabaugh, *Am. Ceram. Soc. Bull.*, 1982, **61**, 814.
- <sup>23</sup> D. R. Biswas, *J. Mat. Sci.*, 1989, **24**, 3791.
- <sup>24</sup> B. I. Lee and L. L. Hench, *Ceram. Bull.*, 1987, **10**, 66.
- <sup>25</sup> C. J. Brinker and G. W. Scherer, *Sol-Gel Science*, Academic Science, San Diego, 1990.
- <sup>26</sup> H. Sobol and K. Tomiyasu, *IEEE Trans. Microwave Theory Tech.*, 2002, **50**, 594.
- <sup>27</sup> G. B. Collins, *Microwave magnetrons*, vol. 6, 1<sup>st</sup> Edition, McGraw-Hill, New York, 1948.

- 
- <sup>28</sup> D. K. Barton, *IEEE Trans. Microwave Theory Tech.*, 1984, **32**, 1161.
- <sup>29</sup> J. M. Osepchuck, *IEEE Trans. Microwave Theory Tech.*, 1984, **32**, 1200.
- <sup>30</sup> S. W. Liu and J. P. Wightman, *J. Appl. Chem. Biotechnol.*, 1971, **21**, 168.
- <sup>31</sup> R. N. Gedye, W. Rank and K. C. Westaway, *Can. J. Chem.*, 1991, **69**, 706.
- <sup>32</sup> R. Hicks and G. Majetich, *J. Microwave Power Electromagn. Eng.*, 1995, **30**, 27.
- <sup>33</sup> W. H. Sutton, *Ceram. Bull.* 1989, **68**, 376.
- <sup>34</sup> J. D. Katz, *Annu. Rev. Mater. Sci.*, 1992, **22**, 153.
- <sup>35</sup> T. Gerdes and M. Willert-Porada, *Mat. Res. Soc. Symp. Proc.*, 1994, **347**, 531.
- <sup>36</sup> D. K. Agrawal, *Curr. Op Solid State Mater. Sci.*, 1998, **3**, 480.
- <sup>37</sup> D. E. Clark and W. H. Sutton, *Annu. Rev. Mater. Sci.*, 1996, **26**, 299.
- <sup>38</sup> D. E. Clark, I. Ahmad and R. C. Dalton, *Mater. Sci. Eng. A*, 1991, **144**, 91.
- <sup>39</sup> A. G. Whittaker and D. M. P. Mingos, *J. Chem. Soc. Dalton Trans.*, 1995, **5**, 2073.
- <sup>40</sup> M. Al-Harashseh, S. Kingman and S. Bradshaw, *Hydrometallurgy*, 2006, **84**, 1.
- <sup>41</sup> S. A. Galema, *Chem. Soc. Rev.* 1997, **26**, 233.
- <sup>42</sup> K. J. Rao, B. Vaidhyanathan, M. Ganguli and P. A. Ramakrishnan, *Chem. Mater.*, 1999, **11**, 882.
- <sup>43</sup> J. D. Houmes and H. C. zur Loye, *Chem. Mater.*, 1996, **8**, 2551.
- <sup>44</sup> D. Vollath and D. V. Sazabo, *Mater. Letters*, 1998, **35**, 236.
- <sup>45</sup> D. J. Brooks, R. E. Douthwaite and L. J. Gillie, *Chem. Comm.*, 2005, 4857.
- <sup>46</sup> O. Jasek, M. Elias, L. Zajickova, V. Kudrle, M. Bublan, J. Matejkova, A. R. J. Bursik and M. Kadlecikova, *Mater. Sci. Eng. C*, 2006, **26**, 1189.

- 
- <sup>47</sup> J. Jiang, W. Cheng, Y. Zhang, H. Zhu and D. Shen, *Mater. Sci. Forum*, 2005, **480-481**, 71.
- <sup>48</sup> K. Tanaka, M. Yoshimura, A. Okamoto and K. Ueda, *Jap. J. Appl. Phys.*, 2005, **44**, 1158.
- <sup>49</sup> H. Kosslick, H. L. Zutowa, U. Lohse, H. Landmesser, R. Fricke and J. Caro, *Ceram. Trans.*, 1997, **80**, 523.
- <sup>50</sup> B. I. Whittington and N. B. Milestone, *Zeolites*, 1992, **12**, 815.
- <sup>51</sup> A. Arafat, J. C. Jansen, A. R. Edaid and H. Van Bekkum, *Zeolites*, 1993, **13**, 162.
- <sup>52</sup> I. Girnus, K. Janke, R. Vetter, J. Richter-Mendau and J. Caro, *Zeolites*, 1995, **15**, 33.
- <sup>53</sup> B. Vaidhyanathan, M. Ganguli and K. J. Rao, *J. Solid State Chem.*, 1994, **113**, 448.
- <sup>54</sup> D. J. Duval, M. J. E. Terjak, S. H. Risbud and B. L. Phillips, *Mater. Res. Soc. Symp. Proc.*, 1996, **430**, 125.
- <sup>55</sup> D. J. Duval, B. L. Phillips, M. J. E. Terjak and S. H. Risbud, *J. Solid State Chem.*, 1997, **131**, 173.
- <sup>56</sup> J. Nagamatsu, N. Nakagawa, T. Muranaka, Y. Zenitani and J. Akimitsu, *Nature*, 2001, **410**, 63.
- <sup>57</sup> A. Agostino, P. Volpe, M. Castiglioni and M. Truccato, *Mat. Res. Innovat.*, 2004, **8**, 75.
- <sup>58</sup> A. Agostino, E. Bonometti, P. Volpe, M. Truccato, C. Manfredotti, P. Olivero, C. Paolini, G. Rinaudo and L. Gozzelino, *Int. J. Mod. Phys. B*, 2003, **17**, 773.
- <sup>59</sup> K. E. Haque, *Int. J. Miner. Process.*, 1999, **57**, 1.

- 
- <sup>60</sup> C. Dong, J. Guo, G. C. Fu, L. H. Yang and H. Chen, *Supercond. Sci. Technol.*, 2004, **17**, 55.
- <sup>61</sup> L. N. Satapathy, P. D. Ramesh, D. Agrawal and R. Roy, *Mater. Res Bull.*, 2005, **40**, 1871.
- <sup>62</sup> J. Aguilar, Z. Valdez, U. Ortiz and J. Rodriguez, *Advances in microwave and radio*, 2006, 645.
- <sup>63</sup> M. Panneerselvam, A. Agrawal and K. J. Rao, *Mater. Sci. Eng. A*, 2003, **356**, 267.
- <sup>64</sup> B. P. Das, M. Panneerselvam and K. J. Rao, *J. Solid State Chem.*, 2003, **173**, 196.
- <sup>65</sup> R. Ahlers and U. Z. Ruschewitz, *Anorg. Allg. Chem.*, 2005, **631**, 1241.
- <sup>66</sup> N. A. Hassine, J. G. P. Binner and T. E. Cross, *Int. J. Refractory Metals & Hard Mater.*, 1995, **13**, 353.
- <sup>67</sup> P. Liu, L. Zeng, H. Wang, X. Cheng, A. Shui, H. Zhang, B. Duan, W. Deng and Y. Liu, *CN1834009-A*, 2006.
- <sup>68</sup> M. Kitiwan and D. Atong, *JSME Int. J. Series A*, 2006, **49**, 85.
- <sup>69</sup> R. Roy, D. Agrawal, J. Cheng and S. Gedevarishvili, *Nature*, 1999, **399**, 668.
- <sup>70</sup> K. Rodiger, K. Dreyer, T. Gerdes and M. Willert-Porada, *Int. J. Refractory Metals & Hard Mater.*, 1998, **16**, 409.
- <sup>71</sup> S. R. Vallance, S. Kingman and D. H. Gregory, *Adv. Mater.*, 2007, **19**, 138.
- <sup>72</sup> M. Lindholm, M. Waldenstroem and M. Ahlgren, *WO200003049-A*, 2000.
- <sup>73</sup> A. Lackner, W. Ferstl, G. Knuenz, A. Dinesh and C. Jiping, *WO200142135*, 2001.

- 
- <sup>74</sup> E. Breval, J. P. Cheng, D. K. Agrawal, P. Gigl, M. Dennis, R. Roy and A. Papworth, *J. Mater. Sci. Eng. A*, 2005, **391**, 285.
- <sup>75</sup> J. P. Cheng, D. K. Agrawal, S. Komarneni, M. Mathis and R. Roy, *Mat. Res. Innovat.*, 1997, **1**, 44.
- <sup>76</sup> S. R. Vallance, S. Kingman and D. H. Gregory, *Chem. Commun.*, 2007, **7**, 742.
- <sup>77</sup> Q. L. Xia, J. H. Yi, J. W. Huang, T. M. Ye, Y. D. Peng and L. Y. Li, *Supercond. Sci. Technol.*, 2006, **19**, 1282.
- <sup>78</sup> J. D. Houmes and H. C. zur Loye, *J. Solid State Chem.*, 1997, **130**, 266.
- <sup>79</sup> C. -Y. Hsieh, C. -N. Lin, S. -L Chung, J. Cheng and D. K. Agrawal, *J. Euro. Ceram. Soc.*, 2007, **27**, 343.
- <sup>80</sup> A. J. Anderson, R. G. Blair, S. M. Hick and R. B. Kaner, *J. Mater. Chem.*, 2006, **16**, 1318.
- <sup>81</sup> B. H. Liu, Y. Zhang, S. X. Ouyang and H. C. Gu, *Acta Metal.Sinica.*, 1998, **11**, 291.
- <sup>82</sup> B. Vaidhyanathan and K. J. Rao, *Chem. Mater.*, 1997, **9**, 1196.
- <sup>83</sup> R. D. Peelamedu, M. Fleming and D. K. Agrawal, *J. Am. Ceram. Soc.*, 2002, **85**, 117.
- <sup>84</sup> A. Jain and K. Brezinsky, *J. Am. Ceram. Soc.*, 2003, **86**, 222.
- <sup>85</sup> S. Craciun and E. Craciun, *Revista Romana De Materiale.*, 2005, **XXXV**, 97.
- <sup>86</sup> M. Iwasaki, H. Takizawa, K. Uheda and T. Endo, *J. Mater. Sci. Lett.*, 2000, **19**, 2033.
- <sup>87</sup> B. Vaidhyanathan, D. K. Agrawal and R. Roy, *J. Am. Ceram. Soc.*, 2004, **87**, 834.

- 
- <sup>88</sup> T. Kimura, H. Takizawa, K. Uheda, T. Endo and M. Shimada, *J Mater. Synthesis and Processing*, 2001, **9**, 57.
- <sup>89</sup> S. Kumar, M. Panneerselvam, P. Vinatier and K. J. Rao, *Ferroelectrics*, 2004, **306**, 165.
- <sup>90</sup> M. Kato, K. Sakakibara and Y. Koike, *Jpn. J. Appl. Phys.*, 1997, **36**, 1291.
- <sup>91</sup> K. Naitoh, T. Takizawa and T. Matsuse, *Jpn. J. Appl. Phys.*, 1999, **38**, 724.
- <sup>92</sup> A. S. Vanetsev, V. K. Ivanov and Yu. D. Tret'yakov, *Doklady Chem.*, 2002, **387**, 332.
- <sup>93</sup> D. Grossin, S. Marinel and J. –G. Noudem, *Ceram. Int.*, 2006, **32**, 911.
- <sup>94</sup> O. P. Thakur, C. Prakash and D. K. Agrawal, *Mater. Lett.*, 2002, **56**, 970.
- <sup>95</sup> A. Harrison, R. Ibberson, G. Robb, G. Whittaker, C. Wilson and D. Youngson, *Faraday Discuss.*, 2002, **122**, 363.
- <sup>96</sup> B. Vaidhyanathan, A. P. Singh, D. K. Agrawal, T. R. ShROUT, R. Roy and S. Ganguly, *J. Am. Ceram. Soc.*, 2001, **84**, 1197.
- <sup>97</sup> M. Iwasaki, H. Takizawa, K. Uheda, T. Endo and M. Shimada, *J. Mater. Chem.*, 1998, **8**, 2765.
- <sup>98</sup> M. P. Selvam and K. Rao, *J. Adv. Mater.*, 2000, **12**, 1621.
- <sup>99</sup> M. H. Bhat, A. Miura, P. Vinatier, A. Levasseur and K. J. Rao, *Solid State Comm.*, 2003, **125**, 557.
- <sup>100</sup> J. Guo, C. Dong, L. Yang, G. Fu and H. Chen, *Mater. Res. Bull.*, 2006, **41**, 655.

## 2: EXPERIMENTAL THEORY AND METHODS

### 2.1 MICROWAVE RADIATION

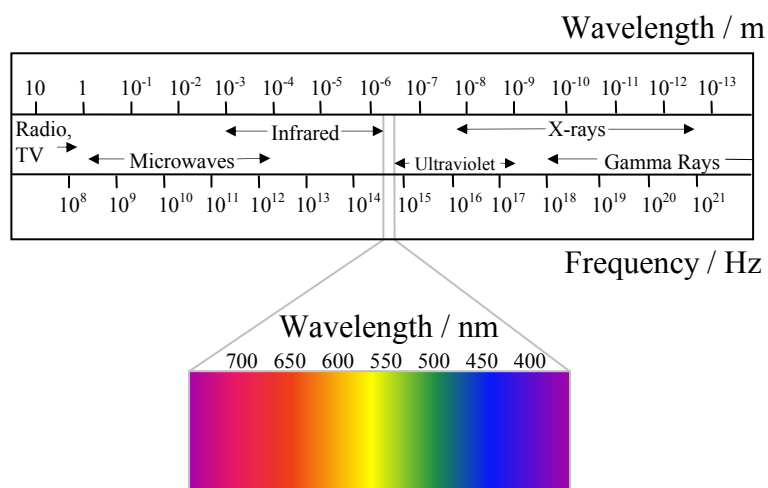


**Figure 2- 1: The electromagnetic spectrum.<sup>1</sup>**

Microwaves are high frequency (0.3 to 300 GHz) electromagnetic waves which are situated between infrared and radio wavelengths in the electromagnetic spectrum (Figure 2- 1).<sup>1</sup> Electromagnetic waves comprise an electric,  $\epsilon$ , and magnetic,  $H$ , portion which propagate perpendicular to each other (Figure 2- 2). Within the microwave region three specific frequencies have been allotted for microwave heating: 433 MHz and ca. 900 MHz (exact value depends on location) and 2.45 GHz, with the last frequency being used predominantly in materials synthesis (all domestic microwave ovens (DMOs) are manufactured at this frequency).<sup>2</sup> These have been chosen by international agreement with the principal aim of minimising interference with communication services.<sup>2</sup>

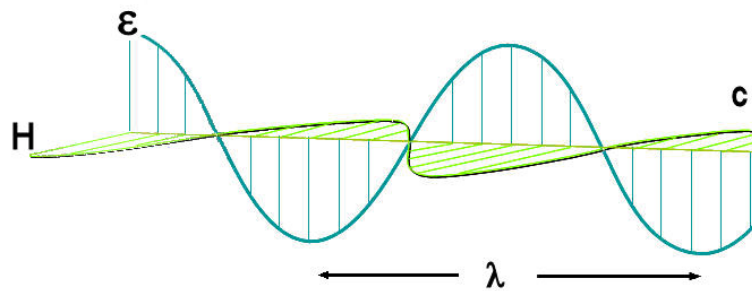


**Figure 2- 2: Electromagnetic wave components ( $\lambda$  is the wavelength and  $c$  is the velocity).<sup>3</sup>**

### **2.1.1 Microwave heating mechanisms**

Microwave radiation heats materials volumetrically. Unlike conventional heating, which relies on conduction and convection, all responsive phases are heated simultaneously with the energy transferred through the material electromagnetically, interacting with polar, ionic or electronic features within the material. This results in numerous advantages:

- Reductions in heating times and energy costs.<sup>2</sup>
- Increased control due to no warm up/cool down of the cavity required.
- Reduced environmental impact.<sup>4</sup>
- Possible improved quality of products and process specific advantages such as improved chemical syntheses and lower reaction temperatures.<sup>5</sup>

The effect of an electric field on a material is dictated by the response of charged particles to the applied field. This applied field results in the

displacement of the charged particles and the generation of induced dipoles (due to distortion of the electron cloud), however naturally occurring dipoles can also be affected. The charged particles begin to migrate or rotate in response to the field inducing further polarisation of neighbouring particles. Due to the rapidly changing direction of the electric field heating occurs because the particles cannot respond instantly to the direction change. Therefore friction is created which manifests as heat.<sup>4</sup> More specifically microwave heating can be divided into three major mechanisms:<sup>2,6</sup>

- Conduction:<sup>2,6</sup>

This mechanism applies specifically to electrical conductors. The externally applied electric field enables the movement of free charge carriers, such as electrons, through the material (Figure 2- 3). However electrical resistance causes non-instantaneous movement of these charge carriers with the change in electric field direction which results in heating.

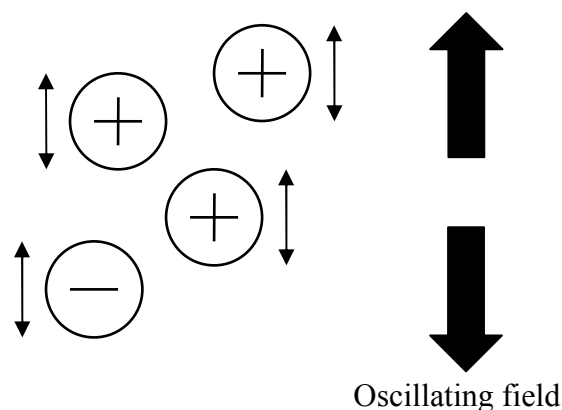


**Figure 2- 3: Representation of the conduction mechanism showing the movement of the electron cloud with the electric field.**

Some samples, such as metals, have a high conductivity resulting in the majority of microwave energy not penetrating the surface and being reflected. This leads to arcing due to huge surface voltages and the breakdown voltage of air exceeded. A finite current exists beneath the surface in diminishing layers running parallel to the surface in alternating directions and this is known as the skin depth.<sup>2</sup>

- Polarisation:<sup>2,6</sup>

The polarisation mechanism covers systems with both temporary and permanent dipoles. Electronic polarisation describes the induced dipoles at an atomic level. The electron cloud is displaced by the electric field inducing a temporary dipole in the atom. Atomic polarisation describes the effect on molecules where the electric field causes the electron cloud to migrate towards the more electrophilic atom and thus inducing a dipole.

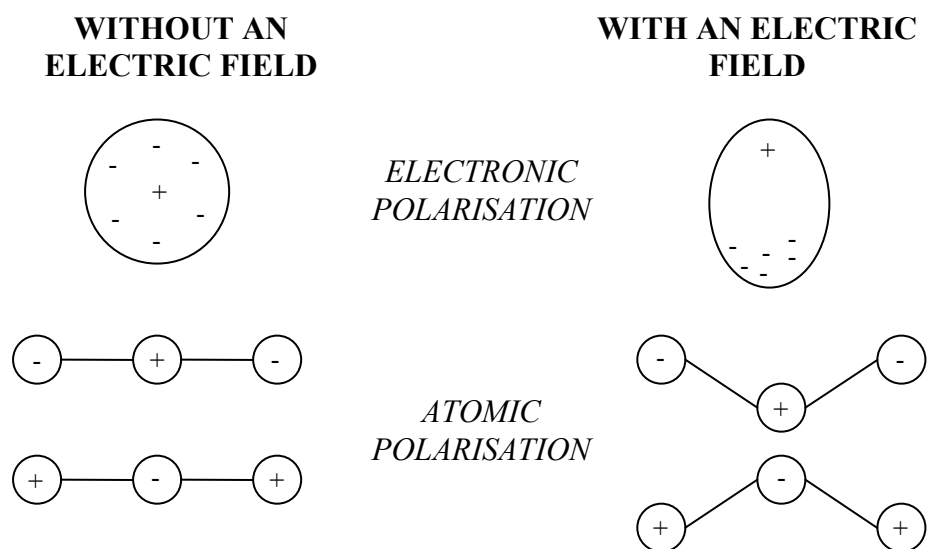


**Figure 2- 4: Representation showing electronic and atomic polarisation.**

Finally dipolar polarisation exists, which describes systems with permanent dipoles, e.g. H<sub>2</sub>O. In this case intermolecular forces stop the molecules instantaneously following the field direction and so heat is produced (Figure 2- 5). Each liquid absorbs best at specific frequencies (relating to the response times of the dipoles) with heating efficiency changing remarkably if this frequency is not used. It is not always desirable, however, to use the microwave frequency that provides maximum absorbance as only surface heating is observed while the sample centre stays relatively cold. This is due to only a finite amount of microwave energy being available which is absorbed completely at the surface, when energy absorption is most efficient due to the dipole response time, leading to penetration depth concerns (section 2.1.2).<sup>6</sup>

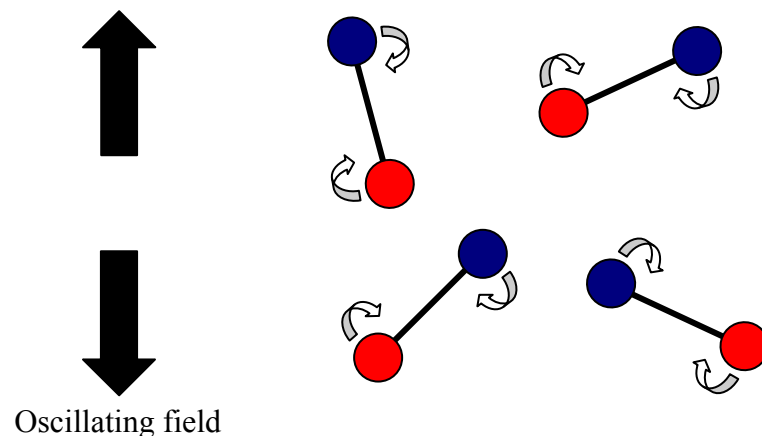


**Figure 2- 5: Simplified representation of dipolar polarisation and the effect of an electric field on polar molecules.**

- Interfacial polarisation:<sup>2, 6</sup>

Interfacial polarisation, although technically a polarisation mechanism, warrants a separate section due to its importance. Unlike the other polarisation

mechanisms it describes the effects of an electric field on a system containing both conducting and non-conducting components. Charge carriers within the system are capable of migrating short distances, however, due to the heterogeneous nature of the system, they can sometimes become trapped and incapable of discharge. At this point charge distortion is observed (Figure 2- 6) resulting in a current induced across the particle leading to a potential difference between the different phases. This mechanism is very complex and it is often easier to consider it as a combination of the conduction and dipolar polarisation mechanisms. For example, when metal particles are dispersed in another medium, the conduction mechanism is no longer accurate as a “drag” effect on the polarisation of particles is observed. This results in the polarisation of particles to lag behind the electric field as observed in dipolar polarisation.

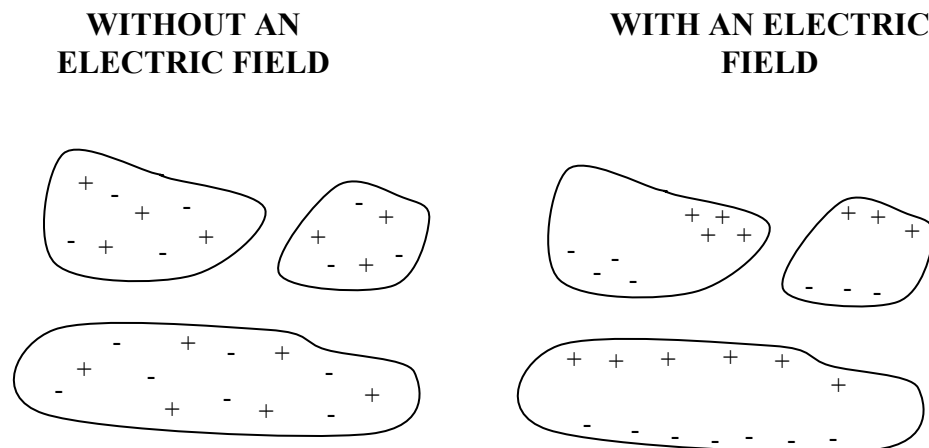


**Figure 2- 6: Representation showing interfacial polarisation.**

The interaction of materials with microwaves can be divided into three categories (Figure 2- 7), which in turn relate to the heating mechanisms

described in this section: transparent (low dielectric loss materials with little or no interaction with microwave fields e.g. quartz), absorbing (high dielectric loss materials which are required to drive reactions e.g. amorphous carbon) and reflective (where the majority of microwave energy is reflected off the surface<sup>7</sup> and for this reason these materials are used for cavity walls within microwave furnaces e.g. aluminium).

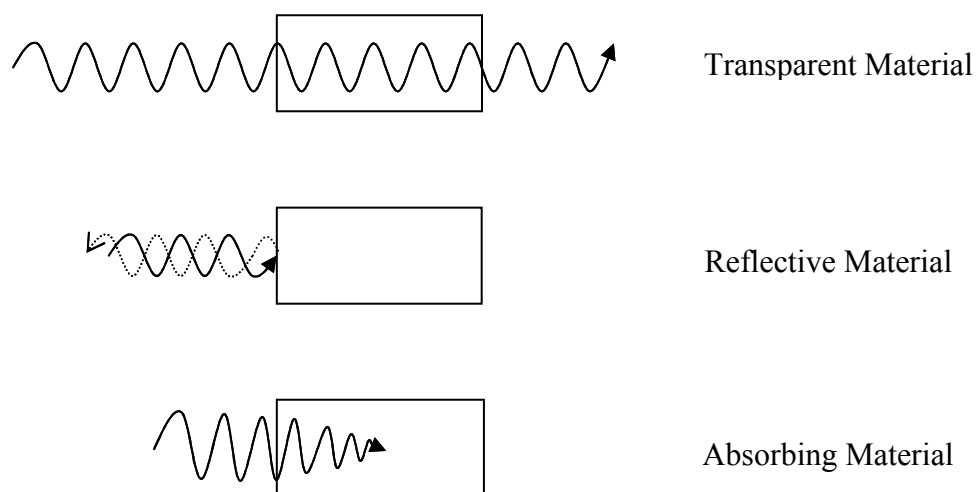


**Figure 2- 7: The interaction of materials with microwave energy.**

During a chemical reaction it is common to use materials from all three categories, however at least one of the materials must absorb microwave energy in order for the reaction to proceed. A list of materials which couple strongly can be found in other articles.<sup>8,9</sup> The dielectric properties of a material control this interaction and pertain to the efficiency of the microwave heating.

## 2.1.2 Dielectric properties

The ability of a material to heat in an applied microwave field directly relates to its dielectric properties which in turn directly relates to conductivity in solids. This interaction is known as dielectric heating and results in thermal energy to ultimately drive the reaction.<sup>10</sup> The dielectric properties of a given medium are quoted as the complex dielectric permittivity,  $\epsilon^*$ , which consists of two parts:<sup>3</sup>

$$\epsilon^* = \epsilon' + i\epsilon'' \quad \text{Equation 2- 1}$$

$\epsilon'$  is the relative permittivity, which is the measure of the ability of a molecule to be polarised by an electric field;  $\epsilon''$  is the dielectric loss, which indicates the ability of the medium to convert the stored energy to heat.

The dielectric loss also relates directly to the electrical conductivity of the material,  $\sigma$ :<sup>2</sup>

$$\epsilon'' = \frac{\sigma}{\epsilon_0 f} \quad \text{Equation 2- 2}$$

Where  $\epsilon_0$  the permittivity of free space and  $f$  is the frequency.

In the case of solids this thermal energy results from the electrical resistance within the material to the movement of charge carriers with the electric field. A more useful value to quote is the loss tangent,  $\tan\delta$ , which defines the ability of a material to absorb microwave energy and dissipate it as heat at a given temperature and frequency:<sup>3</sup>

$$\tan\delta = \frac{\epsilon''}{\epsilon'} \quad \text{Equation 2- 3}$$

Even though the frequency is usually fixed the loss tangent is important as temperature has been shown to vastly affect the dielectric properties of a material.<sup>11,12</sup> As the temperature increases the relaxation time for the dipoles decreases. This allows them to more easily follow the electric field resulting in further heating.<sup>13, 14</sup> As a material absorbs microwave energy the temperature will increase.<sup>2</sup> For a dielectric heating process, assuming uniform heating, the following equation applies:<sup>15</sup>

$$\frac{dT}{dt} = \frac{K \cdot \epsilon'' \cdot f \cdot E^2}{\rho \cdot C} \quad \text{Equation 2- 4}$$

where  $(dT/dt)$  is the rate of change of temperature of the material,  $K$  is a constant,  $\rho$  is the density of the material ( $\text{kg/m}^3$ ) and  $C$  is the specific heat capacity of the material ( $\text{J/kg}^\circ\text{C}$ ).

It is imperative to also take into account the energy loss, and thus decrease in temperature due to radiation from the surface.<sup>15</sup>

$$\frac{dT}{dt} = \frac{-e \cdot \alpha \cdot A_s}{\rho \cdot C \cdot V_s} \cdot T^4 \quad \text{Equation 2- 5}$$

where  $e$  is the sample emissivity ratio,  $\alpha$  is the Stefan-Boltzmann constant,  $A_s$  is the surface area of the sample ( $\text{m}^2$ ) and  $V_s$  is the volume of the sample ( $\text{m}^3$ ).

The conversion of microwave energy into heat depends on both the dielectric and thermal properties of the material. It is clear that one directly

affects the other, however, accurately determining temperature rise is difficult due to the non-uniformity often observed with the microwave field and changes in dielectric properties of a material with temperature. This latter observation is important, particularly in the case of solids, which do not absorb microwave energy at room temperature, but can often absorb at higher temperatures. In these cases often a susceptor material, such as graphite which is a good absorber at room temperature, is used to raise the reaction temperature to a point where the dielectric properties are more favourable for the reactant.<sup>16</sup> An example of this is in the MW heating of alumina which becomes 3000 % more efficient when the temperature is raised from 200 °C to 1200 °C.<sup>17</sup> However this increase in heating efficiency can cause problems like thermal runaway (where an increase in temperature results in a change in reaction rate which leads to a further increase in temperature) and without careful monitoring the temperature can increase exponentially.<sup>18</sup>

As well as frequency and temperature, density plays an important factor in the dielectric properties of a material.<sup>19</sup> The powder is believed to act like a two phase system with air and as the packing density increases so do the dielectric properties. This has been quantified by looking at a simple two component system, although expansion for additional components is possible, for both the volume fractions and density/mass fractions.<sup>20, 21</sup>

$$\varepsilon' = \left[ v_1 (\varepsilon_1')^{\frac{1}{3}} + v_2 (\varepsilon_2')^{\frac{1}{3}} \right]^3 \quad \text{Equation 2- 6}$$

$$\varepsilon' = \left[ \frac{\rho}{\rho_1} m_1 (\varepsilon_1')^{\frac{1}{3}} + \frac{\rho}{\rho_2} m_2 (\varepsilon_2')^{\frac{1}{3}} \right]^3 \quad \text{Equation 2- 7}$$

$$\varepsilon'' = \left[ v_1 \sqrt{(\varepsilon_1'' + e)} + v_2 \sqrt{(\varepsilon_2'' + e)} \right]^2 \quad \text{Equation 2- 8}$$

$$\varepsilon'' = \left[ \frac{\rho}{\rho_1} m_1 \sqrt{(\varepsilon_1'' + e)} + \frac{\rho}{\rho_2} m_2 \sqrt{(\varepsilon_2'' + e)} \right]^2 \quad \text{Equation 2- 9}$$

Where  $v_1$  and  $v_2$  are the volume fractions of components 1 and 2 respectively;  $\varepsilon_1$  and  $\varepsilon_2$  are the dielectric constants of components 1 and 2;  $\rho$ ,  $\rho_1$  and  $\rho_2$  are the densities of the bulk sample and components 1 and 2 ( $\text{kg/m}^3$ );  $m_1$  and  $m_2$  are the mass fractions of components 1 and 2;  $e$  is a small constant ( $\sim 0.001$ , but material dependent);  $\varepsilon_1''$  and  $\varepsilon_2''$  are the loss factors for components 1 and 2.

Equation 2- 6 indicates the relationship between the dielectric constants and volume fractions for the two components which can also be expressed in terms of the mass fractions and densities (Equation 2- 7). Likewise Equation 2- 8 and Equation 2- 9 show the same relationship, but for the dielectric loss of the components. In both cases when the cubed root of the dielectric constant/loss is plotted against sample density, a linear relationship is observed.<sup>21</sup> This directly shows the effect of density on dielectric properties and should be taken into account when heating materials, particularly powders.

The dielectric properties also determine the amount of power absorbed,  $P$  ( $\text{W}/\text{m}^3$ ), by the sample:

$$P = \sigma |E|^2 = 2\pi f \epsilon_0 \epsilon'' |E|^2 = 2\pi f \epsilon_0 \epsilon' \tan \delta |E|^2 \quad \text{Equation 2- 10}$$

$\sigma$  is the total effective conductivity ( $\text{S}/\text{m}$ );  $E$  is the magnitude of the internal electric field ( $\text{V}/\text{m}$ );  $T$  is the temperature;  $t$  is the time.

Ultimately microwave heating is a result of this as the majority of the power absorbed is converted into heat:<sup>7</sup>

$$\frac{\Delta T}{\Delta t} = \frac{2\pi f \epsilon_0 \epsilon'' |E|^2}{\rho C_p} \quad \text{Equation 2- 11}$$

$\rho$  is the density;  $C_p$  is the heat capacity.

As the microwave progresses into a material, its amplitude diminishes as its power is absorbed. Disregarding internally reflected waves, the field intensity and power density falls exponentially further from the materials surface.<sup>2</sup> For this reason an absorbance loss factor needs to be considered as energy is absorbed by the medium. This is represented by the penetration depth,  $D_p$ , for a substance. Penetration depth is defined as the depth into the material at which the power flux has fallen to  $\frac{1}{e}$  ( $\approx 0.368$ ) of its value at the surface:<sup>2</sup>

$$D_p = \frac{\lambda_0 \sqrt{\epsilon'}}{2\pi \epsilon''} \quad \text{Equation 2- 12}$$

$\lambda_0$  is the wavelength of the microwave radiation ( $\text{m}$ ).

It is clear that the dielectric properties of a material play an important role in penetration depth and consequently should always be taken into account when designing an experiment. Materials with large dielectric properties will tend towards surface heating, while smaller dielectric properties lead to more volumetric heating.

### **2.1.3 Microwave applicators**

Three principal classes of microwave applicators exist; travelling wave applicators, single mode cavities and multimode cavities. A number of variables determine the choice of applicator, such as sample size, shape and volume, all of which play an important role in the microwave heating process. Multimode cavities are by far the most common of the three, the only cavity to be used as a domestic appliance. This is mostly due to the fact that they are inexpensive, flexible in their design and readily available. Alternatively single mode cavities offer a number of key advantages, such as higher field strength, over their multimode counterparts. The increasing use of microwave heating in both industry and laboratories has also called for more precise and controllable equipment. Although many choose to design and build bespoke equipment for specific tasks, there are many which are available from commercial companies such as IMS Ltd, CEM Corporation and Cober Electronics Inc which have varying powers and cavity designs. Travelling wave applicators, the final applicator, are mainly used for continuous flow systems which are not applicable to the work discussed in this thesis, therefore they will only be discussed briefly.

### 2.1.3.1 Multimode cavities

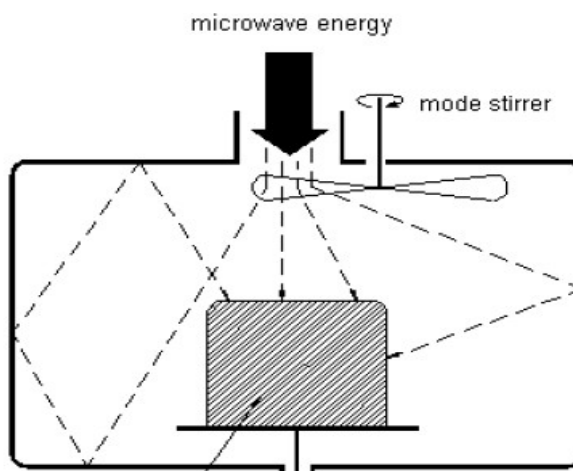


**Figure 2- 8: Illustration of a multimode cavity with a sample present.**

The mechanical design of multimode furnaces is fairly simple, relying on a rectangular cavity with a magnetron connected. However the electromagnetic analysis of these furnaces is very complex. In principle, the cavity supports multiple standing waves (a wave which has no change in amplitude at a given point along itself) resulting in a certain electric field or mode pattern. However, the load and electrical properties of the sample being heated have a huge effect on the distribution of the established field pattern and therefore the performance of the system. Small loads or loads with low dielectric loss result in negligible absorption of the microwave energy by the sample (observed in work discussed in chapter 1, section 1.4) which leads to numerous reflected modes, due to lack of absorption of the microwave energy, within the cavity (the mode is the field pattern that exists within the applicator). Interaction of these modes can then lead to excitation close to their cut-off frequency which results in huge variations in performance.<sup>2</sup> Location of the

load is also very important and misplacing it can also result in a similar loss of performance. In contrast for larger samples or materials with a good dielectric loss these furnaces are ideal as the majority of microwave energy is absorbed leading to more uniform heating compared to single mode furnaces. In a single mode furnace only one mode is observed providing maximum energy in only one position, whereas with multiple modes a number of positions within the cavity allow for efficient heating.

Two different types of multimode cavity were used for the work discussed in this thesis: A DeLonghi M8021P-B1 (analogue control) and a Matsui TS-206SF (digital control). Both were programmable up to 800 W and ran at a frequency of 2.45 GHz with a maximum continuous heat time of 35 minutes and many hours respectively. The Matsui microwave also had a digital timer whereas the DeLonghi was a dial. All experiments in the domestic microwave ovens were run at the maximum power of 800 W due to the nature of the power supplies. Below maximum power the microwaves become pulsed to simulate a “lower power” and so in practice just result in lower reaction times with respect to carbide synthesis. If genuine variable power experiments were to be attempted, a domestic microwave with a fully rectified power supply would have to be purchased.

### ***2.1.3.2 Single mode cavities***

Compared to multimode cavities, single mode cavities are more complex due to the requirement to tune the microwave radiation. Nonetheless a

single mode cavity provides many advantages over a multi mode furnace. In a single mode cavity a single standing wave is formed within the waveguide by superimposing the forward and reflected waves using a short circuit tuner. The tuner is then finely adjusted so that its centre is at the peak of the wave and so at the point of maximum electric field strength. This technique has been used to great effect in the processing of ores and other solid materials.<sup>22</sup> Knowing that the power density is proportional to the square of the electrical field strength within the material (section 2.1.2, Equation 2- 10), it has been demonstrated that increasing microwave power dramatically reduces the heating time required to break apart coal particles.<sup>23</sup> This same principle can be applied to synthesis in numerous solid state systems leading to very short reaction times in a single mode cavity due to increased power density.

Single mode cavity experiments constitute the bulk of work reported in this thesis due to the process control gained, the accurate positioning of the sample in the electric field and the range of heating rates. Three different cavities were used, all with a microwave frequency of 2.45 GHz:

- Sairem 3 -15 kW GMP 150SM microwave generator, connected through WR430 waveguide to an automatic E-h tuner for impedance matching purposes. The tuner was connected to an 82mm internal diameter  $TE_{10n}$  single mode cavity (Figure 2- 9). The waveguide was terminated by a short circuit tuner. The majority of experiments were carried out in this applicator.

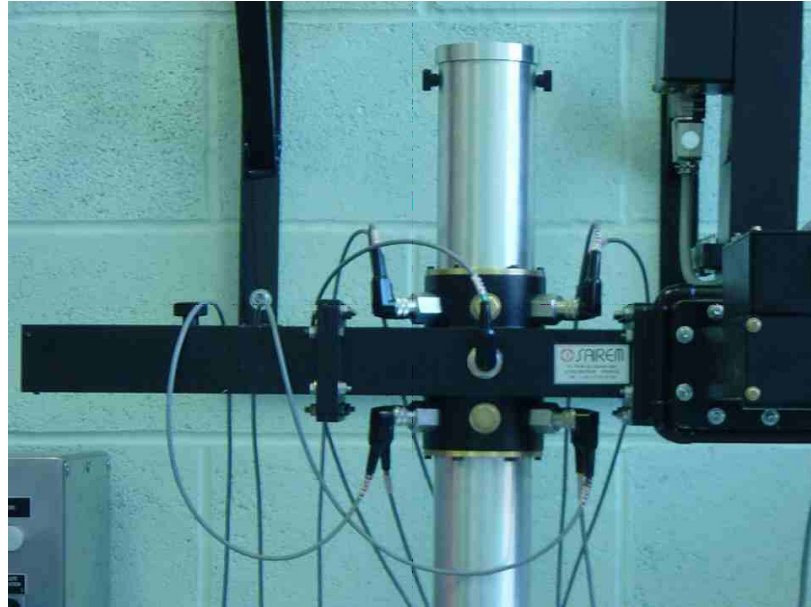


**Figure 2- 9: Picture of the single mode cavity in the 3 – 15 kW applicator.**

- 0 - 1 kW microwave applicator produced by Industrial Microwave Systems Ltd, using WR430 waveguide and a 3 stub tuner to allow matching of the impedance of the transmission line to that of the load.

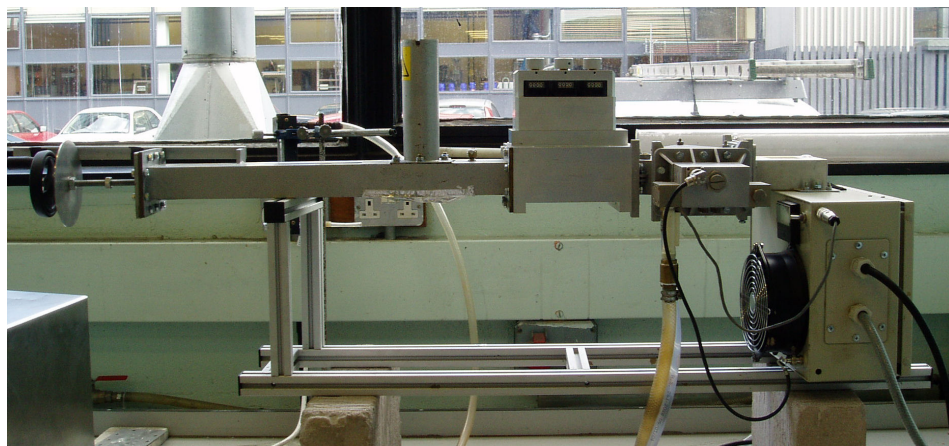


**Figure 2- 10: Picture of 1 kW single mode applicator.**

- Magnetronics 0 - 1.5 kW microwave generator attached to the single mode cavity using WR430 waveguide. A 3 stub tuner is also present, similar to the 1 kW microwave applicator.

### ***2.1.3.3 Travelling wave applicators<sup>24</sup>***

In this type of applicator microwave energy is fed directly into the chamber with the majority being absorbed by any sample present. Any residual power is absorbed by a dummy load, usually water. The setup is only suitable for high loss materials so the majority of the power is not absorbed by the dummy load resulting in inefficient heating. The design of travelling wave applicators is ideal for continuous flow systems, usually with a conveyor belt, allowing for large volumes of sample to be treated.

## **2.2 SYNTHESIS AND PROCESSING**

Effective and reproducible synthesis of the transition metal carbides constituted the majority of this thesis. Although in principle the carbides, particularly binary systems, are simple to synthesise, honing the experimental setup proved to be a challenge. Partly this was due to the lack of current knowledge about microwave heating in the solid state as well as the need to build on the understanding of the heating mechanism and reaction profile in order to further improve the synthesis.

<b>Attempted Reactions</b>	
<i>Metal reactants</i>	<i>Metal oxide reactants</i>
$W + C \rightarrow WC$	$2WO_3 + 5C \rightarrow 2WC + 3CO_2$
$2W + C \rightarrow W_2C$	$2MoO_3 + 7C \rightarrow Mo_2C + 6CO$
$W + xC \rightarrow WC + xC$	$2Ta_2O_5 + 9C \rightarrow 4TaC + 5CO_2$
$2Mo + C \rightarrow Mo_2C$	$2Nb_2O_5 + 9C \rightarrow 4NbC + 5CO_2$
$Ta + C \rightarrow TaC$	
$Nb + C \rightarrow NbC$	
$1-xNb + xTa + C \rightarrow Nb_{1-x}Ta_xC$	

**Table 2- 1: Table of all attempted transition metal carbide reactions**

The synthesis of a number of carbides was attempted from both the elemental metal powders and the appropriate oxides (Table 2- 1). In all cases the carbon used to form the carbide was graphite. This was chosen due to its excellent heating profile in a microwave field and its lack of severe thermal runaway which is observed with amorphous carbon. In all cases the required stoichiometric amount of starting materials (Table 2- 2) to afford the desired products was ground together with an agate pestle and mortar for at least 10 minutes. Using an 8 mm diameter steel die, pellets were then pressed using a hand press. Pellets were kept under pressure for 10 minutes before being removed. Pellets, unless specified, were 2 g for the metal powder plus graphite, and 1 g for the metal oxides plus graphite. Pellets were then imbedded into 0.35 g of graphite powder (to act as a reaction susceptor) within a 10 mm diameter open top quartz tube (microwave transparent), with the top face of the

pellet visible. In some circumstances, particularly when longer heating times were used, the quartz tube was replaced with a 20 mm diameter alumina crucible. This was to stop melting of the quartz tube and often to aid observation of the pellet during the reaction. In all cases starting materials were of a high purity and underwent X-ray diffraction analysis prior to their initial use to check the purity.

Reactant	Manufacturer	Purity / %	Notes
Graphite (C)	BDH	> 99.5	<50 $\mu\text{m}$ particle size
Tungsten (W)	BDH	> 99	Small Mo impurity
Tungsten Oxide ( $\text{WO}_3$ )	BDH	> 99	
Molybdenum (Mo)	BDH	> 99	
Molybdenum Oxide ( $\text{MoO}_3$ )	Aldrich	> 99	
Tantalum (Ta)	Aldrich	> 99.5	
Tantalum Oxide ( $\text{Ta}_2\text{O}_5$ )	Aldrich	> 99	
Niobium (Nb)	Aldrich	> 99.5	
Niobium Oxide ( $\text{Nb}_2\text{O}_5$ )	Aldrich	> 99	

**Table 2- 2: Information for all reactants**

Using these reactants synthesis was attempted for a number of transition metal carbide systems: W-C, Mo-C, Ta-C, Nb-C and Ta-Nb-C. The majority of syntheses were based around binary systems, however ternary carbide synthesis was also attempted. In the case where synthesis was attempted from metal powders, reactions were designed to afford no by-products. For metal oxide experiments the mass of starting materials used was

based on the presumption that  $\text{CO}_2$  was the only resultant by-product. Synthesis was conducted in both multimode and single mode microwave applicators. Sections 2.2.1 and 2.2.2 cover the experimental configuration for the synthesis of all materials in this thesis; however, as described earlier, development of appropriate experimental configurations required much time and trial and error. For this reason these sections are a non-specific setup, covering the majority of materials synthesised. More specific details and variations will be reported in the results chapters (chapters 3, 4 and 5).

### 2.2.1 Synthesis using a Domestic Microwave Oven (DMO)

After initial preparation of the samples had been completed the quartz tube was inserted into silica flour (ground silica) in the centre of a glass beaker such that the top of the graphite was level with the silica flour (Figure 2- 11). The silica flour/beaker was used to both add stability to the tube and to help maintain the high temperatures required for synthesis around the pellet (through insulation).

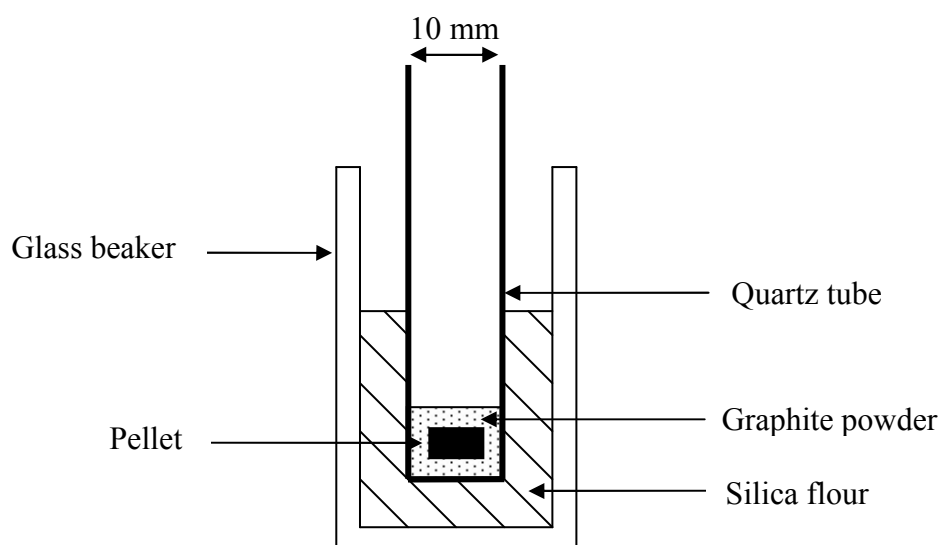


**Figure 2- 11: Diagram of the experimental setup in the DMO.**

The beaker was then placed in the cavity of the domestic microwave oven in a specific location on top of a heat proof mat (Figure 2- 12). This location remained the same to reduce the experimental variables, however, a stationary sample is not ideal given the modes within a multimode cavity change position depending on cavity load, temperature and the dielectric properties of the material being heated. Unfortunately, a turntable could not be used as the high temperature obtained during the experiment would melt the plastic components of the turntable mechanism.



**Figure 2- 12: Picture indicating the position of the beaker within the DMO.**

Heating was then carried out for a given period and typically in less than five seconds the graphite within the tube began to glow indicating that it had been positioned in the correct location within the cavity.

### **2.2.2 Synthesis using a single mode microwave cavity**

After initial preparation of the samples, as above, the quartz tube was loaded into a 72 mm quartz tube, with a fire brick base, containing silica flour (ground silica). This tube was designed to slide into the single mode cavity (78 mm diameter) and thus improves the stability of the experiment as well as providing a degree of protection to the applicator in case of a problem. The silica flour was a specific height to allow imbedding of the quartz tube containing the sample, while also allowing the tube to be positioned within the waveguide to ensure efficient heating. The larger quartz tube was then inserted into the single mode cavity and held in place using a Teflon rod (microwave transparent) (Figure 2- 13). Samples were then irradiated at 3 kW (in the Sairem system) for a set time, varying with each sample. The applicator was allowed to reach the desired power before timing of the reaction was initiated (around 1 second). Reflective power was also monitored on a display to account for any anomalies. For samples heated in the other single mode applicators, a power of 1 kW was used.

In all cases, the single mode applicator was tuned prior to a series of experiments. This was achieved by running a “dummy” experiment during which time the short circuit tuner was adjusted so that maximum energy was absorbed by the sample.

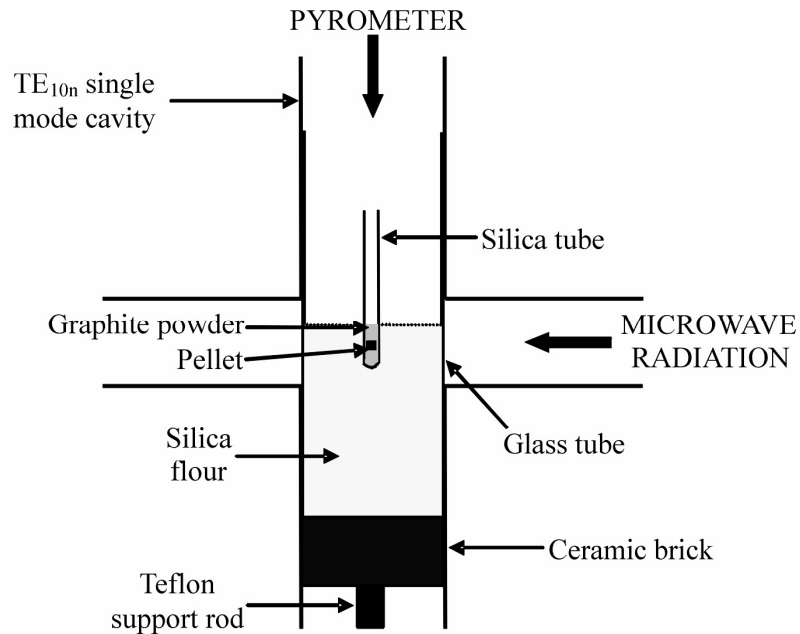


**Figure 2- 13: Diagram showing experimental setup in the single mode applicator.**

During all experiments an optical pyrometer (LAND System4 Thermometer M1 600/1600 °C;  $\pm 1$  °C accuracy with a 5 mm diameter spot centred on the sample surface) was used to monitor the surface temperature of the sample. This was supported over the top of the cavity by a lighting rig (2 stands and a crossbar manufactured by Manfrotto) and could be manually adjusted to make sure the pyrometer spot was in the correct place. For one series of experiments high speed video (Photo-Sonics Phantom V7 Colour, 4800 to 150,000 frames per second) and thermal imaging (FLIR ThermaCAM SC3000, -20 °C to 2000 °C with an accuracy of  $\pm 1$  °C) was also used to monitor the sample *in-situ*. These were provided by the EPSRC engineering loan pool.

## **2.3 CHARACTERISATION TECHNIQUES**

A variety of characterisation techniques are reported in this thesis. Techniques, such as powder X-ray diffraction, were used to help identify and analyse all samples, with techniques such as scanning electron microscopy only used on a finite number of products.

### **2.3.1 Powder X-ray Diffraction (PXD)**

PXD was by far the most common characterization method used with each sample routinely being examined after the completion of any given experiment. PXD is an extremely useful tool for solid state chemists and provides a rapid and accurate method for identifying all known crystalline phases present in the sample.<sup>25</sup> This allows the immediate identification of the desired phases and requires a relatively small amount of sample to perform the analysis. In addition, the resultant model can be refined to obtain crystallographic information and accurate phase percentages.

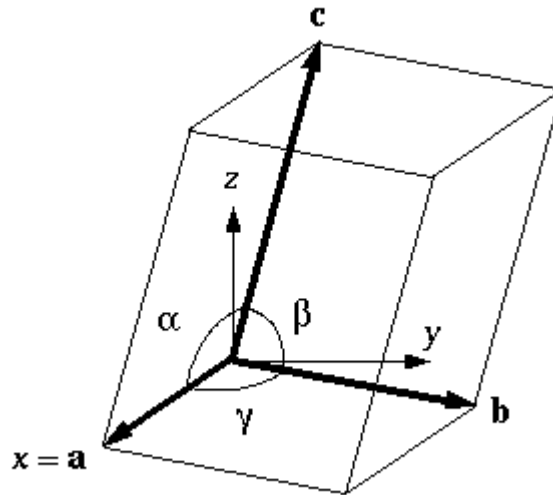


**Figure 2- 14: General unit cell parameters.**

Before we look at diffraction it is important to first understand the structure of crystals.<sup>25,26</sup> Due to only a finite number of atom positions within a crystal, 7 crystal systems exist (cubic, hexagonal, tetragonal, trigonal, orthorhombic, monoclinic and triclinic). Multiple arrangements of these crystal systems results in a total of 14 unique systems which are known as the Bravais lattices. Crystals constitute regular repeating units, the smallest of which is called the unit cell. This can be described in three dimensions, consisting of the axes a, b and c (making up the lattice parameters and so lengths of the cell) with the angles between these denoted as  $\alpha$ ,  $\beta$  and  $\gamma$  (Figure 2- 14). The unit cell can then be used to specify the exact position of an atom in any given crystal by giving it co-ordinates relating to a, b and c. The positions are referenced from a point, known as a lattice point, within the unit cell which is often located at a, b, c co-ordinates 0, 0, 0. Ultimately any point within the crystal can be defined in terms of these co-ordinates, however conventionally this is usually described in terms of the reciprocal of a, b and c, which are

referred to as Miller indices. These have the notation  $h$ ,  $k$  and  $l$  (where  $h = 1/a$ ,  $k = 1/b$  and  $l = 1/c$ ) and are used, for example, to indicate planes within a crystal.

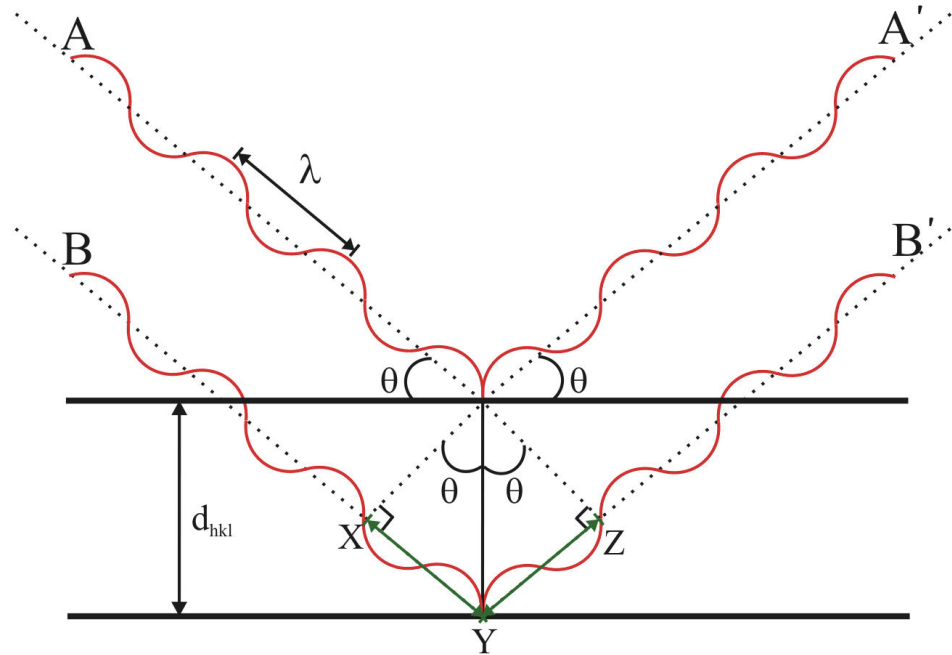


**Figure 2- 15: Schematic representing diffraction of X-rays on planes within a crystal.**

With the knowledge of crystal structures Bragg was able to derive a relationship between diffraction angle and atomic spacing.<sup>26</sup> Diffraction occurs when the inter-atomic distances ( $\sim 2\text{-}3 \text{ \AA}$ ) within the sample being investigated are comparable to the wavelength of the incident radiation ( $\sim 1 \text{ \AA}$  for X-rays). For this reason copper ( $\text{Cu K}_\alpha \lambda = 1.5418 \text{ \AA}$ ) or molybdenum ( $\text{Mo K}_\alpha \lambda = 0.7107 \text{ \AA}$ ) targets are used to generate the required X-rays. The diffraction of X-rays by crystal layers (Figure 2- 15) is analogous to that observed when light passes through an optical grating and results in either constructive or

destructive interference leading to regions of light and dark. In order for constructive interference to occur, the X-ray beams must be in phase and a diffraction maximum, which is formed following this interference, is termed a reflection. In Figure 2- 15 this is only possible if the two parallel incident X-ray beams, A and B, are in phase. Beam B must travel the extra distance XYZ compared to A and so for A' and B' to still be in phase the distance XYZ must be an integer number of wavelengths,  $n\lambda$  (*where n is an integer and  $\lambda$  is the wavelength of radiation*). It can be seen from Figure 2- 15 how the distance XYZ is related to the interplanar spacing  $d_{hkl}$  and the angle of incident radiation  $\theta$  by the equation:

$$\mathbf{XYZ = 2d\sin \theta} \qquad \text{Equation 2- 13}$$

*Where  $d$  = plane separation in  $\text{\AA}$ ,  $\theta$  = Bragg angle and XYZ is the path difference.*

Bragg's law can then be obtained by combining Equation 2- 13 with the knowledge that XYZ must be an integer number of wavelengths for constructive interference to occur:

$$\mathbf{n\lambda = 2d\sin \theta} \qquad \text{Equation 2- 14}$$

The result of Bragg's law is that reflections are only observed at specific angles. This angle depends upon unit cell type and size as well as the inter-atomic plane spacing,  $d$ . Diffraction intensity is also dependent upon atomic number; the X-rays interacting directly with the electron cloud around

the nucleus leading to a relationship between diffraction strength and atomic number: the heavier the atom the greater the intensity. Ultimately these factors lead to compounds having unique diffraction patterns; however it is important that crystallites are randomly orientated during PXD ensuring that all possible lattice planes are present in every direction. If this is not the case preferred orientation is observed resulting in certain peaks being more or less intense than they should be.

### ***2.3.1.1 Powder X-ray diffraction sample preparation, data collection and analysis***

Samples were prepared by grinding them thoroughly in an agate pestle and mortar to ensure random orientation of crystallites. They were then packed into a circular depression on a sample slide and pressed level with a glass slide (Figure 2- 16). This is imperative due to displacement errors if the sample sits above the surface of the slide.

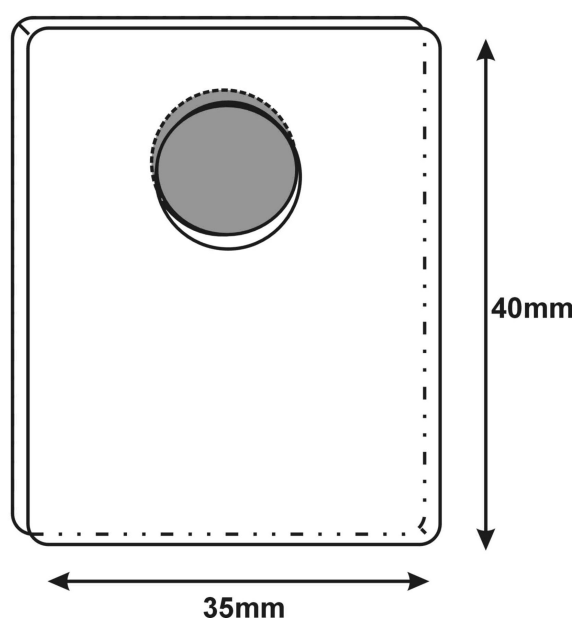


**Figure 2- 16: Diagram showing PXD slide.**

The sample is then irradiated, in the Bragg-Brenato geometry (for flat samples), from a stationary source and a moving detector measures the intensity of the diffracted X-rays (Figure 2- 17). All measurements were collected using a Philips X-pert machine with a PW3710 diffractometer control unit. The radiation used was Cu K $\alpha$  ( $\lambda = 1.5418 \text{ \AA}$ ). A Ni monochromator was used to eliminate Cu K $\beta$  radiation. The standard operating power for the X-ray tube was 40 kV and 40 mA. The X-ray beam was collimated using a 10 mm beam mask, 1 $^\circ$  entrance slit, 0.2 $^\circ$  divergence slit and a 1 $^\circ$  scatter slit on a standard run, in order to prevent both horizontal and vertical divergence of the X-ray beam. Two types of scan were run: a standard 20 minute phase identification scan or a 12 hour overnight scan for more detailed structural refinement. The standard scan was run between 10 and 80  $2\theta$ , step size of 0.2 $^\circ$   $2\theta$  whereas the overnight scan was run between 10 and 120  $2\theta$ , step size of 0.02 $^\circ$   $2\theta$ .

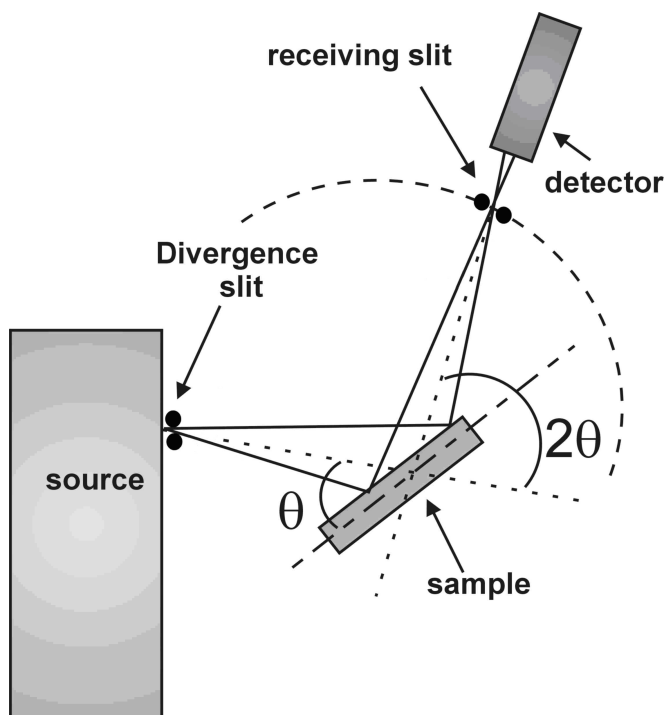


**Figure 2- 17: Setup of the Powder X-ray diffractometer.**

After the scan is complete all patterns are exported and converted to .raw files where they are then displayed as plots of intensity against  $2\theta$  in PowderCell 2.3 software.<sup>27</sup> Known structures are then downloaded from the Inorganic Crystal Structure Database (ICSD)<sup>28</sup> and compared directly to the diffraction patterns resulting in the identification of any phases present. The crystal system and unit cell dimensions were found by indexing using Dicvol91.<sup>29, 30</sup> Structural refinement using the Rietveld method was also undertaken on the majority of scans, specifically those from overnight runs, using the General Structure Analysis System (GSAS) software.<sup>31</sup> This is discussed in section 2.3.3.

### 2.3.2 Powder Neutron Diffraction (PND)

Powder neutron diffraction, like PXD, can be used to identify phases present within a given sample, but its principal use is in the determination of crystal structure. The wavelength of a neutron relates directly to its mass and velocity, as shown by the de Broglie equation:

$$\lambda = \frac{h}{p} = \frac{h}{mv} \quad \text{Equation 2- 15}$$

*where  $\lambda$  = wavelength,  $h$  = Planck's constant,  $p$  = momentum,  $m$  = mass of a neutron and  $v$  = velocity of a neutron.*

Although neutrons diffract much like X-rays, intensity is not directly related to atomic number. Interaction occurs with the nuclei of the atom and not the electron cloud allowing for identification of lighter atoms, isotopes and

iso-electronic species which is not possible with PXD. The reason diffraction is possible is the resultant wavelength, one of which is 1.798 Å, due to the standard velocity for neutrons of 2200 ms<sup>-1</sup> at 273 K. This is similar to X-rays and thus the size of the inter-atomic spacing in crystals.

PND constituted only one part of the characterisation of the materials studied, however it provided some vital results. Two neutron sources were used for the experiments: reactor and spallation. The first, D1A, was situated at Institut Laue-Langevin (ILL) and the second, POLARIS, at ISIS at Rutherford Appleton Laboratory (RAL).

### 2.3.2.1 D1A at ILL

D1A is a high resolution powder diffractometer with a constant wavelength (monochromated) neutron source (Figure 2- 18). This means the scan times are fixed with multiple scans taken to increase the resolution of the diffraction pattern. The diffracted beams are detected by a bank of 25 <sup>3</sup>He counters at 5 atm.

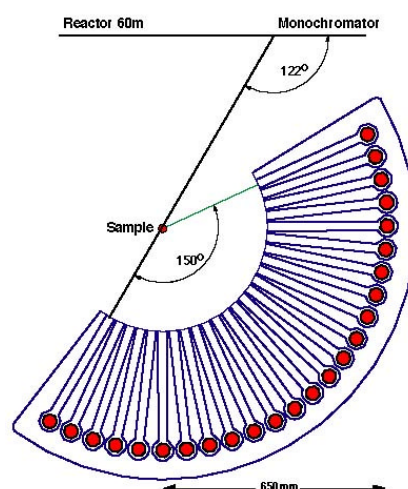


Figure 2- 18: D1A detector layout<sup>32</sup>

A reactor provides the neutrons at the ILL with a single fuel-element used to provide a thermal power of 58 MW. To achieve cooling and regulation of the temperature, heavy water and heat exchangers are utilised.

All experiments were run with the assistance of Dr Clemens Ritter at a wavelength of 1.39 Å, step size 0.1 ° between 0 and 158 ° in 2θ. Powdered samples were prepared in a clean room (2-6 g) and placed into a vanadium canister (5 mm in diameter) before being attached to the diffractometer. Vanadium canisters are used as they are practically transparent to neutrons and so do not interfere with the scan. Samples were typically run between 2 and 8 hours depending on the quantity of sample and the scattering power of the material. All resultant diffraction patterns were analysed with General Structure Analysis System (GSAS) software<sup>31</sup> as discussed in section 2.3.3.

### ***2.3.2.2 POLARIS at ISIS (RAL)***

Neutrons at ISIS are generated using a spallation source and hence POLARIS uses the time of flight method.<sup>33</sup> Hydrogen gas is ionised to H<sup>+</sup> ions within a ring and these ions accelerate around the ring resulting in the stripping of electrons to produce a high energy proton beam. This beam bombards a tantalum target and the interaction between protons and the nuclei of this heavy metal target causes neutrons to be released. These neutrons can interact with more neutrons from the target resulting in an intranuclear cascade. For each proton fired at the target approximately 15-30 neutrons are released. The acceleration of these protons within the ring occurs in pulses less than 1 μs

wide and at frequencies between 10 and 120 Hz. Therefore neutrons produced are also pulsed and so have a range of velocities and corresponding wavelengths. These wavelengths are calculated by measuring the time of flight,  $t_f$ , of a given neutron which is the known distance,  $L$ , it travels from the source to the fixed  $2\theta$  angle detector via the sample. The time of flight of the neutron is directly proportional to its wavelength:

$$t_f = \frac{\lambda L m}{h} \quad \text{Equation 2- 16}$$

POLARIS is a high intensity, medium resolution powder diffractometer. It has four detector banks: two at low angles (one ZNS detector and one  $^3\text{He}$  detector), one at  $\sim 90^\circ$   $2\theta$  (ZNS detector), and one at back scattering angles  $\sim 145^\circ$   $2\theta$  ( $^3\text{He}$  detector) (Figure 2- 19). The incident radiation wavelength ranges from 0.1 – 6 Å.

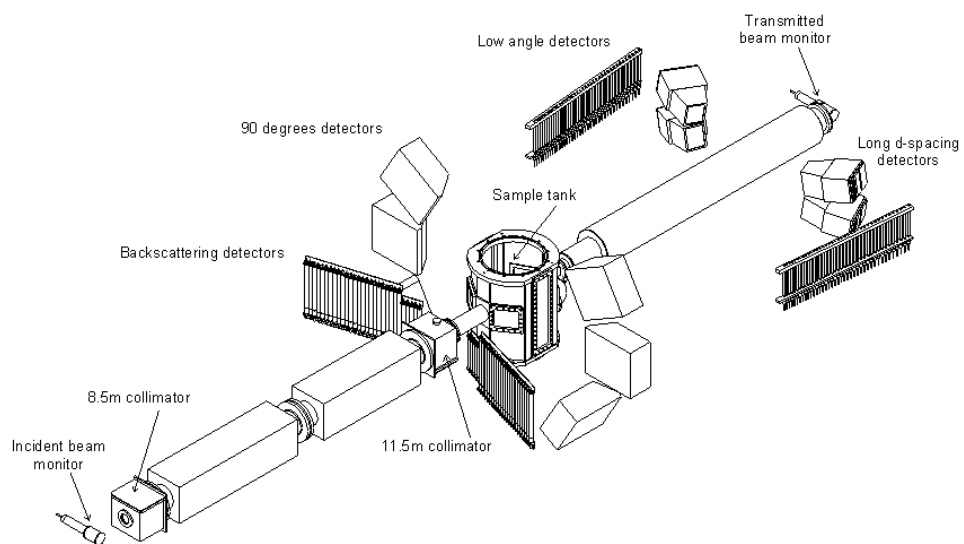


**Figure 2- 19: Schematic of POLARIS<sup>34</sup>**

Samples were prepared in a similar manner as described in section 2.3.2.1 with powdered samples, varying between 1 and 3 g, placed into vanadium canister. The canister is then attached to a sample rod (Figure 2- 20) and lowered into the sample tank of the diffractometer. With the aid of Dr Ron Smith (POLARIS beamline scientist), data were typically collected between 2 and 4 hours depending on the scattering power and quantity of sample. Since all d-spacings are collected simultaneously, the experiments were run until the error on the diffraction patterns was deemed suitably small so that all diffraction peaks were visible. All resultant diffraction patterns were analysed using the General Structure Analysis System (GSAS) software<sup>31</sup> as discussed in section 2.3.3.

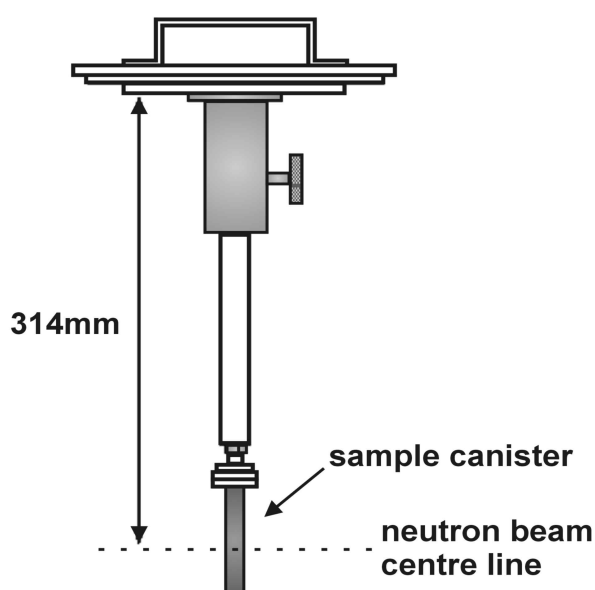


**Figure 2- 20: POLARIS sample rod and vanadium canister**

### 2.3.3 Rietveld refinement

All PND data and overnight data collected from PXD were refined using the Rietveld method through the General Structure Analysis System (GSAS) software and its graphical user interface (EXPGUI).<sup>31, 35</sup> The Rietveld method was developed in the late 1960's when Rietveld published a method for refining crystal structures using data collected from diffraction experiments.<sup>36,37</sup> Refinement is achieved by minimising the difference in intensities between the observed data and the known model over the full diffraction profile resulting in the maximum amount of crystallographic information being obtained. The method involves a least squares minimization between calculated and observed intensities at each profile point. Calculated intensities are generated from a crystallographic model, instrument parameters and a peak profile shape model.

In this work the Rietveld refinement method has been applied to both PND and PXD. PND produces near Gaussian peaks which can be modelled using a Gaussian (or related) function, however for PXD the peak shape is more complicated: The data has to be modelled using a combination of Gaussian (G) and Lorentzian (L) functions known as a pseudo-Voigt function (pV):

$$pV = \eta L + (1 - \eta)G \quad \text{Equation 2- 17}$$

where  $\eta$  is the mixing parameter.

The intensity,  $y$ , at each point,  $i$ , in the diffraction pattern is given below:

$$y_{ci} = s \sum_K L_K |F_K|^2 \phi(2\theta_i - 2\theta_K) P_K A + y_{bi} \quad \text{Equation 2- 18}$$

where  $s$  is a scale factor,  $K$  represents the Miller indices,  $L_K$  contains Lorentz, polarisation and multiplicity factors,  $\phi$  is the reflection profile function,  $P_K$  is a preferred orientation function,  $A$  is an absorption factor,  $F_K$  is the structure factor for the  $K^{\text{th}}$  Bragg peak and  $Y_{bi}$  is the background intensity at point  $i$ .

In order to obtain a “good fit” between the experimental data and the model the model is minimised iteratively until a satisfactory value is reached. This occurs when the generated pattern from the model matches the observed pattern and the residual,  $S_y$ , is minimised:

$$S_y = \sum_i w_i (y_i - y_{ci})^2 \quad \text{Equation 2- 19}$$

where  $w_i$  is the weighting factor ( $=1/y_i$ ),  $y_i$  is the observed intensity at the  $i^{\text{th}}$  step and  $y_{ci}$  is the calculated intensity at the  $i^{\text{th}}$  step.  $S_y$  is summed over all points.

Progression of the refinement is measured by the residual or R-factors. These note the quality of the refinement by providing a quantitative comparison between the observed and calculated model. Five R-factors are generated by various types of refinement software:  $R_p$  (profile),  $R_{wp}$  (weighted profile),  $R_B$  (R-Bragg),  $R_I$  (R-Intensity) and  $R_e$  (R-expected):

$$R_p = \frac{\sum |y_i - y_{ci}|}{\sum y_i} \quad \text{Equation 2- 20}$$

$$R_{wp} = \left\{ \frac{\sum w_i (y_i - y_{ci})^2}{\sum w_i (y_i)^2} \right\}^{1/2} \quad \text{Equation 2- 21}$$

$$R_B = \frac{\sum I_{Ki} - I_{Kci}}{\sum I_{Ki}} \quad \text{Equation 2- 22}$$

$$R_I = \frac{\sum |I_{Ki}^2 - I_{Kci}^2|}{\sum I_{Ki}^2} \quad \text{Equation 2- 23}$$

$$R_e = \left\{ \frac{(N - P + C)}{\sum w_i (y_i)^2} \right\}^{1/2} \quad \text{Equation 2- 24}$$

where  $I_{Ki}$  and  $I_{Kci}$  are observed and calculated Bragg intensities of reflection  $K$  given respectively,  $N$  is the number of observations,  $P$  is the number of independently refined parameters and  $C$  is the number of constraints.

Parameters are refined sequentially and concurrently. An alternative way to measure the quality of a fit is to look at the ‘Goodness of Fit’ value,  $\chi^2$  (Equation 2- 25). A perfect fit has a value of one.

$$\chi^2 = \left( \frac{R_{wp}}{R_e} \right)^2 = \left( \frac{\sum w_i (y_i - y_{ci})^2}{(N - P + C)} \right) \quad \text{Equation 2- 25}$$

### 2.3.4 Dielectric property measurements

Of the methods available for dielectric property measurement, only two are applicable: Coaxial line and cavity perturbation. This is due to their ability to take measurements in the microwave frequency range (433 MHz to 2.45 GHz).<sup>38</sup> Due to sample size and the fact that all materials were powder, the later technique was utilised.

The cavity perturbation technique allows the measurement of the dielectric properties of a sample, at a specific frequency, in solid, powdered or liquid state, at either room or elevated temperatures. The frequency however is dependent on the resonance modes of the cavity meaning measurements can only be made at specific frequencies. Despite this drawback the equipment is simple to use and very versatile, while maintaining accuracy, particularly for low loss materials.<sup>39</sup> Common design for this technique involves a circular cylindrical cavity mounted beneath a conventional furnace, but insulated so as to enable measurements to be taken at elevated temperatures without compromising the cavity (Figure 2- 21).

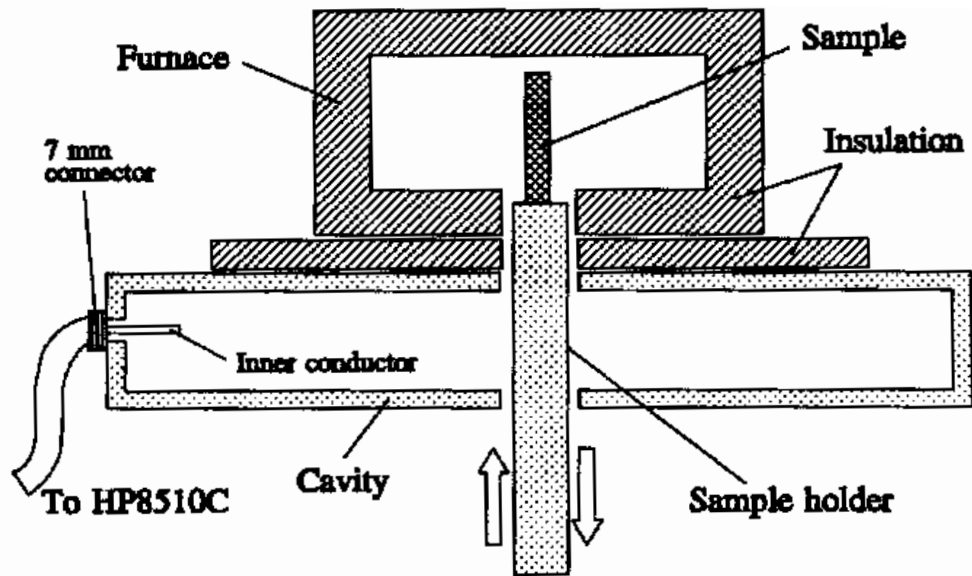


Figure 2- 21: Schematic for cylindrical cavity.<sup>40</sup>

The cavity is defined as a dielectric region surrounded by conducting walls and resonance occurs if the stored electrical energy in the cavity is equal to the stored magnetic energy. As mentioned above, this occurs at specific “resonant” frequencies depending on the dimensions of the cavity. When the cavity is at one of these frequencies, energy is dissipated in the conducting walls and this loss is quoted as a quality factor (Q): a ratio of the total energy stored to the energy dissipated in the walls per cycle. A sample inserted into the cavity will obviously alter this energy dissipation resulting in a shift in the resonant frequency of the cavity and so a change in the quality factor. These changes can be used to calculate the dielectric properties of the sample.

Dielectric measurements were performed utilising a Hewlett Packard-8753-C-300-KHz-6Hz network analyser. Results were obtained at a frequency of 2.47 GHz to enable comparison with the MW treatments, which were carried out at 2.45GHz. Due to resonance modes only being available at specific frequencies

an exact frequency of 2.45 GHz was not possible with this cavity, however, this difference of 0.8 % is well within accepted limits given the 5 % frequency variability of a typical magnetron. Samples were prepared by packing a known amount into a quartz tube (with a quartz shelf) which is then tapped down until no change in the sample height is observed. The quartz tube was then raised by an arm into the cavity and the measurements taken. In the case where elevated temperature readings were recorded the sample was held in the furnace by the arm until the desired temperature was reached. At this point, when the temperature had stabilised, the arm was used to lower the sample into the cavity so that a measurement could be taken.

## **2.3.5 Magnetism**

### ***2.3.5.1 Superconductivity***

A number of the transition metal carbides exhibit superconductivity. Although this phenomenon occurs at fairly low temperatures the superconducting temperature ( $T_c$ ) varies considerably for different phases. A superconductor is a compound that conducts electricity, without resistance, below a certain temperature. Once conduction begins, if the system is a closed loop, an electrical current will flow forever in the superconducting material.<sup>41</sup>

In 1911 superconductivity was first observed in mercury,<sup>42</sup> but it was in 1933 that Walter Meissner and Robert Ochsenfeld discovered what is now commonly known as the Meissner effect (Figure 2- 22).<sup>43</sup> A magnet is used to

induce a current in the superconductor that exactly mirrors the magnetic field from the magnet causing them to repel. Superconductors have zero electrical resistance which means the generated magnetic field can instantaneously change to compensate for the magnet. This phenomenon is known as perfect diamagnetism and is so strong that levitation of the magnet can occur. Over the many decades since this discovery many more superconductors have been synthesised and at present the highest  $T_c$  recorded is 138 K.<sup>44</sup>



**Figure 2- 22: Photograph showing levitation of a magnet above the superconductor,  $\text{YBa}_2\text{Cu}_3\text{O}_{7-x}$ .**<sup>45</sup>

The phenomenon of low temperature superconductivity is believed to be due to the existence of Cooper pairs in the sample.<sup>26</sup> These occur when one electron interacts with the cations in the metal lattice making an area of positive charge. Another electron is attracted to this region and an indirect electron-electron attraction occurs over a distance of hundreds of nanometres. This is called a Cooper pair and makes up the basis for the BCS theory of superconductivity.<sup>26</sup> The effective net attraction between the normally

repulsive electrons produces a pair binding energy on the order of milli-electron volts, enough to keep them paired at extremely low temperatures. This relatively stable pair of electrons is able to move through the lattice avoiding electron-phonon collisions, associated with “normal” metallic behaviour, resulting in zero resistance and superconductivity below the superconducting temperature.

### 2.3.5.2 Magnetic measurements

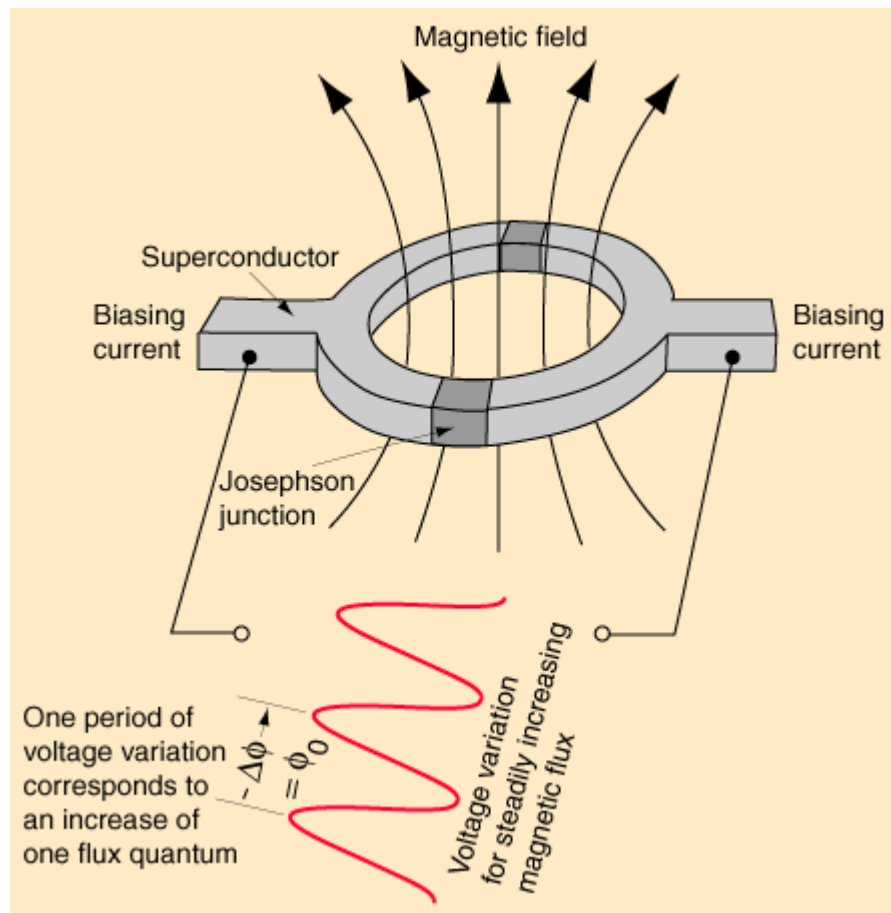


Figure 2- 23: Diagram showing a Josephson junction

Magnetic measurements were carried out using a Quantum Design MPMS-XL SQUID (Superconducting Quantum Interference Device) magnetometer, which detects the magnetic moment of a sample, from which the magnetic susceptibility can be calculated. The SQUID consists of one or more superconducting loops with two weak links between them. These links, called Josephson Junctions, are made of a non-superconducting material (Figure 2- 23). The sample passes between these loops inducing an electric current. The variation in this current is measured and converted to voltage which is proportional to the magnetic moment of the sample. The design of the instrument allows for very sensitive measurements to be taken under a variety of conditions: with a temperature range of 1.8-400 K and a magnetic field strength of  $\pm 5$  Tesla. In order to obtain a value for the magnetisation of the sample ( $M$ ) the machine moment ( $MM$ ) must be corrected to account for dielectric contributions of an empty sample gelatine capsule ( $GC$ ):

$$M = MM - GC \quad \text{Equation 2- 26}$$

From this it is then possible to calculate the gram susceptibility,  $\chi_g$ , and the molar susceptibility  $\chi_m$ , for the sample as the sample mass ( $SM$ ), molecular weight ( $MW$ ) and applied magnetic field ( $H$ ) are already known:

$$\chi_g = \frac{M}{H \cdot SM} \quad \text{Equation 2- 27}$$

$$\chi_m = \chi_g \cdot MW \quad \text{Equation 2- 28}$$

Finally the sample has a diamagnetic contribution from the gelatine capsule and this must be accounted for and corrected by subtraction from  $\chi_m$ . The values for these corrections can be found in a published table.<sup>46</sup>

Samples are prepared loading a pre-weighed gelatine capsule with the powdered sample and noting the mass. The lid of the capsule is then inverted to seal in the powder and prevent it spilling during the measurement. The capsule is then placed in the centre of a plastic straw and held in place by two shorter straw sections. The straw is then pierced to facilitate evacuation of any air during the helium purge process prior to sample measurement. The straw is then attached to the sample rod and securely inserted into the SQUID magnetometer. After the sample is purged and sealed it was centred prior to measurement. Samples were then measured between 1.8 K and 300 K with a constant magnetic field of 10 Oe and a detailed scan carried out around the suspected superconducting transition temperature for the material. The resultant data were then displayed graphically with  $\chi_g$  against temperature, in K, and in all cases the superconducting transition could be clearly observed.

### **2.3.6 Scanning Electron Microscopy (SEM)**

Scanning electron microscopy (SEM) is designed for the direct study of the surface features, morphology and texture of solid objects. By scanning with an electron beam, an image is formed which provides a good representation of the three-dimensional sample. A beam of electrons (incident beam) is produced at the top of the microscope by heating a metallic filament. This beam passes through electromagnetic lenses which focus it directly onto the sample. Once it

hits the sample, other electrons (backscattered and secondary) are ejected from the sample (Figure 2- 24). Some electrons from the incident beam are elastically scattered by the nucleus of the target and so are similar in energy to the incident electrons. These are known as backscattered electrons and the degree of scattering of these is related to the number of electrons in the sample and hence the chemical composition of the sample. Secondary electrons occur when interactions happen between incident electrons and weakly bonded conduction-band electrons in metals or the valence electrons in insulators and semiconductors. Due to the vast difference in energies between the two electrons only a small amount of kinetic energy can be transferred to the secondary electrons and so these electrons originate within a few nanometres from the surface. Detectors collect the secondary or backscattered electrons, and convert them to a signal that is sent to a viewing screen producing an image. Particles can be observed in the nm range; however the majority of samples observed were in the  $\mu\text{m}$  range.

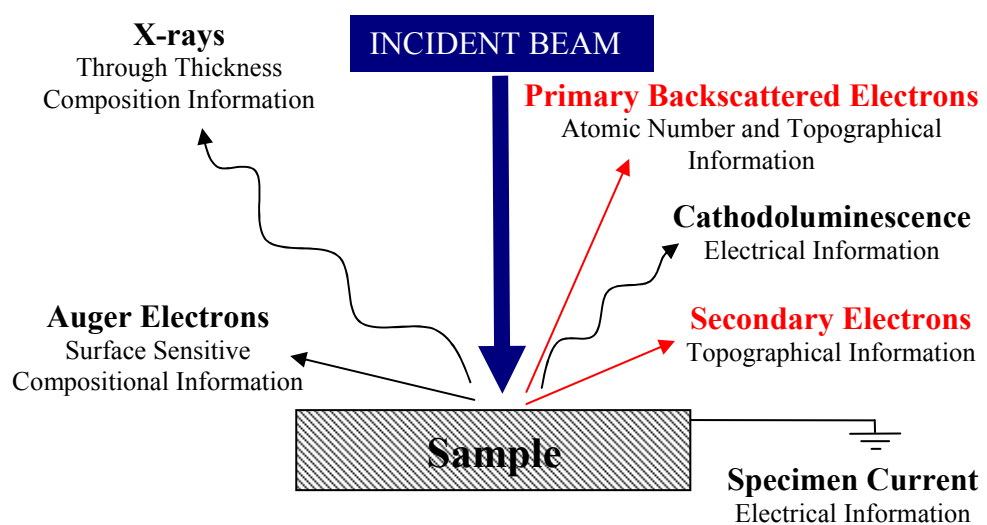


**Figure 2- 24: Diagram of sample/electron interactions in SEM**

All SEM analysis was carried out using a Quanta 600 SEM machine. The powdered sample was then sprinkled onto a carbon tab (stuck to an aluminium stub) until it was completely coated. The sample was then loaded into the chamber and the SEM images taken in high vacuum mode with a voltage of either 20 kV or 25 kV.

### ***2.3.6.1 Energy Dispersive X-ray spectroscopy (EDX)***

While a sample is undergoing SEM it is possible to obtain elemental analysis using Energy Dispersive X-ray spectroscopy (EDX). Elemental information is acquired by bombarding the sample with high energy electrons prompting the ejection of a ground state electron. In turn an electron with higher energy within the sample takes its place and the excess energy of that electron is released in the form of an X-ray. The energies of the X-rays emitted directly relate to the atomic orbital energies of a given atom and so it is possible to calculate the elemental composition of the sample. Like XRD however this technique has its flaws when analysing lighter atoms. For this reason it is hard to detect, with any accuracy, light elements such as carbon. Compounding this problem is the fact that these low energy X-rays, emitted from carbon for example, are readily absorbed by heavier elements, such as tungsten, and so distort the elemental composition. Using this technique it is also hard to detect elements of similar atomic number, such as carbon and oxygen, due to the X-rays emitted being of similar energy. It should also be remembered that the sample is adhered to a carbon tab and so one must be careful not to include any of the tab in the elemental analysis otherwise the

carbon content of the sample becomes skewed. This is easily overcome by visually checking the image before collecting data, but is none the less worth mentioning.

### 2.3.7 X-ray Photoelectron Spectroscopy (XPS)

XPS is a surface characterisation technique that can analyze a sample to a depth of 2 to 5 nm. XPS reveals which chemical elements are present at the surface and the nature of the chemical bond that exists between these elements. The technique is able to detect all of the elements except hydrogen and helium. XPS works by irradiating a sample with X-rays of sufficient energy (in a range 5-40 eV) resulting in excitation of electrons in specific states.<sup>47</sup> Provided sufficient energy is available the electron breaks away from the nuclear attraction force of the element (Figure 2- 25).

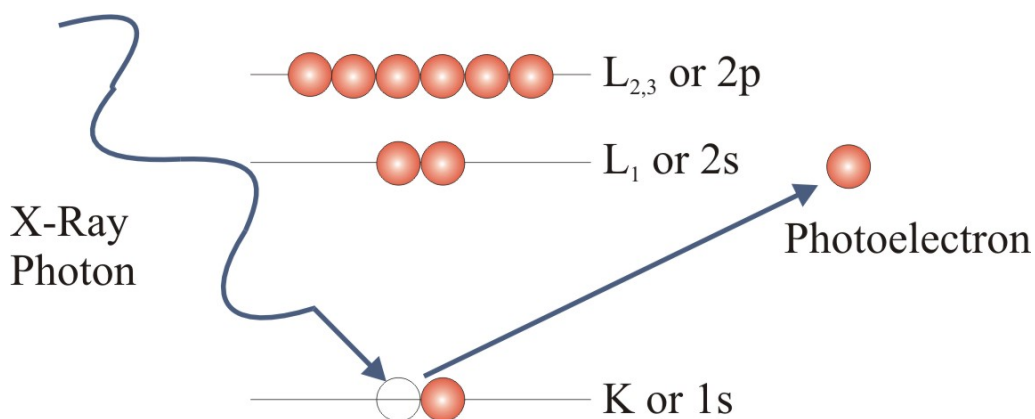


**Figure 2- 25: Diagram showing the excitation of specific electrons and their subsequent emission.**

Some of these photo-ejected electrons inelastically scatter through the sample on their way to the surface, while others undergo prompt emission and suffer no energy loss in escaping the surface and into the surrounding vacuum. Once these photo-ejected electrons are in the vacuum, they are collected by an electron analyzer that measures their kinetic energy. An electron energy analyzer produces an energy spectrum of intensity (number of photo-ejected electrons versus time) versus binding energy (the energy the electrons had before they left the atom). Each prominent energy peak on the spectrum corresponds to a specific element as well as its oxidation state. It is also possible to obtain information on the electronic structure from these peaks. Besides identifying elements in the specimen, the intensity of the peaks also indicates the percentage of the element present in the sample. Each peak area is proportional to the number of atoms present in each element.

Measurements were run with the assistance of Martin Roe at the school of mechanical, materials and manufacturing engineering at the University of Nottingham using a VG ESCALab Mark II X-ray photoelectron spectrometer with AlK- $\alpha$  radiation (non-monochromated), an anode potential of 10kV and 20Ma filament emission current. Samples, still in pellet form, were loaded onto carbon tabs (adhered to aluminium stubs) and characterisation was subsequently carried out and the data analysed. In certain cases the samples can be argon etched to remove a few surface layers allowing analysis deeper into the material.

### 2.3.8 X-ray Fluorescence (XRF) and CHN analysis

X-ray Fluorescence spectroscopy is primarily used as an elemental analysis technique providing fast and accurate results. It relies on the emission of “secondary” X-rays from a sample by bombarding it with high energy X-rays of specific wavelengths. Table 2- 3 indicates the discrete wavelengths for a rhodium tube indicating the heaviest element which can be excited with each specific line. Rhodium is used as it is simultaneously suitable for exciting both heavy and light elements allowing a multitude of elements to be tested for, however, for elements heavier than molybdenum (such as tungsten) a generator setting of 60 kV is required for detection to be possible.

Line	Energy /keV	Wavelength /nm	Heaviest Element
Rh K $\alpha_1$	20.214	0.0613	Mo
Rh K $\alpha_2$	20.072	0.0617	Mo
Rh K $\alpha_1$	22.721	0.0546	Ru
Rh L $\alpha_{1,2}$	2.694	0.4601	S
Rh K $\alpha_2$	2.834	0.4374	Cl

**Table 2- 3: Rhodium’s characteristic lines**

In some cases, when the energy of the radiation exceeds the ionisation potential of the atom, ionisation occurs resulting in the ejection of one or more electrons from the atom. The energy of the X-rays is high enough to expel electrons from the inner orbitals resulting in electrons from outer orbitals

“dropping down” to fill their place. When this occurs a photon is released with energy equal to the difference in orbital energies. This photon, with energy unique to the atom, is then detected and as multiple atoms are bombarded, and so releasing photons, accurate elemental percentages for the material are observed.

For these experiments wavelength dispersive XRF (WDXRF) was used. The main difference between this and energy dispersive XRF (EDXRF) is in the detection system, otherwise the principals are the same. In EDXRF a whole spectrum is measured simultaneously with the detector capable of measuring the different energies of the characteristic radiation coming directly from the sample. This is known as deconvolution. The area of the peaks is then analysed, determining the concentration of a given element. This is similarly the case for WDXRF with this latter technique being more sensitive for lighter elements due to the different detection mechanism. All radiation coming from a sample falls onto a crystal which acts like a prism and disperses different wavelengths in different directions. With the detector at a certain angle, the intensity of X-rays of a certain wavelength can be measured. The detector can then be moved to analyse additional wavelengths resulting in data being collected sequentially.

Unfortunately, like XRD, issues exist with XRF. Lighter elements are inherently harder to observe due to lower sensitivity. Sample fusion is also required to minimise particle size effects during the measurement. The sample is dissolved in a flux material such as di-lithium tetra-meta borate, which is transparent to X-rays, and a spherical glass bead formed, but refractory

materials, such as carbides, dissolve slowly and do not always give satisfactory fusions. It is also recommended to tune the spectrometer for the elements being analysed if the best results are to be achieved. Bad calibration can lead to poor results.

XRF experiments were out-sourced to London and Scandinavian Metallurgical Co Ltd (LSM) where a Panalytical PW1480 was used to conduct the analysis. The sample was weighed onto a Lanthanum Oxide bed in a platinum crucible. The crucible was then placed in a furnace at 1000°C initially and subsequently moved to a furnace at 1270°C. The furnace at 1270°C has oxygen piped to it, completing the oxidation of the sample. The glass fusion mixture (Lithium Tetraborate) is added to the platinum and this is fused at 1270°C. The glass material containing the sample is then cast into a bead form which is analysed on the XRF instrument. The XRF instrument is calibrated using pure materials with the sample quality control materials (BCS/ECRM standards) analysed to confirm the calibration.

LSM also carried out combustion analysis, using a Leco CS-444 system, in order to obtain the percentage of carbon present in a given sample. Approximately 0.2 to 0.5 g of sample was weighed out into a ceramic crucible. This was then placed into the instrument furnace and heated under a current of oxygen. The Carbon in the sample forms CO<sub>2</sub> (any CO formed is converted to CO<sub>2</sub>), which is measured using an infra-red cell. The instrument is calibrated using BCS/ECRM standards or Leco Carbon standards.

### **2.3.9 Thermal Analysis, evolved gas analysis and Mass Spectrometry (MS)**

Thermo gravimetric analysis (TGA) is used to determine sample weight changes in relation to change in temperature in specific atmospheres. This can be used to determine oxidation or reduction of a given sample as well as structural changes. The apparatus comprises a precise balance, a small furnace (encasing the sample) and a sensitive thermocouple to accurately measure the furnace temperature. It is also possible to purge the furnace with a variety of gases, usually an inert gas, such as argon or nitrogen, to prevent oxidation or undesired reactions. The attached computer then records all the data during the measurement including the weight change on the balance and the furnace temperature. It is also possible to attach a mass spectrometer to the equipment so that gases being evolved can be monitored and thus the weight change quantified.

Two different analyzers were used to observe the thermal effects on various materials. Firstly the TA Instruments Q600, based at the University of Nottingham and secondly the STA 409 PC based at the University of Glasgow. Despite the differences in experimental setup, both gave similar results with the latter having a mass spectrometer attached to it for additional information (section 2.3.10). In both cases a variety of experiments were run with either argon or standard atmosphere flowing during the measurement. All crucibles were tared prior to the addition of sample and subsequently heated to 1000 °C in the case of the TA Q600, or 1400 °C for the STA 409 PC. In both cases the

ramp rate was 10 °C/min, with occasional experiments also involving a hold temperature so further information on a sample could be obtained at a specific temperature.

Mass spectroscopy is used to measure the mass-to-charge ration of ions and a resultant spectrum is generated representing the masses of sample components. The technique works by firstly generating ions which are consequently affected by electromagnetic fields. The electric field accelerates the ions into a magnetic field which applies a force to each ion perpendicular to the plane defined by its direction of travel and the magnetic field lines. This results in the ions travelling in a curve, not a straight line, in differing arcs and path lengths depending on their mass-to-charge ratio. Lighter atoms are deflected more as according to Newton's second law of motion acceleration of a particle is inversely proportional to its mass:

$$f = ma \quad \text{Equation 2- 29}$$

*Where  $f$  is the force,  $m$  is the mass and  $a$  is the acceleration.*

The detector then measures this deflection and consequently the number of ions of each specific mass is calculated and a mass spectrum generated. A general schematic of a mass spectrometer can be see in Figure 2-26.

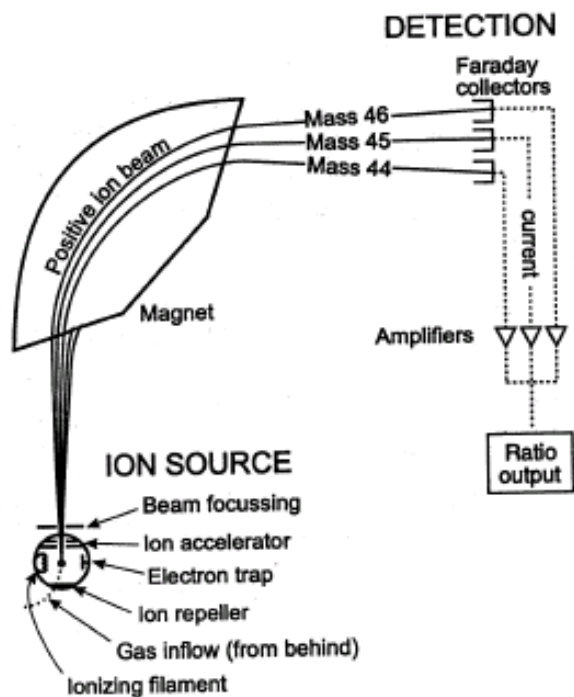


Figure 2- 26: General schematic of a mass spectrometer<sup>48</sup>

Measurements were taken on a Hiden HPR20 based at the University of Glasgow. This was attached to the STA 409 PC (section 2.3.9) so that gases evolved were monitored *in-situ*. The aim was to provide quantitative analysis for the by-products of the carbide synthesis as well as looking at the carbothermal reduction of a number of the starting materials with increasing temperature *in-situ*.

## 2.4 REFERENCES

- 
- <sup>1</sup> <http://www.colourware.co.uk/cpfaq/q1-1.html>
- <sup>2</sup> R. Meredith, *Engineers' handbook of industrial microwave heating*, 1<sup>st</sup> Edition, Short run press ltd, Exeter, 1998.
- <sup>3</sup> G. Whittaker, *A Basic Introduction to Microwave Chemistry*, 1997
- <sup>4</sup> S. A. Galema, *Chem. Soc. Rev.*, 1997, **26**, 233.
- <sup>5</sup> G. Whittaker and D.M.P. Mingos, *Journal of microwave power and electromagnetic energy*, 1994, **29**, 195.
- <sup>6</sup> <http://homepages.ed.ac.uk/ah05/basicintro.html>
- <sup>7</sup> D. E. Clark, D. C. Folz and J. K. West, *Mater. Sci. Eng.*, 2000, **A287**, 153.
- <sup>8</sup> R. G. Ford, *Mater. Process. Rep.*, 1988, **3**, 1.
- <sup>9</sup> K. E. Haque, *Int. J. Miner. Process.*, 1999, **57**, 1.
- <sup>10</sup> C. Gabriel, S. Gabriel, E. H. Grant, B. S. J. Halstead and D. M. P. Mingos, *Chem. Soc. Rev.*, 1998, **27**, 213.
- <sup>11</sup> V. Kenkre, L. Skala, M. Weiser and J. Katz, *Mater. Sci.*, 1991, **26**, 2483.
- <sup>12</sup> G. J. Kriegsmann, *Appl. Phys.*, 1992, 1960.
- <sup>13</sup> S. O. Nelson and P.G. Bartley, *IEEE transactions on instrumentation and measurement*, 2002, **51**, 589.
- <sup>14</sup> J. E. Atwater and R.R.J. Wheeler, *Applied Physics A - Materials science and processing*, 2004, **79**, 125.
- <sup>15</sup> D. M. P. Mingos and D.R. Baghurst, *Chem. Soc. Rev.*, 1991, **20**, 1.
- <sup>16</sup> J. H. Peng, J. Binner, S. Bradshaw, *Mater. Sci. Tech.*, 2002, **18**, 1419.
- <sup>17</sup> W. H. Sutton, *Am. Ceram. Soc. Bull.*, 1989, **68**, 376.
- <sup>18</sup> D. M. P. Mingos and D. R. Baghurst, *Br. Ceram. Trans. J.*, 1992, **91**, 124.

- 
- <sup>19</sup> J. B. Salsman, *Materials research society symposium proceedings*, 1991, **189**, 509.
- <sup>20</sup> L. D. Landau, E.M. Lifshitz and L.P. Pitaevski, *Electrodynamics of Continuous Media*, 2nd Edition, England: Pergamon Press, Oxford, 1984.
- <sup>21</sup> S. O. Nelson, *Journal of microwave power and electromagnetic energy*, 1996, **31**, 215.
- <sup>22</sup> J. Robinson and S. Kingman, *Chem. Eng.*, 2005, **772**, 26.
- <sup>23</sup> E. Lester, S. Kingman and C. Dodds, *Fuel*, 2005, **84**, 423.
- <sup>24</sup> P. Hulls, *Dielectric heating for industrial processes*, U.I.E., 1992.
- <sup>25</sup> P.W. Atkins, *Physical Chemistry*, 6<sup>th</sup> Edition, Oxford University Press, Oxford, 1998, 625.
- <sup>26</sup> A.R. West, *Basic Solid State Chemistry*, 2<sup>nd</sup> Edition, John Wiley and Sons, Ltd, Chichester, 1999.
- <sup>27</sup> W. Kraus and G. Nolze, Federal Institute for Materials Research Testing, Berlin, Germany, 1998.
- <sup>28</sup> ICSD: <http://icsdweb.fiz-karlsruhe.de/>
- <sup>29</sup> D. Louer and M Louer, *J. Appl. Crystallogr.*, 1972, **5**, 271.
- <sup>30</sup> A. Boulouf and D. Louer, *J. Appl. Crystallogr.*, 1991, **24**, 987.
- <sup>31</sup> A. C. Larson and R.B. Von Dreele, "The General Structure Analysis System", Los Alamos National Laboratories, Report LAUR086748, LANL, Los Alamos, N. M., USA, 1999.
- <sup>32</sup> <http://www.ill.fr>
- <sup>33</sup> R. I. Smith and S. Hull, *User Guide for the Polaris Powder Diffractometer at ISIS*,. 1997, Rutherford Appleton Laboratory.
- <sup>34</sup> <http://www.isis.rl.ac.uk/>

- 
- <sup>35</sup> B. H. Toby, *J. Appl. Crystallogr.*, 2001, **34**, 210.
- <sup>36</sup> H. M. Rietveld, *J. Appl. Cryst.*, 1969, **2**, 65.
- <sup>37</sup> H. M. Rietveld, *Acta Crystallogr.*, 1967, **22**, 151
- <sup>38</sup> A. C. Metaxas and R.J. Meredith, *Industrial Microwave Heating*, the Institution of Electrical Engineers, London, 1983.
- <sup>39</sup> A. W. Kraszewski and S.O. Nelson, *Journal of microwave power and electromagnetic energy*, 1996, **31**, 178.
- <sup>40</sup> M. Arai, High temperature dielectric property measurements of engineering ceramics, *Microwaves II*, 1993.
- <sup>41</sup> D. F. Shriver and P. W. Atkins, *Inorganic Chemistry*, 3<sup>rd</sup> Edition, Oxford University Press, Oxford, 1999, 112.
- <sup>42</sup> H. K. Onnes, *Comm. Phys. Lab. Univ. Leiden*, 1911, **122**
- <sup>43</sup> W. Meissner and R. Ochsenfeld, *Naturwissenschaften*, 1933, **21**, 787f
- <sup>44</sup> <http://superconductors.org/History.htm>
- <sup>45</sup> <http://superconductors.org/>
- <sup>46</sup> F.E. Mabbs, D. J. Machin, *Magnetism and Transition Metal Complexes*, Chapman and Hall Ltd., London, 1973.
- <sup>47</sup> P.W. Atkins, *Physical Chemistry*, 6<sup>th</sup> Edition, Oxford University Press, Oxford, 1998, 852.
- <sup>48</sup> <http://pubs.usgs.gov/of/2001/ofr01-257/images/figure1.gif>

## 3: TUNGSTEN CARBIDE INVESTIGATIONS

### 3.1 INTRODUCTION

Tungsten carbide is arguably the most important of the transition metal carbides. It is the hardest binary carbide at elevated temperatures ( $\sim 1000$  kg/mm<sup>2</sup> at 1000 °C). Its properties include a high melting point (2600 – 2850 °C), high hardness (16 – 22 GPa 500 g load Vickers), high fracture toughness (28 MPa m<sup>1/2</sup>), high compressive strength (5 GPa at 20 °C) and a high resistance to both oxidation and corrosion.<sup>1</sup> Although tungsten carbide has many industrial applications, it is predominantly mass produced for use in various tools and drills, but has now even found new applications as a substitute for noble metals in catalysis.<sup>2, 3</sup>

Two different binary phases exist in the tungsten carbide (W-C) system. The principal phase used in industry is WC, but W<sub>2</sub>C also exists and is notoriously difficult to synthesise without any impurities.<sup>5</sup> WC has the more favourable properties for industrial purposes, however W<sub>2</sub>C has a superconducting transition between 2.8 K and 3.9 K.<sup>4</sup> The phase diagram (Figure 3- 1) shows how these different phases can be synthesised in a conventional furnace. For low weight percentages of C, W<sub>2</sub>C is synthesised preferentially to WC, although this changes as the amount of carbon present increases. There is only a narrow carbon weight percent window for pure W<sub>2</sub>C synthesis and equally pure WC is only possible at very high temperatures

(~2600 °C). In most cases it is preferred to react with excess carbon to ensure WC synthesis with a view to removing the excess carbon post-synthesis.

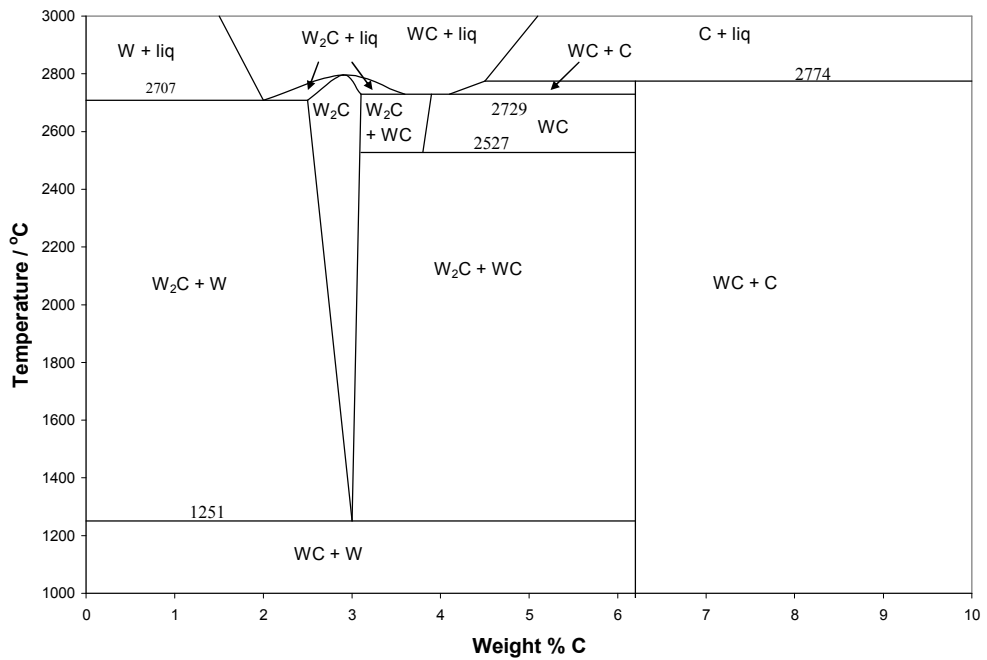


**Figure 3- 1: Phase diagram of the W-C system.<sup>5, 6</sup>**

WC has a hexagonal structure, space group  $P\bar{6}m2$ ,  $a = 2.9065 \text{ \AA}$ ,  $c = 2.8366 \text{ \AA}$ <sup>7</sup>;  $W_2C$  has a hexagonal structure, space group  $P6_3/mmc$ ,  $a = 2.9920 \text{ \AA}$ ,  $c = 4.7250 \text{ \AA}$ .<sup>8</sup>

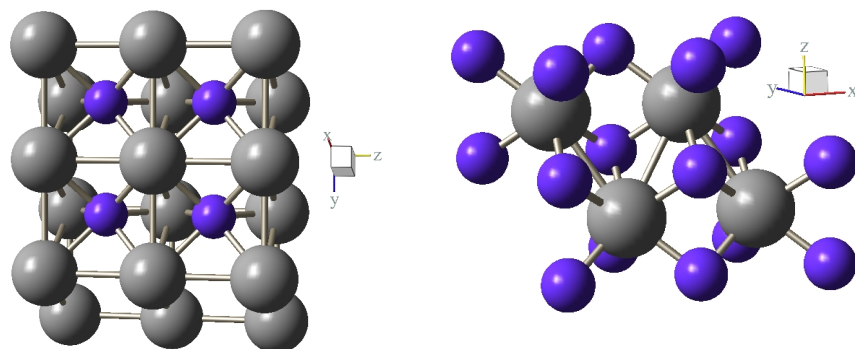


**Figure 3- 2: Structures of WC (left) and W<sub>2</sub>C (right). The grey atoms correspond to W and the purple to C.**

The current synthesis for tungsten carbide involves direct carburization of tungsten powder, requiring firing for 2 – 10 h at elevated temperatures (1400 – 1600 °C). Control of grain size and carbon content can further lengthen this process.<sup>5, 9</sup> Separation is often required to obtain a specific grain size or reheating the product with additional carbon to aid the synthesis of a non-carbon deficient carbide. In recent years, a number of articles have been published providing alternative synthetic methods for this energy intensive process. These include variations in the current synthesis, for example coating WO<sub>3</sub> particles with between 13 and 17 wt % carbon prior to heating.<sup>10, 11</sup> Alternatively combustion synthesis has been reported, again from tungsten oxide, but also using magnesium, carbon and sodium salts to afford the desired WC product.<sup>12</sup> Synthesis has also been reported using the metal halide, WCl<sub>4</sub>, reduced at room temperature with LiBEt<sub>3</sub>H resulting in the formation of monodispersed ~2nm W<sub>2</sub>C colloids.<sup>13</sup> Using the same halide, with the addition of Al<sub>4</sub>C<sub>3</sub> or CaC<sub>2</sub>, solid state metathesis was used to synthesise WC. However, unlike many of the other synthetic methods, this was possible at much lower temperatures (~350 °C with CaC<sub>2</sub>) and on a rapid timescale.<sup>14</sup> Synthesis of WC has even been reported without the use of a furnace. Ball milling alone was used in the formation of WC from the reactants W and C; however the timescales involved were over 60 hours.<sup>15, 16</sup>

As discussed in chapter 1, the search for novel synthetic methods for the transition metal carbides is a necessity for the advancement of modern processing. Microwave heating is one such method which has been reported for the synthesis of many types of carbide (chapter 1, section 1.4). The

synthesis and sintering of WC and the cemented WC-Co has been reported, with synthesis and sintering achieved on the sub-hour timescale with usually lower reaction temperatures.<sup>17, 18</sup> Patents also exist for the successful microwave synthesis<sup>19</sup> and sintering<sup>20</sup> of WC. For the former, a multimode microwave system is used with successful production of the carbide achieved in 70 min with a reaction temperature between 1200 and 1700 °C. In principle these synthesis methods seem adequate with a significant improvement on synthesis time compared to conventional methods, however, neither process is perfect. Lackner reports the requirement for a protective gas atmosphere and/or in vacuo<sup>19</sup> whereas the constraint of Lindholm's process is the requirement of wet mixing of the reactants.<sup>20</sup>

In contrast to the WC patents, synthesis is not always the priority for some authors. The importance of changes in morphology and properties of samples processed using microwave irradiation has also been investigated. For example Cheng et al. observe a much smaller grain size (~1 µm) and enhanced densification in the sintering of WC-Co.<sup>17</sup> Looking at the effects of microwave irradiation on samples, Rodiger et al. examined penetration depth in the sintering of WC-Co, highlighting the importance of understanding the reaction process.<sup>18</sup> Breval et al. showed using Transmission Electron Microscopy (TEM), that the cobalt phase dissolves nearly no tungsten, whereas conventionally up to 20 % can be dissolved into the Co binder phase in WC-Co.<sup>21</sup> In addition, finer WC grains are observed and a more uniform, homogenous distribution of the Co binder resulting in a material 1-5 GPa harder than the conventionally synthesised material. The MW synthesised

sample was found to be also six times more resistant to corrosion and twice as resistant to erosion, however no explanation was given for this phenomenon.<sup>21</sup>

Although numerous papers report successful rapid sintering/synthesis of carbides comparatively little work has been carried out to probe reaction mechanism or to attempt to quantify experimental observations. With this in mind this chapter looks at the work carried out on the synthesis and study of the W-C system. In particular, focus is given to the design and progress of the synthetic method to the study of the products and investigation of the reaction mechanism. The W-C system was used as a basis, in all cases, for the other systems investigated in later chapters (chapters 4 and 5). The majority of work carried out for W-C was later adapted for the other transition metal carbide systems.

### **3.2 EXPERIMENTAL: SYNTHESIS OF W-C**

The principal aim of work regarding the W-C synthesis was the successful synthesis of both the targeted WC and W<sub>2</sub>C phases using microwave energy (Table 3- 1). In addition, an examination of the reaction profile was deemed key to building upon the understanding of microwave heating in the solid state as well as the processing of transition metal carbides. In order to achieve this, a great deal of time was spent developing the experimental technique, particularly with the W-C system (**1**), which was the first transition metal carbide system to be investigated. It would then be possible to replicate this synthesis across the series of group IV, V and VI carbides.

Experiment	Applicator	Reaction	Purpose
1	DMO	$W + C \rightarrow WC$	Experimental design; synthesis of WC
2	DMO	$2W + C \rightarrow W_2C$	Synthesis of $W_2C$
3	DMO	$WC + W \rightarrow W_2C$	Synthesis of $W_2C$ from WC
4	DMO; Single mode cavity	$W + C \rightarrow WC$	Applicator and power investigation
5	Single mode cavity	$W + C \rightarrow WC$	Synthesis and study of W-C reaction profile
6	Single mode cavity	$W + C \rightarrow WC$	Study carbon stoichiometry of WC through PND
7	Single mode cavity	$W + xC \rightarrow WC_x$	Study the effect of excess carbon on WC synthesis
8	Single mode cavity	$W + C \rightarrow WC$	Study the effect of sample size on synthesis time
9	Single mode cavity	$W + C \rightarrow WC$	In-situ study of the reaction using thermal imaging and high speed photography
10	Single mode cavity	$WO_3 + 5C \rightarrow 2WC + 3CO_2$	Synthesis of WC

**Table 3- 1: Summary of all experiments carried out on the W-C system.**

Initially it was unknown how the reactants would behave under microwave treatment. Both tungsten (W) and graphite (C) heat using the conduction mechanism (section 2.1.1) with the latter known to be a good microwave absorber, reaching temperatures in excess of 1000 °C in less than 2 min.<sup>22, 23</sup> This is due to the movement, in response to the electric field, of the limited free charge present in the material which allows the material to behave like a poor electrical conductor. Resultant heating is possible through electrical resistance. W, on the other hand, is a conductive metal and was expected to

behave as such. In this case, the majority of microwave energy is reflected off the surface resulting in observed high surface voltages. A finite diminishing current exists beneath the surface, known as the skin depth, which is directly affected by the microwave frequency, allowing deeper microwave penetration with frequency variation.<sup>26</sup>

With reactant behaviour in mind, the experimental technique was developed through the investigation of stand-alone heating of the pellet, the use of susceptors, such as carbon, variations in reaction vessels, issues with microwave penetration depth, changes in power input and sample positioning within the cavity (1). The experimental development and consequential results are discussed in detail in section 3.3 with the final experimental method reported in section 2.2.

Synthesis was attempted in multimode domestic microwave ovens (section 2.2.1) and single mode cavities (section 2.2.2), with direct comparisons made between the two applicators (4). For lab work, a single mode cavity offers many advantages over its multimode counterpart. Detailed in chapter 2 (section 2.1.2.2), a single mode applicator allows for increased power density leading to a decrease in reaction time. Reproducibility is also facilitated due the precise definition of the electric field, with fine tuning of the sample within the cavity possible despite the difficulties the small sample sizes lend to accurate tuning. This, coupled with the increased power available (up to 15 kW), meant rapid heating was capable in the single mode cavity. Although direct comparisons were made between power input and synthesis time in both applicators (4) (section 3.4); the single mode proved more successful, with

heating investigated using powers up to 10 kW. In addition changes to the reaction were also investigated, using the 3- 15 kW single mode applicator (section 2.1.2.2), including changes in carbon content (7) (section 3.4.2), and variation in sample size (8) (section 3.4.3)

The majority of work concentrated around synthesis of the carbide, from the metal powder, W (1-9) (sections 3.3 and 3.4), but processing involving the oxide (10) (section 3.4.6),  $WO_3$ , was also investigated. WC was almost always the targeted phase, for reasons explained in section 3.1, however, the synthesis of  $W_2C$  was also studied (2, 3). One of the key areas of work revolved around the reaction profile (5) (section 3.4.1). Investigations, using *in-situ* temperature studies, *ex-situ* phase analysis from PXD and *ex-situ* dielectric property measurements, revealed information on possible reaction mechanisms, which were aided by further *in-situ* studies using thermal imaging and high speed photography (9).

High speed video (Photo-Sonics Phantom V7 Colour, 4800 to 150, 000 frames per second, courtesy of EPSRC engineering pool) was used to record the synthesis of WC from W + C within the 3 – 15 kW single mode applicator (9). The camera was positioned above the cavity in place of the optical pyrometer, and with the aid of additional lighting, focused on the sample within the cavity. Experiments were run at 3 kW with the sample, embedded in graphite, placed in an alumina crucible rather than a quartz tube. This was purely to aid in the video of the sample, and through previous experiments, was shown not to affect the synthesis of the carbide. The pellet was heated for 30 s and footage was taken at time intervals of 139  $\mu$ s between frames (7200 frames

per second) resulting in footage of key initial steps of the reaction (Video file, WC\_high\_speed.avi, attached on CD). The camera was operated as soon as the flash was observed from the reaction and, using time delay and an onboard storage buffer of footage, the frames were collected during this crucial reaction initiation step.

For the thermal imaging (9), an FLIR ThermaCAM SC3000 (-20 °C to 2000 °C with an accuracy of  $\pm 1$  °C; courtesy of EPSRC engineering pool) was used, with a view to recording live video footage of the temperature changes during the reaction;  $W + C \rightarrow WC$ . Similar to the work with the high speed photography, the thermal imager was situated above the cavity in place of the optical pyrometer. The imager was set to record temperatures ranging from 500 °C to 2000 °C, chosen due to results collected with the optical pyrometer. An alumina crucible was used in place of the quartz tube to house the pellet to facilitate the thermal imaging process. Unfortunately the quartz tube both obscured the pellet and masked any thermal information as it conducted heat from the reaction. Footage was then recorded in real-time throughout the 30 second reaction. 9 s of the footage, taken during reaction initiation, can be viewed on the attached CD (WC\_thermal.wmv). Due to video storage on the thermal imager and subsequent video formatting, 9 s was the maximum length of footage available.

In all reactions (1-10) stoichiometric amounts of the starting materials to afford the desired product were ground together and pelleted; 2 g pellets for non-oxide reactions and 1 g pellets for oxide reactions. This method is

described in detail in section 2.2. In the case of the scale up experiment (7) standard pellets weighing 2 g were pressed as well as pellets weighing 10 g and 20 g. This was carried out using a large scale press (custom built automated mechanical press capable of pressing up to 20 tonnes) available in the School of Mechanical, Materials and Manufacturing Engineering at the University of Nottingham. Due to the compressive strength of tungsten, pressing proved difficult, with the fragility of the pellets providing difficulty in initial setup of the experiment. However, it was possible to use a small amount of acetone to act as a pellet binder which evaporated after 24 hours. Pellets were exposed to microwave energy for up to 1 min.

Regardless of the applicator used, all experiments were repeated a minimum of three times. A fixed power was always used; 800 W for DMO experiments and 3 kW for single mode applicator experiments. Although, as mentioned above, other powers were investigated, 800 W and 3 kW, for the DMO and single mode cavity experiments respectively, proved the most successful in the synthesis of the carbide. This is commented on in more detail in sections 3.4 and 3.5. After the desired heating time samples were removed from the cavity and left to cool prior to characterisation.

Various classes of characterisation technique were used to investigate the resultant products. PXD was carried out on all samples post-synthesis by first grinding the sample to a fine powder with subsequent loading onto a glass slide (section 2.3.1). Samples were typically scanned for 20 min with a finite number of samples scanned for 12 h so that structural refinement could be

carried out (section 2.3.3). In addition specific samples were characterised using PND (6), enabling detailed structural refinement and phase analysis (section 2.3.2). Dielectric property measurements were carried out on the majority of samples (section 2.1.2). These were crucial in the investigation of the reaction profile and involved the powder, used in PXD, being loaded into a quartz tube. Samples, weighing no more than 0.5 g, were then inserted into the cavity and five measurements taken so an average value could be obtained. From these results, coupled with the PXD data and *in-situ* temperature information obtained during the reactions, it was possible to study the reaction profiles and the direct relationships observed between these three variables. Other techniques such as SEM (section 2.3.6), EDX (section 2.3.6.1), XRF and CHN analysis (section 2.3.8) and thermal analysis (section 2.3.9) were also carried out to reinforce results from other characterisation techniques.

### **3.3 RESULTS AND DISCUSSION: W-C SYNTHESIS AND EXPERIMENTAL DEVELOPMENT USING A DOMESTIC MICROWAVE OVEN (DMO)**

A DMO was used for the initial experiments. With its ease of use and relative inexpense it was an ideal starting point for synthetic work of this nature. All work was carried out at 800 W (max power) so continuous power output was achieved due to the lack of a rectified power supply. In an effort to synthesise the more desirable WC phase (1), stoichiometric amounts (1:1) of W and C were ground together and pelletised (section 2.2). The pellet was then placed in a 10 mm diameter silica tube (microwave transparent), supported in a

fire brick, and heated, on a turntable, in a DMO (DeLonghi model M8021P-B1) for 30 min. It was hoped this would be sufficient time for a partial or complete reaction to occur, however, after grinding the pellet to a fine powder post-reaction, powder X-ray diffraction (PXD, section 2.3.1) revealed only the reactants, W and C. In addition, the turntable system failed due to the melting of the plastic component of the turning mechanism. From this point forward all DMO experiments were carried out in a specific location inside the microwave cavity. Although this is not ideal as the mode positions within the cavity are known to vary with temperature, volume and dielectric properties of the load, no alternative was available.

The DMO was again set to 30 min with the pellet this time remaining in a stationary location within the cavity, but no reaction was observed with the pellet remaining shiny; PXD confirmed the presence of only reactants. In response, the experiment was repeated, but with a pellet contained in a silica tube sunk into a beaker containing powdered graphite. It was hoped that using a susceptor such as graphite, a well documented approach<sup>24, 25</sup>, would aid the synthesis of WC. Heating for 30 min revealed a reaction had occurred, however on analysis with PXD only a small amount of WC was observed as well as the unwanted W<sub>2</sub>C phase, with the majority of the pellet comprising starting materials. Although some carbide had been formed, after looking at the phase diagram (section 3.1), it was decided that it was unlikely the pellet was reaching 1000 °C, the minimum temperature for WC synthesis. With the pellet not in direct contact with the graphite powder it is likely that heat is rapidly dissipated from the graphite into the surrounding atmosphere/silica glassware resulting in insufficient heat for WC synthesis to occur. For this reason a pellet

was placed directly into the beaker of graphite powder and heated for 30 min, however again this resulted in minimal WC formation. Thankfully the graphite powder surrounding the pellet was easily brushed off post- reaction.

As mentioned in the introduction (section 3.1) Rodiger et al. published a paper discussing the effect of penetration depth on WC-Co sintering.<sup>18</sup> It is vital to take penetration depth (discussed in chapter 2, section 2.1.2) into account when designing experiments in microwave applicators. The microwave irradiation only penetrates a finite distance into the sample<sup>26</sup> and so high dielectric loss materials, such as carbon, have a low penetration depth. With this in mind graphite powder was placed, along with the pellet, in a silica tube which in turn was stabilised in a beaker containing silica flour (ground silica). Silica flour is essentially microwave transparent and as well as supporting the silica tube retains heat emitted from the graphite and thus maintains the high temperature required for carbide synthesis. As discussed in the preparations section of chapter 2 (section 2.2) this setup became the basis for all transition metal carbide reactions.

Although it is still not fully understood why the graphite susceptor is required, it is possible that without it the power density is too low for the sample size used. It also seems that the insulation provided by the silica flour is important in maintaining a sufficient reaction temperature, initially provided by the graphite susceptor. It is certainly this initial heating of the susceptor that enables the temperature to become adequate for the W and C present in the pellet, given the small load, to produce sufficient heat for WC formation. With this in mind, it is possible that with a much larger load the graphite susceptor

may not be required, however by that stage, as discussed by Rodiger,<sup>18</sup> microwave penetration depth becomes an important issue.

Following the new experimental procedure, the pellet was heated for 30 min in the DMO; PXD (Figure 3- 3) revealed a pure phase of WC with indexed lattice parameters  $a = 2.908(1) \text{ \AA}$  and  $c = 2.839(1) \text{ \AA}$ . Lattice parameters are in excellent agreement (identical within 1 ESD) with previous studies of stoichiometric WC.<sup>27</sup> Repetitions of this experiment at 5 min intervals (between 0 and 30 min) allowed the phases to be studied at specific intervals during the reaction. Figure 3- 4 shows pure-phase WC synthesis was achieved in 20 min with further study revealing a possible reaction mechanism:



Formation of the carbide does not begin until around 10 min (temperature related), at which point  $W_2C$  is the first phase to form. As the reaction proceeds WC becomes the dominant phase, with  $W_2C$  decaying rapidly to form WC.

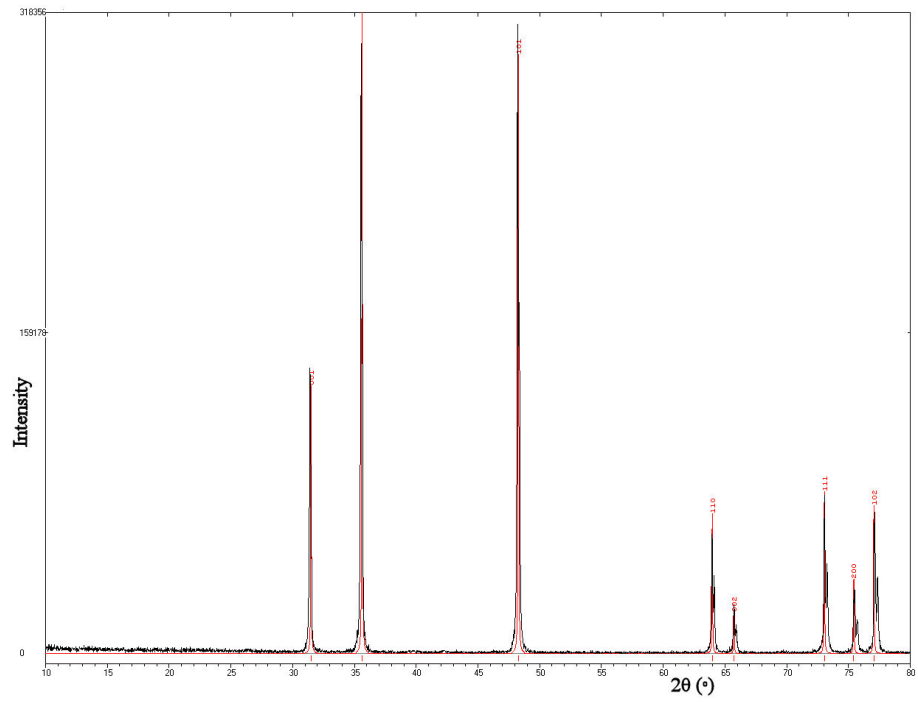


**Figure 3- 3: Overnight PXD pattern of pure WC sample (black) synthesised in 30 min in DeLonghi DMO. Calculated pattern is red.**

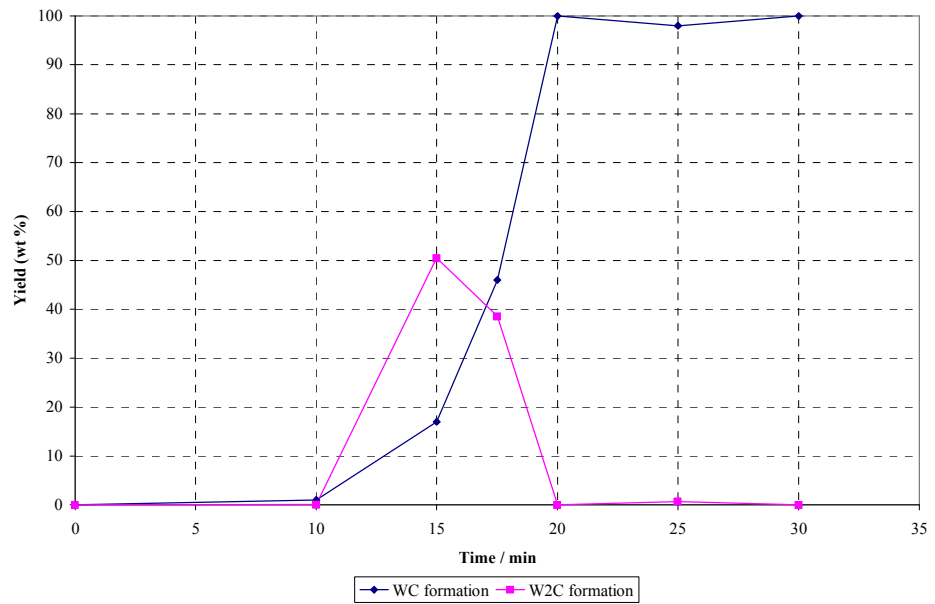


**Figure 3- 4: Graph showing WC and W<sub>2</sub>C formation against time in the DMO.**

Although  $W_2C$  was never present in the final product, in an effort to bypass any formation the reactions were repeated with 20 wt % excess graphite in the starting mixture ( $W + 1.2C \rightarrow WC + 0.2C$ ). Analysis of the products, however, revealed no change in the reaction profile with  $W_2C$  still a prominent phase during initial stages of the reaction. Clearly synthesis of this phase is important in the mechanism of WC synthesis.

Given the important of  $W_2C$  in the successful synthesis of WC, a pure-phase synthesis of this phase was attempted (2, 3). Using the same experimental setup (section 2.2.1) pellets were pressed to afford the  $W_2C$  phase and individually heated up to 30 min, in 10 min intervals, in order to investigate multiple reaction times. Unfortunately formation of the  $W_2C$  phase was impossible to achieve regardless of heating times with PXD revealing WC and W as the major phases after successful phase matching with structure downloads from the ICSD database. In an effort to force the synthesis of  $W_2C$ , reactions were first undertaken to synthesise WC. Following reaction (3), additional W was ground into the reactants and, after pressing, the pellet was heated for 25 min in the DMO. After a further two additions of W and re-heating it was possible to achieve a sample containing 83 %  $W_2C$ , which after further experimentation was determined to be the best result. Repetitions using the single mode cavity at a later date still produced no better results. The lack of temperature control during the reaction and the preferential formation of WC go some way to explaining the difficulty in synthesis of the  $W_2C$  phase.

### 3.4 RESULTS AND DISCUSSION: W-C SYNTHESIS USING A SINGLE MODE CAVITY

Experiments (experimental procedure: section 2.2), to produce WC from W and C, were carried out initially in two separate applicators: 0 -1 kW IMS system (ran at 1 kW) and a 3 – 15 kW Sairem system (ran at 3 kW) (section 2.1.2.2). Samples were heated for a given time in a specific reactor and subsequently characterised, using PXD, to verify the phases present in each sample so that reaction times in each system could be obtained. Comparisons of these times, along with previous work in the domestic microwave oven revealed an expected trend between applied power, cavity type and WC phase fraction (4) (Figure 3- 5). Pure-phase synthesis of the carbide was possible in 20 min in the DMO (section 3.3), however, a change in cavity type, from multimode to single mode, resulted in a significant decrease in synthesis time as discussed in the literature.<sup>28</sup> With an increase of only 200 W of applied power in addition to the increased efficiency in irradiation of the sample (described in section 2.1.2.2), reaction time is decreased by a factor of 20: from 20 min to only 1. Increasing the applied power to 3 kW resulted in a further decrease in reaction time to only 20 s, for greater than 95 % WC purity. To achieve 100 % purity a total heating time of 40 s was required, suggesting that the homogeneity of the reaction mixture plays a crucial role in the final stages of WC formation. Grinding the reaction mixture in a pestle and mortar for up to 20 min made no difference to the phase purity; however, this is not surprising given the rapid timescale of the reaction and the fact “perfect” mixing is impossible to achieve.

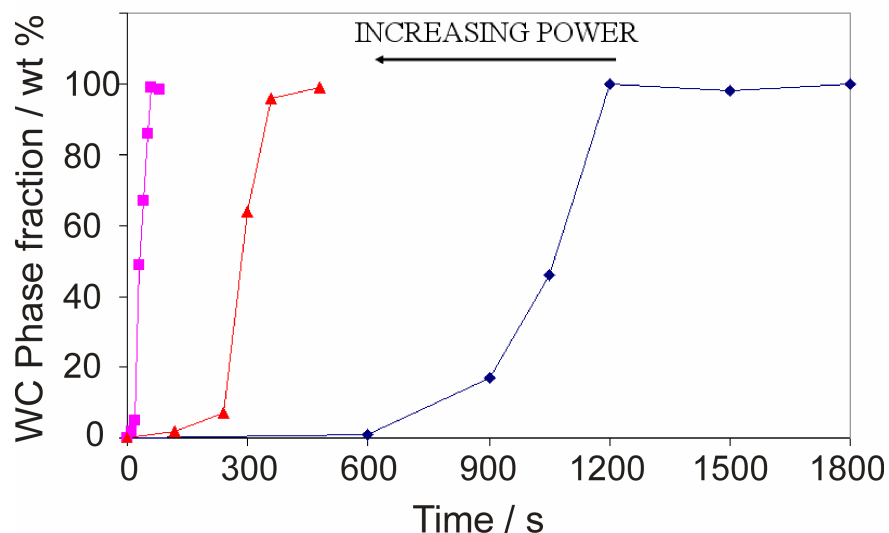


**Figure 3- 5: WC phase fraction vs. reaction time for varying applicator-type and applied power. (Diamonds represent multimode DMO data, triangles 1 kW single mode data and squares 3 kW single mode data.)**

Regardless of the microwave reactor used, synthesis of WC was achieved on a much more rapid timescale than previously reported in the literature.<sup>19, 20</sup> Using a single mode cavity and 3 kW applied power, 100 % WC phase purity was achieved in 40 s.<sup>29</sup> This result directly compares to conventional synthesis of ~2 h for a sample of a similar volume;<sup>30</sup> a drastic improvement with the use of microwave heating. Figure 3- 6 displays the resultant refined diffraction pattern for the WC product. Table 3- 2 comprises the crystallographic parameters post-refinement. Lattice parameters are in excellent agreement with previous studies of stoichiometric WC.<sup>27</sup> Bond distances are identical to within 0.0002 Å for both metal-metal and metal-carbon bonds (previous studies found in the literature report bond distances of W-C: 2.1972 and W-W: 2.9060 and 2.8370). Refinement of carbon stoichiometry was attempted, but resulted in an unstable refinement due to problems associated with light element detection and PXD (section 2.3.1).

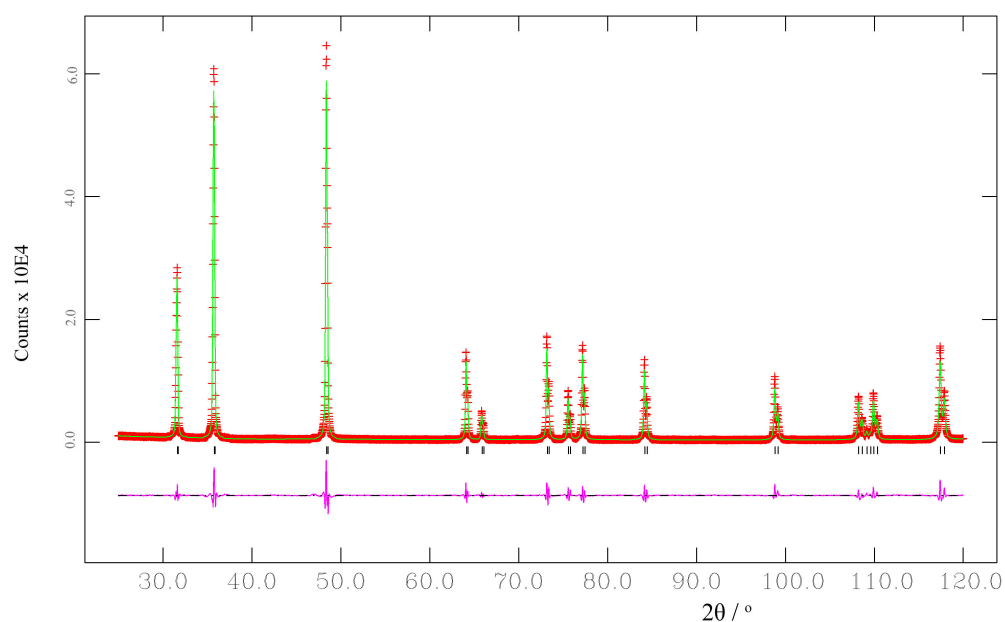


**Figure 3- 6: Observed (plusses), calculated and difference profile plot for the Rietveld refinement against PXD data for tungsten carbide produced in 40 s at 3 kW. Tick marks denote WC diffraction peaks.**

Empirical formula	WC
Crystal system, Space group	Hexagonal, $P\bar{6}m2$
Unit cell formula weight, $M_w$	105.85
$a, c$ -parameter, $\text{Å}$	2.9062(1), 2.8371(1)
Unit cell volume, $\text{Å}^3$	20.751(1)
$Z$ , Calculated density, $\rho_x / \text{g cm}^{-3}$	1, 15.673
Observations, parameters	4765, 28
$R_p, R_{wp}, \chi^2$	0.045, 0.060, 4.705
Interatomic distance: W-C, $\text{Å}$	2.1973(1)
Interatomic distance: W-W, $\text{Å}$	2.9062(1), 2.8371(1)

**Table 3- 2: PXD crystallographic and bond information for WC synthesised in 40 s at 3 kW in a single mode cavity.**

Thermogravimetric analysis (TGA) of the final product in air revealed negligible weight loss (of CO, CO<sub>2</sub>) until the oxidation of WC (to WO<sub>3</sub> as confirmed by PXD) begins at *ca.* 400 °C (with a corresponding weight gain) with rapid onset occurring at 550 °C (Figure 3- 7). The TGA data are hence commensurate with the complete conversion  $W + C \rightarrow WC$ , in the carburisation reaction.

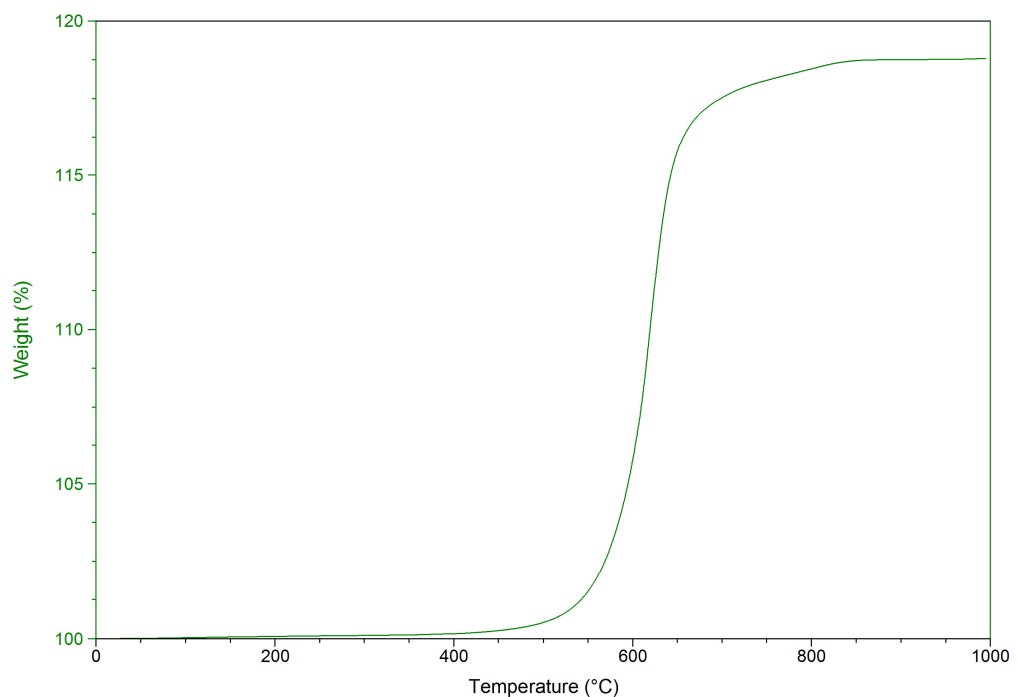


**Figure 3- 7: TGA data indicating oxidation of WC beginning at 400 °C with rapid onset occurring at 550 °C.**

Scanning electron microscopy of a cleaved pellet (SEM) reveals the carbide exists as block-like, irregular crystallites with a typical range of grain sizes from 5-10 μm (Figure 3- 8). The observed morphology and grain size did not vary appreciably irrespective of the reaction temperature, reactor type or applied power. From energy dispersive analysis by X-rays (EDX) we were able

to derive a W:C ratio of 1:1.0(2). There was no evidence from SEM/EDX of W, C or  $W_2C$  in the final product. XRF and combustion analysis also confirmed the presence of only tungsten and carbon in the ratio 1:0.98(1), strongly suggesting the formation of WC.

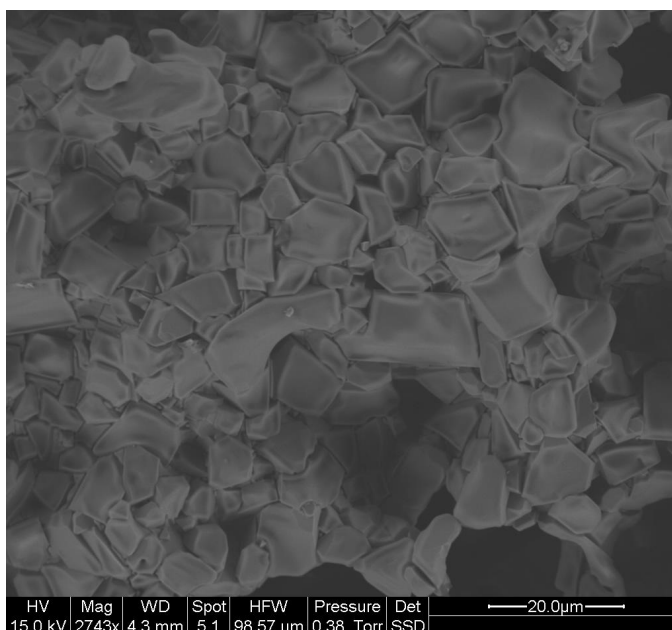


**Figure 3- 8: SEM micrograph of a cross-section of a tungsten carbide pellet produced in 40 s at 3 kW.**

The expected trend observed in Figure 3- 5 identified one of the major advantages, in this case, of single mode cavities i.e. ultra-rapid reaction times. The increased electric field clearly improves power dissipation within the carbide system resulting in successful synthesis on the sub-minute timescale. In an effort to improve reaction speeds further, applied powers up to 10 kW were used. Samples were heated using the 3 – 15 kW microwave applicator for times up to 40 s, however a number of problems were encountered. With such a small load (sample volume compared to cavity size) the reflective power increased, as applied power was augmented, indicating that the sample was

incapable of absorbing the increasing microwave energy. With fine tuning it was possible to better match the system thus decreasing the reflective power; however, this often resulted in termination of the reaction due to failure of the quartz tubing or alumina crucibles. After a number of attempts it was determined, for both safety and practicality reasons, that no more than 3 kW applied power would be used.

### 3.4.1 W-C reaction profile

Although synthesis of WC had been achieved on a rapid timescale and it was known that  $W_2C$  played an important role in its formation, it was still not understood how or why this reaction was occurring so quickly. For this reason a more detailed investigation was carried out at all stages of the reaction:  $W + C \rightarrow WC$  (5). Firstly the experiment was adapted to take *in-situ* temperature measurements during any given experiment (section 2.2.2).

Temperature measurements have been an area of controversy with regards to the accurate description and understanding of microwave heating. Three principal options are available: thermocouples, fibre optics and optical pyrometers. The latter two methods are similar, but differ technically and in terms of applications hence they are considered separately. Each technique has its merits, but ultimately none fulfil all the criteria for unequivocal reaction temperature measurement. These being that the technique is non-invasive, and produces both accurate surface and bulk temperature measurement. Bulk temperature measurement is of particular importance since the internal

temperature of a material in a microwave field is higher than the surface due to the volumetric MW heating mechanism and heat transfer from the surface.<sup>31</sup> This phenomenon results from the balance between heat loss from the surface, conduction of heat to/from the interior and volumetric dissipation of energy in the body.<sup>32</sup>

Thermocouples are by far the most common method of temperature measurement and many modifications have been attempted for successful operation within a microwave field.<sup>33,34,35</sup> Due to perturbation of the field by the thermocouple a sheath is required for the probe, however this is not 100% effective and local field distortion can be observed.<sup>33</sup> Direct contact with the material, required for thermocouple readings, also can cause interference and measurement error. In an effort to improve the thermocouple technique a number of alternatives have been investigated, mostly with the aim of minimising the extension of the thermocouple in the microwave cavity. This has been achieved, for example, by embedding the thermocouple into the reaction vessel, however this results more strictly in the measurement of the reaction vessel temperature and not that of the sample which can be vastly different.<sup>34,35,36</sup> An alternative is to stop heating and manually insert the thermocouple into the sample and take a reading.<sup>37</sup> However the error associated with this technique is considerable due to the large temperature gradient between the sample and the surrounding atmosphere.

Another method of temperature measurement is using fibre optics. A novel experimental procedure has been published by Iwasaki et al. in which they use two such devices, one to measure the external temperature and a second to measure the internal temperature by drilling a hole in the pelletised sample (in their case  $\text{LaCrO}_3$ ).<sup>38</sup> Despite the obvious precision required in drilling into a sample and the limitations due to material fragility, this method showed some promising results. However, it is unclear as to whether the fibre optic cables had any perturbation effect on the microwave field. It has also been shown that the metal tip of the cable can interact locally with the field.<sup>33</sup> In addition the use of fibre optics is limited as they can only operate at relatively low temperatures ( $< 300\text{ }^\circ\text{C}$ ). Another optical method is to use an infrared pyrometer situated outside the cavity, but focused onto the material. This results in no interference with the microwave field and gives an accurate surface temperature reading. However no internal temperature measurements can be made by this method and the temperature range of the apparatus is much more limited than that using a thermocouple. For both optical methods the sensitivity to emissivity can also be an issue which can result in significant temperature errors.<sup>33</sup> The emissivity of materials is also known to change with temperature and accounting for this is difficult in rapid reactions.

Overall it is clear that no single approach yet provides a complete solution. Optical pyrometers at present, probably offer the most economical and most widely applicable solution if calibrated correctly, resulting in accurate measurement of surface temperatures without any perturbation of the microwave field. For this reason a LAND pyrometer (System4 Thermometer

M1 600/1600 °C;  $\pm 1$  °C accuracy) was used in the following experiments. The pyrometer was positioned over the single mode cavity and focused so that the 5 mm diameter spot was centred on the sample surface. The information from the pyrometer was then fed to a control box and the temperature monitored and recorded throughout the experimental process. This enabled accurate surface temperature measurement of the pellet at any given point during the reaction. A number of pellets were then heated at 3 kW in the single mode cavity (following the recognised experimental procedure (section 2.2.2)) between 0 and 40 s, in 5 s intervals, with multiple repeats at each time (5). Repetitions of this experiment, with sample quenching in ice cold water, resulted in less than 5 % difference in phase fractions present at any given heating time. Given this is the error calculated during any given experiment, the result was deemed insignificant with quenching having no noticeable effect. Due to the microwave heating effect, samples are heated instantaneously with the application of microwave energy. However, the atmosphere around the sample receives no direct heating, as observed in a conventional furnace, and so remains significantly cooler than the sample. This results in rapid cooling of the sample once the microwave radiation has been terminated. This is observed with the optical pyrometer during all experiments; the temperature dropping to below 600 °C (the lower detection limit of the optical pyrometer) in under 5 s. This in itself could be considered air quenching and in any case by the time the sample is removed from the cavity and quenched in the water the temperature is going to be too low for any reaction to be occurring. For this reason quenching, post-synthesis has little or no effect on the reaction.

All samples, post-reaction, underwent ex-situ PXD and dielectric property measurements. PXD plots are presented in Figure 3- 9 which show the existence of W + C in the early stages of the reaction and the formation of  $W_2C$  at 5 s which decays away as WC is formed as the reaction proceeds. By 20 s a near-pure phase of WC exists and by 40 s pure WC is afforded.<sup>29</sup>

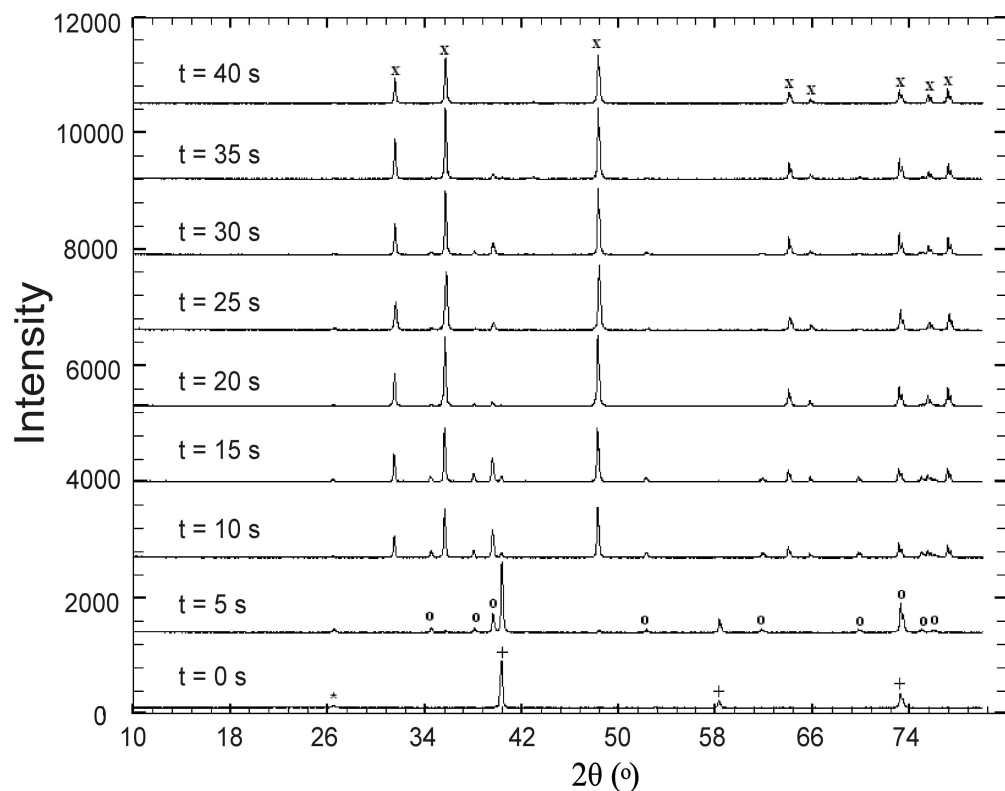


**Figure 3- 9: PXD patterns taken *ex-situ* from the W + C reaction, performed at 3 kW. W diffraction peaks are denoted by plusses, C by asterisks,  $W_2C$  by circles and WC by crosses.**

Dielectric property measurements were carried out using the cavity perturbation technique (section 2.1.2) for all microwave treated samples. The resultant data, along with phase fraction information obtained from PXD and temperature data from the optical pyrometer, is plotted in Figure 3- 10.<sup>29</sup> The

lines drawn on the graphs act only as a visual guide. It is important to remember that dielectric properties are temperature dependant and so the results reported are not absolute, however the relative difference and thus the important trend should always remain constant.<sup>39</sup>

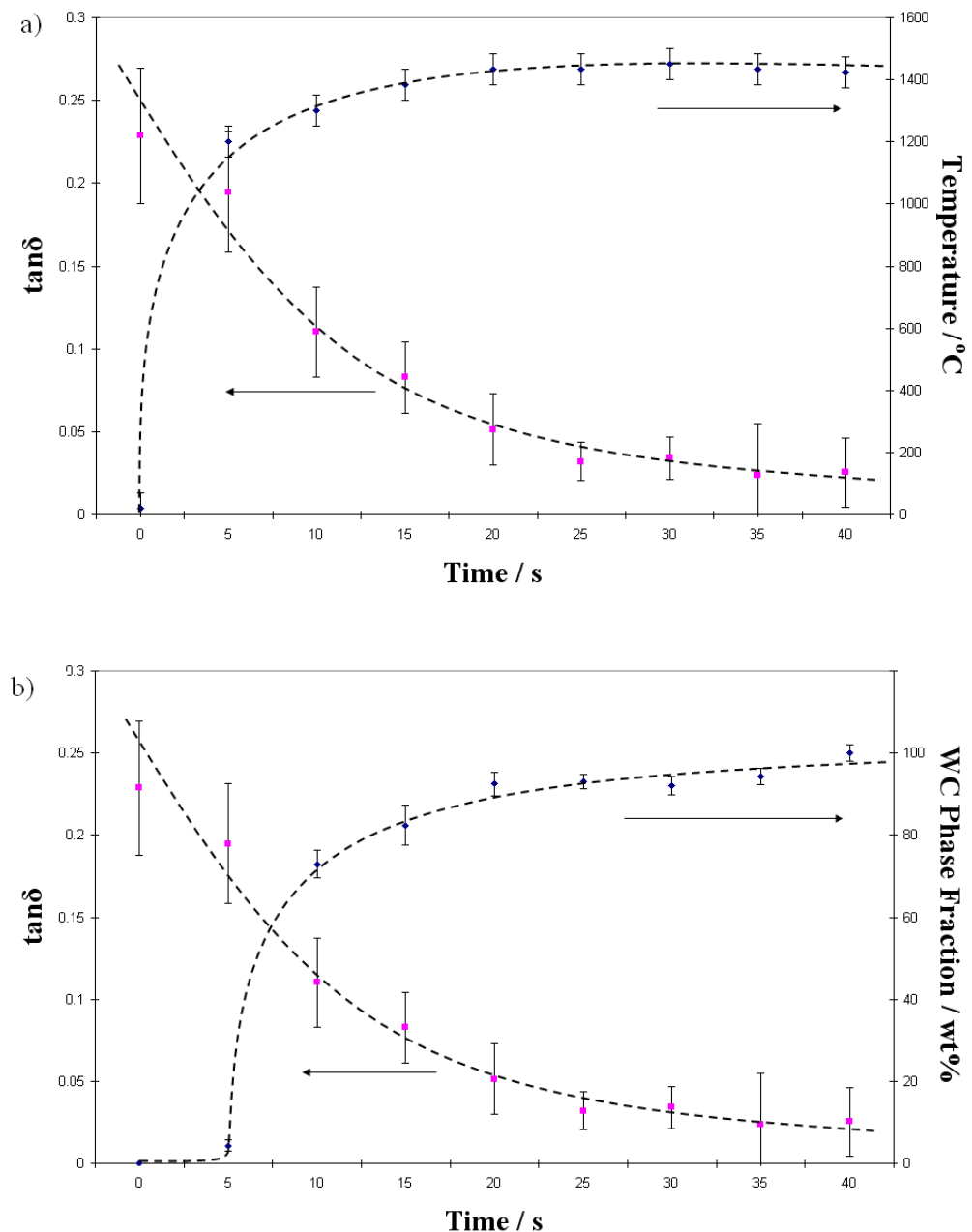


**Figure 3- 10: Plot of the loss tangent,  $\tan \delta$  (squares) vs. reaction time (for 0 wt % excess C; 3 kW) superimposed with (a) WC phase fraction (diamonds) and (b) reaction temperature (diamonds) data.**

The dielectric constant,  $\epsilon'$  decreases only slightly with reaction time, whereas the dielectric loss factor  $\epsilon''$  decreases more markedly over the same period. This is likely due to the loss in conductivity as W + C are used to form the product WC. From the data collected it is unequivocal that the dielectric properties play a pivotal role in the MW carburisation process. Hence the loss tangent,  $\tan \delta$  (ratio of the loss factor to the dielectric constant,  $\epsilon''/\epsilon'$ ), decreases as one progresses from a mixture predominantly containing the starting materials towards, after 20 s, a composition containing in excess of 90 wt % WC (Figure 3- 11). The absorbed power per unit volume is directly proportional to the dielectric loss factor in addition to the electric field strength inside the material squared. Over the initial 20 s period, the temperature rises to over 1400 °C but from this point forward, the rate of heating is very low. From the combined sets of data, one can thus define two unambiguous heating regimes; the first in which dielectric heating initiates the reaction and the second in which heating is dominated by conventional conduction. The highest rate of heating occurs before most of the W and C has produced WC (or  $W_2C$ ) and one can thus infer that the exothermic formation of WC ( $\Delta H_{f, 298} = -40.46 \text{ kJ mol}^{-1}$ )<sup>40</sup> is not a major contributor to the initial rapid heating. Various forms of carbon couple strongly to microwaves<sup>41</sup> and one might expect finely divided metals such as tungsten to contribute to heating ohmically in a high frequency electric field (section 2.1.1).<sup>41,42,43</sup> By comparison, the dielectric properties of the mixture after 20 s (when the composition is mainly WC) are not particularly conducive to further coupling with the electric field. These observations carry great significance in that the reaction essentially “self-terminates”, there is no evidence of thermal runaway and hence the reaction ends with the desired product and no

decomposition, melting, oxidation or safety issues save the reaction vessel temperature. This behaviour in the W-C system is brought about by the phenomenon of self-limiting heating, where  $d\epsilon''/dT$  decreases sharply above a certain temperature<sup>44</sup> (in this case, coincident with the majority phase formation of WC), contrasting to the rapid heating effect that occurs in the early stages of the reaction. This allows a degree of control over the various phases of the reaction which is certainly significant for industrial scale up. It is also an important distinction between many other microwave heating solid state reactions where thermal runaway occurs due to the dielectric properties of materials increasing with temperature.<sup>45</sup> The evident control in addition to a total reaction time (< 60 s), initial rapid heating and the final self-termination suggest that with appropriate cavity design, one could engineer a continuous, flow process to rapidly produce large amounts of crystalline, single phase WC in a highly efficient way.

Further investigation lead to dielectric property measurements being made at elevated temperature. These were carried out every 100 °C up to the maximum furnace temperature of 1000 °C (Figure 3- 11). The aim was to analyse the effect of temperature on the dielectric properties of the W + C mixture. A 2 g mixture of tungsten and graphite powder, weighed out stoichiometrically to give the product WC, was loaded into a quartz tube identical to those used in other dielectric property measurements. The tube was sealed, to avoid any oxidation of the reactants during the experiment, then positioned in the sample arm and raised into the furnace. The furnace was set to a ramp rate of 4 °C/min and was stabilised for 10 min every 100 °C. After

stabilisation the tube was lowered into the cavity and five sequential measurements taken. This technique is detailed in section 2.1.2. PXD was taken pre- and post-reaction verifying the presence of only the starting materials, W and C in both cases.

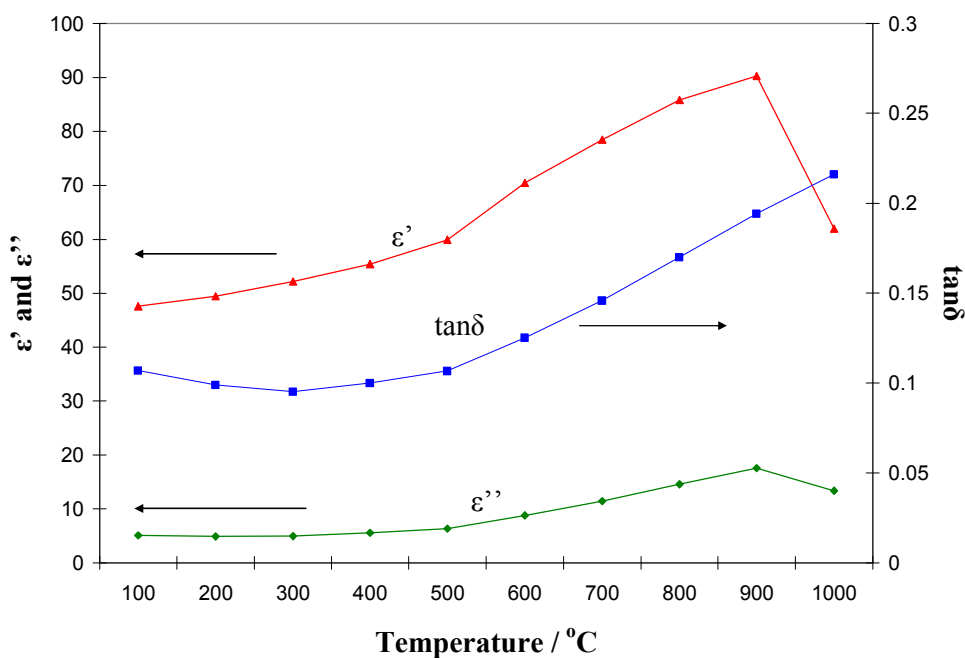


**Figure 3- 11: Plot of relative permittivity ( $\epsilon'$ ), dielectric loss ( $\epsilon''$ ) and resultant loss tangent data with increasing temperature for W + C reaction mixture.**

Figure 3- 11 clear shows that, with increasing temperature,  $\epsilon'$  increases greatly compared to  $\epsilon''$ . This would suggest that, as the reaction temperature rises, the reaction mixture becomes more susceptible to the electric field. At ambient temperature the loss tangent is relatively low for the mixture, remaining so until between 500 °C and 600 °C. At this point the loss tangent begins to increase with temperature and continues to do so until the maximum

furnace temperature is reached. This helps to explain the lack of product until a susceptor is used to initiate the synthesis of the carbide, with the susceptor heating initially and raising the temperature to a point where the dielectric properties of the reactant mixture has improved sufficiently so that formation of the carbide can begin. Although this explains the initial lack of WC formation in the early stages of the reaction, further expansion of this result would require *in-situ* dielectric property measurements. This task in itself requires a lot of thought, but is worth consideration if one truly wants to control and understand what is occurring in the few s that this reaction takes to go to completion.

#### ***3.4.1.1 PND study of WC***

Powder Neutron Diffraction (PND) was carried out on the sample heated for 40 s to closely examine the crystal structure of WC as well as confirming it as the only phase present (6). In addition an examination of the carbon stoichiometry in the final product was carried out which, as mentioned previously, was not possible to refine using PXD data. PND data were collected on D1A at the ILL in Grenoble (section 2.3.2.1). D1A operates with fixed scan times over a specified  $2\theta$  range, with multiple scans taken to increase the resolution of the diffraction pattern. The resultant pattern looks similar to PXD with  $2\theta$  plotted against intensity.

Approximately 2 g of the sample was loaded into a 5mm diameter vanadium canister which was then attached to the diffractometer. The sample

was scanned, between 0 and 158 ° in 2  $\theta$  at a wavelength of 1.39 Å with a step size of 0.1 °, and data collected for 4 h. Rietveld refinement (section 2.3.3) of the data were performed using the General Structure Analysis System (GSAS)<sup>46</sup> through the windows based EXPGUI interface.<sup>47</sup> Data were refined concurrently against the WC structure proposed by Leciejewicz,<sup>7</sup> starting with the background coefficients, followed by the unit cell, atomic positions, profile parameters and isotropic temperature factors. Finally the absorption/reflectivity correction and carbon occupancy were refined. The resultant profile plot is seen in Figure 3- 12 and Table 3- 3 comprises selected crystallographic parameters post-refinement.

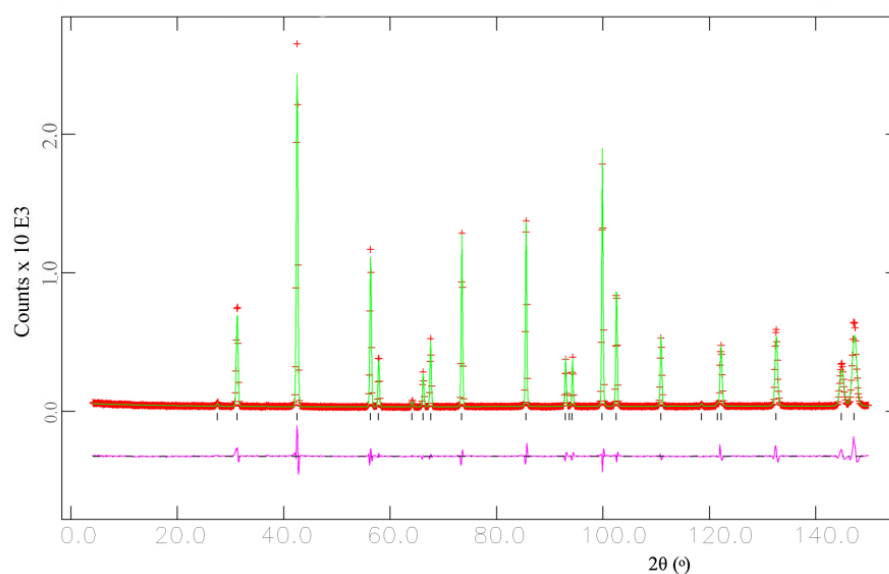


**Figure 3- 12: Observed (plusses), calculated and difference profile plot for the Rietveld refinement against PND data for WC produced in 40 s at 3 kW. Tick marks denote WC diffraction peaks.**

Empirical formula	WC
Crystal system, Space group	Hexagonal, $P\bar{6}m2$
Unit cell formula weight, $M_w$	105.85
$a, c$ -parameter, $\text{\AA}$	2.91828(4), 2.84549(4)
Unit cell volume, $\text{\AA}^3$	21.162(2)
Z, Calculated density, $\rho_x / \text{g cm}^{-3}$	1, 15.965
Observations, parameters	1459, 15
$R_p, R_{wp}, \chi^2$	0.0675, 0.0872, 5.853
W (0, 0, 0) occupancy, $U_{iso} / \text{\AA}^2$	1.00, 0.0014(1)
C ( $\frac{2}{3}, \frac{1}{3}, \frac{1}{2}$ ) occupancy, $U_{iso} / \text{\AA}^2$	0.972(5), 0.0014(1)
Interatomic distance: W-C, $\text{\AA}$	2.2053(1)
Interatomic distance: W-W, $\text{\AA}$	2.9183(1), 2.8455(1)

**Table 3- 3: PND Crystallographic and bond information for WC synthesised in 40 s at 3 kW in a single mode cavity.**

PND revealed a pure phase of WC synthesised in 40 s at 3 kW. Interestingly the lattice parameters are slightly higher than those reported previously (section 3.4). This is reflected in the interatomic distances which are around  $0.01 \text{\AA}$  longer than the reported structure of WC.<sup>7</sup> PND does not suffer from the problem of light atom detection like PXD, thus it was possible to refine accurately carbon stoichiometry. This revealed slight carbon non-stoichiometry in the product which explains the expanded crystal structure observed and hence the longer interatomic distances. Phase purity and carbon stoichiometry was confirmed with XRF and combustion analysis; a ratio of tungsten to carbon 1:0.98(1) was observed, suggesting WC formation. SEM of the powdered product indicates the expected angular grains, all of similar size, with EDX confirming tungsten to carbon ratio of 1:1.0(2) (Figure 3- 13).

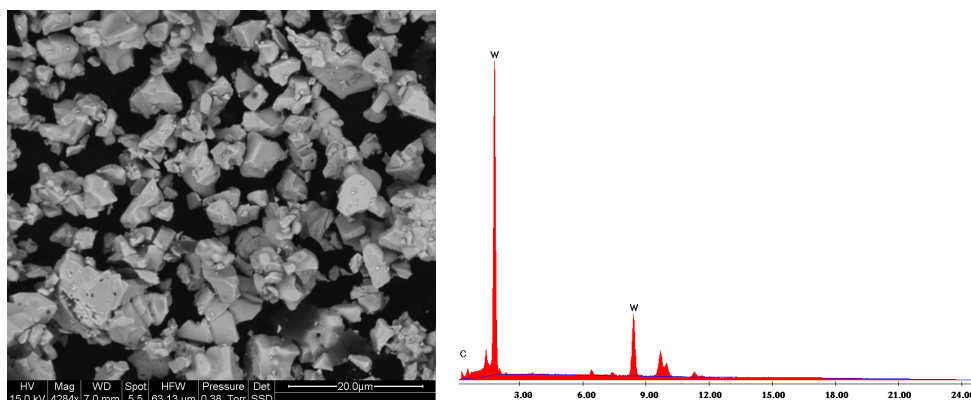


**Figure 3- 13: Left: SEM micrograph indicating WC grains in powdered sample heated for 40 s at 3 kW. Right: EDX graph indicating presence of only W and C in the sample.**

Despite the inaccuracy of EDX for light atoms it supported the results from both PND and XRF/combustion analysis. The confirmation of carbon non-stoichiometry in the product also explains the observation of small, yet significant differences in lattice parameters for a number of WC products. Table 3- 4 reports a series of pure-phase WC products synthesised in 30 s in the single mode cavity and their corresponding lattice parameters and W and C occupancy (achieved via XRF/combustion analysis).

a-parameter, Å	c-parameter, Å	W: C occupancy
2.9074(4)	2.8387(5)	-
2.9103(5)	2.8416(2)	1.00:0.98(1)
2.9081(8)	2.8395(3)	1.00:0.98(1)
2.9086(1)	2.8391(4)	-

**Table 3- 4: Variation in lattice parameters for synthesised WC**

This carbon non-stoichiometry is no-doubt prevalent in the WC products due to the synthesis method. The ultra-rapid reaction time means homogeneity of the reaction mixture is extremely important. Unfortunately “perfect” homogeneity is impossible to achieve so carbon non-stoichiometry seems inevitable. Regrinding and re-heating the sample makes little difference to the crystal structure with the possibility of reaching a 1:1 ratio of W:C being difficult due to the short irradiation time of the sample. Unfortunately XRF was not accurate enough to notice the subtle changes in carbon stoichiometry with lattice parameters. However, PND could be used to characterise additional samples for a comparison, which could confirm this hypothesis about carbon non-stoichiometry affecting the crystal structure. Regrettably, beam time is difficult to obtain and is certainly not within the scope of this thesis. Despite this, carbon deficiency is only slight, with samples tested recording a ratio of greater than 0.7:1, C:W, which is within the reported specifications for industrially manufactured WC.<sup>5</sup>

As an extension of this work, the study of carbon stoichiometry *in-situ*, as the reaction progressed, would provide invaluable information on WC formation. PND would be ideal for this, as described in this section it is possible to accurately refine C stoichiometry. This technique could also provide information on the formation of the carbide, from the reactants and the decay of  $W_2C$ , but importantly could shed light on the carbon stoichiometry in the WC product throughout the reaction. Harrison et al. have begun to look at in-situ analysis with successful experiments using PND to study phase behaviour and thermal expansion of  $BaTiO_3$  during microwave heating at 1 kW.<sup>48</sup> In this instance the authors used a pyrometer to monitor the sample

surface temperature and collected data at specific temperatures resulting in some unexpected structural observations compared to a sample heated conventionally. A larger cubic cell parameter, but smaller anisotropic displacement parameters (ADPs) were observed in the MW heated sample. It was suggested that the increased cell volume was due to higher temperatures within the sample than are recorded at the surface. However the low ADPs, which contradict this, arise from damping of certain forms of ion motion by the microwave field. The data also suggested, due to a significant increase in fitted peak width parameters, the existence of hot spots or at least thermal gradients within the sample. Although this experiment was carried out over a much longer timescale than the work reported in this thesis, this experimental technique is still worth taking into consideration.

Similar work by Kisi et al. studying combustion synthesis of  $\text{Ti}_3\text{SiC}_2$ ,  $\text{Ti}_3\text{AlC}_2$ ,  $\text{Ti}_5\text{Si}_3$  and compounds in the system Ni-Al-Ti-C was carried out using neutron diffraction to monitor phases at specific times.<sup>49</sup> The temperature was ramped at 100 to 200 °C/min towards 1100 °C and diffraction patterns were recorded for 200 to 500 ms with detector read-out times between 80 and 300 ms over the given reaction period. Phase fractions and sample temperatures were determined *in-situ* and so the kinetics and activation energies of diffusion controlled phase transitions could be determined. Although the samples were heated conventionally it would be possible to perform very similar treatments using microwave irradiation with a similar setup to Harrison et al.<sup>48</sup> In addition, with the data collection timescale used by Kisi, it would be possible to collect *in-situ* phase information for the formation of WC despite the total reaction

time over less than 60 s. This data could well reveal, in detail, the phase progression throughout the reaction as well as structural information on each phase providing further understanding on the microwave heating reaction mechanism.

### 3.4.2 Effect of excess graphite on WC formation

The role of carbon was considered by evaluating the effect of various wt % excesses on reaction temperature and product phase composition (7). Figure 3- 14 shows the variation in sample temperature and WC phase fraction during the reaction process at 3 kW in the single mode cavity. Arrows presented on the graph are purely to guide the eye.

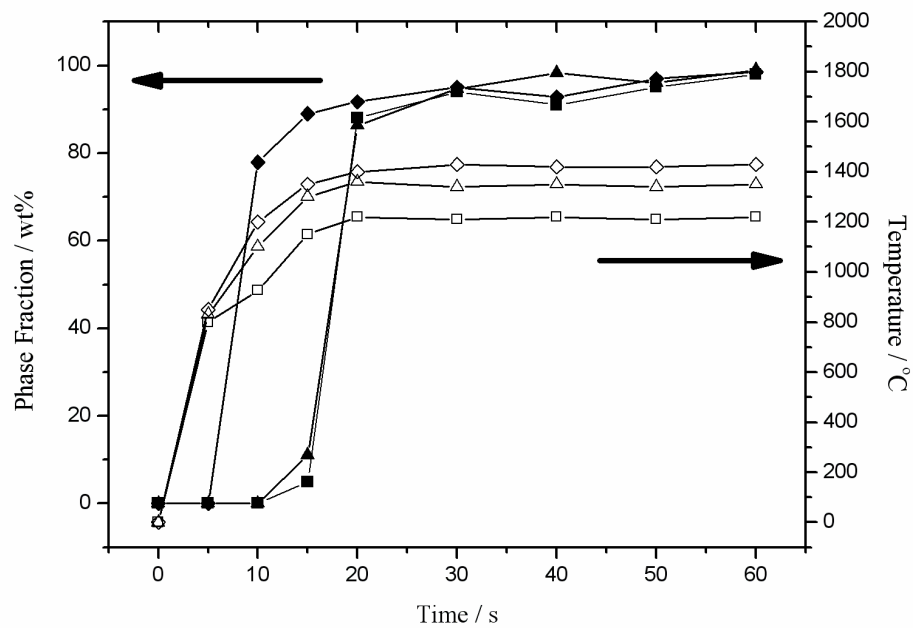


**Figure 3- 14: Reaction temperature and WC phase fraction vs. reaction time at 3 kW applied power for 0 wt % (squares), 10 wt % (triangles) and 20 wt % (diamonds) excess C. Open symbols denote temperature and filled symbols denote WC phase fraction.**

From Figure 3- 14 it was seen that within 20 s for each reaction, the sample temperature (at the pellet surface) had exceeded 1200 °C. Increasing the wt % of carbon beyond the stoichiometric amount leads both to an increase in heating rate over the initial stages of the reaction and an increase in overall reaction temperature. The reaction temperature plateaus in each case after 20 s. Using a 20 wt % excess C leads to almost 80 wt % WC within 10 s, approximately half the time taken for reactions with a 0 or 10 wt % excess to reach a similar stage. All three reactions produce ~ 95 wt % WC within 30 s (Figure 3- 15).

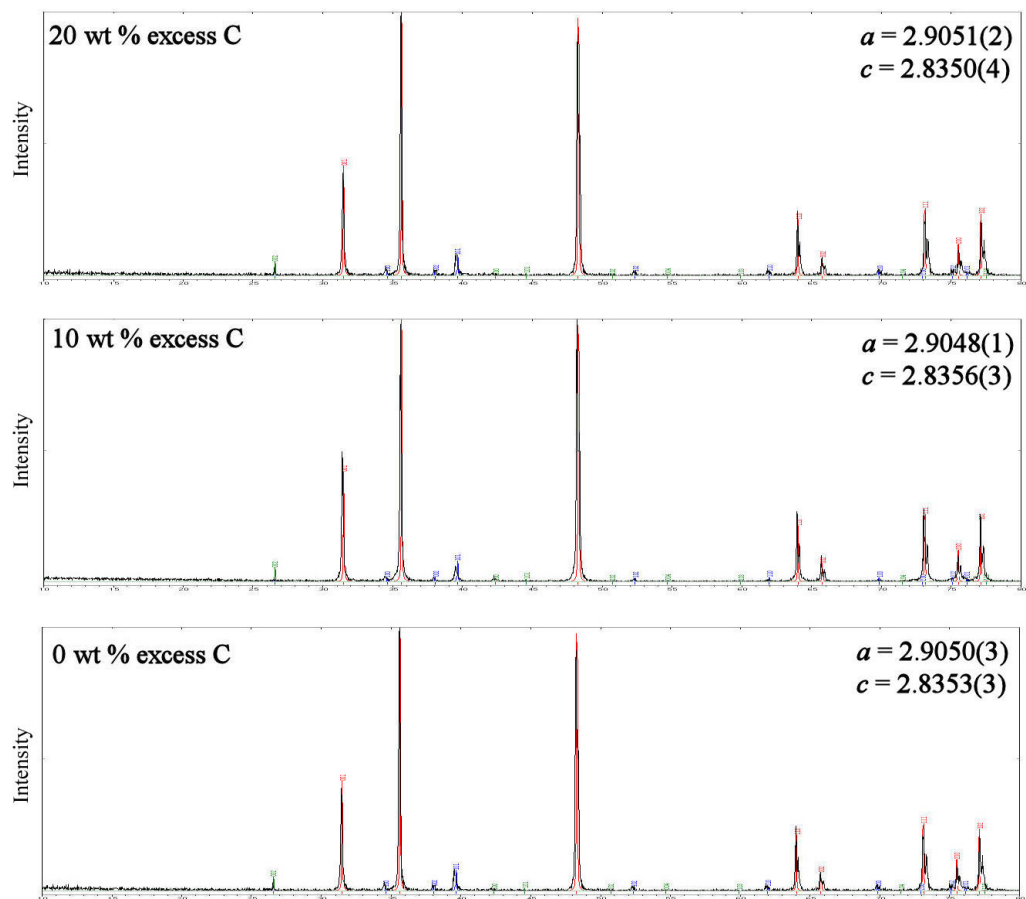


**Figure 3- 15: PXD patterns for samples (black lines) heated for 30 sec in the single mode cavity with 3 kW applied power compared to calculated patterns for WC (red line), W<sub>2</sub>C (blue line) and graphite (green line).**

Importantly, the indexed cell parameters of the product, WC, do not change significantly as the C excess is varied (Figure 3- 15), suggesting again that a 1:1 W:C starting ratio produces stoichiometric WC and also that the excess C either remains as an amorphous by-product or is oxidised to CO/CO<sub>2</sub>. Similar behaviour, for example, is observed in the MW synthesis of  $\beta$ -SiC using an excess of carbon (in either air or relatively inert atmospheres).<sup>50,51</sup>

Perhaps the main result of significance from Figure 3- 14 is the correlation of WC phase fraction with temperature. Below 20 s the formation rate of WC is extremely rapid, but after this point the rate slows dramatically coinciding with the temperature plateau. From phase sampling, it is observed that WC formation is rapid when the reaction temperature reaches *ca.* 1200 °C. With reference to the changes in loss tangent observed in Figure 3- 10 and the data observed in Figure 3- 14, it is clear that as one increases the wt % of excess C the heating rate dT/dt increases over the early period of the reaction (especially  $5 < t < 15$  s) suggesting that the bulk dielectric loss of the reaction mixture is further improved by a greater proportion of C (vs W and evolving WC). However, at least as important is the evidence that the addition of 10-20 wt % excess C not only has little effect on final product composition and phase purity but also little effect on the self-limiting heating phenomenon, suggesting again that at  $T > 1700$  K excess C is lost as CO/CO<sub>2</sub>. Hence adding  $\leq 20$  wt % excess C provides the benefit of faster heating without leading to thermal runaway or loss of sample purity.

During phase sampling, as mentioned above,  $W_2C$  was observed to decline steadily with the formation of WC (Figure 3- 16). This observation is not unusual, however, the subtle differences between observations in the DMO and single mode are worth discussing, as well as the effect of excess carbon on  $W_2C$  formation. The existence of  $W_2C$  in the final product is not uncommon and as a consequence it is a recognised by-product in the industrial synthesis of the mono-carbide.<sup>40</sup> However, the role of  $W_2C$  in the formation of WC has never been fully investigated. Provided  $< 2$  wt % is present in the final product the sample is deemed satisfactory.<sup>52</sup>

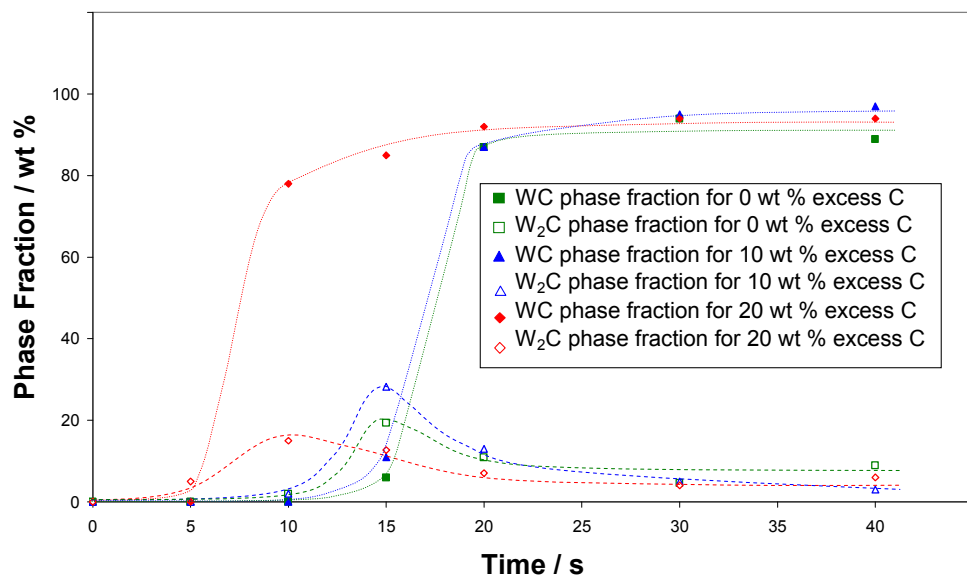


**Figure 3- 16: WC (dotted lines, filled symbols) and  $W_2C$  (dashed lines, open symbols) Phase fraction vs. time at 3 kW applied power. Red lines apply to 20 wt % excess carbon reactions, blue lines apply to 10 wt % excess carbon reactions and green lines apply to 0 wt % excess carbon reactions.**

As discussed in section 3.3,  $W_2C$  seems to play a role in the formation of the desired carbide, WC. As an intermediate phase,  $W_2C$  is formed prior to WC at *ca* 1000 °C and begins to decay away above 1200 °C with the rapid formation of WC. Due to the rapid reaction times involved the  $W_2C$  phase fraction never reaches much more than 25 %, unlike experiments using a DMO (section 3.3). This is no doubt due to the rapid temperature rise and resultant formation of WC, however, there is still a clear preference for  $W_2C$  formation in initial stages of the reaction. This is most obvious in reactions involving 10 wt % excess carbon or less, where the temperature rise is not as rapid (Figure 3- 14). For experiments involving a carbon excess of 20 wt %, formation of  $W_2C$  does occur, but is overshadowed by the formation of WC. This is observed in the shallower trend line observed in Figure 3- 16. Encouragingly though it seems  $W_2C$  synthesis still occurs despite the temperature reaching 1200 °C in only 10 s. This indicates that this phase does indeed play a part in the synthesis of the mono-carbide with much of the tungsten present preferentially forming this phase prior to decaying into WC.

### **3.4.3 Sample volume variation: Experimental scale up**

Experimental scale up, from laboratory to industrial, is an important part of industrial relevant materials. Tungsten carbide is obviously such a material and is used in numerous applications with an estimated 20, 000 tons manufactured annually.<sup>5</sup> For this reason experimental scale up is vitally important if microwave synthesis of WC is going to have any “real world” applications.

In these experiments, samples of varying masses were treated up to 60 s (8); any longer than this and the experiments became unsafe (for example reaction vessel failure) with unpredictable results. For the 10 g pellets, surface temperatures in excess of 1000 °C were observed after 10 s with the temperature rising rapidly initially, followed by the expected plateau. However, unlike experiments with the smaller pellet volumes the temperature never truly levelled off, but continued to slowly rise. Heating of the 20 g pellets resulted in a relatively slow temperature rise compared to previous small volume experiments. More graphite susceptor (~ 5 g) was required to counter this, to a point where penetration depth of the microwaves became an issue (~ > 4 mm).

Analysis of all the pellets revealed little formation of WC. Figure 3- 17 shows two PXD patterns collected *ex-situ* post-reaction. Samples (weighing 10 g and 20 g) had been heated for 60 s in both cases.

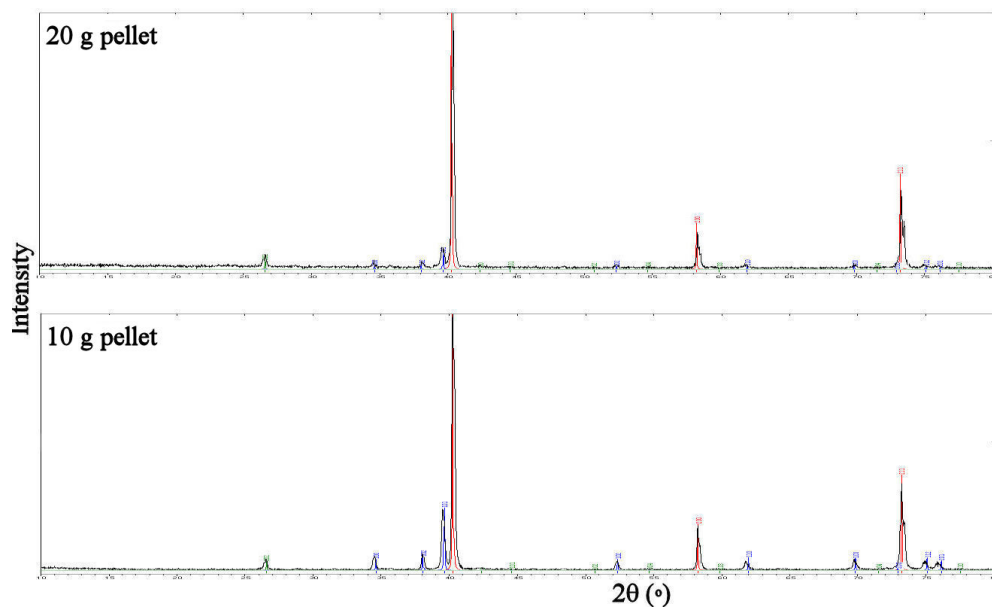


**Figure 3- 17: PXD patterns for samples (black lines) heated for 60 s in the single mode cavity with 3 kW applied power compared to calculated patterns for W (red line), W<sub>2</sub>C (blue line) and graphite (green line).**

It can be clearly seen from Figure 3- 17 that the pellets mostly constitute the reactants, W and C, with some  $W_2C$ . Even with heating times of 60 s no WC is observed. It was concluded that the sample volumes involved required longer heating times for complete WC formation to occur, however this was not possible with the present configuration. The reactor would need to be designed to suit the load (sample volume) as well as adapting the experimental procedure. In addition the graphite susceptor was still required, despite the larger sample volume; however, this is not unexpected given the dielectric property measurements reported in section 3.3.1. At present, batch processing of large scale tungsten carbide, with the current reactor, is not possible within the timescales hoped due to both safety issues and the issues associated with increasing the mass of the susceptor used. However, it would be possible to irradiate multiple small-volume samples, which could then be ground together post-reaction and sintered. This is one possible route, using the current single mode applicator; however, development of a new reactor would be more prudent. For the sample sizes investigated a much smaller cavity size would be ideal, allowing for better tuning of the microwave energy and thus maximising the power density at the sample position. This would result in less power being reflected and more absorbed by the sample which should allow for larger volumes of sample to be irradiated in any given batch experiment. It could also be possible, if the batch process was going to be pursued, to install an automatic sample arm which could raise samples into the cavity where they are irradiated for a given time while their temperature is monitored. The sample could then be lowered, a new sample positioned in the arm and the

process restarted. Despite the need for sample changes, the rapid reaction time more than makes up for this.

Another alternative for cavity design is to take a continuous processing approach. In theory this may provide the best solution for WC synthesis. Although this is not possible to test with the current setup, it would be possible to irradiate multiple small pellets at once, or one at a time on a belt system. The W + C pellet, imbedded in graphite, could be fed through the single mode cavity with the WC pellet removed post treatment. The graphite susceptor could then be recycled to heat more of the reactant mixture. Unfortunately cavity design and modelling is beyond the scope of this thesis.

#### **3.4.4 *In-situ* analysis**

Most analysis at present, with respect to microwave heating, is performed *ex-situ*. Obviously within the microwave field at high temperature, samples can have vastly different properties than at room temperature, but these are very challenging to measure *in-situ* due to awkward cavity design and rapid synthesis times and interaction of any probes with the electric field. Although efforts have been made to look at sample properties at elevated temperature, for example dielectric property measurements (section 3.3.1), it is still performed *ex-situ* and so is not a completely accurate representation of what is occurring during the reaction. If microwave heating in the solid state is truly to be understood then *in-situ* analytical techniques must be employed. The information obtained from these techniques, such as both surface and bulk

temperature measurements, is invaluable in explaining and understanding the reaction mechanisms, specifically those of carbide synthesis.

As part of an effort to develop these *in-situ* techniques, reported here are experiments involving high speed photography and thermal imaging. It was hoped that such techniques could shed more light on visualising the reaction process within the cavity over very short timescales.

#### ***3.4.4.1 High speed Photography***

High speed video was carried out using a Photo-Sonics Phantom V7, on loan from the EPSRC engineering equipment pool (9). With the use of this camera it was hoped that real-time footage could be obtained of the reaction process, particularly at the point at which WC formation is initiated. With the aid of previous results this was determined to be around 5 s (section 3.4.1). The initiation of the reaction also seems to be concurrent with a flash observed from within the cavity, which can easily be spotted with a conventional video camera. However, this is over in a fraction of a second and so impossible to analyse without the use of high speed photography. The camera records permanently on a loop and contains a buffer which permanently stores a given amount of frames. The camera can then be set up to, when a button is pressed, permanently record a set number of frames stored before the button is pressed, as well as a certain number after. This can account for delay from the naked eye thus allowing the user to record information as it is observed making sure that none of the crucial footage is missed.

The video of footage taken from the reaction  $W + C \rightarrow WC$  (8), is located on the attached CD (WC\_high\_speed.avi) where it can be seen in its entirety. Figure 3- 18 shows two stills taken from this footage, which identify key moments in the synthesis of the carbide. The top still is taken 5 s into the reaction and the bottom still 417  $\mu$ s after (5.000417 s after reaction initiation). Both stills contain the pellet, surrounded by graphite powder, within an alumina crucible.

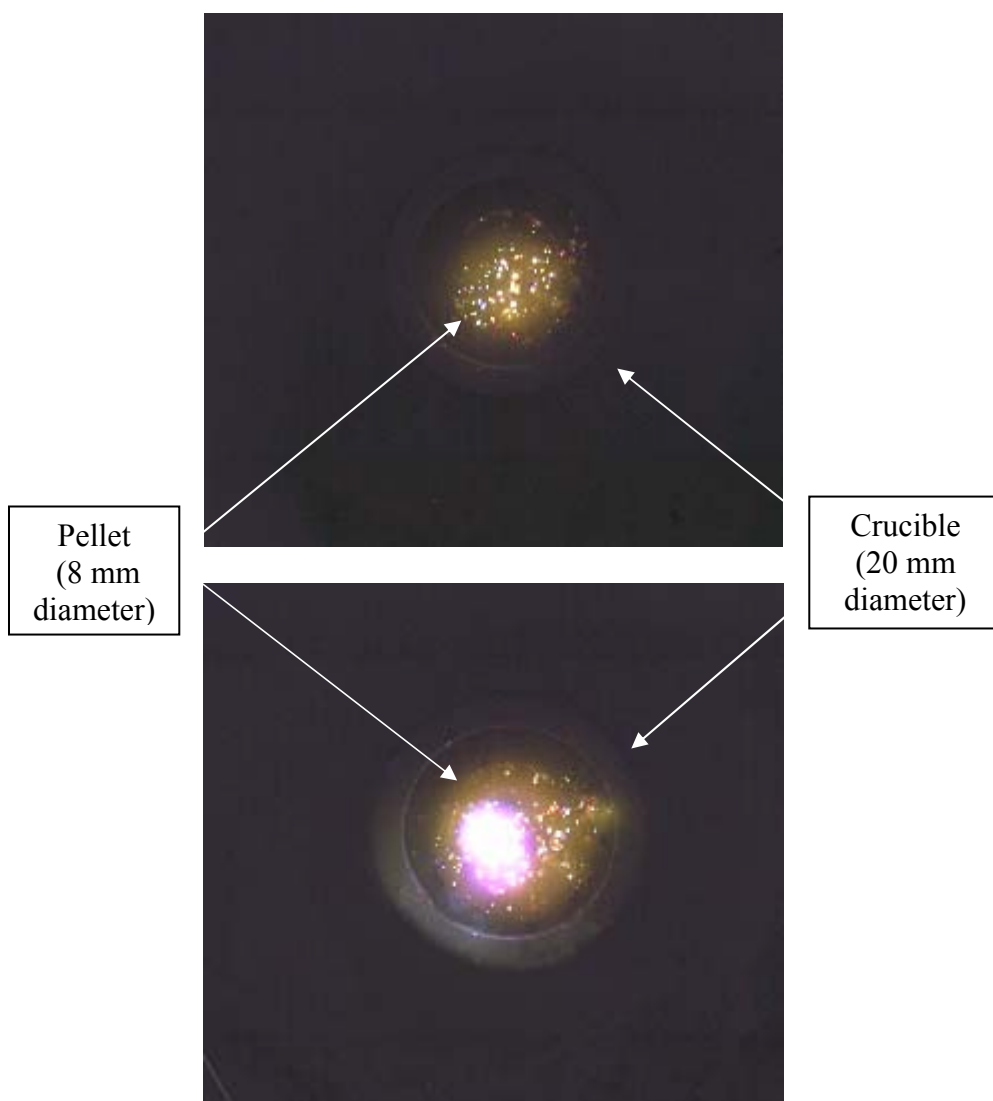
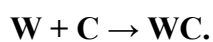


**Figure 3- 18: Stills taken in-situ using a high speed camera of the reaction**



It can be seen from the top still in Figure 3- 18 that after five seconds localised heating is occurring at the surface of the pellet. It appears that heating by the microwave field is occurring selectively, although it is unclear whether this heating is exclusively C or W, or a mixture of both reactants. One, however, could suggest that the observed heating is C due its known reactivity and rapid heating rates in microwave fields.<sup>22, 23</sup> The rapid and effective heating of graphite powder has also been observed in the single mode cavity, when heated at 3 kW, with temperatures rising rapidly to over 1000 °C in 5 s. Conversely W powder, when heated in the same applicator at 3 kW for 1 min, showed no registered change in temperature with the optical pyrometer (minimum recorded temperature is 600 °C).

The rapid heating of graphite can be explained by the complex structure of graphite. Electrical conductivity parallel to the layers is reported as  $3 \times 10^6 \text{ Sm}^{-1}$ , similar to a metal, whereas perpendicular to the layers graphite behaves as a semiconductor with electrical conductivity reported as  $5 \times 10^2 \text{ Sm}^{-1}$ .<sup>53</sup> As a semiconductor the conductivity increases with temperature, whereas for a metal the opposite applies.<sup>53</sup> This low conductivity perpendicular to the layers allows the material to absorb microwave energy efficiently at room temperature unlike the high surface voltages observed for high conductivity metals e.g. W is reported as  $17.9 \times 10^6 \text{ Sm}^{-1}$  at room temperature, decreasing to  $4.7 \times 10^6 \text{ Sm}^{-1}$  at 900 K.<sup>54</sup> The high electrical conductivity exhibited by metals does not allow for efficient bulk microwave heating and it is not until higher temperatures are reached that the conductivity of the metal decreases to facilitate heating.

A few frames later (417  $\mu$ s) (bottom still) a flash is observed which corresponds to the initial formation of WC measured ex-situ using PXD. Currently, as seen in section 3.4.1, the reaction profile is recorded by analysing pellets at 5 s intervals. With the observation seen in the second still, and the short time between frames, it is possible that the formation of WC is almost instantaneous, however this is difficult to verify with the current experimental setup. Unfortunately accurate results can only be obtained at a minimum of 5 s intervals, below this the errors involved in controlling reactor power, monitoring heating time and sample removal from the cavity are too great, resulting in no noticeable difference in phase analysis post-reaction. In other words, it is easy to over or under react the sample by a few seconds and if only 2.5 s exist between sample reaction times, it is easy for results to overlap.

Analysing the video (WC\_high\_speed.avi), the progress of the reaction can be seen clearly. The heating observed locally, shown in the stills above (Figure 3- 18), is also observed in the graphite susceptor surrounding the pellet. Although this again suggests that the selective heating initially observed in the pellet could indeed be graphite, it is by no means proof. However this selective heating does point towards some possible reaction mechanisms. It is possible that interfacial polarisation is occurring with the carbon being heated dielectrically and the existence of very high temperatures between the grains. This would explain the ultra-rapid synthesis time of WC; knowing the optical pyrometer is only capable of acquiring an average temperature over an area and so would not be able to observe these localised temperatures. Although at present it is difficult to confirm this mechanism, it could well be possible to use

infrared microscopy to achieve this, as demonstrated by Sato et al.<sup>55</sup> In an important piece of work, Sato examined the microwave heating of bronze using IR microscopy showing it is possible to observe the selective heating of particles and follow their diffusion through the sample. If this could be applied to the work reported here, it may be possible to investigate the reaction mechanism further. However, the microscope needs to be very close to the sample which is not possible in the current single mode applicator.

An alternative heating mechanism is that the W is purely heated by conduction from C. If the localised heated observed in still 1 (Figure 3- 18) is indeed C, coupled with the evidence above indicating the poor heating of W in the microwave field, it is possible that carbon is being heated selectively and the heat generated being conducted by W. In turn the temperature of W is raised, along with its loss tangent as seen in section 3.4.1, to a point where it too begins to absorb microwave energy (as the electrical conductivity of the metal decreases with temperature). One must ask now if this is possible given the temperatures observed and the reaction times for pure-phase synthesis of WC? In truth there is no evidence to confirm or deny this mechanism, but the lack of understanding as to the procedure of solid state microwave reactions means an answer is going to be difficult. However, research to build on this understanding is being conducted. For example Whittaker has presented proof that microwaves can directly influence ion transport during a high temperature sintering process.<sup>56</sup> In the experiment  $\text{YbBa}_2\text{Cu}_3\text{O}_7$  was embedded in  $\text{YBa}_2\text{Cu}_3\text{O}_7$  and the diffusion of  $\text{Y}^{3+}$  into the former sample was reliably observed. Pellets of the materials were heated in a single mode cavity for

between 2 and 12 days with enough power to maintain a constant temperature of 750 °C. Pellets were subsequently dissected and the phase interface was found using Scanning Electron Microscopy (SEM). Elemental mapping of the ion distributions was carried out locally using X-ray Fluorescence (XRF) spectroscopy. By simply comparing the ratio of diffusion coefficients for motion parallel and perpendicular to the electric field it can clearly be seen that in the initial stages of the reaction (first few days) the diffusion of the ions is enhanced by the microwave field. This influence decreases with time however as the sample microstructure changes during sintering: the grains fuse together resulting in diminished diffusion enhancement.

Clearly future work in this area is required, particularly if further understanding of solid state microwave heating is to be obtained. Regardless, the *in-situ* high-speed photography has produced exciting results. The clear observation of localised heating, probably graphite, and the subsequent reaction flash, suggest possible reaction mechanisms. In addition the observations agree with PXD information obtained from single mode experiments (section 3.4.1). The ultra-rapid nature of the reaction is also observed with the reaction initiation occurring in less than 500  $\mu$ s implying the reaction may be almost instantaneous.

#### ***3.4.4.2 Thermal imaging***

Although the optical pyrometer provides accurate *in-situ* temperature measurements, it is not possible to view the changes in specific temperature over the pellet surface. For this thermal imaging was used (FLIR ThermaCAM

SC3000, courtesy of EPSRC engineering pool) with a view to recording live video footage of the temperature changes during the reaction;  $W + C \rightarrow WC$  (9). Data were collected in real-time and the subsequent 9 s of recorded footage, surrounding the reaction initiation, is available on the attached CD (WC\_thermal.wmv).

Figure 3- 19 shows two stills taken from the recorded footage. Still 1, on the left, was taken 3 s after the experiment begun. Still 2, on the right, was taken 2 s after still 1, a total of 5 s from the beginning of the experiment. The position of the crucible, graphite susceptor and pellet are indicated on both stills.

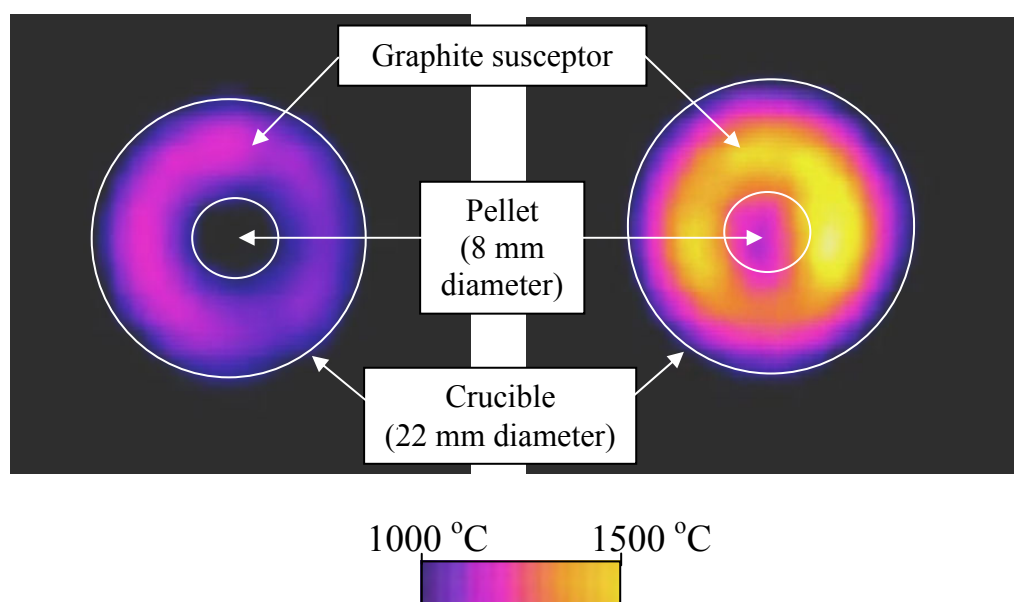


**Figure 3- 19: Stills taken in-situ using a thermal imaging camera of the reaction  $W + C \rightarrow WC$ .**

Although only capable of surface imaging, the thermal imaging footage was able to show the initial heating of the graphite susceptor (Figure 3- 19, left

still). Prior to 5 s (before still 2) this is all that is observed, with the black spherical shape in the centre indicating the presence of the pellet. The black around the crucible is the silica flour which is supporting the crucible within the cavity. At 5 s the temperature of the reaction, observed with the thermal imaging camera, is already much hotter with the pellet now higher than 1200 °C. Specifically, at 5 s, the temperature of the pellet was recorded at 1178 °C in the centre (see arrow point on right still in Figure 3- 19), however, the temperature of the pellet varied across the surface. This can be seen in still 2, with a variation in colour across the pellet, indicating slightly different temperatures. This is no doubt due to the influence from the much hotter graphite susceptor, seen clearly in Figure 3- 19, which surrounds the pellet. Crucially, the footage collected corroborates the temperature data obtained from the optical pyrometer regarding the pellet surface temperature. Unfortunately, due to the placement of the thermal imaging camera, the optical pyrometer could not be used in conjunction with the camera; however, the comparison of the data collected is sufficient to confirm the accuracy of the temperature measurements collected with the optical pyrometer.

The thermal imaging results can also be directly compared to the footage collected from the high speed photographic experiments. As discussed in section 3.4.4.1, the reaction was observed to initiate at 5 s with a recognisable flash from the pellet. This coincided with the initial stages of carbide formation observed from the PXD data collected from the reaction profile study (section 3.4.1). Prior to this localised heating of the pellet was observed, thought to be graphite powder present in the reaction mixture.

Although thermal imaging and high speed photography could not be run concurrently, a comparison between the data collected in both cases revealed an agreement between the changes observed at 5 s. The sudden increase in temperature at 5 s, observed with thermal imaging, was no doubt due to the flash observed at the same time through thermal imaging. Unfortunately the thermal imaging camera was not able to pick up the localised heating observed in the high speed footage. This could be due to the sensitivity of the camera, but is more likely due to the rapid nature of the reaction initiation. Thermal imaging footage was captured in real time and thus was not capable of observing the temperature changes on the  $\mu\text{s}$  scale. Despite this the footage collected was encouraging with the data agreeing with observed results from phase fraction and high speed photographic experiments. However, the technique is still only capable of *in-situ* surface temperature measurements. Therefore it is not possible to verify the temperature gradient between the centre of the pellet and the surface with the high internal temperatures suspected to be the cause of the ultra-rapid synthesis times.

### **3.4.5 WC synthesis from tungsten oxide, $\text{WO}_3$**

Synthesis of tungsten carbide from tungsten oxide is far more economical than from pure  $\text{W} + \text{C}$ . The oxide is much cheaper than tungsten metal and for this reason industry favours reduction of the oxide prior to synthesis of the carbide. This is usually achieved by reduction involving carbon as well as a reducing hydrogen atmosphere. It is well known that the oxide,  $\text{WO}_3$ , proceeds through intermediates, such as  $\text{WO}_2$ , to afford  $\text{W}$ , however, the

carbide is only formed after the oxide has been completely eliminated.<sup>40</sup> Conventional synthesis is usually a two-step process with tungsten oxide being reduced to tungsten metal prior to reaction with carbon to form the carbide.<sup>57</sup>

Microwave synthesis of WC from WO<sub>3</sub> was attempted in a one-step process **(10)**:



It was hoped that reduction of the oxide would occur *in-situ* to afford tungsten metal, which would subsequently react with graphite to afford WC. Section 3.2 describes the experiment carried out, with detail of the experimental procedure found in section 2.2. Heating of the pellets was carried out with 3 kW applied power with heating times varying up to 60 s. However, with the experimental configuration used, a major problem was encountered in the synthesis of WC: the pellet was often observed to shatter into multiple pieces. Due to the rapid temperature rise in the initial stages of the reaction, rapid evolution of CO/CO<sub>2</sub> gas occurs, causing the pellet to fracture. This evolution was confirmed by thermal analysis and mass spectrometry (section 2.3.9) (Figure 3- 20). Stoichiometric amounts of the reactants WO<sub>3</sub> and C were ground together to afford the products WC and CO<sub>2</sub>. The sample was heated from 20 °C to 1400 °C with a ramp rate of 10 °C/min under flowing argon. A mass spectrometry scan was taken every 60 s. Thermal analysis revealed the reduction of the oxide beginning at ~900 °C and mass spectrometry indicated the majority of gas evolved was CO with small amounts of CO<sub>2</sub>. All other

peaks present in the mass spectrograph are due to the argon gas and its associated impurities. The optical pyrometer recorded a temperature of over 800 °C in less than 5 s for any given experiment, with reduction of the oxide expected at this point due to the data collected from thermal analysis. By 5 s an average temperature in excess of 1200 °C was recorded. No doubt this rapid temperature rise on such a short timescale is the main contributing factor to the pellets becoming bloated and disintegrating due to gas evolution.

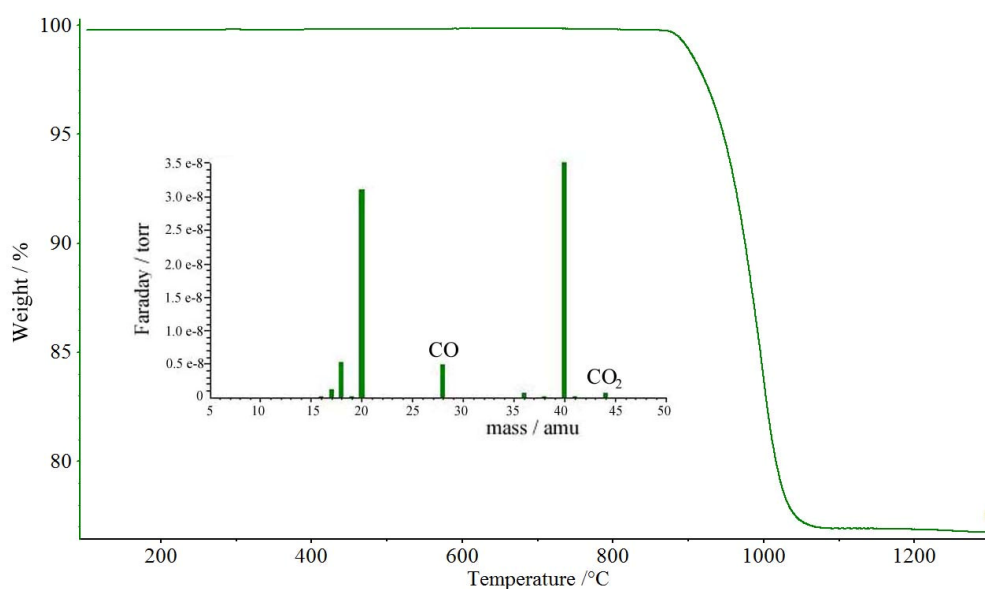


**Figure 3- 20: Thermal analysis and mass spectrometry result for the reaction  $2\text{WO}_3 + 5\text{C} \rightarrow 2\text{WC} + 3\text{CO}_2$  showing the reduction of  $\text{WO}_3$  beginning at  $\sim 900$  °C and the corresponding  $\text{CO}/\text{CO}_2$  evolution indicated by mass spectrometry.**

Unfortunately reducing the applied power, and so the decreasing the temperature ramp rate, was not possible in the 3-15 kW applicator. At this time the 1 kW reactor was also unavailable and so in an effort to improve the synthesis of WC the cavity was deliberately “un-tuned”. By un-tuning the

cavity the electric field is offset from the sample position resulting in a decrease in the power density at the samples location. In order to achieve this, the automatic tuner was set to manual and adjusted to increase the total power being reflected back towards the generator. This resulted in only around 1 kW of microwave energy being absorbed by the sample. Although this did not solve the problem entirely, with some pellets still disintegrating, a number of pellets were successfully heated with reaction times up to 60 s. Figure 3- 21 shows PXD data collected for samples heated for 0, 30 and 60 s.

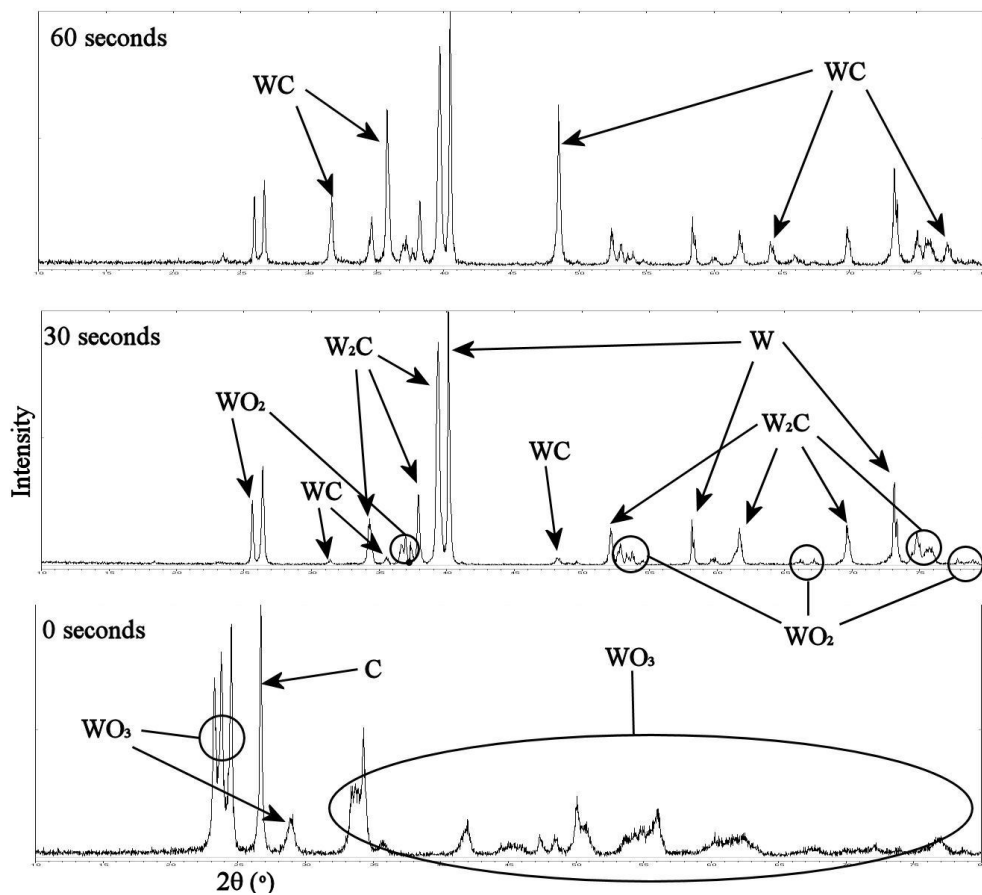
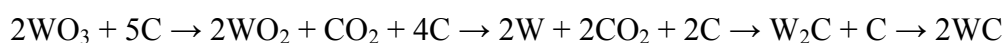


**Figure 3- 21: PXD patterns for reaction  $2WO_3 + 5C \rightarrow 2WC + 3CO_2$ .**

**Pellets were heated at 3 kW for 0, 30 and 60 s respectively.**

At 0 s the only phases to exist are the reactants,  $\text{WO}_3$  and C. As the reaction progresses the reduction of  $\text{WO}_3$  to  $\text{WO}_2$  is observed and by 30 s the complete reduction of the tri-oxide to the di-oxide has occurred. 30 s also shows the existence of W (~22 wt %), indicating  $\text{WO}_2$  has reduced further to the metal. Crucially two carbide phases are also observed,  $\text{W}_2\text{C}$  (~32 wt %) and a small quantity of WC (~2 wt %). The formation of these W-C phases contradicts previous reports that this is not possible until all the oxide has been reduced,<sup>40</sup> By 60 s the phase profile has changed drastically once again. Although all phases present at 30 s are still visible, WC is much more prominent (~26 wt %) with  $\text{W}_2\text{C}$  still a major phase (~24 wt %). The oxide,  $\text{WO}_2$ , still exists as well as W metal, although both phases have diminished slightly. Within the timescale, 0 – 60 s, it is apparent that the one step reaction attempted was successful. The reduction of the oxide and subsequent formation of the carbide, WC, was achieved, although within the 60 s reaction a pure-phase of WC was not observed. However, from the PXD data, it appears the reaction occurs as follows:



As the reaction progresses, however, it is possible that WC is formed preferentially to  $\text{W}_2\text{C}$  as the reaction temperature increases. This is observed in reactions involving the metal powder and C, however, in this case no evidence supports this observation. It is likely though that the *in-situ* formation of the carbide from W, post-reduction of the oxide, closely follows the synthesis of WC from W and C.

An important visual observation between the PXD patterns at 30 and 60 s is the relative similarity in the profiles, bar the obvious change in WC wt %. Perhaps this small relative change in all phases, save WC, verifies  $W_2C$  acting as an intermediate phase for the production of WC. In addition the reduction of the oxide to the metal must occur before any carbide is formed. However, the presence of W in the diffraction patterns indicates that the formation of the carbide is slow in comparison to the reduction of the oxide. In fact the reduction of  $WO_3$  to  $WO_2$  seems to be rapid, with no evidence of the phase by 30 s. The literature supports this information, with an *in-situ* PXD study of the synthesis of WC from  $WO_3$ , using a  $CH_4/H_2$  mixture for reduction of the oxide and as the source of the carbon, indicating the rapid reduction of the tri-oxide between 600 – 650 °C.<sup>58</sup> As soon as the required temperature is reached, complete reduction to  $WO_2$  is rapid, with  $W_2C$  formation also observed. Interestingly W metal is never observed in the PXD data, seemingly, as it is formed, it must react instantaneously with C to form the carbide, WC. The majority of PXD data were collected every 100 °C, with the temperature increased at 1 °C/min. This results in a time between scans of 100 min, which results in a complete reaction time of around 240 min. Due to this long reaction time, it is likely the W metal is never observed as sufficient time allows for the formation of the carbide, unlike the observations in the rapid microwave reactions. A second important observation to note is that by 80 min the reduction of the oxide is almost complete, with only  $W_2C$  and WC observed in the PXD phase profile. The reaction is observed for a further 160 min before a near-pure phase of WC is witnessed. However, small amounts of both  $WO_2$  and  $W_2C$  still exist after a total of 240 min heating, which reinforce the results

obtained through microwave heating. The relatively slow formation of the carbide is probably due to the occurrence of phase separation in conjunction with gas evolution from reduction of the oxide. This would result in a non-intimate mix of W and C and thus slow formation of the carbide. However, with the supporting data from the literature, it seems certain that with increased heating times microwave synthesis of the carbide should be possible.

Although synthesis of the carbide, WC, was achieved, analysis revealed a mixed phase product. With a reaction time of 60 s the increase in wt % of WC is clear and one would assume this trend would continue until ultimately a pure-phase WC product was achieved. This prediction is supported by dielectric property measurements at elevated temperature for the reaction mixture  $2\text{WO}_3 + 5\text{C}$  (Figure 3- 22). These results suggest that after 600 °C the loss tangent improves significantly with increasing temperature due to the much greater increase in  $\epsilon''$  compared to  $\epsilon'$ . This would explain the need for a susceptor to initiate the reaction with tungsten oxide as well as suggesting that at high temperature reduction of the oxide and formation of the carbide is probably inevitable given enough time.

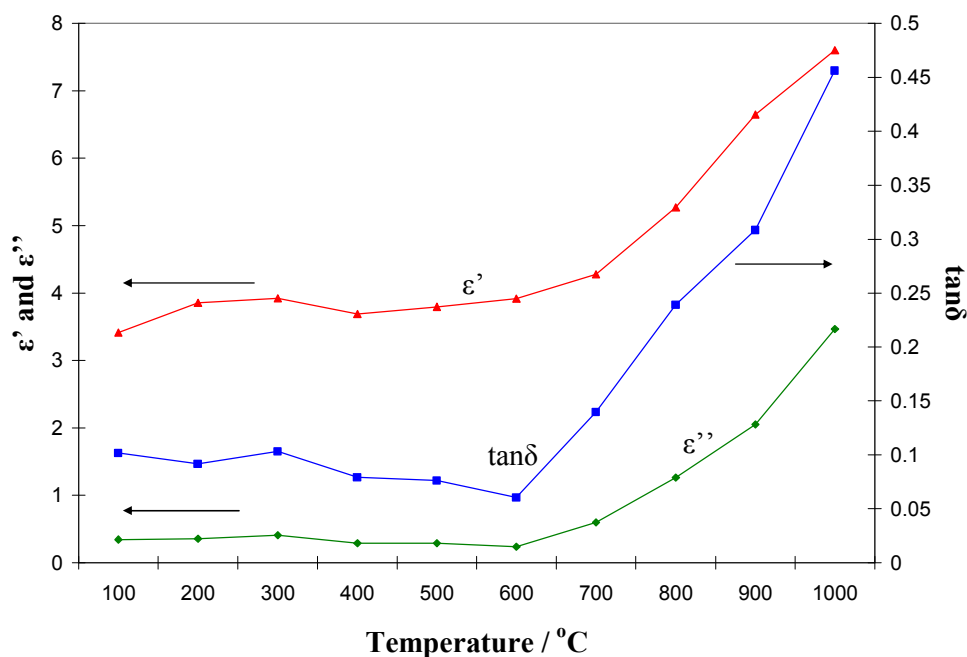


**Figure 3- 22: Plot of relative permittivity ( $\epsilon'$ ), dielectric loss ( $\epsilon''$ ) and resultant loss tangent data with increasing temperature for  $\text{WO}_3 + \text{C}$  reaction mixture.**

Despite the observation, using thermal analysis, that reduction of the oxide began at  $\sim 900$  °C (mentioned earlier in this section), reduction is reported to begin at  $\sim 600$  °C.<sup>52, 59</sup> This would coincide with the change in loss tangent observed in Figure 3- 22 at this temperature. PXD data collected *ex-situ* for a sample,  $2\text{WO}_3 + 5\text{C}$ , heated to  $800$  °C in a conventional furnace (attached to the dielectric property measurement cavity) revealed the existence of  $\text{WO}_2$  and  $\text{W}$  at this temperature (Figure 3- 23). This sample phase change is no doubt related to the increase in loss tangent and would agree with the literature, which reports the reduction of the oxide is carried out in industry between  $800$  and  $1000$  °C to afford  $\text{W}$ .<sup>59</sup>

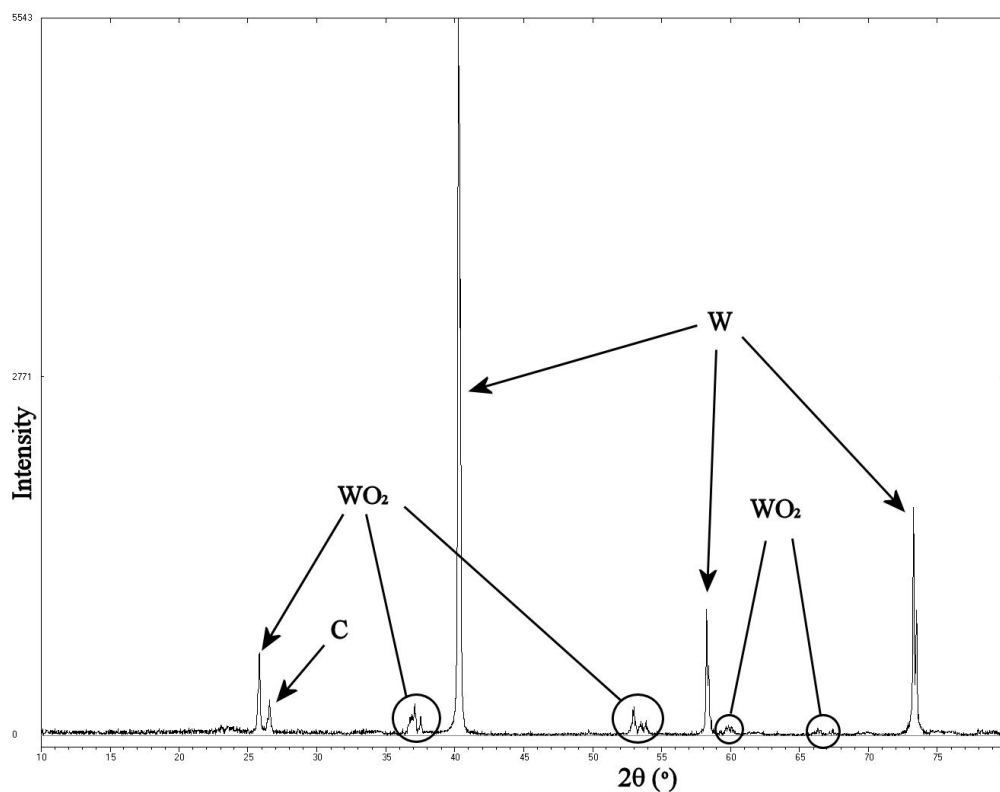


**Figure 3- 23: PXD pattern for  $2\text{WO}_3 + 5\text{C}$  reaction mixture heated to 800 °C in a conventional furnace.**

Unfortunately, due to safety reasons, it was not possible to heat samples for greater than 60 s in order to attempt pure-phase synthesis of WC. Numerous problems were encountered including arcing within the cavity, failure in the reaction vessel and breakdown of the experimental setup. In some cases the heat produced from the reaction was enough to melt the quartz tubing in which the pellet was situated, rendering the pellet impossible to retrieve post-reaction. In rare cases the quartz tube acting as a guide in the single mode cavity, which contained the silica flour, melted resulting in the reaction vessel becoming stuck within the cavity. The possibility of igniting the carbon was also greatly increased with increasing reaction time and so for these reasons experiments were not run for more than 60 s.

Although it was not possible for the experiments described in this section, a variety of novel approaches could result in the successful synthesis of WC from the oxide,  $\text{WO}_3$ . Firstly a better matched cavity, allowing greater control over tuning of the electric field and sample position, would certainly assist in the experimental development. A lower applied power would also be applicable, with work being carried out at a maximum of 1 kW. Although synthesis time may be sacrificed, a greater degree of control over reaction temperature should be possible and ultimately failure of the reaction vessel should not occur. Alternatively it could be possible to design a feedback system which links the applied power directly to the monitored reaction temperature. With slower temperature ramp times, it could be possible to vary the power with regards to the current reaction temperature, to gain further control of synthesis temperature and the reaction itself. If this was the case it could be possible to maintain lower temperatures (between 800 and 1000 °C) while reduction of the oxide occurs. Post-reduction the applied power, and so temperature, could be increased to facilitate carbide synthesis. This however is beyond the scope of this thesis, but is worth considering for future development in this field.

### **3.5 CONCLUSIONS**

Experiments to investigate and synthesise the carbide, WC, have been at the core of the work presented in this chapter. It was the first carbide to be studied using microwave heating and the resulting reactions, carried out in the DMO, resulted in the experimental procedure which was subsequently used in

all transition metal carbide preparations reported in this thesis. Methodical variations in reaction vessels, reaction times, cavity locations, susceptor quantity and pellet placement resulted in the final experimental setup. This was then used to successfully synthesis the carbide, WC, in 30 min in the DMO. Alongside this, the second carbide phase, W<sub>2</sub>C, was also investigated and shown to play a vital role in the synthesis of the mono-carbide. However, successful synthesis of this phase was not possible, although a purity of ~80 % was achieved.



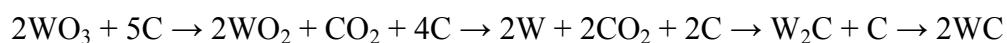
Following the DMO experiments, a single mode reactor was used to continue investigating the synthesis of WC. A direct comparison of the two reactors, as well as a variation in applied power, resulted in a suspected trend in power versus reaction time. From this it was possible to successfully synthesise, at 3 kW in the single mode applicator, a pure-phase of WC in 40 s, with high purity observed at 20 s.<sup>29</sup> Through the study of dielectric properties and *in-situ* temperature measurements an understanding of how the reaction proceeds was then established. The direct relationship between dielectric properties, temperature and WC phase fraction was observed. In initial stages of the reaction (< 5 s), until the temperature reached ~1200 °C, WC formation was minimal. At this point rapid formation of the carbide began and within 15 s (a total of 20 s) an almost pure-phase of WC was observed. In addition the rapid temperature rise, observed initially, had achieved a plateau at ~1400 °C. This confirmed a self terminating reaction as well as, with reference to the very

low loss tangent observed when WC is formed, a link between temperature and the dielectric properties of the sample. Dielectric property measurements with increasing temperature explained the initial lack of WC formation, with the loss tangent not increasing until a temperature above 600 °C was reached. This also explains the need for a susceptor to aid in reaction initiation and synthesis of the carbide. PND analysis of the final product (sample heated for 40 s) confirmed a pure-phase of WC, but also identified C non-stoichiometry in the product, which is believed to be due to the short reaction times combined with non-perfect homogeneity.

The WC reaction has been studied further through the use of in-situ high speed photography and thermal imaging. Both techniques complement the results already collected from previous work, showing agreement with reaction times and the initiation point for carbide formation (5 s). Specifically, the high speed photography has revealed possible reaction mechanisms, interfacial polarisation or conduction, with localised heating being observed. Due to the intense glow observed it is also possible these localised areas are much hotter than expected, although this could not be verified with thermal imaging. This could account for the rapid product formation, although at present this can only be speculated. Thermal imaging was able to verify the temperature data collected from the optical pyrometer as well as confirming the use of the susceptor in the reaction initiation. However, thermal imaging is only a surface imaging technique and was not able to confirm or deny the existence of higher temperatures within the sample.

Additional variables have also been studied related to the formation of WC from W and C. These include the effect of excess carbon within the reaction mixture, showing that, with increasing carbon content, reaction temperature increases more rapidly and plateau at a higher temperature in addition to the formation of the carbide beginning earlier. The presence of  $W_2C$ , as an intermediate phase, was also confirmed in all cases regardless of carbon excess. The effect of pellet volume was also investigated, with various problems encountered with fragility and product formation. With reaction times up to 60 s, only W and C with small amounts of  $W_2C$  were observed with pellet masses up to 20 g. It was concluded, with a view to industrial scale up of the reaction that a continuous system may best suit the production of WC, although it would be possible to implement a batch synthesis system with multiple pellets heated simultaneously. However further study in this area is definitely required with the development of a specific single mode applicator.

Finally the synthesis of WC from the oxide,  $WO_3$ , was also attempted with only moderate success. Synthesis was achieved in 60 s, however, only to ~26 wt %. Despite the dielectric property observations with temperature, indicating that the loss tangent improves as temperature increases, the reaction times were deemed too short for a complete reaction to occur. Longer synthesis times were ultimately required, which were not possible with the current experimental procedure and applicators available. Despite this a great deal was learnt about the one step synthesis of WC from the oxide, indicating a possible reaction procedure:



From these results, it is almost certain that synthesis of the pure-phase carbide is possible given a longer reaction time. However, development of both the experimental technique and applicator must be carried out prior to this, with a suggestion that a decrease in applied power and cavity size may contribute to the successful synthesis of WC from WO<sub>3</sub>.

In conclusion, successful synthesis of WC has been achieved in rapid timescales, with a degree of understanding about the reaction mechanism achieved. The development of an experimental procedure has also been successful, which can be applied to the microwave synthesis of numerous other transition metal carbides. The investigation into *in-situ* characterisation methods was also carried out, with high speed photography and thermal imaging shedding light on possible reaction mechanisms, as well as confirming previous results collected both *in-* and *ex-situ*. Finally the investigation into a number of variables directly affecting the formation of WC was studied, such as carbon excess and changes in sample mass. Through these results further understanding about the reaction,  $W + C \rightarrow WC$ , was gained.

### 3.6 REFERENCES

- 
- <sup>1</sup> R. Koc and S. K. Kodambaka, *J. Euro. Ceram. Soc.*, 2000, **20**, 1859.
- <sup>2</sup> M. J. Ledoux, C. H. Pham, J. Guille and H. Dunlop, *J. Catalysis*, 1992, **134**, 383.
- <sup>3</sup> T. Xiao, A. Hanif, A. P. E. York, J. Sloan and M. L. H. Green, *Phys. Chem. Chem. Phys.*, 2002, **4**, 3522.
- <sup>4</sup> N. Morton, B. W. James, G. H. Wostenholm and D. C. B. Hepburn, *J. Less-Common Metals*, 1972, **29**, 423.
- <sup>5</sup> H. O. Pierson, *Handbook of Refractory Carbides and Nitrides*, 1<sup>st</sup> Edition, Noyes, Park Ridge NJ, 1960.
- <sup>6</sup> A. S. Kurlov and A. I. Gusev, *Inorg. Mater.*, 2006, **42**, 121.
- <sup>7</sup> J. Leciejewicz, *Crystallographica*, 1961, **14**, 200.
- <sup>8</sup> P. Stecher, F. Benesovsky and H. Nowothny, *Planseeberichte fuer Pulvermetallurgie*, 1964, **12**, 89.
- <sup>9</sup> A. S. Hester, A. D. Mitchell and R. W. Rees, *Ind. Eng. Chem.*, 1960, **52**, 94.
- <sup>10</sup> G. A. Swift and R. Koc, *J. Mater. Sci.*, 2000, **35**, 2109.
- <sup>11</sup> R. Koc and S. K. Kodambaka, *J. Euro. Ceram. Soc.*, 2000, **20**, 1859.
- <sup>12</sup> H. H. Nersisyan, H. I. Won and C. W. Won, *Mater. Lett.*, 2005, **59**, 3950.
- <sup>13</sup> D. Zeng and M. J. Hampden-Smith, *Chem. Mater.*, 1992, **4**, 968.
- <sup>14</sup> A. M. Nartowski, I. P. Parkin, M. MacKenzie, A. J. Craven and I. MacLeod, *J. Mater. Chem.*, 1999, **9**, 1275.
- <sup>15</sup> M. S. El-Eskandarany, A. A. Mahday, H. A. Ahmed and A. H. Amer, *J. Alloy and Compounds*, 2000, **312**, 315.
- <sup>16</sup> G. M. Wang, S. J. Campbell, A. Calka and W. A. Kaczmarek, *J. Mater. Sci.*, 1997, **32**, 1461.

- 
- <sup>17</sup> J. P. Cheng, D. K. Agrawal, S. Komarneni, M. Mathis and R. Roy, *Mat. Res. Innovat.*, 1997, **1**, 44.
- <sup>18</sup> K. Rodiger, K. Dreyer, T. Gerdes and M. Willert-Porada, *Int. J. Refractory Metals & Hard Mater.*, 1998, **16**, 409.
- <sup>19</sup> Lackner, A.; Ferstl, W.; Knuenz, G.; Dinesh, A.; Jiping, C. *WO200142135*, 2001.
- <sup>20</sup> Lindholm, M.; Waldenstroem, M.; Ahlgren, M. *WO200003049-A*, 2000.
- <sup>21</sup> E. Breval, J. P. Cheng, D. K. Agrawal, P. Gigl, M. De<sup>21</sup> Lackner, A.; Ferstl, W.; Knuenz, G.; Dinesh, A.; Jiping, C. *WO200142135*, 2001.
- <sup>21</sup> E. Breval, J. P. Cheng, D. K. Agrawal, P. Gigl nnis, R. Roy and A. J. Papworth, *Mater. Sci. Eng. A.*, 2005, **391**, 285.
- <sup>22</sup> R. G. Ford, *Mater. Process. Rep.*, 1988, **3**, 1.
- <sup>23</sup> J. W. Walkiewicz, G. Kazonich and S. L. McGill, *Miner. Metall. Processing*, 1998, **5**, 39.
- <sup>24</sup> A. Agostine, E. Bonometti, P. Volpe, M. Truccato, C. Manfredotti, P. Olivero, C. Paolini, G. Rinaudo and L. Gozzelino, *Int. J. Mod. Phys. B.*, 2003, **17**, 773.
- <sup>25</sup> J. H. Peng, J. Binner and S. Bradshaw, *Mater. Sci. Tech.*, 2002, **18**, 1419.
- <sup>26</sup> R. Meredith, *Engineers' handbook of industrial microwave heating*, 1<sup>st</sup> Edition, Short run press ltd, Exeter, 1998.
- <sup>27</sup> E. Parthe, V. Sadagopan, *Monat. Chem.*, 1962, **93**, 263.
- <sup>28</sup> Vaidhyanathan, B.; Singh, A. P.; Agrawal, D. K.; Shrout, T. R.; Roy, R.; Ganguly, S.; *J. Am. Ceram. Soc.* **2001**, *84*, 1197.
- <sup>29</sup> S. Vallance, S. Kingman and D. H. Gregory, *Adv. Mater.*, 2007, **19**, 138.

- 
- <sup>30</sup> T. Ya. Kosolapova, *Carbides: Properties, Production and Applications*, 1<sup>st</sup> Edition, Plenum Press, New York, 1971.
- <sup>31</sup> J. G. P. Binner and T. E. Cross, *J. Hard Mater.*, 1993, **4**, 177.
- <sup>32</sup> J. H. Peng, J. Binner and S. Bradshaw, *Mater. Sci. and Technology.*, 2002, **18**, 1419.
- <sup>33</sup> E. Pert, Y. Carmel, A. Birnboim, T. Olorunyolemi, D. Gershon, J. Calame, I. K. Lloyd and O. C. J. Wilson Jr., *Am. Ceram. Soc.*, 2001, **84**, 1981.
- <sup>34</sup> A. G. Whittaker and D. M. P. Mingos, *J. Chem. Soc. Dalton. Trans.*, 1995, 2073.
- <sup>35</sup> A. Agostino, P. Volpe, M. Castiglioni and M. Truccato, *Mat. Res. Innovat.*, 2004, **8**, 75.
- <sup>36</sup> O. P. Thakur, C. Prakash and D. K. Agrawal, *Mater. Lett.*, 2002, **56**, 970.
- <sup>37</sup> J. D. Houmes and H. C. zur Loye, *J. Solid State Chem.* 1997, **130**, 266.
- <sup>38</sup> M. Iwasaki, H. Takizawa, K. Uheda and T. Endo, *J. Mater. Sci. Lett.*, 2000, **19**, 2033.
- <sup>39</sup> D. J. Brooks, R. E. Douthwaite and L. J. Gillie, *Chem. Comm.*, 2005, **38**, 4857.
- <sup>40</sup> E. K. Storms, *The Refractory Carbides*, 1<sup>st</sup> Edition, Academic Press, New York, 1967.
- <sup>41</sup> K. J. Rao, B. Vaidhyanathan, M. Ganguli, P. A. Ramakrishnan, *Chem. Mater.*, 1999, **11**, 882.
- <sup>42</sup> D. K. Agrawal, *Curr. Op. Solid State Mater. Sci.*, 1998, **3**, 480.
- <sup>43</sup> R. Roy, D. Agrawal, J. Cheng, S. Gedeveanishvili, *Nature*, 1999, **399**, 668.
- <sup>44</sup> D. E. Clark, W. H. Sutton, *Annu. Rev. Mater. Sci.*, 1996, **26**, 229.
- <sup>45</sup> D. M. P. Mingos and D. R. Baghurst, *Br. Ceram. Trans. J.*, 1992, **91**, 124.

- 
- <sup>46</sup> A. C. Larson and R. B. von Dreele, "*The General Structure Analysis System*", 2000, Los Alamos National Laboratories: Los Alamos, NM.
- <sup>47</sup> B. H. Toby, *J. Appl. Crystallogr.*, 2001, **34**, 210.
- <sup>48</sup> Harrison, A.; Ibberson, R.; Robb, G.; Whittaker, G.; Wilson, C.; Youngson, D. *Faraday Discuss.* **2002**, *122*, 363.
- <sup>49</sup> Kisi, E. H.; Riley, D. P.; Curfs, C. C. *Physica B.* **2006**, *385-386*, 487.
- <sup>50</sup> L. N. Satapathy, P. D. Ramesh, D. Agrawal, R. Roy, *Mater. Res. Bull.*, 2005, **40**, 1871.
- <sup>51</sup> P. D. Ramesh, B. Vaidhyanathan, M. Ganguli, K. J. Rao, *J. Mater. Res.*, 1994, **2**, 3025.
- <sup>52</sup> E. Lassner and W. D. Schubert, *Tungsten: Properties, Chemistry, technology of the element, alloys and chemical compounds*, 1<sup>st</sup> edition, Springer, 1999.
- <sup>53</sup> D. F. Shriver and P. W. Atkins, *Inorganic Chemistry*, 3<sup>rd</sup> Edition, Oxford University Press, 1999.
- <sup>54</sup> D. R. Lide, *Handbook Of Chemistry And Physics*, 88<sup>th</sup> Edition, CRC Press, 2007.
- <sup>55</sup> M. Sato, S. Takayama, Y. Yasunaga and Y. Saitou, *9<sup>th</sup> international conference on microwave and RF heating*, **2003**.
- <sup>56</sup> Whittaker, A. G. *Chem. Mater.* **2005**, *17*, 3426.
- <sup>57</sup> L. E. Toth, *Transition Metal Carbides and Nitrides*, 1<sup>st</sup> edition, Academic Press, New York and London, 1971.
- <sup>58</sup> A. Lofberg, A. Frennet, G. Leclercq, L. Leclercq and J. M. Giraudon, *J. Catalysis*, 2000, **189**, 170.
- <sup>59</sup> G. S. Upadhyaya, *Cemented tungsten carbides*, 1<sup>st</sup> edition, Noyes publications, 1998.

# 4: MOLYBDENUM CARBIDE INVESTIGATIONS

## 4.1 INTRODUCTION

Molybdenum carbide,  $\text{Mo}_2\text{C}$ , like other refractory carbides, has high hardness and strength coupled with good thermal and electrical conductivity as well as a high chemical stability and melting point.<sup>1</sup> Specifically its high melting point (2520 °C) and its hardness (15.5 – 24.5 GPa 500 g load Vickers) make it comparable to the tungsten carbide, and although it does not perform as well at high temperatures, is a viable alternative for less demanding applications.<sup>1</sup> Found in steel alloys and as a tool/blade coating, it is often favoured over the more expensive tungsten carbide, WC.<sup>2</sup>

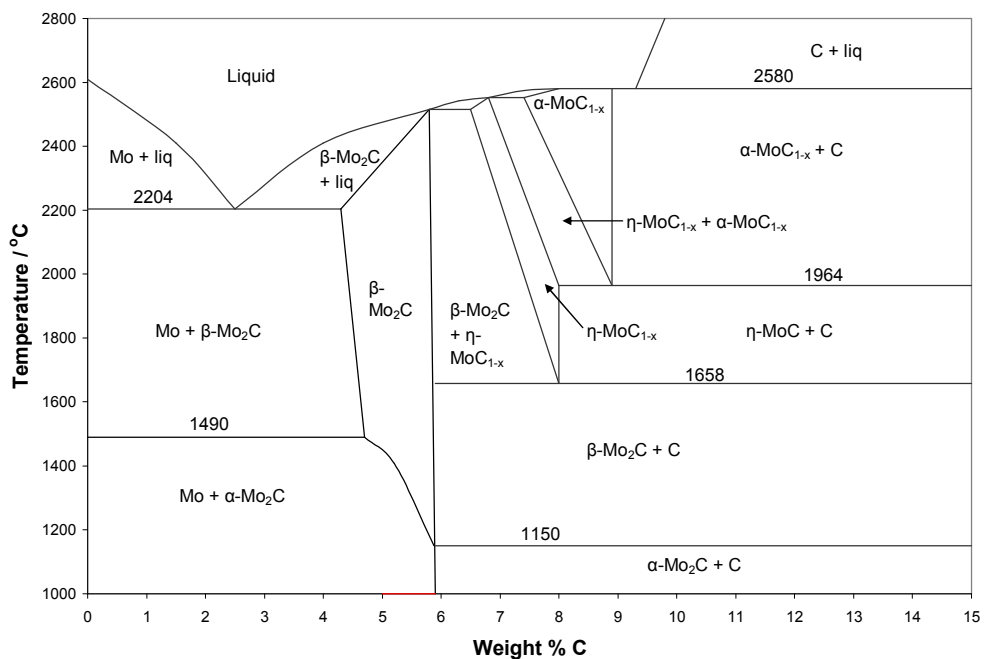
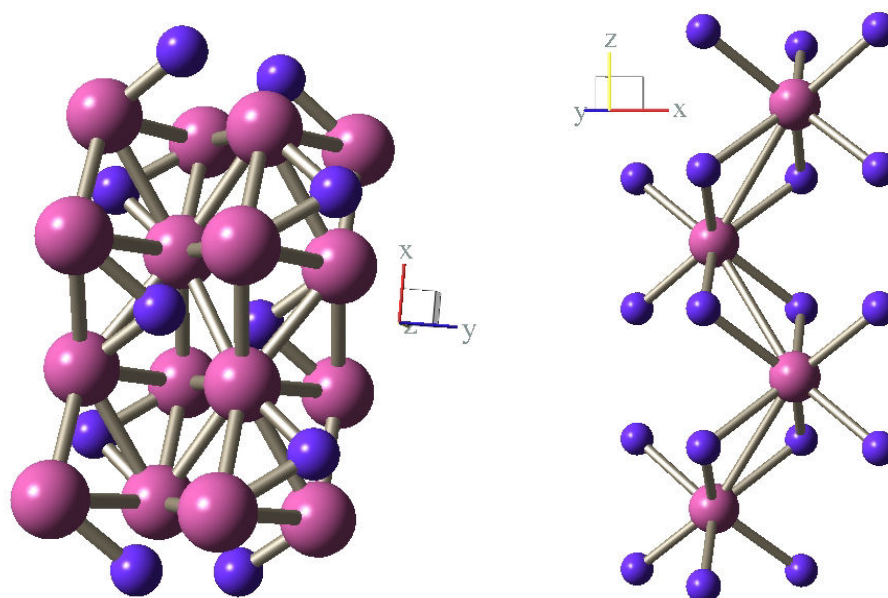


Figure 4- 1: Phase diagram of Mo-C system.<sup>3</sup>

The molybdenum-carbon system comprises three known stoichiometric compositions: MoC ( $\alpha$ -MoC), Mo<sub>3</sub>C<sub>2</sub> ( $\eta$ -MoC) and Mo<sub>2</sub>C (Figure 4- 1). Direct synthesis of any given phase is notoriously difficult due to several of the phases being stable only at high temperatures. In addition slight variations in reactant stoichiometry can result in unwanted phases.<sup>4</sup> Mo<sub>2</sub>C, the only phase stable at room temperature,<sup>3</sup> forms two known phases: orthorhombic  $\alpha$ -Mo<sub>2</sub>C and hexagonal  $\beta$ -Mo<sub>2</sub>C. The latter phase adopts an ABAB stacking sequence of the metal layers and a distortion in the carbon atom ordering. At lower synthesis temperatures, the structure converts into an orthorhombic structure with an ordered distribution of the carbon atoms in the interstitial sites.<sup>5</sup>  $\beta$ -Mo<sub>2</sub>C belongs to the space group  $P6_3/mmc$  with lattice parameters  $a = 3.011 \text{ \AA}$ ,  $c = 4.771 \text{ \AA}$ ;<sup>6</sup>  $\alpha$ -Mo<sub>2</sub>C belongs to space group  $Pbcn$  with lattice parameters  $a = 4.735 \text{ \AA}$ ,  $b = 6.025 \text{ \AA}$ ,  $c = 5.210 \text{ \AA}$  (Figure 4- 2).<sup>7</sup>



**Figure 4- 2: Structures of  $\alpha$ -Mo<sub>2</sub>C (left) and  $\beta$ -Mo<sub>2</sub>C (right). The pink atoms correspond to Mo and the purple atoms to C.**

Mo<sub>2</sub>C also exhibits superconductivity, although there is some inconsistency in the reported superconducting transition temperature, T<sub>c</sub>. Early work and later specific heat measurements agree that the T<sub>c</sub> lies between 2.4 and 3.2 K for β-Mo<sub>2</sub>C,<sup>8, 9</sup> however values between 3.45 and 7.2 K have also been reported.<sup>10</sup> The superconducting transition is believed to be slightly higher for α-Mo<sub>2</sub>C, between 6 and 7.3 K.<sup>10</sup> Again, however, this value is disputed with values being reported as low as 4 K,<sup>9</sup> and as high as 12.2 K.<sup>11</sup> These discrepancies are thought to be due to the synthetic procedure as well as the carbon stoichiometry; the electron-phonon coupling and hence T<sub>c</sub> is especially sensitive to the latter. It is possible that reported Mo<sub>2</sub>C phases with higher T<sub>c</sub> in fact contain hexagonal or cubic polymorphs of MoC<sub>1-x</sub>. It is believed, however, that synthesis of MoC<sub>1-x</sub>, is only possible with rapid quenching post-reaction.<sup>3</sup> If this is not carried out Mo<sub>2</sub>C + C is observed.

Current synthesis methods for molybdenum carbide target the only industrially useful phase, Mo<sub>2</sub>C (no polytype preference). Preferentially the metal is reacted directly with carbon at around 1500 °C under flowing hydrogen to afford the carbide.<sup>12</sup> Alternatively the metal oxide, MoO<sub>3</sub>, can be used as a starting material under similar conditions, however, controlling the carbon content of the desired carbide is difficult. For this reason reduction of the oxide is usually carried out prior to carbide synthesis. Alternatively this is bypassed altogether with the direct use of Mo metal.

In an effort to improve on this process many articles have been published within the last decade discussing novel methods of synthesis. These include Solid State Metathesis (SSM) reactions which are a subclass of Self propagating High temperature Synthesis (SHS) reactions.<sup>13</sup> Driven largely by the lattice energy of a coproduced salt, these reactions involve chemical exchange of the reacting partners. Through the use of  $\text{Al}_4\text{C}_3$  or  $\text{CaC}_2$  and  $\text{MoCl}_3$ , the successful synthesis of  $\text{Mo}_2\text{C}$  in under a minute has been reported.<sup>14</sup> This work was later followed up by Nartowski et al. with the successful synthesis of the carbide from the oxide using SSM.<sup>15</sup> Although the reaction times were longer, it was noticed that  $\alpha\text{-Mo}_2\text{C}$ , the more thermodynamically stable product, was synthesised and not  $\beta\text{-Mo}_2\text{C}$ , the kinetic phase, as observed from the halide precursor. This was explained by the reaction times involved in both cases, the oxide reactions taking significantly longer (hours over minutes).

In addition to improving the bulk synthesis, manipulation of the structure and properties of the carbide has also been investigated. Using metal-halides, specifically  $\text{MoCl}_3$ , and  $\text{LiBEt}_3\text{H}$  it is possible to synthesise monodispersed nanoparticles of  $\text{Mo}_2\text{C}$  at room temperature.<sup>16</sup> Transition metal carbides are also used as active catalysts in a number of processes with the synthesis of high surface area forms of these materials attracting considerable attention. Successful synthesis of  $\text{Mo}_2\text{C}$  was achieved using flowing methane and ethane gas at relatively low temperatures ( $< 1000\text{ }^\circ\text{C}$ ) resulting in suitable catalytic materials.<sup>17</sup>

## 4.2 EXPERIMENTAL: SYNTHESIS OF Mo-C

Based on experimental work carried out using the W-C system (chapter 3), a great deal was already understood about microwave synthesis of the transition metal carbides prior to the investigation of the Mo-C system. The application of the successful experimental procedure (section 2.2) developed in the synthesis of WC allowed for immediate results to be collected for Mo<sub>2</sub>C formation.

Experiment	Applicator	Reaction	Purpose
1	DMO	$2\text{Mo} + \text{C} \rightarrow \text{Mo}_2\text{C}$	Synthesis of Mo <sub>2</sub> C
2	DMO	$2\text{Mo} + \text{C} \rightarrow \text{Mo}_2\text{C}$	Study carbon stoichiometry and structure of Mo <sub>2</sub> C through PND
3	DMO	$\text{Mo} + \text{C} \rightarrow \text{MoC}$	Synthesis of MoC
4	DMO	$3\text{Mo} + 2\text{C} \rightarrow \text{Mo}_3\text{C}_2$	Synthesis of Mo <sub>3</sub> C <sub>2</sub>
5	Single mode cavity	$2\text{Mo} + \text{C} \rightarrow \text{Mo}_2\text{C}$	Synthesis and study of Mo <sub>2</sub> C reaction profile
6	Single mode cavity	$2\text{Mo} + \text{C} \rightarrow \text{Mo}_2\text{C}$	Study the effect of power variation on Mo <sub>2</sub> C synthesis
7	Single mode cavity	$2\text{Mo} + \text{C} \rightarrow \text{Mo}_2\text{C}$	Study the effect of sealed reaction tubes on Mo <sub>2</sub> C synthesis
8	DMO	$2\text{MoO}_3 + 6\text{C} \rightarrow 2\text{Mo} + \text{C} \rightarrow \text{Mo}_2\text{C}$ $\text{MoO}_3 + 7\text{C} \rightarrow \text{Mo}_2\text{C} + 7\text{CO}$	Synthesis of Mo <sub>2</sub> C from oxide
9	Single mode cavity	$\text{MoO}_3 + 7\text{C} \rightarrow \text{Mo}_2\text{C} + 7\text{CO}$	Reaction study of oxide to carbide

**Table 4- 1: Summary of all experiments carried out on the Mo-C system.**

As described in section 4.1, the Mo-C system is more complicated than any carbide from groups IV and V. The possible existence of three different phases makes the targeted formation of specific phases much more difficult. With this in mind a great deal of care was taken over the synthesis of the desired phase. Reactants were weighed out accurately (to 4 decimal places) knowing that stoichiometry greatly affects the final product; the reaction temperature was constantly monitored for all single mode experiments and a number of characterisation techniques were utilised from the outset to confirm and analyse the product. In particular the Mo<sub>2</sub>C phase has a superconducting transition which, unlike for WC, provides an additional tool for analysis in the form of magnetic measurements using a SQUID magnetometer (section 2.3.5.2). In this case a small pre-weighed sample of the powdered product was loaded into a gelatine capsule. The capsule was then inserted into a plastic straw, fixed in place and attached to the sample rod prior to being lowered into the SQUID chamber. The chamber was then purged and the sample aligned within the machine before the scan was begun. Samples were typically scanned between 1.8 and 300 K with a magnetic field of 10 Oe. Data collection was concentrated around the suspected superconducting transition of the material; between 1.8 and 20 K, so accurate results could be obtained.

In addition to SQUID a number of other characterisation techniques were utilised. PXD was carried out on all samples post-synthesis by first grinding the sample to a fine powder with subsequent loading onto a glass slide (section 2.3.1). Samples were typically scanned for 20 min with a finite number of samples scanned for 12 h so that structural refinement could be

carried out (section 2.3.3). Dielectric property measurements were carried out on the majority of samples (section 2.1.2). No more than 0.5 g of sample was inserted into the cavity and five measurements taken so an average value could be obtained. Other techniques such as SEM (section 2.3.6), EDX (section 2.3.6.1), XRF and CHN analysis (section 2.3.8) and thermal analysis (section 2.3.9) were also carried out to reinforce results from other characterisation techniques.

This chapter comprises work carried out primarily on the synthesis of Mo<sub>2</sub>C (experiments **1, 2, 5-9**), although other phases were also investigated (**3, 4**). However, unlike work concerning WC synthesis, synthesis of Mo<sub>2</sub>C from the oxide precursor (**8, 9**), MoO<sub>3</sub>, comprised much of the work centred on this carbide. This was carried out concurrently with experimental work on the synthesis of Mo-C phases from the metal, Mo, and carbon (**1-7**). In all reactions (**1-9**) stoichiometric amounts of the starting materials to afford the desired product were ground together and pelleted; 2 g pellets for non-oxide reactions and 1 g pellets for oxide reactions. This method is described in detail in section 2.2. Regardless of the applicator used, all experiments were repeated a minimum of three times and errors calculated where appropriate. A fixed power was always used; 800 W for DMO experiments and 3 kW for single mode applicator experiments. The only exception to this is experiments carried out between 0 and 1 kW during the investigation of Mo<sub>2</sub>C synthesis from the oxide (section 4.5.2.2). After the desired heating time samples were removed from the cavity and left to cool prior to characterisation.

As well as Mo-C synthesis reactions (1, 3, 4, 8) in which the sole purpose was the formation of the desired product, a number of other experiments were undertaken. PND was used to examine the Mo<sub>2</sub>C phase (2) enabling detailed structural refinement and phase analysis (section 2.3.2). Crucially this revealed the structure of the Mo<sub>2</sub>C phase. The reaction profile for Mo<sub>2</sub>C synthesis, from Mo metal powder and C, was also studied in the 3-15 kW single mode cavity (5). Using the experimental technique described above, samples were heated for specific times between 5 and 30 s, at 5 s intervals. *In-situ* temperature measurements were taken throughout the experiment (described in detail in chapter 3) which, combined with the *ex-situ* PXD and dielectric property data, allowed the study of the reaction profile and resultant observation of a direction relationship between temperature, phase fraction and loss tangent.

The affect of variations in applied power on Mo<sub>2</sub>C synthesis was investigated (6). Specifically this was to correlate the effect of temperature on Mo<sub>2</sub>C formation, but also served to see if increased power significantly affected synthesis time. Experiments, using Mo and C starting materials, were also carried out to investigate the affect of a sealed reaction tube on the final product (7). It had been observed for WC synthesis that an open reaction silica tube in the experimental procedure resulted in no oxide observed in the final product. Despite the rapid reaction times this was investigated by carrying out the standard synthesis reaction and repeating with the tube sealed at both ends. Products were then analysed using X-ray Photoelectron Spectroscopy (XPS) (section 2.3.7) in order to detect the presence of any surface oxidation. This was necessary as PXD showed no oxidation of the metal in the bulk sample.

As mentioned previously a lot of time was invested in the synthesis of  $\text{Mo}_2\text{C}$  from the oxide,  $\text{MoO}_3$ . Both a single step synthesis was attempted (8) as well as the study of this reaction, carried out using PXD and PND (section 2.3.2) in which a number of samples, both pure  $\text{Mo}_2\text{C}$  product and intermediate multi-phase samples, were investigated (9). It was hoped that this may shed light on the reaction profile and enable a reproducible reaction to be developed. Due to the problems with oxide reactions, namely the pellet fracturing due to rapid gas evolution, a reproducible reaction was hard to achieve. In fact much time was taken in the attempt of a successful reaction with a number of reactions repeated due to inadequate samples. To remedy this, the experimental procedure was modified by investigating lower microwave powers, temperature monitoring and various temperature ramp rates. This is described fully in the results and discussion section 4.5.

## **4.3 RESULTS AND DISCUSSION: Mo-C SYNTHESIS USING A DOMESTIC MICROWAVE OVEN (DMO)**

### **4.3.1 $\text{Mo}_2\text{C}$ synthesis**

Owing to the successful synthesis of tungsten carbide in a DMO (section 3.2) similar methods were used in the approach to the synthesis of molybdenum carbide (1). The experimental setup (section 2.2.1) refined from WC synthesis was used, with a 2 g pellet (constituting stoichiometric amounts of Mo and C to afford  $\text{Mo}_2\text{C}$ ) placed in graphite powder in an open-top silica

tube. With the tube supported in silica flour the pellet was heated in the DeLonghi DMO for 30 min at a continuous power output of 800 W. Heating for 30 min yielded a pure phase of Mo<sub>2</sub>C (confirmed by PXD) and this reaction was subsequently refined to achieve a successful reaction in only 90 s. (The lack of discussion of the resultant pattern and the carbide structure at this juncture is deliberate and will be examined later in this section.) Reactions carried out with heating times of 60 s or less resulted in only the reactants, Mo and C, indicating that the reaction must reach a specific point, no doubt temperature related as observed for the W-C system, before formation of the product can occur. However, once this is reached, synthesis of the carbide is rapid and to a very high purity. Unfortunately, confirmation of the relationship between reaction time and temperature was not possible with this setup and so was postponed until synthesis in the single mode cavity with the use of an optical pyrometer could be carried out.

In addition to PXD, further analysis of the sample using EDX was carried out, revealing an Mo:C ratio of 2.0:0.9(4) with no other elements present. This confirmed the formation of the desired phase, however, although EDX reinforces the results from PXD, accurate carbon stoichiometry is impossible to obtain from this information due to the inaccuracy observed for light atoms with EDX (section 2.3.6). SEM showed the formation of approximately spherical crystallites with a uniform grain size across the sample of between 2 and 6 μm (Figure 4- 3). SEM of samples heated up to 30 min was also carried out revealing no change in grain size with heating time.

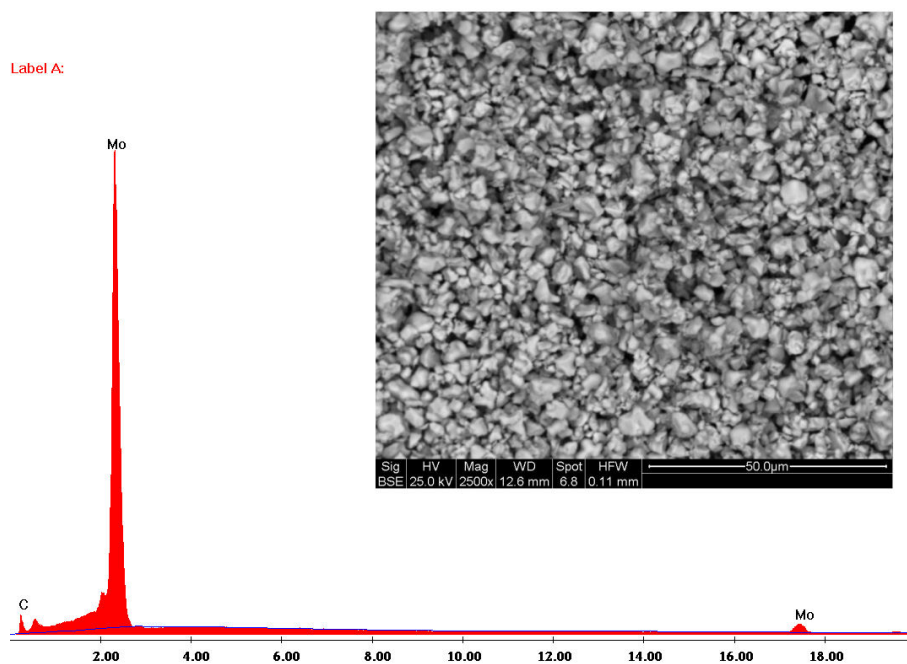


**Figure 4- 3: EDX and SEM images for Mo<sub>2</sub>C sample heated for 90 s at 800 W in a DMO.**

Despite the successful synthesis of Mo<sub>2</sub>C, confirmed by PXD, this technique could not distinguish completely between the orthorhombic and hexagonal Mo<sub>2</sub>C phases. Refinement of PXD data collected overnight, using the Rietveld least squares refinement method and EXPGUI (section 2.3.3),<sup>18, 19</sup> was unable to differentiate unequivocally between these phases (Figure 4- 4). Furthermore crystallographic parameters post-refinement (Table 4- 2) for both structures show no appreciable difference in the “goodness of fit” parameter,  $\chi^2$ . In fact both the hexagonal and orthorhombic structures result in acceptable refinements and in both cases the lattice parameters are in excellent agreement with previous studies of stoichiometric Mo<sub>2</sub>C.<sup>20</sup>

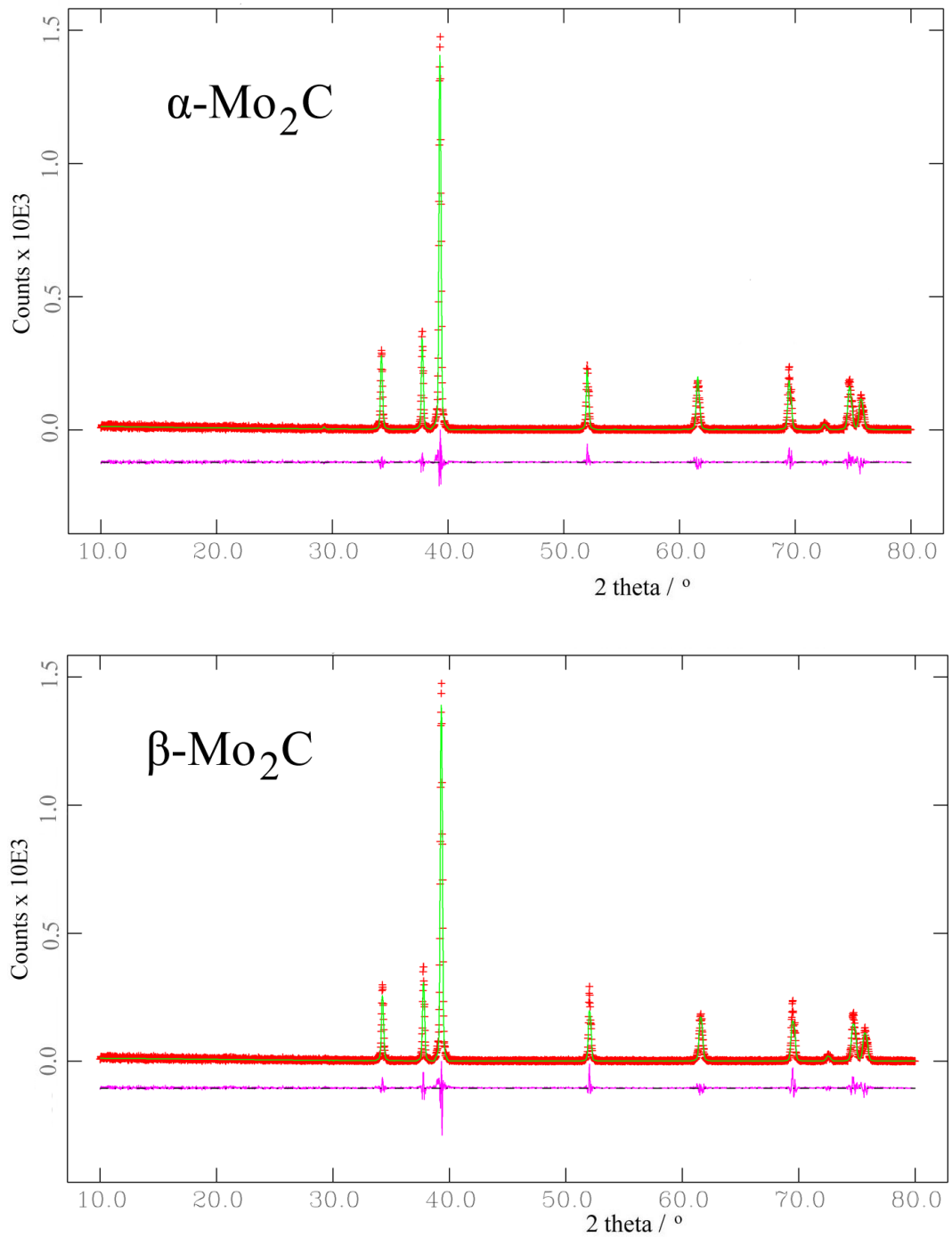


**Figure 4- 4: Observed (plusses), calculated and difference profile plots for Rietveld refinements of  $\alpha\text{-Mo}_2\text{C}$  and  $\beta\text{-Mo}_2\text{C}$  against PXD data for  $\text{Mo}_2\text{C}$  produced in 90 s at 800 W in a DMO.**

Sample	$\alpha$ -Mo <sub>2</sub> C	$\beta$ -Mo <sub>2</sub> C
Empirical formula	Mo <sub>2</sub> C	
Unit cell formula weight, M <sub>w</sub>	107.9507	
Crystal system, Space group	Orthorhombic, Pbcn	Hexagonal, P6 <sub>3</sub> /mmc
<i>a</i> , <i>b</i> , <i>c</i> -parameter, Å	4.7287(2), 6.0054(4), 5.1883(3)	2.9999(6), 2.9999(6), 4.7498(1)
Unit cell volume, Å <sup>3</sup>	147.34(1)	36.86(4)
Z, Calculated density, ρ <sub>x</sub> / g cm <sup>-3</sup>	1, 9.192	1, 13.129
Observations, parameters	3323, 17	3323, 13
R <sub>p</sub> , R <sub>wp</sub> , χ <sup>2</sup>	0.1689, 0.2598, 1.168	0.1842, 0.2716, 1.275

**Table 4- 2: PXD Crystallographic information for Mo<sub>2</sub>C synthesised in 90 s at 800 W in a DMO.**

A detailed examination of the two structures,  $\alpha$ -Mo<sub>2</sub>C and  $\beta$ -Mo<sub>2</sub>C, using PXD shows the existence of a number of reflections (denoted by the blue tick marks) for the orthorhombic phase which are not present in the hexagonal phase. However, all of these reflections are very weak and any diffraction that exists in the product is masked by the PXD background. Even with the reduced background from an overnight scan any diffraction is still obscured. In fact the only noticeable reflections, as seen in Figure 4- 4, are shared by both the  $\alpha$ -Mo<sub>2</sub>C and  $\beta$ -Mo<sub>2</sub>C phases. This makes it impossible to confirm the preference of one phase over the other using this technique. As a side note it was also impossible to accurately determine carbon stoichiometry in either refinement. Due to problems associated with light element detection and PXD (section 2.3.1), a resultant unstable refinement occurred when the occupancy was varied.

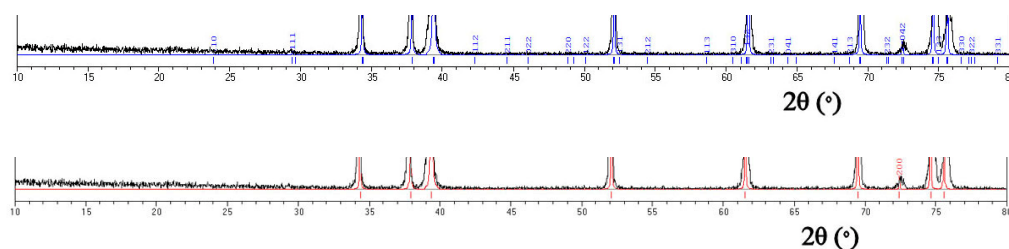


**Figure 4- 5: PXD data for an Mo<sub>2</sub>C sample (black) heated for 90 s at 800 W in a DMO. Calculated pattern for  $\alpha$ -Mo<sub>2</sub>C is blue and red for  $\beta$ -Mo<sub>2</sub>C.**

As discussed in section 4.1, Mo<sub>2</sub>C has a superconducting transition temperature,  $T_c$ , between 2.4 and 12.2 K.<sup>8, 9, 10, 11</sup> This is a known area of controversy and carbide samples have been reported to have numerous transition temperatures within this temperature range with the exact value depending strongly on carbon stoichiometry and structure. The orthorhombic phase,  $\alpha$ -Mo<sub>2</sub>C, is reported to have a lower  $T_c$  than the hexagonal phase,  $\beta$ -Mo<sub>2</sub>C, however, an overlap between the two exists with values reported as high as 7.2 K for  $\alpha$ -Mo<sub>2</sub>C<sup>10</sup> and as low as 4 K for  $\beta$ -Mo<sub>2</sub>C.<sup>9</sup> This makes it difficult to confirm the structure using the  $T_c$ , however it certainly indicates which phase may be present.

Magnetic measurements were carried out using SQUID (section 2.3.5.2) on Mo<sub>2</sub>C synthesised in 90 s in the Delonghi DMO. This indicated a  $T_c$  of 3.83(6) K with a superconducting volume fraction of 97.6 % confirming the formation of the desired phase Mo<sub>2</sub>C and suggesting intrinsic superconductivity in the bulk phase. This result also suggests the formation of the hexagonal carbide,  $\beta$ -Mo<sub>2</sub>C, with the  $T_c$  located towards the upper end of the values reported by Meissner.<sup>8</sup> However, this  $T_c$  is also situated just below

the low end of the reported  $T_c$  values for the orthorhombic phase,  $\alpha$ - $\text{Mo}_2\text{C}$ ,<sup>9</sup> making it difficult to draw an absolute conclusion from this SQUID result.

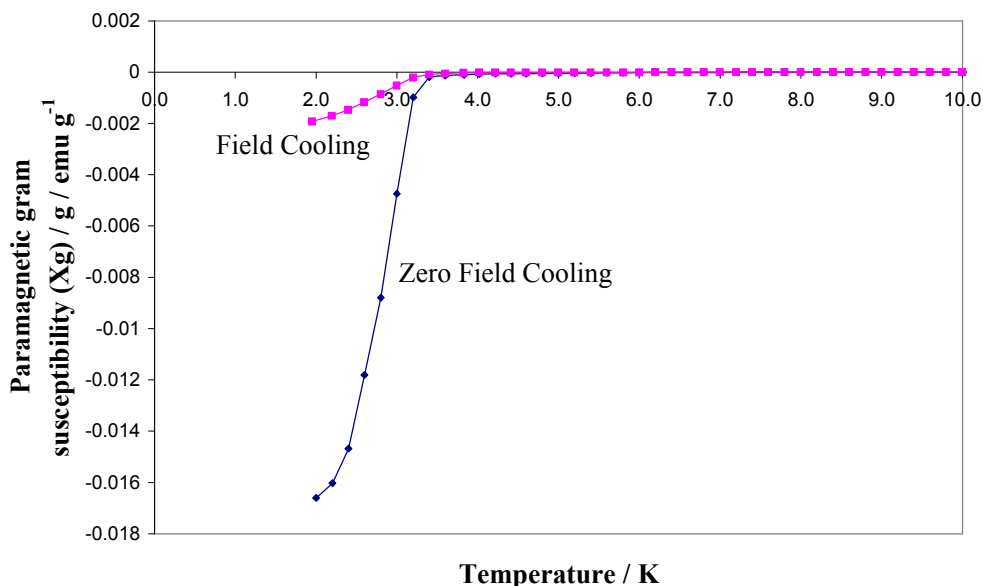


**Figure 4- 6: Plot of mass susceptibility,  $\chi_g$ , against temperature, for superconducting  $\text{Mo}_2\text{C}$  synthesised in 90 s at 800 W in a DMO, showing a  $T_c$  onset at 3.83(6) K.**

Examination of the phase diagram for the Mo-C system (section 4.1, Figure 4- 1) indicates that, with excess C,  $\alpha$ - $\text{Mo}_2\text{C}$  is exclusively formed below 1150 °C. Above this temperature only  $\beta$ - $\text{Mo}_2\text{C}$  exists until temperatures higher than 1658 °C. With excess Mo the sole formation of the orthorhombic phase is possible up to temperatures of 1490 °C, above this synthesis of the hexagonal phase is possible. However, as the reaction mixture nears a stoichiometric mixture of Mo and C to afford  $\text{Mo}_2\text{C}$ , this temperature rapidly decreases to 1150 °C. This indicates that two factors primarily control the ultimate  $\text{Mo}_2\text{C}$  structure: temperature and reactant stoichiometry. As discussed earlier, the

Mo<sub>2</sub>C phase was targeted by grinding together stoichiometric amounts of the reactants, Mo and C. A great deal of care was taken over this due to the known sensitivity of carbon stoichiometry on carbide properties and structure. By a process of elimination this leaves temperature, but unfortunately *in-situ* monitoring of this variable was not achievable in the DMO setup and without these results prediction of either phase was difficult.

Nartowski et al., as discussed in section 4.1, investigated alternative synthetic methods to the carbide Mo<sub>2</sub>C.<sup>14, 15</sup> Although successful synthesis of the carbide was presented, reaction times differed significantly with varying experimental parameters. Crucially, however, one important observation was made from the results collected in that short reaction times, using the halide, resulted in the kinetic product  $\beta$ -Mo<sub>2</sub>C, and long reactions time, using the oxide, resulted in the thermodynamic product  $\alpha$ -Mo<sub>2</sub>C. One could then assume that, in the case of the ultra-rapid microwave treated samples, the kinetic phase,  $\beta$ -Mo<sub>2</sub>C, is most likely produced, however this assumption is tenuous at best.

It is apparent that, with the characterisation techniques available, no conclusion can be drawn as to the polytype associated with the Mo<sub>2</sub>C phase. SQUID results confirm a T<sub>c</sub> of 3.8(1) K which falls within the region for the hexagonal structure, however, this alone is not enough to confirm the existence of this phase due to the known controversy in the superconducting transition temperature for this system. For this reason, Powder Neutron Diffraction (PND) proved a necessity in confirming the existence of either the orthorhombic or hexagonal phase.

### 4.3.2 Mo<sub>2</sub>C Powder Neutron Diffraction (PND) study

PND was carried out on the sample heated for 90 s at 800 W in the Delonghi DMO (2). It was hoped that this technique would verify phase purity and allow examination of the crystal structure and thus reveal the existence of either  $\alpha$ -Mo<sub>2</sub>C or  $\beta$ -Mo<sub>2</sub>C. This technique was carried out successfully by Parthé in 1963 in which the difference structures were observed.<sup>21</sup> In addition the examination of the carbon stoichiometry in the final product was investigated which, as mentioned previously, was not possible to refine using PXD data. PND data was collected on D1A at the ILL in Grenoble (section 2.3.2.1). D1A operates with fixed scan times over a specified  $2\theta$  range, with multiple scans taken to increase the resolution of the diffraction pattern.

Approximately 2 g of the sample was loaded into a 5mm diameter vanadium canister which was then attached to the diffractometer. The sample was scanned, between 0 and 158 ° in  $2\theta$  at a wavelength of 1.39 Å with a step size of 0.1 °, and data collected for 4 h. Rietveld refinement (section 2.3.3) of the data was performed using the General Structure Analysis System (GSAS)<sup>18</sup> through the windows based EXPGUI interface.<sup>19</sup> Data were refined concurrently against the  $\alpha$ -Mo<sub>2</sub>C structure proposed by Epicier<sup>7</sup> and the  $\beta$ -Mo<sub>2</sub>C structure proposed by Rudy<sup>6</sup>. In both cases refinement was started with the background coefficients, followed by the unit cell, atomic positions, profile parameters and isotropic temperature factors. Finally the absorption/reflectivity correction and carbon occupancy were refined. Resultant profile plots can be observed in Figure 4- 7 and Table 4- 3 is comprised of selected crystallographic parameters post-refinement.

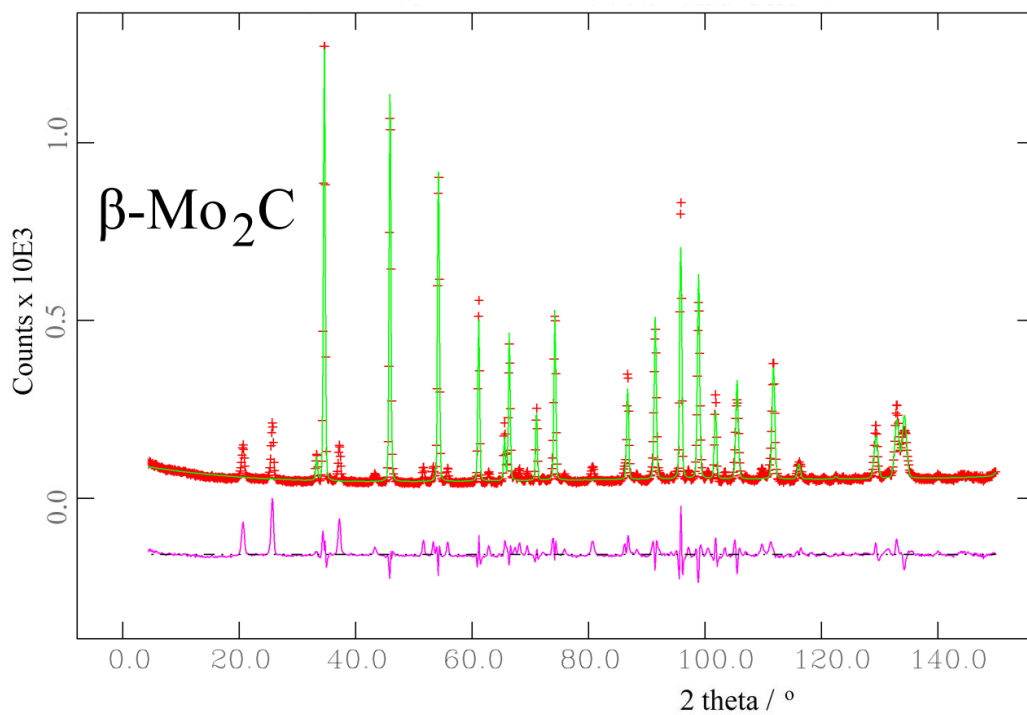
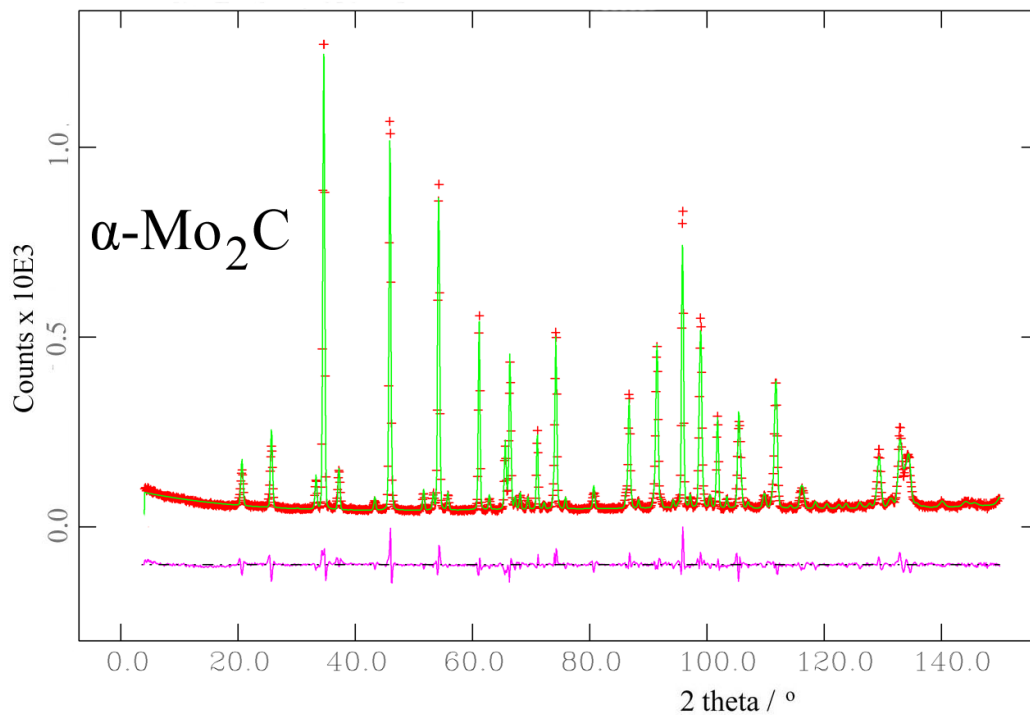


**Figure 4- 7: Observed (plusses), calculated and difference profile plots for Rietveld refinements of  $\alpha\text{-Mo}_2\text{C}$  and  $\beta\text{-Mo}_2\text{C}$  against PND data for  $\text{Mo}_2\text{C}$  produced in 90 s at 800 W in a DMO.**

Sample	$\alpha$ -Mo <sub>2</sub> C	$\beta$ -Mo <sub>2</sub> C
Empirical formula	Mo <sub>2</sub> C	
Unit cell formula weight, M <sub>w</sub>	107.9507	
Crystal system, Space group	Orthorhombic, Pbcn	Hexagonal, P6 <sub>3</sub> /mmc
<i>a</i> , <i>b</i> , <i>c</i> -parameter, Å	4.7403(1), 6.0289(3), 5.20518(1)	3.008(6), 3.008(6), 4.738(9)
Unit cell volume, Å <sup>3</sup>	148.76(1)	37.15(4)
Z, Calculated density, ρ <sub>x</sub> / g cm <sup>-3</sup>	1, 9.057	1, 11.154
Observations, parameters	1459, 18	1459, 16
R <sub>p</sub> , R <sub>wp</sub> , χ <sup>2</sup>	0.0568, 0.0747, 8.153	0.0998, 0.1501, 32.90
Mo position, occupancy, U <sub>iso</sub> / Å <sup>2</sup>	(0.2452(3), 0.127(2), 0.0816(6)), 2.00, 0.0023(2)	( <sup>1</sup> / <sub>3</sub> , <sup>2</sup> / <sub>3</sub> , <sup>1</sup> / <sub>4</sub> ), 1.00, 0.0036(4)
C position and occupancy, U <sub>iso</sub> / Å <sup>2</sup>	(0, <sup>3</sup> / <sub>8</sub> , <sup>1</sup> / <sub>4</sub> ), 0.9696(2), 0.0023(2)	(0, 0, 0), 0.4692(3), 0.0036(4)
Interatomic distance: Mo-C, Å	2.0919(1), 2.1132(1), 2.1186(1)	2.1023(1)
Interatomic distance: Mo-Mo, Å	3.0079(1), 2.9778(1), 3.0148(1), 2.9387(1), 2.9013(1)	2.9376(1)

**Table 4- 3: PND Crystallographic and bond information for Mo<sub>2</sub>C synthesised in 90 s at 800 W in a DMO**

PND was able to show categorically that  $\alpha$ -Mo<sub>2</sub>C is the phase formed in the microwave synthesis reaction. Analysis of the refinement data for both structures reveals a much better fit for the orthorhombic structure represented by much lower R factors and goodness of fit ( $\chi^2$ ); 8.153 compared to 32.90 for  $\beta$ -Mo<sub>2</sub>C. This fit comparison is also apparent in the profile plots; Figure 4- 7. Greater accuracy in the refinement of the unit cell was also possible, with final values obtained matching very closely with previously studied  $\alpha$ -Mo<sub>2</sub>C.<sup>7</sup>

Interatomic distances directly related to the lattice parameters of the unit cell and subsequently are observed to be identical to within 0.001 Å for all values.

Unlike PXD, PND does not suffer from detection problems of light atoms so it is possible to determine carbon stoichiometry for the carbide. The ratio of Mo:C is 2.00:0.9696(2), indicating slight carbon non-stoichiometry for  $\alpha$ -Mo<sub>2</sub>C. EDX results, reported in section 4.3.1, agree with this result, although the stoichiometry observed with PND is clearly far more accurate. In fact this carbon deficiency could well explain the slight difference in lattice parameters compared to those previously studied for stoichiometric  $\alpha$ -Mo<sub>2</sub>C. The result is not unexpected given stoichiometries observed for other carbides as well as information concerning their conventional synthesis. The rapid reaction times observed for  $\alpha$ -Mo<sub>2</sub>C synthesis, combined with the impossibility of perfect homogeneity, go some way to explaining the slight carbon deficiency in the final product. Despite this, the Mo:C ratio is within the range for industrially acceptable materials.<sup>1</sup>

### 4.3.3 MoC and Mo<sub>3</sub>C<sub>2</sub> synthesis

Although much research to date has concentrated on the synthesis of Mo<sub>2</sub>C, two other phases exist within the Mo-C system; MoC and Mo<sub>3</sub>C<sub>2</sub>. One of the reasons for the lack of investigation into these other phases is their instability at room temperature,<sup>3</sup> however, it has been indicated that synthesis may be possible, certainly for MoC, with rapid quenching of the reaction post-heating.<sup>3</sup> The physics behind microwave heating result in the direct heating of

the sample within the cavity. Unlike a conventional furnace, in which the contained atmosphere is heated initially resulting in subsequent sample heating, heating of the sample begins instantaneously with the input of microwave energy into the cavity. Equally, heating stops immediately when the microwave energy generation is terminated. This phenomenon was documented in the chapter on WC synthesis (chapter 3) where an optical pyrometer was used *in-situ* to monitor the reaction temperature within the single mode cavity. Applying this knowledge to the synthesis of Mo-C phases, it can be assumed that the reaction temperature will decrease rapidly with the cessation of microwave power, resulting in air quenching. In addition the sample was removed and placed into ice cold water, quenching it further to assure the rapid termination of the reaction. Despite the lack of temperature monitoring in the DMO, the phase diagram (Figure 4- 1) was consulted in order to estimate the reaction temperatures required for phase formation. In both cases existence of MoC and Mo<sub>3</sub>C<sub>2</sub> was reported only above 1964 °C and 1658 °C respectively, very high temperatures.

For both MoC and Mo<sub>3</sub>C<sub>2</sub> experiments, stoichiometric amounts of the starting materials (Mo and C) were ground together to afford the desired phase (MoC (3) or Mo<sub>3</sub>C<sub>2</sub> (4)). Heating was carried out between 90 s and 30 min for a number of pellets, however, successful synthesis of either phase was never achieved. In all cases Mo<sub>2</sub>C was produced with a mixture of Mo and/or C present. This can be seen clearly in the overnight PXD patterns for both the MoC (Figure 4- 8) and Mo<sub>3</sub>C<sub>2</sub> (Figure 4- 9) experiments.

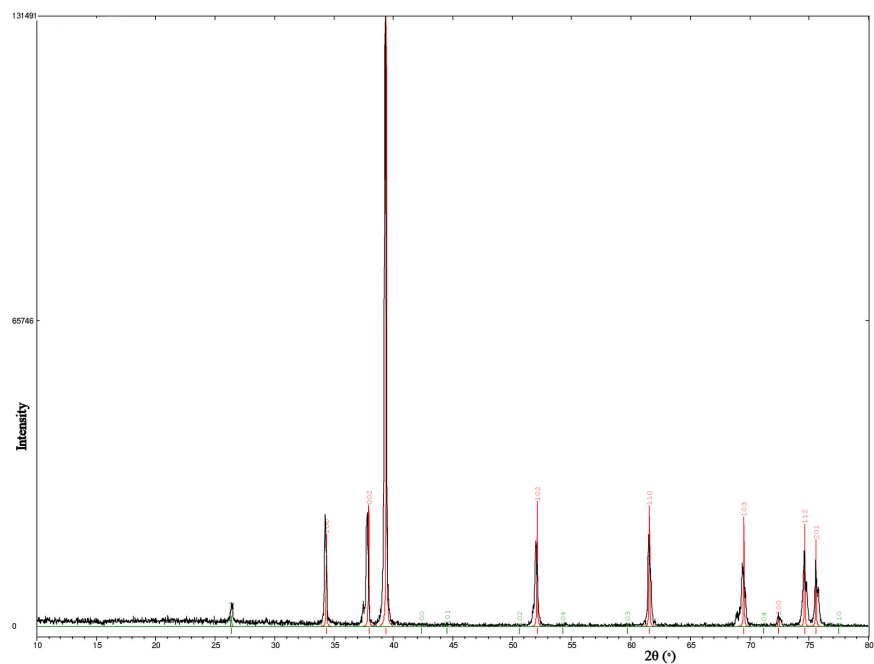


**Figure 4- 8: Overnight PXD pattern of MoC sample (black) heated for 30 min in DeLonghi DMO. Mo<sub>2</sub>C calculated pattern is red, C calculated pattern is green.**

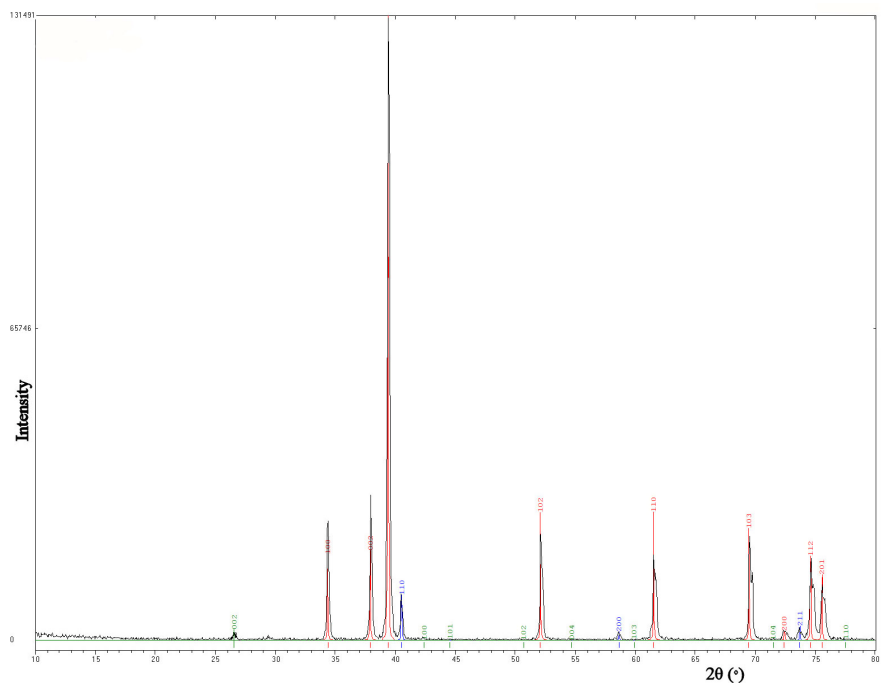


**Figure 4- 9: Overnight PXD pattern of MO<sub>3</sub>C<sub>2</sub> sample (black) heated for 30 min in DeLonghi DMO. Mo<sub>2</sub>C calculated pattern is red, C calculated pattern is green, Mo calculated pattern is blue.**

In the attempted synthesis of MoC, PXD showed the preferential formation of Mo<sub>2</sub>C resulting in excess C present in the final sample (Figure 4-8). Similarly, for the synthesis of Mo<sub>3</sub>C<sub>2</sub>, Mo<sub>2</sub>C was formed instead along with small amounts of the reactants, Mo (~ 2 %) and C (~ 5 %). Multiple repeats of the experiments still resulted in no evidence of the synthesis of Mo-C phases, bar Mo<sub>2</sub>C, despite the use of quenching post-reaction. It was therefore reasonable to conclude that the reaction temperature never reached ~ 1650 °C, which was later confirmed in the single mode cavity using an *in-situ* optical pyrometer, meaning Mo<sub>2</sub>C was formed exclusively during the reaction.

#### **4.4 RESULTS AND DISCUSSION: Mo<sub>2</sub>C SYNTHESIS USING A SINGLE MODE CAVITY**

Although much success was achieved in the DMO, progression to the single mode cavity was required for further study of the Mo-C system. With the increased power densities it was hoped shorter reaction times would be possible, as observed for the WC system, but crucially the *in-situ* monitoring of the temperature would be possible. This would answer a number of questions posed from the DMO work, plus allow the study of the reaction profile for  $\alpha$ -Mo<sub>2</sub>C synthesis.

#### 4.4.1 Mo<sub>2</sub>C synthesis and investigation

The merits of single mode cavities are discussed in detail in chapter 2, but in general they are known to enhance reaction times due to greater microwave power density. Due to precise matching of the transmission line to the applicator it is possible to allow maximum energy absorption by the material. With this in mind, experiments were carried out to determine the required heating time to produce a pure phase of  $\alpha$ -Mo<sub>2</sub>C from the metal powder, Mo, and C. Using the experimental procedure described in section 2.2.2, the synthesis of  $\alpha$ -Mo<sub>2</sub>C was attempted using the 3-15 kW microwave generator with a TE<sub>10n</sub> single mode cavity (5). 2 g pellets were produced from stoichiometric amounts of the Mo and C to afford the desired product,  $\alpha$ -Mo<sub>2</sub>C. The pellets were then heated, in turn, for a given amount of time between 5 and 30 s within the single mode cavity at 3 kW. Multiple repeats at each time allowed the determination of reproducibility. Characterisation post-reaction, using PXD, revealed the phases present after each reaction time which ultimately indicated a complete reaction had occurred within 20 s (Figure 4-10), much faster than the multiple hours required for conventional synthesis.<sup>1,4</sup>

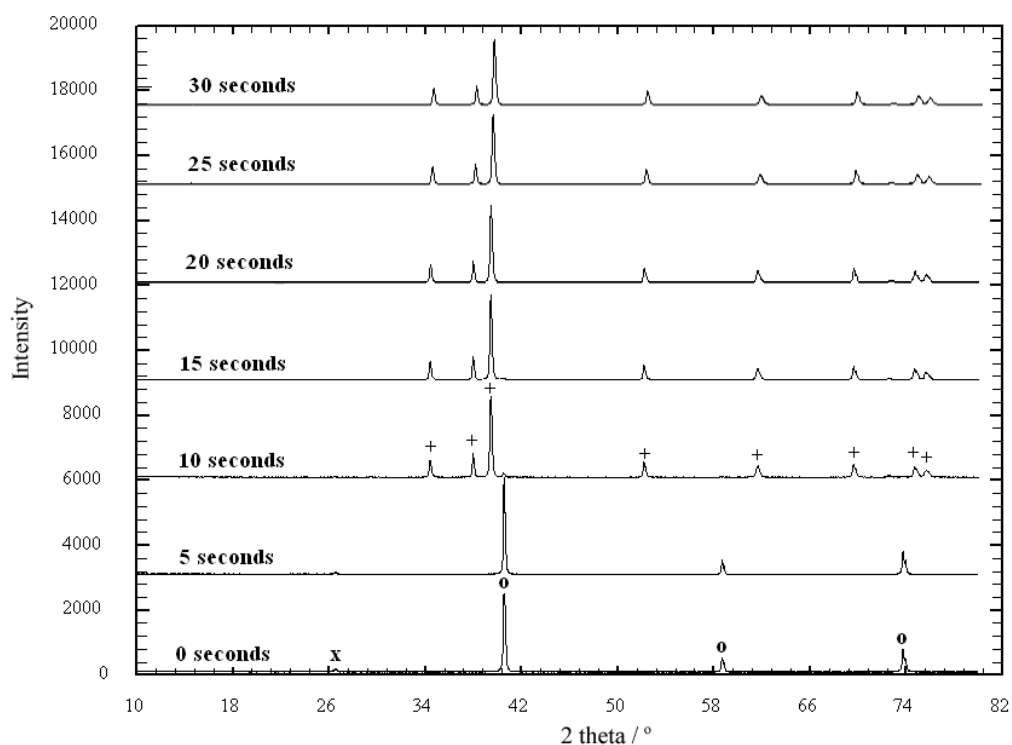


**Figure 4- 10: PXD patterns taken *ex-situ* from the Mo + C reaction, performed at 3 kW. Mo diffraction peaks are denoted by circles, C by crosses and  $\alpha$ -Mo<sub>2</sub>C by plusses.**

Although 20 s was required for 100 % Mo<sub>2</sub>C phase purity to be observed, it is clear from Figure 4- 10 that only 10 s was required for an almost complete reaction with only minor impurities observed due to Mo and C. Prior to 10 s the only phases to exist are the reactants Mo and C. Figure 4- 10 also indicates that no intermediate phase exists between the reactants and product. Therefore Mo and C react directly to form  $\alpha$ -Mo<sub>2</sub>C. In fact this transformation occurs primarily over only a 5 s interval. In principle this reaction could be even faster than this, but 5 s is the minimum gap between reactions due to experimental error. Below this the errors involved in controlling reactor power, monitoring heating time and sample removal from the cavity are too great, resulting in no noticeable difference in phase analysis post-reaction.

To confirm the result at 20 s, Rietveld refinement was carried out on the final product as well as magnetic measurements, TGA and elemental analysis. Table 4- 4 compiles the crystallographic parameters post-refinement. Figure 4- 11 displays the resultant refined diffraction pattern for the  $\alpha$ -Mo<sub>2</sub>C product. Lattice parameters are in excellent agreement with previous studies of stoichiometric  $\alpha$ -Mo<sub>2</sub>C, a difference of only 0.004 Å for *a* and *b* parameters and 0.01 Å for the *c* parameter.<sup>7</sup> Refinement of carbon stoichiometry was attempted, but resulted in an unstable refinement due to problems associated with light element detection and PXD (section 2.3.1).

Empirical formula	$\alpha$ -Mo <sub>2</sub> C
Crystal system, Space group	Orthorhombic, Pbcn
Unit cell formula weight, M <sub>w</sub>	107.9507
<i>a</i> , <i>b</i> , <i>c</i> -parameter, Å	4.73193(6), 6.0217(1), 5.2040(1)
Unit cell volume, Å <sup>3</sup>	148.287(5)
Z, Calculated density, ρ <sub>x</sub> / g cm <sup>-3</sup>	1, 9.133
Observations, parameters	5500, 21
R <sub>p</sub> , R <sub>wp</sub> , χ <sup>2</sup>	0.0596, 0.0798, 6.959
Mo position, U <sub>iso</sub> / Å <sup>2</sup>	(0.247(2), 0.1158(1), 0.0813(7)), 0.0012(1)
C position, U <sub>iso</sub> / Å <sup>2</sup>	(0, <sup>3</sup> / <sub>8</sub> , <sup>1</sup> / <sub>4</sub> ), 0.0012(1)
Interatomic distance: Mo-C, Å	2.0894(1), 2.1117(1), 2.1160(1)
Interatomic distance: Mo-Mo, Å	3.0065(1), 2.9741(1), 3.0112(1), 2.9343(1), 2.8978(1), 2.8978(1)

**Table 4- 4: PXD crystallographic and bond information for  $\alpha$ -Mo<sub>2</sub>C synthesised in 20 s at 3 kW in a single mode cavity.**

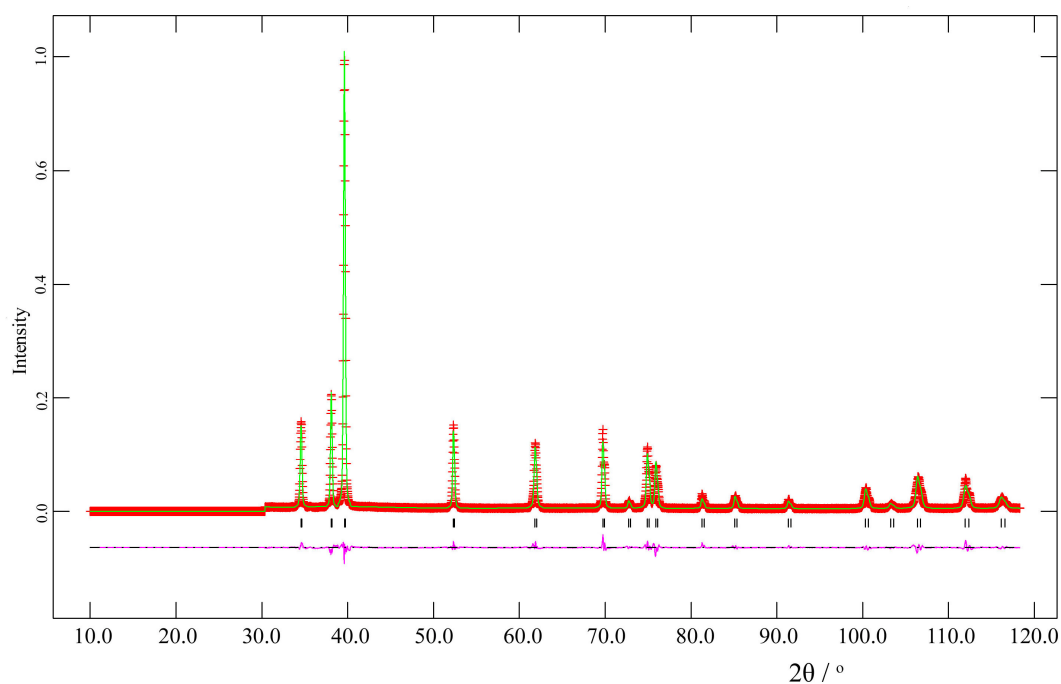


**Figure 4- 11: Observed (plusses), calculated (solid line) and difference (below) profile plot for the Rietveld refinement against PXD data for Mo<sub>2</sub>C product synthesised in 20 s at 3 kW in a single mode cavity. Tick marks denote Mo<sub>2</sub>C reflection positions.**

No obvious amorphous content is observed with PXD and thermogravimetric analysis (TGA) of the final product under oxygen revealed only a weight gain (141.6 %) corresponding to the oxidation of  $\alpha$ -Mo<sub>2</sub>C at 475 °C (to MoO<sub>3</sub>, as confirmed by PXD) (Figure 4- 12). The sample was heated from 20 °C to 650 °C with a ramp rate of 2 °C/min. The temperature was then held at 650 °C for 3 h to ensure complete oxidation of the carbide. The temperature was never increased beyond 650 °C due to previously observed weight loss above 700 °C until only elemental Mo is left (confirmed by PXD). It is believed that any elemental carbon, which may exist after the carbide is oxidised, is responsible for the reduction of the metal oxide.

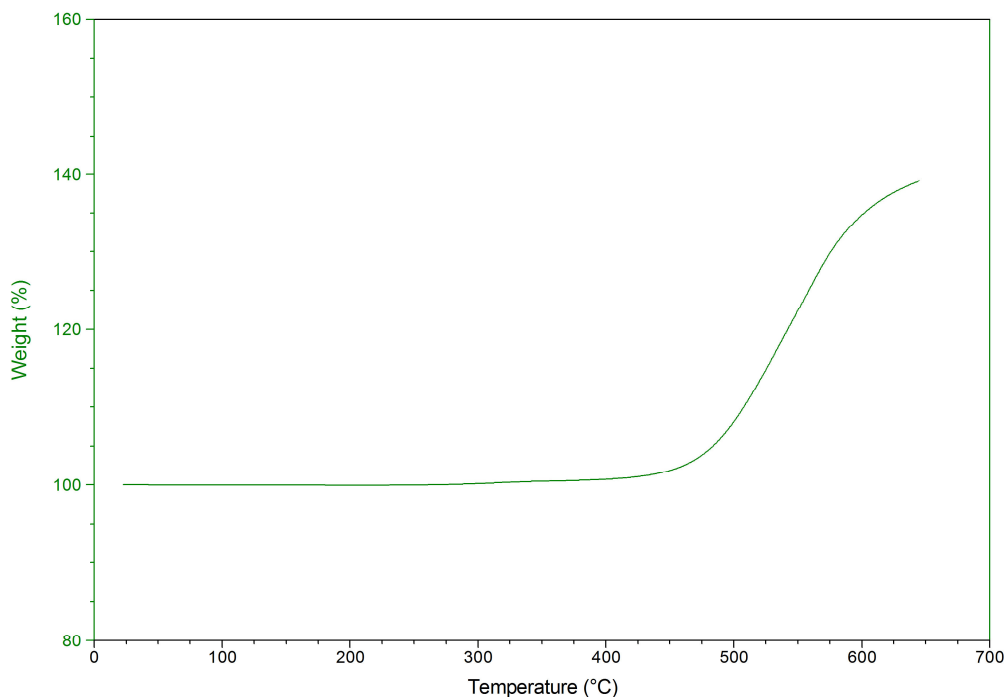


**Figure 4- 12: TGA plot indicating the oxidation of  $\alpha$ -Mo<sub>2</sub>C beginning at 475 °C.**

Energy dispersive analysis by X-rays (EDX) yielded an Mo:C ratio of 2:0.99(3), with no other elements present. Analysis for Mo and C by X-ray fluorescence spectroscopy (XRF) and combustion analysis respectively yielded an Mo:C ratio of 2:0.99(1). Both these results strongly suggest the formation of stoichiometric  $\alpha$ -Mo<sub>2</sub>C.

Magnetic measurements using SQUID resulted in an observed superconducting transition temperature ( $T_c$ ) at 3.5(1) K and a superconducting volume fraction of 97 %. This confirms the formation of the desired product and indicates the presence of no other superconducting phase.

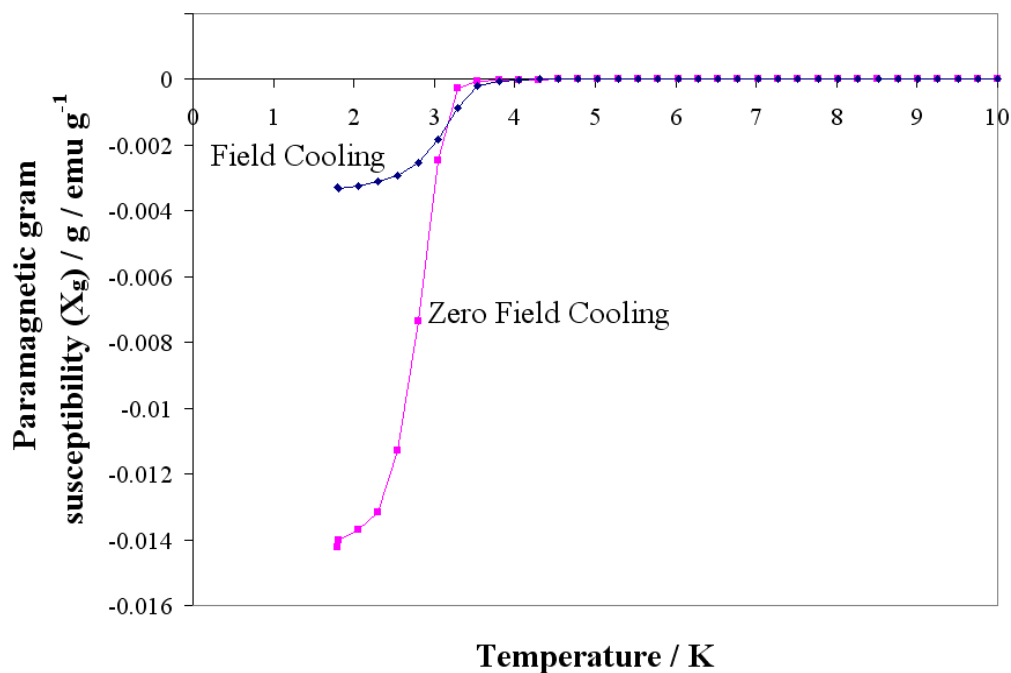


**Figure 4- 13: Plot of mass susceptibility,  $\chi_g$ , against temperature, for superconducting  $\alpha$ -Mo<sub>2</sub>C synthesised in 20 s at 3 kW in a single mode cavity. Plot shows a  $T_c$  onset at 3.5(1) K.**

Similar to work observed in the DMO, the product synthesised using the single mode cavity resulted in a  $T_c$  lower than expected for the observed phase. In fact this superconducting transition temperature is associated with the upper end of  $\beta$ -Mo<sub>2</sub>C,<sup>8</sup> however, the low value could be associated with the final structure of the carbide. Although no formal investigation has been carried out in the literature to the effect of carbon non-stoichiometry on the superconducting transition temperature of Mo<sub>2</sub>C, it is well documented that, in general,  $T_c$  onset decreases with increasing C vacancy for transition metal carbides.<sup>22, 23</sup> PND refinements performed on successfully synthesised Mo<sub>2</sub>C in the DMO resulted in a Mo:C ratio of 2.00:0.9696(2). It is this carbon non-stoichiometry which could explain the reduction in  $T_c$ , however it is by no means certain that this is the case.

#### ***4.4.1.1 Powder Neutron Diffraction (PND) structural investigation***

Due to the uncertainty over the Mo<sub>2</sub>C phase synthesised, raised by the magnetic measurement results, it was deemed necessary to investigate, using PND, the Mo<sub>2</sub>C product formed in 20 s at 3 kW in the single mode cavity to see if a)  $\alpha$ -Mo<sub>2</sub>C had been formed and b) to compare the refinement parameters with those reported in Table 4- 4 for PXD as well as the supporting characterisation data.

PND data was collected on POLARIS at ISIS, Rutherford Appleton Laboratory (RAL) in Oxfordshire (section 2.3.2.2). POLARIS operates by simultaneously collecting all d-spacings with data collected across 4 banks of detectors until the error on the diffraction patterns was deemed suitably small so that all diffraction peaks were visible (3 h). Before a scan was taken approximately 2 g of the sample was loaded into a 5mm diameter vanadium canister which was then lowered into the sample tank of the diffractometer. Post-collection, Rietveld refinement (section 2.3.3) against the data was performed using the General Structure Analysis System (GSAS)<sup>18</sup> through the windows based EXPGUI interface.<sup>19</sup> Data were refined concurrently against the  $\alpha$ -Mo<sub>2</sub>C structure proposed by Epicier<sup>7</sup> and the  $\beta$ -Mo<sub>2</sub>C structure proposed by Rudy<sup>6</sup>. In both cases refinement was started with the background coefficients, followed by the unit cell, atomic positions, profile parameters and isotropic temperature factors. Finally the absorption/reflectivity correction and carbon occupancy were refined. The resultant profile plot can be seen in Figure 4- 14 with Table 4- 5 comprising selected crystallographic parameters post-refinement.

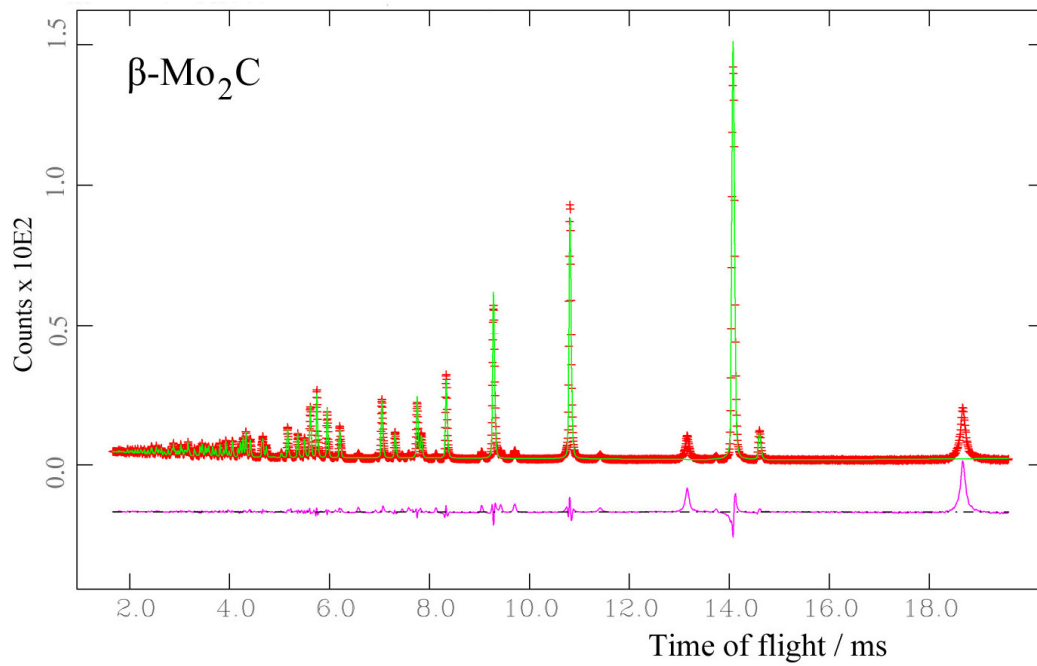
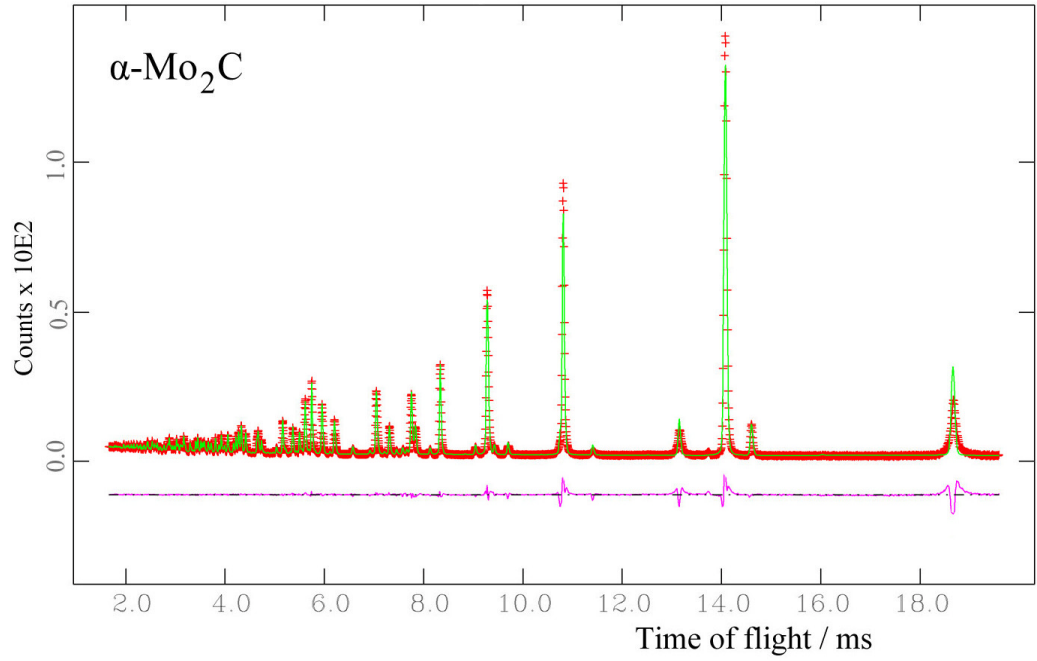


**Figure 4- 14: Observed (plusses), calculated and difference profile plots for Rietveld refinements of  $\alpha$ -Mo<sub>2</sub>C and  $\beta$ -Mo<sub>2</sub>C against PND data (bank c) for Mo<sub>2</sub>C produced in 20 s at 3 kW in a single mode cavity.**

Sample	$\alpha$ -Mo <sub>2</sub> C	$\beta$ -Mo <sub>2</sub> C
Empirical formula	Mo <sub>2</sub> C	
Unit cell formula weight, M <sub>w</sub>	107.9507	
Crystal system, Space group	Orthorhombic, Pbcn	Hexagonal, P6 <sub>3</sub> /mmc
<i>a</i> , <i>b</i> , <i>c</i> -parameter, Å	4.73978(4), 6.02846(8), 5.20408(7)	3.00949(4), 3.00949(4), 4.74000(9)
Unit cell volume, Å <sup>3</sup>	148.699(3)	37.179(3)
Z, Calculated density, ρ <sub>x</sub> / g cm <sup>-3</sup>	1, 9.068	1, 27.67
Observations, parameters	15569, 49	15655, 45
R <sub>p</sub> , R <sub>wp</sub> , χ <sup>2</sup>	0.0781, 0.0325, 5.071	0.1153, 0.0628, 27.67
Mo position and occupancy, U <sub>iso</sub> / Å <sup>2</sup>	(0.24531(8), 0.1223(1), 0.0803(1)), 2.00, 0.00323(4)	( <sup>1</sup> / <sub>3</sub> , <sup>2</sup> / <sub>3</sub> , <sup>1</sup> / <sub>4</sub> ), 1.00, 0.0037(1)
C position and occupancy, U <sub>iso</sub> / Å <sup>2</sup>	(0, <sup>3</sup> / <sub>8</sub> , <sup>1</sup> / <sub>4</sub> ), 0.947(2), 0.00313(6)	(0, 0, 0), 1.48(1), 0.0042(1)
Interatomic distance: Mo-C, Å	2.0914(1), 2.1125(1), 2.1180(1)	2.1029(1)
Interatomic distance: Mo-Mo, Å	3.0069(1), 2.9768(1), 3.0142(1), 2.9379(1), 2.9004(1)	2.9385(1)

**Table 4- 5: PND Crystallographic and bond information for Mo<sub>2</sub>C synthesised in 20 s at 3 kW in a single mode cavity.**

From the data and profiles observed in Table 4- 5 and Figure 4- 14 respectively it is apparent that  $\alpha$ -Mo<sub>2</sub>C has been formed. Examination of Figure 4- 14 clearly shows a difference in the orthorhombic and hexagonal structure: A number of reflections are observed, for example *hkl* 112 and 111 (both situated at the right end of the pattern), which exist in the former structure, but not the latter. This directly affects the data analysis, resulting in a more stable refinement for  $\alpha$ -Mo<sub>2</sub>C indicated by a much better fit between the recorded and calculated pattern; a  $\chi^2$  of 5.071 compared to 27.67 for the  $\beta$ -Mo<sub>2</sub>C structure.

The results obtained from PND are a clear indication that  $\alpha$ -Mo<sub>2</sub>C is indeed the observed phase. The resultant crystallographic data agree with previously discussed PXD results (section 4.4.1), but, crucially, possible refinement of carbon occupancy was possible indicating a Mo:C ratio of 2: 0.947(2). This is lower than elemental analysis and EDX indicated, but is likely to be more accurate due to the sensitivity of PND. More particularly, PND relates to C present only within the Mo<sub>2</sub>C phase as opposed to the entire sample. Similar to previous PND results for DMO synthesised  $\alpha$ -Mo<sub>2</sub>C, this refinement of carbon occupancy shows a definite carbon non-stoichiometry which could explain the relatively low T<sub>c</sub> observed for this material (Figure 4-13). As discussed earlier, although the topic has had only a few publications, T<sub>c</sub> onset is known to decrease dramatically with increased C non-stoichiometry. In particular, in the investigation of T<sub>c</sub> variation in the NbC<sub>1-x</sub> and TaC<sub>1-x</sub> carbides, this non-stoichiometry was shown to bring about a rapid reduction in T<sub>c</sub> with superconductivity completely lost at *ca* 15 % C vacancies.<sup>22, 23</sup> There is no doubt though that it is the  $\alpha$ -Mo<sub>2</sub>C with a low T<sub>c</sub> that is formed and not  $\beta$ -Mo<sub>2</sub>C with a T<sub>c</sub> at the upper end of previously reported results.<sup>8</sup>

#### ***4.4.1.2 Mo<sub>2</sub>C reaction profile study***

An important aspect of the experimental procedure for single mode cavity reactions (section 2.2.2) was the *in-situ* measurement of the surface temperature of the pellet during the reaction. An optical pyrometer was deemed most suitable for this situation due to its accuracy, if calibrated correctly, and its ability to measure surface temperatures without perturbing the microwave

field. A more detailed discussion of optical pyrometers as well as a critique on *in-situ* temperature measurements can be found in section 3.4.1. Specifically a LAND optical pyrometer was used (System4 Thermometer M1 600/1600 °C;  $\pm 1$  °C accuracy), positioned over the single mode cavity and focused so that the 5 mm diameter spot was centred on the pellets surface. With the aid of a control box the temperature could be recorded throughout the experiment resulting in temperature data for all stages of the reaction which could be compared directly with the phase fractions observed.

In addition to PXD, as discussed in section 4.4.1 (Figure 4- 10), all samples, post-reaction, underwent ex-situ dielectric property measurements; carried out using the cavity perturbation technique at room temperature (20 °C) (section 2.1.2). The resultant data, along with phase fraction information obtained from PXD (Figure 4- 10) and temperature data from the optical pyrometer, is plotted in Figure 4- 15 thus allowing the examination of the reaction profile (5).<sup>24</sup> The lines drawn on the graphs act only as a visual guide. It is important to remember that dielectric properties are temperature dependant and so the results reported are not absolute, however the relative difference and thus the important trend should always remain constant.<sup>25</sup>

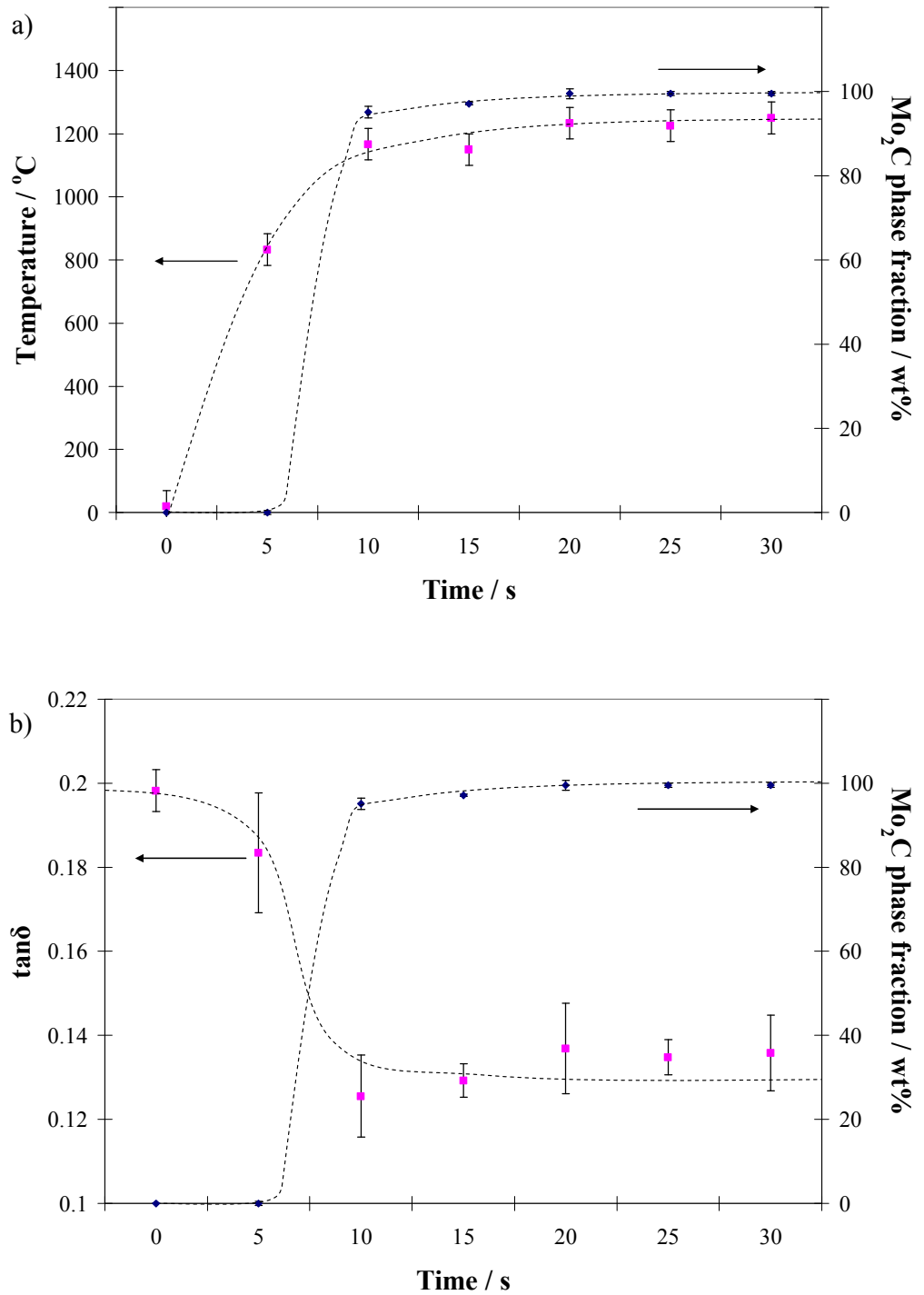


**Figure 4- 15: Plot of a) temperature and Mo<sub>2</sub>C phase fraction vs. reaction time; b) loss tangent, tan δ and Mo<sub>2</sub>C phase fraction vs. reaction time.**

Figure 4- 15 shows formation of the product is negligible below 5 s, however the rate of change of temperature at this point is high. From 5 – 10 s  $\alpha$ -Mo<sub>2</sub>C formation is observed with a commensurate and significant change in gradient of the temperature curve. At 10 s the composition of the sample is close to 100 %  $\alpha$ -Mo<sub>2</sub>C and at this point the temperature begins to stabilise. Considering the dielectric data, little difference in the real part of the permittivity,  $\epsilon'$ , was observed over the course of the reaction, however a noticeable decrease in the imaginary part,  $\epsilon''$ , was observed as the reaction progressed. Hence we observe an overall decrease in the loss tangent,  $\tan\delta$ , over the period of the reaction (20 s and beyond), possibly due to the consumption of the C reactant.

Comparison of the results in Figure 4- 15 highlights a relationship between dielectric properties, phase fraction and temperature. A noticeable reduction in  $\tan\delta$  is observed between 5 and 10 s coinciding with the rapid formation of the  $\alpha$ -Mo<sub>2</sub>C phase and the sharp change in gradient of the temperature curve (towards the  $x$  axis). The absorbed power per unit volume is directly proportional to the dielectric loss factor in addition to the electric field strength inside the material squared. Over the initial 10 s period the temperature rises to around 1200 °C, but from this point forward the rate of heating is very low with the temperature always remaining lower than the 1500 °C necessary for conventional synthesis. From the combined sets of data, one can thus define two unambiguous heating regimes; the first in which microwave dielectric heating mediates the reaction and the second in which heating is dominated by conventional conduction.

The highest rate of heating occurs before most of the Mo and C has produced  $\alpha$ -Mo<sub>2</sub>C and one can thus infer that the exothermic formation of  $\alpha$ -Mo<sub>2</sub>C ( $\Delta H_{f, 298} = -46.05 \pm 2.9 \text{ kJ mol}^{-1}$ )<sup>3</sup> is not a major contributor to the initial rapid heating. Manifestly, the dielectric properties of the components play a central role in the reaction, with self-termination resulting from the loss of components, C and Mo, with superior microwave absorbing properties. That the initial interaction of the mixture with the applied microwaves is so favourable is not unexpected given that ordered forms of carbon couple strongly to microwaves<sup>26</sup> (partly due to their conductivity, as discussed in section 3.4.4.1) and one might expect finely divided metals such as molybdenum to contribute to heating ohmically in a high frequency electric field (electrical conductivity is  $1.914 \times 10^7 \text{ Sm}^{-1}$  at room temperature, decreasing with increasing temperature).<sup>26, 27, 28</sup> Hence, as in the W-C system (section 3.4.1),<sup>29</sup> the accelerated self terminating formation of the carbide produces phase-pure product with no decomposition, melting, oxidation or safety issues that would arise from thermal runaway. Once again, as observed for the W-C system, these observations raise the possibility of industrial scale-up. Given optimisation of the cavity, the overall reaction time ( $\approx 20 \text{ s}$ ), initial enhanced heating and the final self-termination imply that one could engineer a continuous, flow process to rapidly produce large amounts of crystalline, single phase Mo<sub>2</sub>C.

Although industrial scale-up is beyond the scope of this thesis a number of important observations have been observed which could facilitate this procedure. A direct link between temperature, dielectric properties and phase

fraction has been noted with the possibility of a degree of control over the reaction established from these results. Using dielectric property measurements it is possible to predict, with reasonable accuracy, the phase fraction of the sample. This would give a good indication as to the progress of the reaction and allows for a degree of control over the product. With the aid of *in-situ* temperature measurements it could also be possible to manufacture a feedback system in which the temperature directly controlled the applied power of the microwave generator allowing precise control over the reaction temperature. In addition, if possible, *in-situ* dielectric property measurements could be taken to allow for phase monitoring concurrent with the reaction.

#### **4.4.2 Mo<sub>2</sub>C synthesis: variations in applied power**

In an effort to examine the synthesis of  $\alpha$ -Mo<sub>2</sub>C further, variations in applied power were investigated (6). Despite the rapid reaction times observed with only 3 kW microwave power, both 5 kW and 10 kW were examined. 2 g pellets, comprising stoichiometric amounts of Mo and C to afford  $\alpha$ -Mo<sub>2</sub>C, were heated for 5 s or 10 s at 3, 5 or 10 kW applied power and their temperature monitored using an *in-situ* optical pyrometer. PXD, carried out *ex-situ* post-reaction, revealed the Mo<sub>2</sub>C phase fraction for a given reaction time at a specific applied power. The results of this experiment can be seen in Figure 4- 16.

At 3 kW,  $\alpha$ -Mo<sub>2</sub>C formation initiates at 5 s and reaches ~95 wt. % by 10 s. This is also observed in Figure 4- 10. At 5 kW applied power,  $\alpha$ -Mo<sub>2</sub>C formation reached a similar phase fraction by 10 s; ~95 wt. %, however, unlike

for 3 kW, formation of the product began by 5 s with ~ 13 wt. %  $\alpha$ -Mo<sub>2</sub>C observed. At 10 kW applied power an almost complete reaction was observed by 5 s; ~91 wt. %  $\alpha$ -Mo<sub>2</sub>C. Unfortunately, termination of reactions longer than 5 s was required due to failure of the reaction vessel. For this reason no further discussion of experiments with 10 kW applied power will take place.

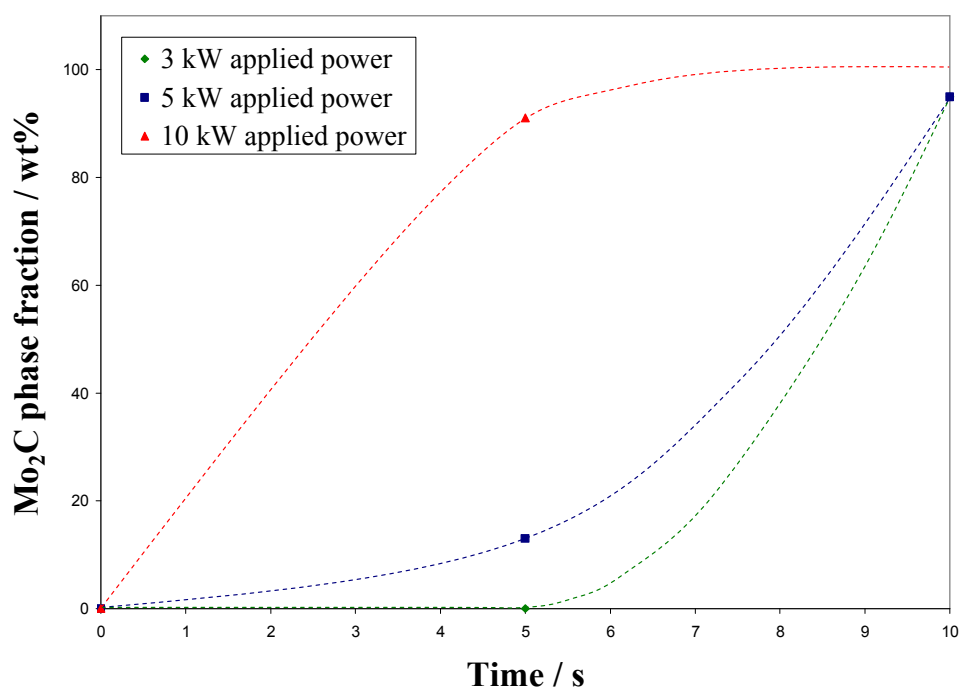


**Figure 4- 16: Plot indicating the affect of applied power on Mo<sub>2</sub>C phase fraction between 0 and 10 s.**

By investigating reaction temperatures it is clear why formation of  $\alpha$ -Mo<sub>2</sub>C is linked to applied power. Monitoring reflective power, it was observed that very little of the applied power was being reflected during any of the reactions. In other words the majority of the 3, 5 or 10 kW was being absorbed by the sample and graphite. Therefore, the more energy available, the more heat produced and so the faster the temperature rise. This hypothesis is

confirmed with data collected from the optical pyrometer. Temperatures were observed at 5 s and are reported in Table 4- 6 along with Mo<sub>2</sub>C phase fraction data.

<b>Applied power / kW</b>	<b>Approximate Temperature / °C</b>	<b>Mo<sub>2</sub>C phase fraction / wt %</b>
3	800	0
5	1050	13
10	>1600	91

**Table 4- 6: Reaction temperature for specific applied powers after 5 s exposure.**

Looking at the results from the reaction profile study, an almost pure phase of  $\alpha$ -Mo<sub>2</sub>C is observed in 10 s with an applied power of 3 kW and a reaction temperature of ~1200 °C (Figure 4- 15). Table 4- 6 indicates that no product is observed at 800 °C for the same applied power. Therefore, between 5 and 10 s,  $\alpha$ -Mo<sub>2</sub>C formation must begin when the temperature becomes appropriate, however, discovering the exact reaction initiation temperature on this timescale is difficult.

If the phase diagram is studied (Figure 4- 1), formation of both  $\alpha$ -Mo<sub>2</sub>C and  $\beta$ -Mo<sub>2</sub>C does not begin until 1000 °C. Examining the information in Table 4- 6 indicates that with an applied power of 5 kW formation of  $\alpha$ -Mo<sub>2</sub>C has already begun at 5 s, although only a low percentage of the product is observed. The reaction temperature of ~1050 °C associated with this experiment narrows down the reaction initiation temperature and crucially agrees with the values reported in the phase diagram. Therefore it appears that

$\alpha$ -Mo<sub>2</sub>C formation begins between 800 and 1050 °C, likely closer to the top end of this bracket due to the low percentage of  $\alpha$ -Mo<sub>2</sub>C observed at 5 s and 5 kW and the relevant data published in the phase diagram (Figure 4- 1).

#### **4.4.3 Sealed reaction investigation (Experiment 7)**

As discussed in the introduction (section 1.1.2), the majority of transition metal carbide synthesis reactions are performed in a vacuum or a flowing inert gas atmosphere, such as argon. The reason being, with the high temperatures required for synthesis, the metal and carbide are readily oxidised resulting in an unsatisfactory product. Synthesis of non-oxygen containing carbides is also particular difficult for targeted carbon non-stoichiometric phases.<sup>4</sup> Oxygen content has, however, been reduced through the use of rapid reaction times and high vacuum conditions.<sup>3</sup>

It is apparent thus far that microwave heating results in rapid reaction times. In fact, within the single mode cavity, reactions have been completed in under 60 s for all carbides investigated in this thesis. Synthesis in the DMO, however, has not been as rapid, but still synthesis times of less than 30 min have been reported. In all cases successful synthesis of the carbide, from their respective metal powders and carbon, was carried out in open top silica tubes in which the pellet (imbedded in graphite powder) was situated (section 2.2). It should also be noted that PXD and PND never indicated the presence of metal oxide in the final product regardless of the applicator used. Considering the reaction temperatures observed, for example ~1200 °C for Mo<sub>2</sub>C synthesis, one might expect the formation of small amounts of metal oxide, however, PXD of

the bulk powder never indicated this. For this reason a more detailed investigation of the resultant powders for molybdenum carbide experiments, using X-ray Photoelectron Spectroscopy (XPS), was conducted as part of sealed system studies (7).

Samples were synthesised, using the experimental procedure described in section 2.2.2, in 20 s at 3 kW applied power in a single mode cavity. Post-reaction samples, still in pellet form, were adhered to carbon tabs and characterisation was then carried out using XPS. This technique is for surface characterisation only and can analyze a sample to a depth of 2 to 5 nm. XPS reveals all chemical elements present, but importantly can also distinguish oxidation states thus allowing the suggestion of chemical bonds between elements. In particular, this would propose if Mo is bonded to oxygen, in the case of the metal oxide, or carbon with respect to the carbide.

Samples were first characterised without any preparation, i.e. straight from the experiment and not etched. Pellets were subsequently etched using a fine jet of argon gas which removes the outer few layers (< 5 nm) of material from the sample. Following this samples were characterised again using XPS. The results from this analysis can be seen in Figure 4- 17 and Figure 4- 18. The plots indicate, for both pre- and post-etching carbon exists in the structure (Figure 4- 17). This is clearly not unexpected given the make-up of the pellet and the carbide. More importantly Figure 4- 18 indicates that, pre-etching, there is definitely some MoO<sub>3</sub> present in the sample; however, post-etching this disappears and the only visible peaks are associated with Mo<sub>2</sub>C.

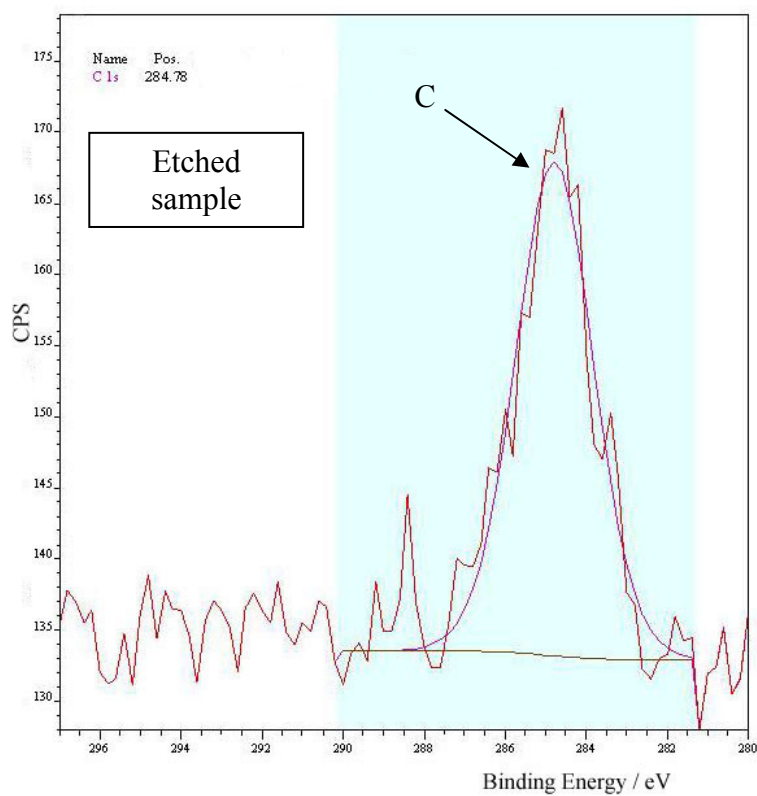
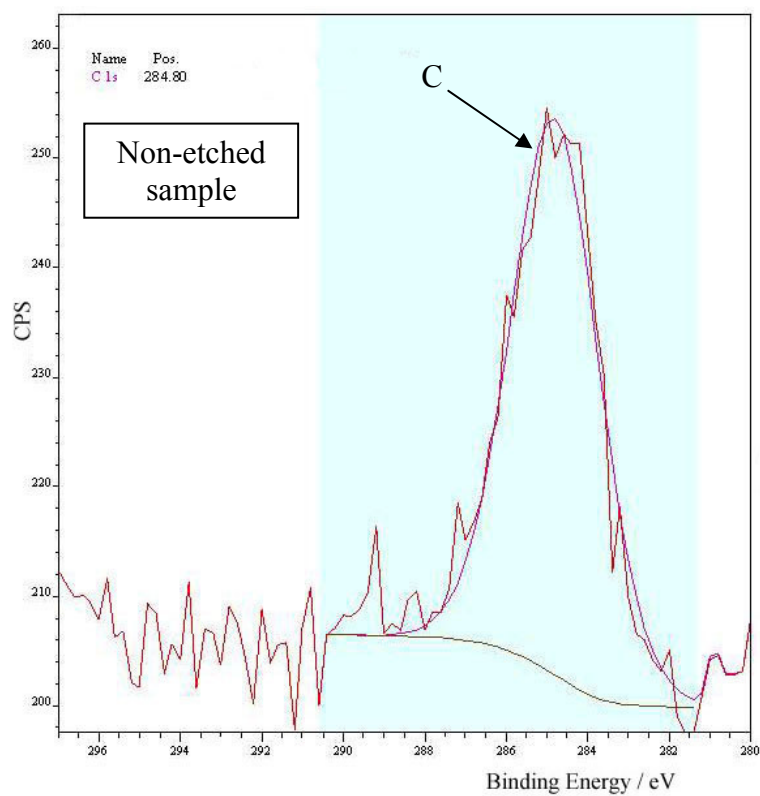


**Figure 4- 17: XPS plots showing C present in Mo<sub>2</sub>C sample synthesised in 20 s at 3 kW in the single mode cavity. Top plot is for non-etched sample, bottom plot is for etched sample.**

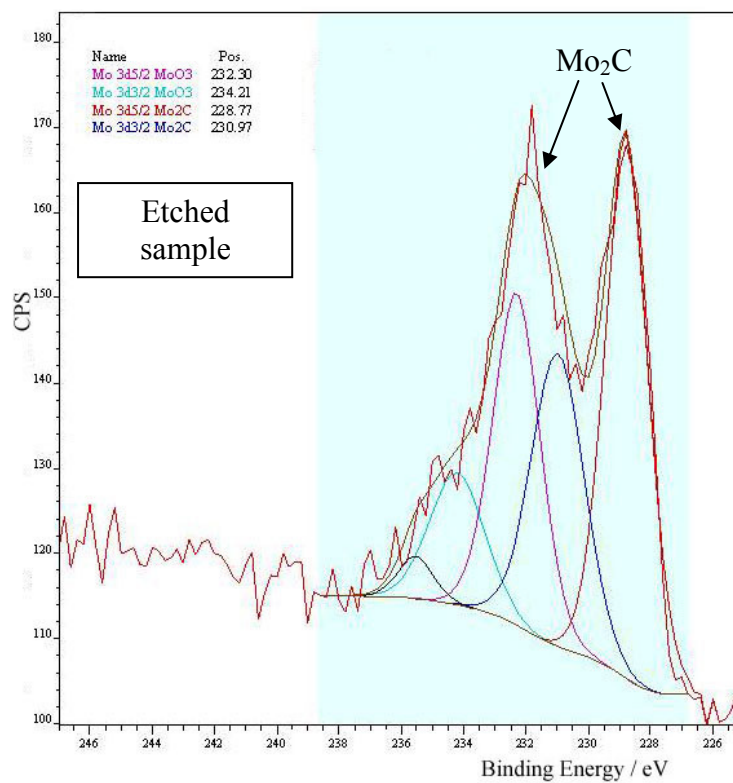
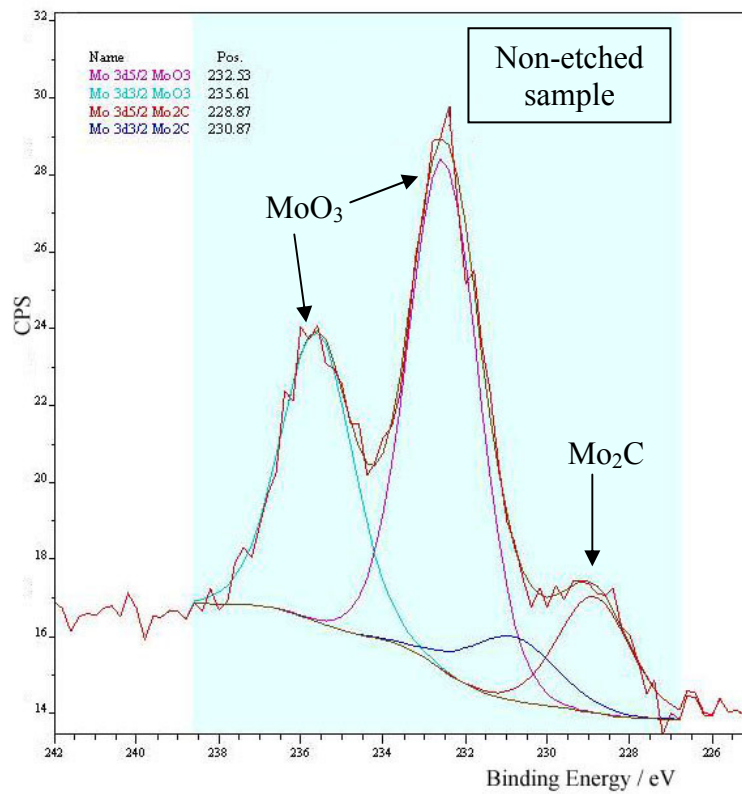


**Figure 4- 18: XPS plots showing Mo present in Mo<sub>2</sub>C sample synthesised in 20 s at 3 kW in the single mode cavity. Top plot is for non-etched sample, bottom plot is for etched sample.**

XPS clearly demonstrates the existence of surface metal oxide, specifically  $\text{MoO}_3$ . This is defined by the two peaks corresponding to Mo found chemically bonded to O (shown on the plot). This plot also indicates the presence of  $\text{Mo}_2\text{C}$  (Mo chemically bonded to C), however only a small amount is observed compared to the metal oxide. With the use of argon etching, however, the metal oxide is almost completely expunged from the plot leaving only Mo associated with the carbide,  $\text{Mo}_2\text{C}$ . Despite the existence of oxide, it is apparent that it is limited to the surface of the carbide given the disappearance of any  $\text{MoO}_3$  peaks with the removal of only a few nm of the surface of the sample. Regardless of reaction times, this oxide coating was also observed, although only ever at the pellet surface, with no other metal oxide (specifically  $\text{Mo}_4\text{O}_{11}$  and  $\text{MoO}_2$ ) present.

In response to the XPS examination of  $\text{Mo}_2\text{C}$  product, sealed system experiments were carried out in the hope that the metal oxide would not form. Experiments were carried out as discussed in section 2.2.2, however, the quartz reaction tube, containing the pellet and graphite powder, was sealed under a vacuum. For this the tube was connected to a rotary vacuum pump, evacuated down to a pressure of  $10^{-4}$  Torr, and then sealed by heating with a glass blow torch (Figure 4- 19). This created a sealed tube which contained the pellet, imbedded in graphite powder, all sealed under a vacuum.

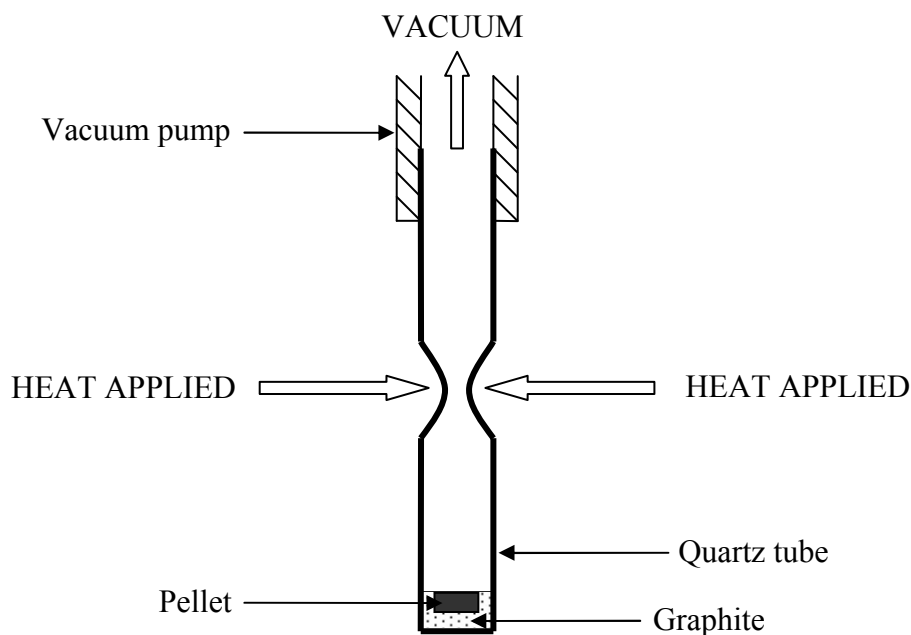


**Figure 4- 19: Simple schematic indicating the sealing of the quartz tube.**

Reactions were then carried out in the single mode cavity at 3 kW with a heating time of 20 s. Although not crucial in these experiments, it was not possible to monitor the reaction temperature during the experiment due to interference between the top of the sealed tube and the IR beam of the optical pyrometer. These experiments were also difficult to carry out with the majority of reactions having to be terminated due to fracturing of the quartz tube. This was most probably due to weakening of the tube during the sealing process and the sudden and rapid onset of high temperatures during the reaction. It is also possible that oxygen was still present in the tube which resulted in the formation of CO/CO<sub>2</sub> gas and the consequent fracturing of the reaction vessel. It has been documented that oxygen bonds readily to carbon and is hard to remove,<sup>3, 12</sup> even under vacuum, or it is possible that the oxygen making up the quartz tube (SiO<sub>2</sub>) reacted directly with the C present under the high temperatures.

Post-reaction samples were analysed with PXD and XPS, however, in all cases PXD indicated the presence of no bulk oxide with observations of surface oxide under XPS. In fact results seemed very similar to experiments carried out in open reaction vessels, indicating that either the tubes were not sealed properly or that minute amounts of oxygen exist within the system prior to microwave heating. Due to the number of repeats carried out it is unlikely the first explanation is plausible which means oxygen must be present, either as described above, or that the high temperatures allow oxygen to be stripped directly from the quartz tube ( $\text{SiO}_2$ ) to form the metal oxide. In any case it seems oxide formation, regardless of the quantity observed, is immensely difficult to remove completely. On a positive note, however, XPS only indicates a diminutive amount of the oxide,  $\text{MoO}_3$ , present which is not even detected with PXD. For this reason it seems that, with these reaction timescales, no sealed systems are required allowing experiments to be carried out open to the surrounding atmosphere. This certainly simplifies and accelerates the experimental procedure and should definitely be taken into account when comparing this synthesis method to other techniques used for carbide production. In fact, it is possible these existing manufacturing techniques may result in surface oxide being present, although this could only be verified with characterisation.

## **4.5 RESULTS AND DISCUSSION: Mo<sub>2</sub>C SYNTHESIS FROM THE OXIDE, MoO<sub>3</sub> (Experiments 8, 9)**

Synthesis of carbides from the metal oxide allows for a much more economical process as the oxide is much cheaper to purchase than the metal powder. However, as discussed in section 1.1, synthesis often results in insufficient purity for industrial applications with the presence of oxygen affecting properties of the material and weakening the carbide structure.<sup>1</sup> For this reason the synthesis process is often carried out in multiple steps, reduction of the oxide to the metal powder, under either a reducing atmosphere or using carbon powder and a vacuum, followed by synthesis of the carbide from the resultant metal.<sup>12</sup> Despite the use of a two step process however, arc melting or high vacuum annealing is often still required to purify the product.<sup>3</sup>

If one is to look towards industrial processing of the carbides, the synthesis of the desired material from the oxide precursors becomes of paramount importance. For this reason the study of microwave synthesis from the oxide was attempted and is discussed here.

### **4.5.1 Mo<sub>2</sub>C synthesis in a Domestic Microwave Oven (DMO)**

Experiments concerning microwave synthesis of the carbide from the metal oxide have not received much interest in the literature. This could well be due to the increased complexity with reduction of the oxide required prior to carbide formation, but it is likely that laboratory experiments are just not concerned with potential scale up reactions at this stage. Mirroring this, most of

the work reported in this thesis concerns synthesis from the metal powders and carbon, however, it would not be prudent if reactions involving the oxide precursor were not investigated. However, the lack of success with respect to the W(-O)-C system (section 3.4.5), meant that little knowledge could be applied to build on results for the Mo-C system. For this reason the experiments were examined from the initial stages of development.

Molybdenum oxide, MoO<sub>3</sub>, is known to heat poorly under microwave energy. In fact temperatures have been recorded to ramp at a slow rate of only 15 °C/min,<sup>30</sup> meaning it is unlikely that a reaction will proceed without the use of a precursor. Fortunately this was not an issue as graphite, which as shown previously is an excellent susceptor, can also be used as a reducing agent. Reactions involving MoO<sub>3</sub> and graphite took two approaches; a one-step synthesis and the traditional two-step synthesis (8). Firstly synthesis was attempted in a similar fashion to conventional manufacturing methods. The oxide was first reduced and then the resultant metal powder was reacted to afford the carbide, α-Mo<sub>2</sub>C. Secondly a single step reaction was attempted with *in-situ* reduction of the oxide, MoO<sub>3</sub>, occurring alongside the formation of the carbide.

#### ***4.5.1.1 1<sup>st</sup> approach: Two-step synthesis***

The two-step process first involved the reduction of the oxide, MoO<sub>3</sub>, to the metal, Mo. Once this was achieved, synthesis of the carbide, α-Mo<sub>2</sub>C, could then be carried out as described in section 4.3.1 (experimental procedure reported in section 2.2.1). Providing the reduction was complete to the metal,

this 2<sup>nd</sup> carbide synthesis step, thanks to previous investigations using the metal powder, was always successful. For this reason only the 1<sup>st</sup> step will be discussed here.

Initially reduction of MoO<sub>3</sub> was attempted as a powdered mixture of the oxide and graphite.



Stoichiometric amounts of the starting materials (1 g total) were ground together to afford the products, Mo and CO. It was assumed that all gas evolved would be in the form of CO and not CO<sub>2</sub>, although in reality it was likely a mixture of the two would exist (as observed for the W-C system). The reaction mixture was kept as a powder and placed into a 10 mm diameter quartz tube which was supported in a beaker of silica flour. A pellet was not used given previous problems observed with the W-C system where pellet destruction was frequent due to rapid gas evolution (section 3.4.5). Subsequent heating of the reaction mixture in the DMO for 30 min resulted in the successful reduction of the oxide (Figure 4- 20). However, although no oxide was present, Mo<sub>2</sub>C was observed alongside the desired Mo (Figure 4- 20). Although a low intensity for the carbide reflections revealed only a small amount present (~5 %), pure Mo would have been ideal. PXD also revealed the existence of no C in the sample, suggesting it reacted entirely to form either CO/CO<sub>2</sub>, Mo<sub>2</sub>C or that some C was X-ray amorphous. If, as expected, carbon formed both CO and CO<sub>2</sub>, it would be in excess, with the quantity used, for the reduction of the oxide. Ultimately this means, if the temperature was high enough, there is potential for Mo<sub>2</sub>C to be formed. In fact, regardless of the gas

being evolved, temperature is crucial if one is to reduce the oxide completely whilst avoiding carbide formation, however, monitoring of this variable is not possible with the DMO setup.

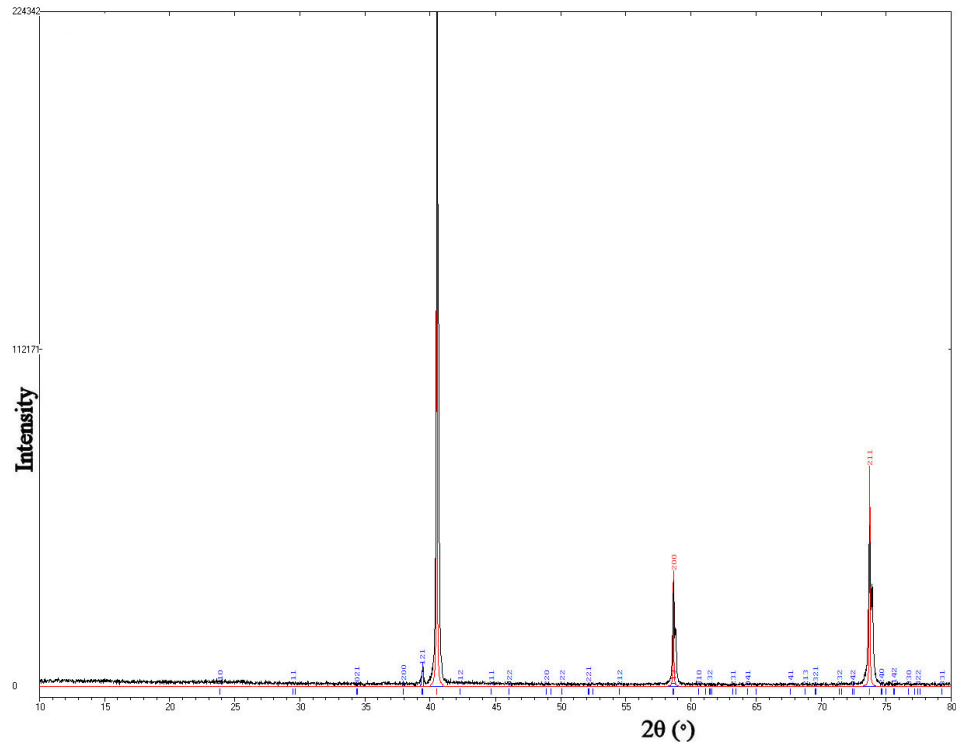


**Figure 4- 20: Overnight PXD pattern of Mo sample (black) heated for 30 min in DeLonghi DMO. Mo calculated pattern is red, Mo<sub>2</sub>C calculated pattern is blue.**

If one is to understand what is occurring, a number of variables must be examined: MoO<sub>3</sub> is known to be reduced, using carbon, at ~600 °C,<sup>31</sup> temperatures, using the single mode cavity have been observed in excess of 1200 °C for the reaction of Mo and C (section 4.4.1); the phase diagram (Figure 4- 1) indicates formation of Mo<sub>2</sub>C begins at 1000 °C, which is supported by the sealed reaction vessel experiments (section 4.4.3). These observations seem to indicate that, despite no monitoring of the temperature in the DMO, a sufficient reaction temperature exists in these oxide reduction

experiments for Mo<sub>2</sub>C formation (Figure 4- 20). It seems, therefore, that in order to reduce the oxide without the formation of the carbide, a control over the reaction temperature is required. Unfortunately this is not possible with the current DMO setup and so will be discussed later during the single mode synthesis section (4.5.2).

Finally it is worth mentioning that, despite the existence of Mo<sub>2</sub>C in the sample, the Mo, although not pure, was used in the attempted synthesis of pure  $\alpha$ -Mo<sub>2</sub>C. The carbide present was deemed insignificant at this stage considering, in the end, the desired phase was the same material. The experiment was carried out as discussed above, using the experimental procedure described in section 2.2.1, which resulted in successful synthesis of the carbide in only 90 s in the DMO at 800 W.

#### ***4.5.1.2 2<sup>nd</sup> approach: One-step synthesis***

Results from the two-step synthesis seemed to indicate that it was possible to produce Mo<sub>2</sub>C from MoO<sub>3</sub> in a single process where the oxide is reduced as the carbide is formed. By chance this was observed, due to the high temperatures probably encountered during the microwave reduction process, when the reduction of the oxide, MoO<sub>3</sub>, to Mo was attempted. Given this was using a powdered reaction mixture, it was hoped that by pelleting the reactants, after intimate grinding, successful synthesis of  $\alpha$ -Mo<sub>2</sub>C might be achieved. However, as mentioned previously (section 4.5.1.1), the rapid gas evolution associated with the microwave heating of these samples could result in disintegration of the pellet.

Pellets were prepared, with stoichiometric amounts of the starting materials to afford to desired product.



Following the experimental procedure described in section 2.2.1, pellets were heated in a Delonghi DMO at 800 W for 30 min with PXD revealing a pure phase of  $\alpha$ - $\text{Mo}_2\text{C}$ . This reaction time was later refined to 90 s; an identical time to the reaction from the metal powder, Mo. Rietveld refinement was carried out on this latter sample and the resultant plot can be seen in Figure 4-21. Table 4-7 contains the crystallographic data associated with this refinement.

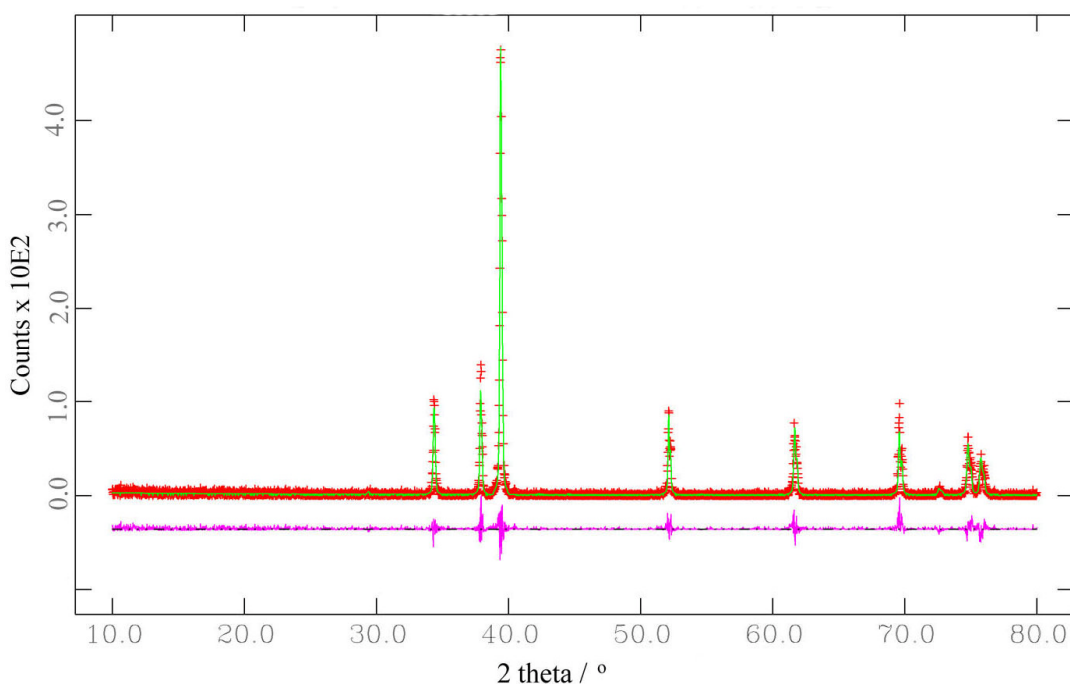


**Figure 4- 21: Observed (plusses), calculated and difference profile plots for Rietveld refinements of  $\alpha$ - $\text{Mo}_2\text{C}$  against PXD data for  $\text{Mo}_2\text{C}$  produced in 90 s at 800 W in a DMO. Tick marks denote  $\text{Mo}_2\text{C}$  diffraction peaks.**

Empirical formula	$\alpha$ -Mo <sub>2</sub> C
Crystal system, Space group	Orthorhombic, Pbcn
Unit cell formula weight, M <sub>w</sub>	107.9507
<i>a</i> , <i>b</i> , <i>c</i> -parameter, Å	4.7274(2), 6.0021(4), 5.1904(4)
Unit cell volume, Å <sup>3</sup>	147.279(3)
Z, Calculated density, ρ <sub>x</sub> / g cm <sup>-3</sup>	1, 9.195
Observations, parameters	2624, 17
R <sub>p</sub> , R <sub>wp</sub> , χ <sup>2</sup>	0.2320, 0.3352, 0.7279
Mo position, U <sub>iso</sub> / Å <sup>2</sup>	(0.247(1), 0.1114(4), 0.084(2)), 0.0047(2)
C position, U <sub>iso</sub> / Å <sup>2</sup>	(0, <sup>3</sup> / <sub>8</sub> , <sup>1</sup> / <sub>4</sub> ), 0.0028(5)
Interatomic distance: Mo-C, Å	2.0843(1), 2.1073(1), 2.1109(1)
Interatomic distance: Mo-Mo, Å	2.9982(1), 2.9695(1), 3.0014(1), 2.9293(1), 2.8933(1), 2.8913(1)

**Table 4- 7: PXD crystallographic and bond information for  $\alpha$ -Mo<sub>2</sub>C synthesised in 90 s at 800 W in a DMO.**

An excellent fit exists for the  $\alpha$ -Mo<sub>2</sub>C sample synthesised in 90 s from the oxide, MoO<sub>3</sub>. Lattice parameters are in excellent agreement with previously studied  $\alpha$ -Mo<sub>2</sub>C,<sup>7</sup> and EDX confirmed the formation of  $\alpha$ -Mo<sub>2</sub>C with a Mo:C ratio of 2.0: 1.0(2) and showed no other elements present. Magnetic measurements also revealed a superconducting onset temperature, T<sub>c</sub>, of 3.4(1) K and a superconducting volume fraction of 97.5 %. These results strongly suggest the formation of stoichiometric  $\alpha$ -Mo<sub>2</sub>C, despite once again the low T<sub>c</sub> observed for this material.

Arguably as important as the successful synthesis of  $\alpha$ -Mo<sub>2</sub>C from the metal oxide, no disintegration of the pellet was observed during the reaction, however pellets in general for these experiments always increased in volume and were fragile post-reaction. This was no doubt due to the gas evolution from the reduction of the oxide during the reaction. At this stage it is difficult to say why the pellet remains intact, especially considering there is no temperature data to examine, but one could hypothesise that it is due to the lower applied power of the DMO which directly influences the power density around the sample. This in turn would result in a slower temperature rise which may contribute to reaction stability; however, none of this can be confirmed using this experimental procedure. In spite of this it is still encouraging that a single step reaction is possible using microwave heating. In fact the reaction is complete on a similar timescale to the elemental powder reaction, which could indicate a more economical process. However, further study of this reaction is required and for that a single mode cavity is ideal; enabling the *in-situ* study of the reaction temperature as well as more precise control over the reaction.

#### **4.5.2 Mo<sub>2</sub>C synthesis in a single mode cavity**

It was hoped that the single mode cavity would allow a more detailed study of the oxide to carbide reaction process. With the exclusive examination of the one-step reaction to form Mo<sub>2</sub>C alongside the reduction of MoO<sub>3</sub> with C, it was hoped that successful synthesis would be possible on a similar timescale to the elemental reaction (20 s), as observed for investigations using the DMO.

Stoichiometric amounts of the starting materials, MoO<sub>3</sub> and C, to afford  $\alpha$ -Mo<sub>2</sub>C, were ground together and pelleted. The experimental procedure, as discussed in section 2.2.2, was followed ultimately resulting in successful synthesis of the carbide, confirmed by PXD, at 3 kW in the single mode cavity in a single step reaction in only 20 s (9). Selected crystallographic data is reported in Table 4- 8 and the resultant Rietveld refinement can be seen in Figure 4- 22.

Empirical formula	$\alpha$ -Mo <sub>2</sub> C
Crystal system, Space group	Orthorhombic, Pbcn
Unit cell formula weight, M <sub>w</sub>	107.9507
<i>a</i> , <i>b</i> , <i>c</i> -parameter, Å	4.7318(5), 6.01994(3), 5.2000(8)
Unit cell volume, Å <sup>3</sup>	148.127(3)
Z, Calculated density, $\rho_x$ / g cm <sup>-3</sup>	1, 9.143
Observations, parameters	2994, 18
R <sub>p</sub> , R <sub>wp</sub> , $\chi^2$	0.1786, 0.2756, 1.871
Mo position, $U_{iso}$ / Å <sup>2</sup>	(0.2474(8), 0.1192(2), 0.084(1)), 0.0040(3)
C position, $U_{iso}$ / Å <sup>2</sup>	(0, <sup>3</sup> / <sub>8</sub> , <sup>1</sup> / <sub>4</sub> ), 0.0036(1)
Interatomic distance: Mo-C, Å	2.0888(1), 2.1105(1), 2.1154(1)
Interatomic distance: Mo-Mo, Å	3.0045(1), 2.9732(1), 3.0103(1), 2.9339(1), 2.8970(1), 2.8958(1)

**Table 4- 8: PXD crystallographic and bond information for  $\alpha$ -Mo<sub>2</sub>C synthesised in 20 s at 3 kW in a single mode cavity.**

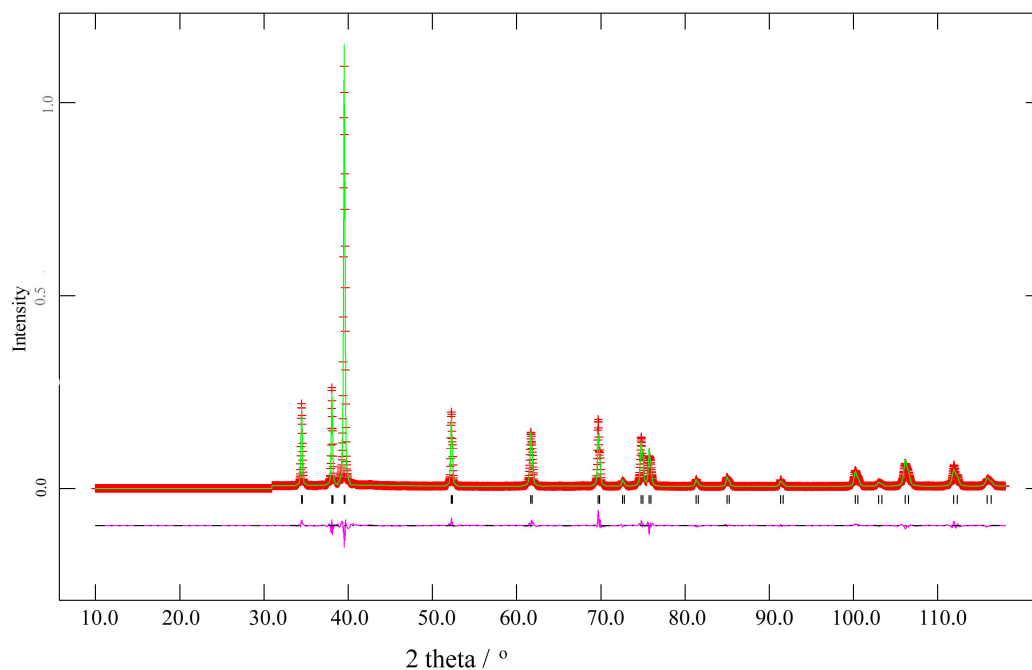


**Figure 4- 22: Observed (plusses), calculated and difference profile plots for Rietveld refinements of  $\alpha$ -Mo<sub>2</sub>C against PXD data for Mo<sub>2</sub>C produced in 20 s at 3 kW in a single mode cavity.**

The synthesis of  $\alpha$ -Mo<sub>2</sub>C from the oxide in the single mode cavity compares favourably with the experiment carried to produce  $\alpha$ -Mo<sub>2</sub>C from the elemental powders, Mo and C. Lattice parameters are in excellent agreement with those studied previously for  $\alpha$ -Mo<sub>2</sub>C.<sup>7</sup> Product formation was also confirmed with EDX; a Mo:C ratio of 2.0: 1.0(1) showing no other elements present. XRF corroborated this result, giving a Mo:C ratio of 2:0.99(1). Magnetic measurements also revealed a superconducting onset temperature,  $T_c$ , of 3.42(6) K and a superconducting volume fraction of 97.7 %. Table 4- 8 also shows an excellent fit between the calculated and observed patterns and, combined with the characterisation discussed previously, strongly suggests the formation of stoichiometric  $\alpha$ -Mo<sub>2</sub>C.

Although successful synthesis of  $\alpha$ -Mo<sub>2</sub>C had been achieved, unfortunately the single mode cavity, with its increased power and precise tuning of the electric field, resulted in one problem; pellet disintegration. Similar to WC synthesis from the oxide (section 3.4.5), the majority of reactions resulted in premature termination due to failure of the reaction vessel due to the rapid gas evolution from the pellet. Consequentially the pellet was often in multiple pieces or completely disintegrated making sample characterisation impossible in such cases.

Using *in-situ* temperature analysis a more detailed examination of the reaction process was undertaken. An optical pyrometer, discussed previously (section 4.4), was used to monitor the surface temperature of the pellet during the reaction. A number of pellets were heated at 3 kW in the single mode cavity (following the recognised experimental procedure (section 2.2.2)) between 0 and 30 s, in 5 s intervals, with multiple repeats at each time (9). It was hoped that, ultimately, a reaction profile might be achieved for the metal oxide and C reaction as had been previously investigated for the metal powder and C. Unfortunately, due to reasons discussed earlier, the majority of pellets did not remain intact during the experiments, resulting in difficulty obtaining phase information for the samples. Many of the fractured samples were lost through ejection from the vessel or integration with the susceptor/quartz tube. However, despite the lack of consistent phase fraction results with reaction time, occasional pellets remained intact for subsequent analysis and it was still hoped that the temperature data might shed some light on the reaction process. These results are reported in Figure 4- 23. It should be noted however, that these results were difficult to obtain due to the volatility of the pellet which

ultimately influenced the collection of the results. A number of results had to be discarded due to erroneous readings from the shifted reaction vessel, usually noted with a rapid drop in the observed temperature. For this reason a degree of care should be taken in the study of these results, but it is still warranted given the relative trend observed.

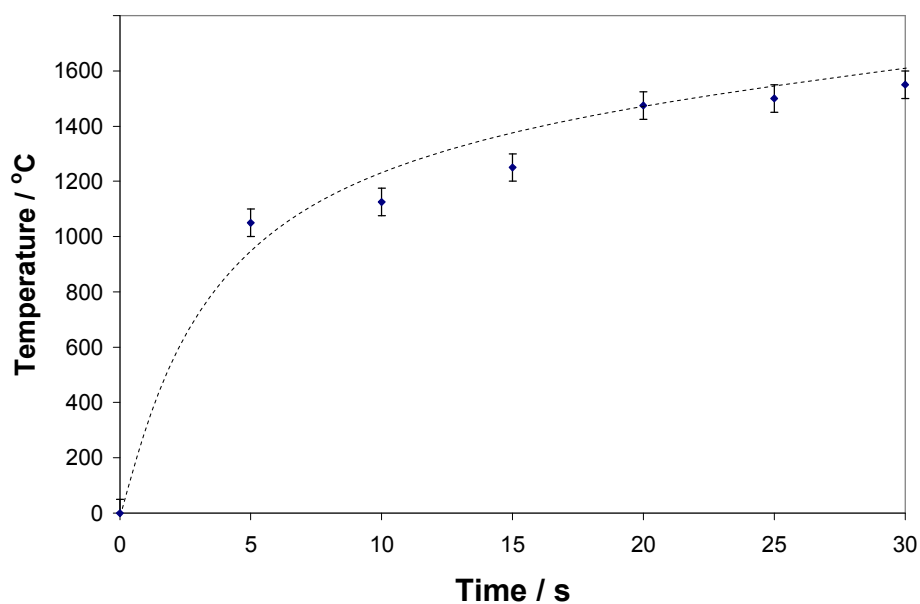


**Figure 4- 23: Plot of temperature versus time for  $\text{MoO}_3 + \text{C}$  reaction. Line acts as a guide only.**

It is apparent from Figure 4- 23 that by 5 s the reaction temperature is already greater than 1000 °C. After 5 s the elevation of the temperature retards, however, a gentle rise is still observed until a temperature of over 1400 °C is reached by the time the reaction is terminated. Noticeably the temperature never plateaus, as observed in the reaction profiles for the elemental reaction  $\text{Mo} + \text{C}$ , due to the reaction never proceeding to completion, a pure phase of  $\alpha\text{-Mo}_2\text{C}$ . Despite the overall lack of phase fraction data, recovery of a finite

number of samples and subsequent PXD revealed negligible  $\alpha$ - $\text{Mo}_2\text{C}$  present right up to 30 s. In fact the samples consisted primarily of  $\text{MoO}_3$ ,  $\text{Mo}_4\text{O}_{11}$ ,  $\text{Mo}_2\text{C}$  and C. Figure 4- 24 is a PXD plot for a sample heated for 10 s in the single mode cavity at 3 kW.

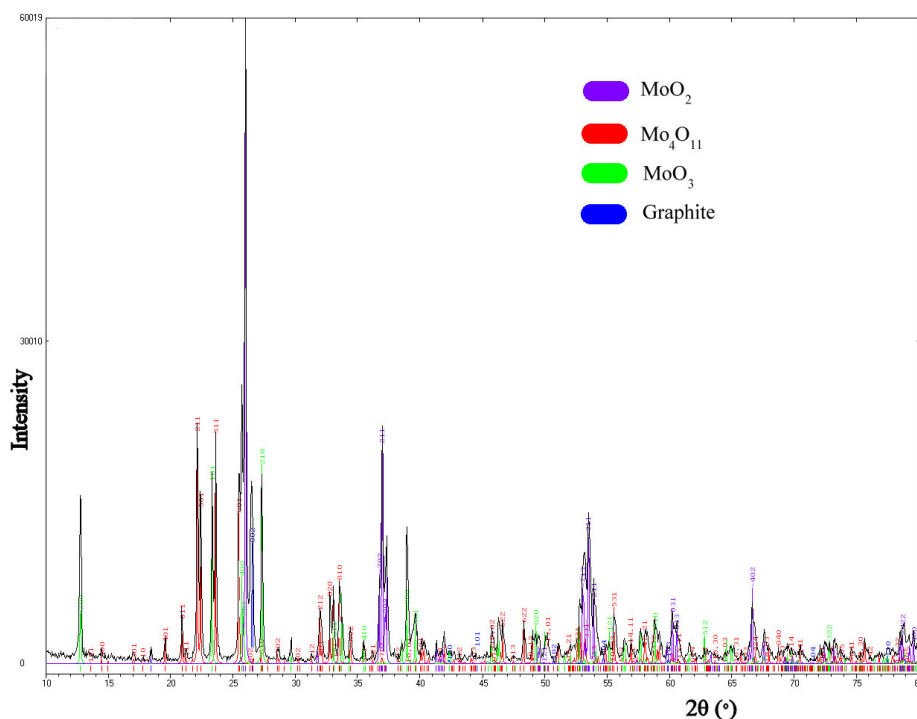


**Figure 4- 24: PXD plot for  $\text{MoO}_3$  + C pellet heated for 10 s at 3 kW in a single mode cavity.**

The majority of the sample is the intermediate oxide  $\text{Mo}_4\text{O}_{11}$  (~37 %), with the starting oxide,  $\text{MoO}_3$  (~25 %), and intermediate oxide,  $\text{MoO}_2$  (~25 %), constituting the majority of the remainder. C is also a visible phase in the PXD, whereas Mo and  $\text{Mo}_2\text{C}$  only make a minute amount of the sample (~0.2 % and ~1.2 % respectively). In fact, negligible amounts of Mo were observed (<0.5 %) at any given point during the reaction with the  $\alpha$ - $\text{Mo}_2\text{C}$  content never exceeding 10 %. What's more PXD seems to indicate that almost as soon as Mo is formed it reacts immediately with C to form the carbide; however, it

appears during the 30 s microwave heating process the oxide is never fully reduced. Further examination of other PXD plots during the reaction profile results in a dynamic shift in the oxides present at a given point during the microwave heating process. These results are summarised as a graph in Figure 4- 25.

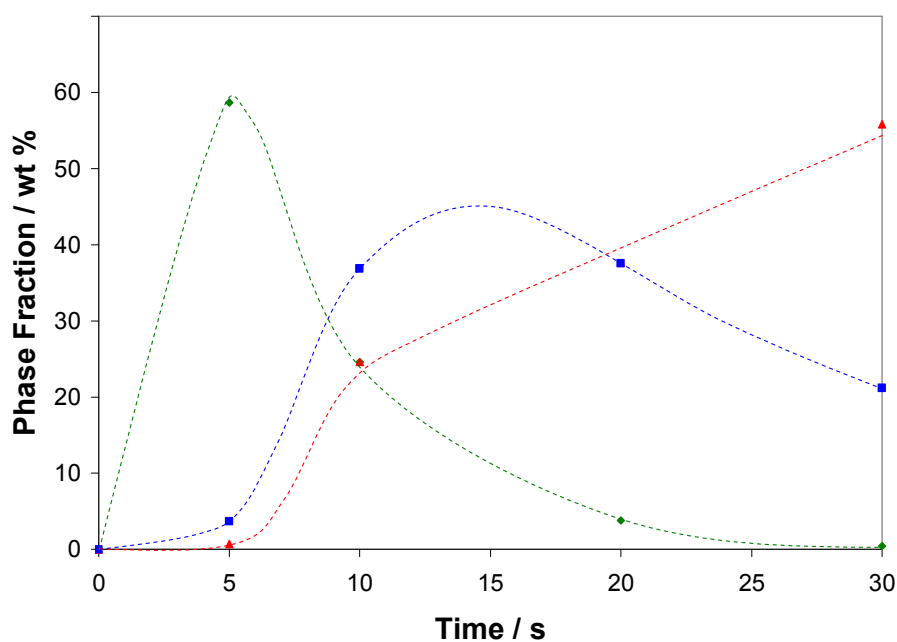


**Figure 4- 25: Plot indicating the phase fraction of various Mo oxides at given times during the reaction, MoO<sub>3</sub> + C. The green line represents MoO<sub>3</sub>, the blue line Mo<sub>4</sub>O<sub>11</sub> and the red line MoO<sub>2</sub>.**

It can be clearly seen that below 5 s MoO<sub>3</sub> is the primary oxide, however, by the time the temperature has reached ~1000 °C (5s) the existence of MoO<sub>2</sub> and the intermediate oxide Mo<sub>4</sub>O<sub>11</sub> is apparent. As the temperature steadily rises, MoO<sub>3</sub> rapidly decays away and is replaced by the other two oxides. At first, Mo<sub>4</sub>O<sub>11</sub> is predominant, but as the reaction progresses this is quickly reduced to MoO<sub>2</sub>. After 30 s, and a reaction temperature of ~1400 °C,

the oxide phase is predominant with MoO<sub>3</sub> practically non-existent. However, by this stage only ~0.4 % Mo and 2 % Mo<sub>2</sub>C are observed. This whole process can be summarised as follows:



Although this reaction pathway is clear, little oxide has fully reduced to the metal, thus allowing formation of the carbide. This raises an immediate question.

1. Why is reduction of the oxide/formation of the carbide not more rapid given the results observed on such rapid timescales for other experiments?

This could be due to the short timescales used, however, it is more likely a result of the breaking apart of the pellet during the reaction. Firstly the fracturing will reduce the efficiency of conductive heat transfer through the pellet, resulting in a significant increase in the overall reaction time required for carbide formation. Secondly the fracturing destroys the local intimacy of the reactants, reducing the efficiency of oxide reduction and carbide formation. Finally the consequence of the pellet breakage often resulted in displacement of the graphite susceptor, or in worst cases, fracturing of the reaction vessel. Again another question needs to be raised.

## 2. Why does pellet fracturing occur?

Fracturing of the pellet is known to occur due to the gas evolution from the pellet in the form of CO and CO<sub>2</sub>. This gas evolution must be violent given the nature of the pellet post-reaction and it appears likely that the rapid temperature rise observed in Figure 4- 23 during the initiation of the reaction is responsible for this. After only 5 s the temperature is already in excess of 1000 °C with PXD showing, from this point onwards, the rapid reduction of MoO<sub>3</sub>. Therefore, perhaps with greater control over the initial reaction conditions fracturing of the pellet can be avoided.

Although successful synthesis of  $\alpha$ -Mo<sub>2</sub>C from the oxide, MoO<sub>3</sub>, has been achieved the circumstances were far from ideal. Good reproducibility was hard to achieve due to the rapid gas evolution corresponding with the reduction of the oxide, believed to be a result of the initial and rapid rise in reaction temperature. Ultimately this outcome led to pellet fracture leading to minimal carbide formation and great difficulty in collecting the sample post-reaction. In turn this meant that in the majority of cases, PXD could not be performed in order to characterise the sample. Where it was possible, the samples constituted primarily Mo oxides, however, accurate phase fractions were problematic to achieve and the vast quantity of reflections observed (seen in Figure 4- 24) presented complexity in identifying all the phases present.

Despite these challenges discussed above, a great deal has been learnt about the microwave heating of metal oxide in an effort to form the corresponding metal carbide. However, if a further understanding of the reaction in

conjunction with the conception of a reproducible reaction is to be achieved, it is clear a number of issues need to be addressed. For this reason dielectric property studies were carried out to examine the effects of temperature on MoO<sub>3</sub>, thermal analysis, coupled with mass spectrometry, allowed the effect of temperature on MoO<sub>3</sub> to be closely monitored, and finally, a smaller, more controllable, single mode applicator was used where applied powers between 0 and 1.5 kW could be investigated in an effort to further study the reaction process, reaction vessel and pellet integrity.

#### ***4.5.2.1 Further reaction study; $2\text{MoO}_3 + 7\text{C} \rightarrow \text{Mo}_2\text{C} + 6\text{CO}$***

The dielectric properties of materials are known to change with temperature.<sup>32, 33</sup> In fact, in the majority of cases (where the sample contains no water) the loss tangent is reported to increase with reaction temperature, which often leads to thermal runaway in the system as more microwave energy is converted into heat. With this in mind the dielectric properties of the reaction mixture, MoO<sub>3</sub> + C, were studied with increasing temperature in order that the results obtained might allow the reaction process to be determined, particularly during the initial stages when pellet fracturing is known to occur.

Stoichiometric amounts of MoO<sub>3</sub> and C, weighing a total of 1 g, were ground together to afford Mo<sub>2</sub>C. The powder was then loaded into a quartz tube and secured on the arm of the dielectric property measurement apparatus (section 2.1.2). This arm allowed the tube to be automatically lowered and raised from the attached furnace into the perturbation cavity so that dielectric

property measurements could be taken. The sample was then heated from 20 °C to 1000 °C with a ramp rate of 5 °C/min with the temperature held for 10 min every 100 °C to allow for stabilisation of the temperature so the dielectric property measurements could be taken. The resultant data is plotted in Figure 4- 26.

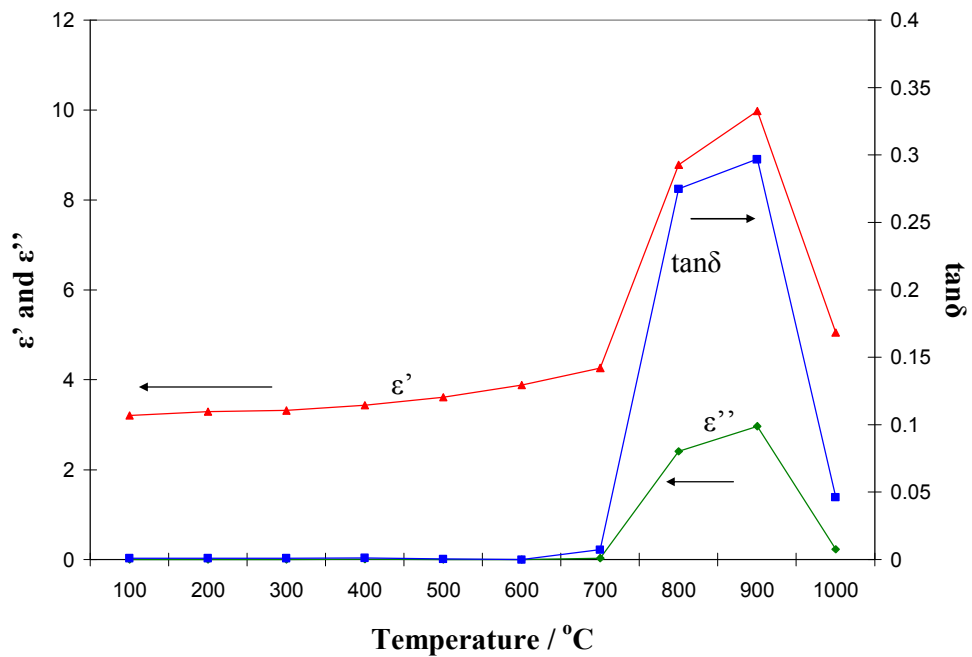


**Figure 4- 26: Plot indicating the relative permittivity ( $\epsilon'$ ), the dielectric loss ( $\epsilon''$ ) and the resultant loss tangent at increasing temperature for  $\text{MoO}_3 + \text{C}$  under air.**

No change is observed in the loss tangent ( $\tan\delta$ ) up to 600 °C with it remaining at almost zero, indicating the sample would heat very little in a microwave field. However, above this temperature the loss tangent begins to rise slowly with a rapid rise observed above 700 °C (caused by the large increase in  $\epsilon'$  compared to  $\epsilon''$ ). By 800 °C, the sample is now a much more

effective microwave absorber and is certainly capable of being heated. Between 900 °C and 1000 °C, however, a sharp drop is observed in the loss tangent indicating, once again, that the sample no longer has favourable properties for microwave heating. PXD of the sample post-heating revealed the presence of Mo metal only.

Figure 4- 26 certainly indicates why a susceptor is required to initiate the reaction process. Below 600 °C the loss tangent is practically zero, indicating the sample ( $2\text{MoO}_3 + 7\text{C}$ ) is essentially microwave transparent. For this reason a susceptor, such as graphite, is required to raise the reaction temperature to a point where the dielectric properties become more favourable ( $> 600$  °C). This change in loss tangent coincides with a temperature above 600 °C which, on examination of TGA data, is the point at which reduction of the oxide  $\text{MoO}_3$  begins (Figure 4- 27). In fact, more accurately, TGA shows the reduction of the oxide begins between 550 °C and 600 °C, at which point steady weigh loss occurs until 1050 °C (Figure 4- 27). PXD confirmed the existence of only Mo metal above this temperature. Mass spectrometry, taken throughout the experiment, revealed CO gas evolution throughout the experiment. At 550 °C the amount of CO observed increased dramatically and  $\text{CO}_2$  was also present in the spectrograph (all be it negligible compared to CO). Other peaks observed during the experiment were due to the Argon gas present which was confirmed by an Argon control experiment. A typical Mass spectrograph can be seen in Figure 4- 27 for the reduction of  $\text{MoO}_3$  with C, taken specifically at 700 °C.

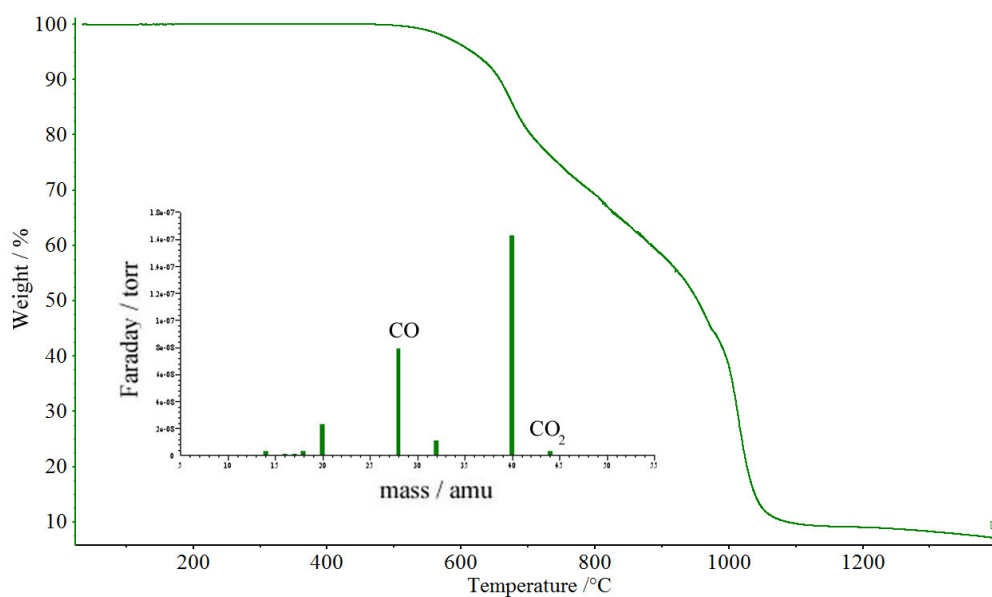


**Figure 4- 27: TGA for MoO<sub>3</sub> + C sample under air. Mass spectrograph represents typical result during the reduction of the oxide (between 550 °C and 1050 °C).**

The TGA and dielectric property results seem to suggest that, with the reduction of MoO<sub>3</sub>, the sample's loss tangent becomes higher. This coincides with the formation of Mo<sub>4</sub>O<sub>11</sub> and MoO<sub>2</sub> suggesting that both these oxides have higher loss than the tri-oxide. As more of these intermediate oxides are formed the loss tangent of the sample becomes more favourable thus allowing the sample to interact favourable with the microwave field. However, as the reduction progresses towards Mo metal (confirmed by PXD) the loss tangent begins to decay towards zero again. This was observed with the W-C system and again with the Mo-C reactions from the elemental powders, Mo and C, where in all cases a susceptor was required to initiate the reaction. It seems, therefore, that if the reaction temperature could be controlled it would be possible to initiate the reduction process by maintaining a desired temperature

which might in turn control the gas evolution from the sample. Without the previously observed high temperatures, one might obtain a slower, more controlled reduction of the oxide resulting in pellet integrity. Once reduction is thought to be complete the temperature can then be increased to a desirable temperature for microwave assisted carbide formation. This would allow for the whole reaction to be completed in one step, although the process control breaks this step down into two individual steps within the one; first the reduction of the oxide which is then followed by the formation of the carbide. It may also be possible, with initial temperature control, to remove the need for a susceptor completely.

#### ***4.5.2.2 Mo<sub>2</sub>C synthesis using Magnetronics 0 - 1.5 kW single mode microwave applicator***

Formation of Mo<sub>2</sub>C from the oxide has already been observed, however, a reproducible synthetic method was yet to be achieved. In part this was due to rapid gas evolution resulting in pellet fracturing as well as a limited understanding about the reaction process. To rectify this, data were collated using a combination of characterisation methods including dielectric property studies, TGA, PXD and reaction temperature monitoring. Ultimately this resulted in a greater understanding of the microwave heating process and allowed for a fresh approach to be taken in the synthesis of the carbide, Mo<sub>2</sub>C, from the oxide, MoO<sub>3</sub>.

From dielectric data collected for the reaction  $\text{MoO}_3 + \text{C}$  the loss tangent was observed to improve greatly at 800 °C (discussed in section 4.5.2.1). TGA also showed the reduction of the oxide,  $\text{MoO}_3$ , began between 700 and 750 °C (discussed in section 4.5.2.1), with PXD indicating the existence of 3 oxides by 1000 °C;  $\text{MoO}_3$ ,  $\text{Mo}_4\text{O}_{11}$  and  $\text{MoO}_2$  (discussed in section 4.5.2, Figure 4- 24). It was also observed that little Mo and  $\text{Mo}_2\text{C}$  were present during the reduction of the oxide. With this in mind, it was hypothesised that if controlled reduction of the oxide could be achieved, resulting in slow release of CO /  $\text{CO}_2$ , fracturing of the pellet would not occur (< 1000 °C). Once reduction has been completed the temperature could then be increased to allow carbide formation to begin (> 1000 °C).

As a susceptor was still required the experimental procedure was kept identical to that used previously in the successful synthesis of  $\text{Mo}_2\text{C}$  (section 2.2). The 1 g pellet was placed into the graphite susceptor and the experimental apparatus secured in the single mode microwave cavity. The Magntronics applicator operated in a similar fashion to the Sairem 3-15 kW applicator, however, only manual tuning was possible unlike the automatic tuner present in the latter applicator. Initial experiments were run at 1 kW applied power, however, it quickly became apparent that this power did not allow for sufficient control over the reaction. The reaction temperature rose rapidly to ~900 °C at which point the temperature increased suddenly accompanied by a flash from the reaction vessel. In all cases the pellet emerged fractured, but the flash still observed, showing a possible link between the temperature rise and the previously studied dielectric properties of the pellet (section 4.5.2.1).

The next series of experiments were conducted at only 500 W applied power. It was hypothesised that with much less applied power available the temperature would rise more slowly than previously observed, allowing for manual adjustments of the power to be carried out, resulting in a degree of control over the reaction temperature. In this case, the temperature was observed to rise relatively slowly, reaching a temperature of 850 °C within 1 min. However, once this temperature was reached the reaction temperature increased rapidly accompanied by the associated flash from the reaction vessel. Surprisingly, despite this occurrence, the pellet was removed intact with PXD revealing the presence of Mo<sub>4</sub>O<sub>11</sub>, MoO<sub>2</sub> and Mo<sub>2</sub>C, all be it only small amounts of the carbide. This encouraging result led to multiple experimental repeats at 500 W allowing for greater control of the reaction in the form of temperature control via variations in the applied power. As the reaction approached 700 °C it was possible to manually adjust the applied power between 0 and 500 W in an effort to maintain the temperature between 700 and 800 °C. It was difficult, however, to stop the temperature rise altogether with only retardation possible. Once a temperature of ~850 °C was reached, usually taking between around 2 min, the characteristic flash was observed followed by a rapid temperature rise to in excess of 1200 °C. By this stage pellet fracturing was no longer an issue and, with further experimentation, at the associated reaction flash the applied power could be increased to 1 kW with pellets still remaining intact. With heating of only 10 s after this power increase, *ex-situ* PXD post-reaction revealed a pure phase of Mo<sub>2</sub>C. This was subsequently characterised using PND to verify phase purity and structure as well as the carbon stoichiometry.

PND data were collected on POLARIS at ISIS, Rutherford Appleton Laboratory (RAL) (section 2.3.2.2). Before a scan was taken approximately 2 g of the sample was loaded into a 5mm diameter vanadium canister which was then lowered into the sample tank of the diffractometer. Post-collection, Rietveld refinement (section 2.3.3) of the data was performed using the General Structure Analysis System (GSAS)<sup>18</sup> through the windows based EXPGUI interface.<sup>19</sup> Data were refined (all banks) concurrently against the  $\alpha$ -Mo<sub>2</sub>C structure proposed by Epicier.<sup>7</sup> Refinement was started with the background coefficients, followed by the unit cell, atomic positions, profile parameters and isotropic temperature factors. Finally the absorption/reflectivity correction and carbon occupancy were refined. Specifically the sample investigated was heated for a total of 130 s. The resultant profile plot can be seen in Figure 4- 28 and Table 4- 9 comprises selected crystallographic parameters post-refinement.

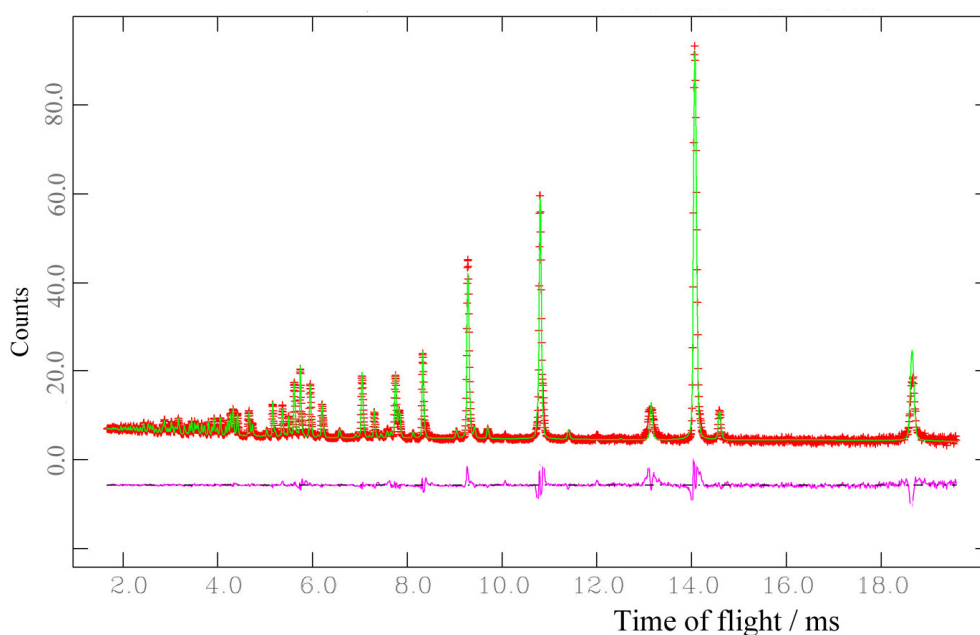


**Figure 4- 28: Observed (plusses), calculated and difference profile plots for Rietveld refinement of  $\alpha$ -Mo<sub>2</sub>C against PND data for Mo<sub>2</sub>C (130 s).**

Sample	$\alpha$ -Mo <sub>2</sub> C
Empirical formula	Mo <sub>2</sub> C
Unit cell formula weight, M <sub>w</sub>	107.9507
Crystal system, Space group	Orthorhombic, Pbcn
<i>a</i> , <i>b</i> , <i>c</i> -parameter, Å	4.73512(7), 6.0253(1), 5.2035(1)
Unit cell volume, Å <sup>3</sup>	148.462(5)
Z, Calculated density, ρ <sub>x</sub> / g cm <sup>-3</sup>	1, 9.090
Observations, parameters	15569, 48
R <sub>p</sub> , R <sub>wp</sub> , χ <sup>2</sup>	0.0581, 0.03, 2.849
Mo position and occupancy, U <sub>iso</sub> / Å <sup>2</sup>	(0.2428(1), 0.1209(7), 0.0812(2)), 2.00, 0.00317(6)
C position and occupancy, U <sub>iso</sub> / Å <sup>2</sup>	(0, <sup>3</sup> / <sub>8</sub> , <sup>1</sup> / <sub>4</sub> ), 0.945(3), 0.0035(1)
Interatomic distance: Mo-C, Å	2.0902(1), 2.1117(1), 2.1169(1)
Interatomic distance: Mo-Mo, Å	3.0064(1), 2.9748(1), 3.0128(1), 2.9356(1), 2.8985(1)

**Table 4- 9: PND crystallographic and bond information for  $\alpha$ -Mo<sub>2</sub>C synthesised in 130 s in a single mode cavity.**

Figure 4- 28 and Table 4- 9 clearly verify the formation of  $\alpha$ -Mo<sub>2</sub>C with the lattice parameters agreeing strongly with those previously studied.<sup>7</sup> Investigation into carbon stoichiometry revealed a Mo: C ratio of 2:0.945(3), indicating slight carbon non-stoichiometry; common amongst carbides synthesised from oxide precursors due to carbon loss in the form of CO/CO<sub>2</sub> during the reaction and the reported existence of oxygen within the structure.<sup>1,3</sup> However, through the use of PXD and PND, no oxygen is observed within the Mo<sub>2</sub>C product synthesised in 130 s in the single mode cavity (O on the C site results in an unstable refinement).

Further analysis of the carbide was carried out using SQUID magnetometry revealing a superconducting transition at 3.4(1) K (Figure 4-29). This is consistent with the Mo<sub>2</sub>C samples reported throughout this chapter and importantly does not seem to vary despite the formation of the carbide from the oxide precursor, MoO<sub>3</sub>, and not directly from the metal, Mo. Once again this T<sub>c</sub> is unusually low for the α-Mo<sub>2</sub>C structure, which would suggest the formation of the hexagonal phase if the PND did not indicate otherwise. However, this low T<sub>c</sub> for α-Mo<sub>2</sub>C can be explained by the carbon non-stoichiometry observed in the structure. As discussed in chapter 1, it is well known that an increase in carbon vacancies dramatically reduces the superconducting transition for the carbide.<sup>3</sup>

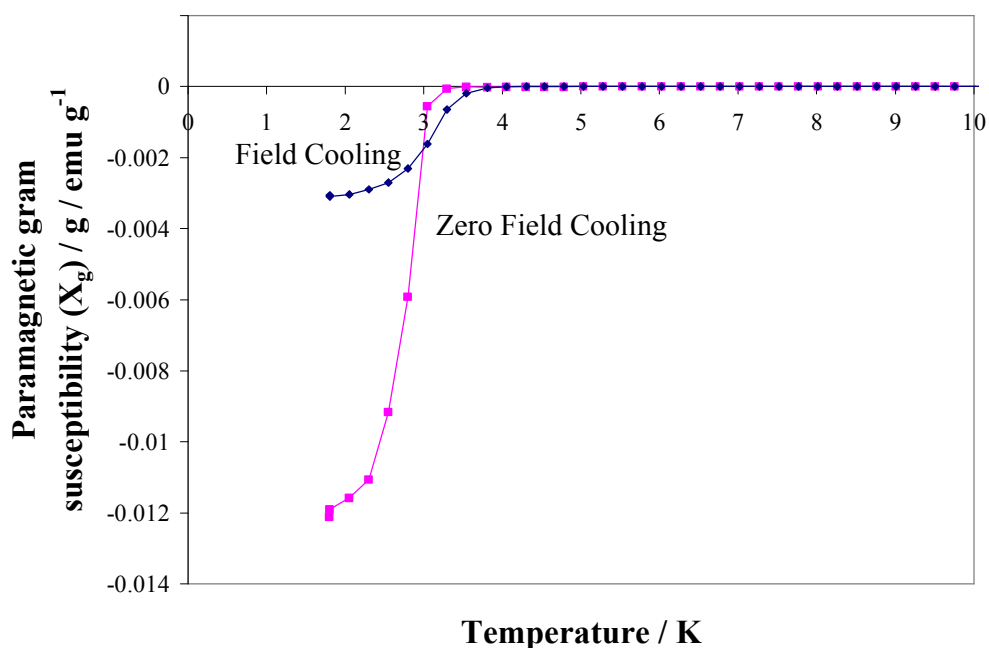


**Figure 4- 29: Plot of mass susceptibility,  $\chi_g$ , against temperature, for  $\alpha$ -Mo<sub>2</sub>C synthesised in 130 s. Plot shows a T<sub>c</sub> onset at 3.4(1) K.**

Examination of cell volume, C occupancy and  $T_c$  onset for samples studied using PND revealed interesting trends. Although limited investigations have been carried out using PND (too few to draw any absolute conclusions), a clear trend is visible between the three variables offered up for study (Figure 4-30). One might expect the observed linear trend between cell volume and C content, with an increase in C vacancies resulting in a decrease in the unit cell; however, it is difficult to verify this with only the 3 compounds investigated. Figure 4-30 also suggests a non-linear relationship between C occupancy and  $T_c$  onset. In fact, rapid decrease in  $T_c$  is observed when a seemingly crucial C occupancy is obtained. Work published by Giorgi et al. reports a similar trend in  $TaC_{1-x}$  and  $NbC_{1-x}$ ,<sup>22</sup> with rapid reduction in  $T_c$  apparent with only minimal reduction in C non-stoichiometry. Although further investigation is warranted to verify this trend in  $Mo_2C_{1-x}$ , it seems this phenomenon may exist across the transition metal carbides as suggested in numerous publications.<sup>3, 12, 22, 23</sup>

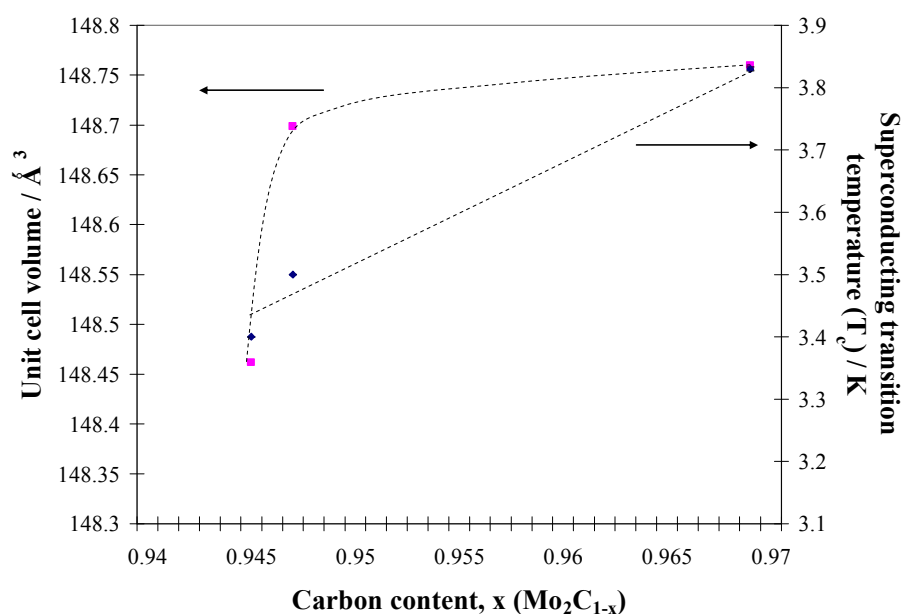


**Figure 4- 30: Plot of unit cell volume and  $T_c$  onset vs. carbon content for  $\alpha$ - $Mo_2C$  samples investigated using PND.**

The successful reproducible synthesis of  $\text{Mo}_2\text{C}$  from the oxide, in a single synthetic step, has been achieved. Through the study of the reaction process it was possible to vary the applied microwave power, thus allowing more stable reduction of the oxide without pellet fracturing. It was then possible to achieve successful synthesis of the carbide from the Mo and C present. However, despite this success, the relationship between the power and reaction temperature could not be controlled sufficiently to maintain a desired temperature, although this may be possible with an automated feedback system. If this could be incorporated into the microwave applicator design it would be possible to program a series of steps which could ultimately result in a single step synthesis from  $\text{MoO}_3$  to  $\text{Mo}_2\text{C}$ . This setup could then subsequently be used in the investigation into the synthesis of other carbides from their oxide precursors.

## 4.6 CONCLUSION

Thanks to the work carried out previously on the W-C system, the investigations into Mo-C had a good basis. With work beginning in the DMO, successful synthesis of  $\text{Mo}_2\text{C}$  was achieved relatively quickly with a reaction time of only 90 s. Characterisation using a variety of techniques including PXD, EDX and SEM confirmed the existence of the desired phase with magnetic measurements indicating a superconducting transition ( $T_c$ ) of 3.83(6) K. This  $T_c$  implied the formation of the hexagonal phase,  $\beta$ - $\text{Mo}_2\text{C}$ , but PXD was unable to confirm this due to no visible difference in the patterns of this phase and the orthorhombic phase,  $\alpha$ - $\text{Mo}_2\text{C}$ . Fortunately subsequent PND was

able to distinguish between the two structures, verifying the formation of the latter phase,  $\alpha$ -Mo<sub>2</sub>C; unexpected due to the observed T<sub>c</sub> of the material. However, the existence of this low T<sub>c</sub> was soon explained due to the carbon non-stoichiometry observed in the structure; indicative of a decreased superconducting transition temperature.<sup>22, 23</sup> This was further indicated by limited examination of the trend between C occupancy and T<sub>c</sub> onset, showing a rapid decrease in T<sub>c</sub> with only a small decrease in C non-stoichiometry.

The success in the DMO naturally led to attempted synthesis in a single mode cavity in an effort to improve synthesis time and reproducibility. Ultimately successful synthesis was achieved on a rapid timescale of only 10 s with PND again confirming the formation of carbon non-stoichiometric  $\alpha$ -Mo<sub>2</sub>C with a superconductivity of 3.5(1) K, confirmed by magnetic measurements. This result was incorporated into a reaction profile study in which the examination of *in-situ* temperature measurements and *ex-situ* dielectric property measurements and PXD allowed for the Mo + C → Mo<sub>2</sub>C to be studied. A direct relationship between these variables was observed, with the loss tangent relating directly to the phases present in any given sample; high for Mo + C and low for Mo<sub>2</sub>C. In turn, the reaction temperature related to the loss tangent with a rapid rise observed, while the loss tangent was high, and a plateau observed coinciding with the formation of Mo<sub>2</sub>C. This plateau occurred above 1200 °C and further investigation by thermal analysis revealed the formation of the carbide begins at ~1000 °C, fitting directly with the results obtained for the reaction profile study.

The possible existence of oxide impurities was also investigated for the Mo-C system. With all the reactions being carried out open to the atmosphere, it was considered that metal oxides could form during the reaction, despite them not being observed with PXD. For this reason, XPS was used to examine the samples post-synthesis revealing small amounts of MoO<sub>3</sub> present on the surface of the pellet sample. However, this oxide was removed with argon etching indicating the presence of this impurity only at the pellet surface; not enough to be detected using PXD. Repetitions of these experiments in sealed systems revealed no difference in XPS results, indicating that small amounts of oxygen impurity must be present within the reaction vessel. Due to this result it was deemed acceptable to continue with experiments open to the atmosphere.

The final section of this chapter was concerned with the synthesis of Mo<sub>2</sub>C from the oxide, MoO<sub>3</sub>. Despite this being possible in both the DMO and single mode cavity, a reproducible reaction was difficult to achieve due to rapid gas evolution resulting in pellet fracturing. For this reason a detailed study of the reaction process using dielectric property measurements at temperature and TGA analysis of the reaction mixture MoO<sub>3</sub> and C was carried out combined with PXD data from successful attempts to synthesis the carbide. It became clear that, as the temperature increased, the dielectric properties of the material changed. TGA also indicated the reduction temperature required for the oxide and using this knowledge it was possible to design an experimental procedure which allowed for successful, reproducible synthesis of the carbide,  $\alpha$ -Mo<sub>2</sub>C. Using a reduced applied power (0-500 W) the controlled reduction of the oxide was achieved resulting in no fracturing of the

sample. It was then possible to increase the applied power which in turn caused the reaction temperature to rise and the carbide to be formed within a total reaction time of 130 s.

Examination of the various reactions, both in the DMO and single mode cavities, reveals an interesting observation. Although the single mode offers faster synthesis times (10 s compared to 90 s) it also seems to result in smaller cell volumes, indicating increased carbon vacancies. This, in turn, is observed in the superconductivity of the respective carbides; lower  $T_c$  onset for  $\text{Mo}_2\text{C}$  formed in the single mode cavity. Interestingly, despite the similarity in reactions times (90 s),  $\text{Mo}_2\text{C}$  formed in the DMO from the oxide  $\text{MoO}_3$ , has a lower  $T_c$  than  $\text{Mo}_2\text{C}$  synthesised from the metal, Mo. This is merely a general observation across the  $\text{Mo}_2\text{C}$  investigations, with specific variations present for each given material, however, it cannot be ignored. The longer reaction times appear to allow for higher C occupancy to be achieved, which in turn directly affects the cell volume and  $T_c$  onset. With reference to the carbide formed from  $\text{MoO}_3$ , the results suggest the reduction of the oxide *in-situ* increases the carbon vacancies within the final carbide structure. Perhaps this could be eliminated with an increase in reaction time.

In conclusion, the successful synthesis of  $\text{Mo}_2\text{C}$  has been achieved from both the oxide and elemental precursors on an ultra-rapid timescale. Through the study of the reaction process a great deal has been learnt beyond just the synthesis of the carbide, particularly from the oxide with adaptation of the experimental procedure resulting in a reproducible one-step synthesis.

Although the exact mechanism of Mo<sub>2</sub>C formation remains elusive, much has been learnt about the interactions of the reactants, intermediates and products with the microwave field and, importantly, a method of monitoring and quantifying these interactions. The direct effect of applied microwave power on synthesis time has also been indicated with additional factors such as reduced synthesis temperatures noted. The study has revealed a number of trends which, with detailed and careful applicator design, could be monitored *in-situ* allowing for both a rapid and controllable process to be developed. Applied on the industrial scale, much faster processing times could be achieved resulting in an attractive alternative to conventional synthesis methods.

## 4.7 REFERENCES

---

- <sup>1</sup> H. O. Pierson, *Handbook of Refractory Carbides and Nitrides*, 1<sup>st</sup> Edition, Noyes, Park Ridge NJ, 1960.
- <sup>2</sup> G. A. Swift, R. Koc, *J. Mater. Sci.*, 2000, **35**, 2109.
- <sup>3</sup> E. K. Storms, *The Refractory Carbides*, 1<sup>st</sup> Edition, Academic Press, New York, 1967.
- <sup>4</sup> L. E. Toth, *Transition Metal Carbides and Nitrides*, 1<sup>st</sup> edition, Academic Press, New York and London, 1971.
- <sup>5</sup> J. Lu, H. Hugosson, O. Eriksson, L. Nordström and U. Jansson, *Thin Solid Films*, 2000, **370**, 203.
- <sup>6</sup> E. Rudy, S. Windisch, A. J. Stosick and J. R. Hoffmann, *Trans. Metallurgical Soc. of Aime*, 1967, **239**, 1247.
- <sup>7</sup> T. Epicier, J. Dubois, C. Esnouf and G. Fantozzi, *Acta Metallurgica*, 1988, **36**, 1903.
- <sup>8</sup> W. Meissner, H. Franz, *Z. Physik*, 1930, **65**, 30.
- <sup>9</sup> L. E. Toth, J. Zbasnik, *Acta Met.*, 1968, **16**, 1177.
- <sup>10</sup> N. Morton, B. W. James, G. H. Wostenholm, D. G. Pomfret, M. R. Davies and J. L. Dykins, *J. Less-Common Met.*, 1971, **25**, 97.
- <sup>11</sup> V. Sadagopan and H. C. Gatos, *J. Phys. Chem. Solids*, 1966, **27**, 235.
- <sup>12</sup> T. Ya. Kosolapova, *Carbides: Properties, Production and Applications*, 1<sup>st</sup> Edition, Plenum Press, New York, 1971.
- <sup>13</sup> I. P. Parkin, *Chem. Soc. Rev.*, 1996, 199.
- <sup>14</sup> A. M. Nartowski, I. P. Parkin, M. MacKenzie, A. J. Craven and I. MacLeod, *J. Mater. Chem.*, 1999, **9**, 1275.

- 
- <sup>15</sup> A. M. Nartowski, I. P. Parkin, M. MacKenzie and A. J. Craven, *J. Mater. Chem.*, 2001, **11**, 3116.
- <sup>16</sup> D. Zeng and M. J. Hampden-Smith, *Chem. Mater.*, 1992, **4**, 968.
- <sup>17</sup> A. P. E. York, J. B. Claridge, V. C. Williams, A. J. Brungs, J. Sloan, A. Hanif, H. Al-Megren and M. L. H. Green, *Studies in Surface Science and Catalysis*, 2000, **130**, 989.
- <sup>18</sup> A. C. Larson and R.B. Von Dreele, "The General Structure Analysis System", Los Alamos National Laboratories, Report LAUR086748, LANL, Los Alamos, N. M., USA, 1999.
- <sup>19</sup> B. H. Toby, *J. Appl. Crystallogr.*, 2001, **34**, 210.
- <sup>20</sup> E. Rudy, S. Windisch, A. J. Stosick and J. R. Hoffmann, *J. Less-Common Met.*, 1986, **120**, 135.
- <sup>21</sup> E. Parthé and V. Sadogopan, *Acta. Cryst.*, 1963, **16**, 202.
- <sup>22</sup> A. L. Giorgi, E. G. Szklarz, E. K. Storms, A. L. Bowman and B. T. Matthias, *Phys. Rev.*, 1962, **125**, 837.
- <sup>23</sup> K. Schwarz, and N. Rösch, *J. Phys. C: Solid State Phys.*, 1976, **9**, 433.
- <sup>24</sup> S. Vallance, S. Kingman and D. H. Gregory, *Chem. Commun.*, 2007, **7**, 742.
- <sup>25</sup> D. J. Brooks, R. E. Douthwaite and L. J. Gillie, *Chem. Comm.*, 2005, **38**, 4857.
- <sup>26</sup> K. J. Rao, B. Vaidhyanathan, M. Ganguli and P. A. Ramakrishnan, *Chem. Mater.*, 1999, **11**, 882.
- <sup>27</sup> D. K. Agrawal, *Curr. Op. Solid State Mater. Sci.*, 1998, **3**, 480.
- <sup>28</sup> R. Roy, D. Agrawal, J. Cheng and S. Gedevarishvili, *Nature*, 1999, **399**, 668.
- <sup>29</sup> S. Vallance, S. Kingman and D. H. Gregory, *Adv. Mater.*, 2007, **19**, 138.

---

<sup>30</sup> K. E. Haque, *Int. J. Miner. Process.*, 1999, **57**, 1.

<sup>31</sup> D. R. Lide, *CRC Handbook of Chemistry and Physics*, 88<sup>th</sup> Edition, CRC press, 2007.

<sup>32</sup> V. Kenkre, L. Skala, M. Weiser and J. Katz, *Mater. Sci.*, 1991, **26**, 2483.

<sup>33</sup> G. J. Kriegsmann, *Appl. Phys.*, 1992, 1960.

## 5: GROUP V CARBIDE INVESTIGATIONS

### 5.1 INTRODUCTION

Three carbides exist containing the metals of Group V; V-C, Nb-C and Ta-C, however, within this thesis only the latter two systems will be discussed. Specifically, the mono-carbides NbC and TaC share a number of similar properties to other refractory carbides including high hardness, fracture toughness and good thermal and chemical stability. They also exhibit some of the highest melting points amongst the transition metal carbides; 3600 °C for NbC and 3950 °C for TaC, with TaC being the most chemically stable of all carbides.<sup>1</sup> These properties allow for a number of uses of these materials with the overall manufacture of TaC estimated at around 500 tonnes per annum in the mid 90's.<sup>2</sup> Both carbides are used to improve the properties of cemented carbides, with NbC used alongside alumina in special grades of these cemented compounds. TaC, on the other hand, sees wider industrial usage in combination with WC to produce cemented carbides with improved cutting characteristics, high temperature hardness, shock resistance and wear and oxidation resistance.<sup>2</sup>

Although NbC and TaC are the two major carbides in terms of industrial interest, secondary phases exist within the Nb-C and Ta-C systems, Nb<sub>2</sub>C and Ta<sub>2</sub>C. In all cases the reported properties of these phases are inferior to the mono-carbide (due to structural differences). Much like the group VI systems, temperature and C stoichiometry are integral to targeting the mono-

carbide phase such that none of the unwanted secondary phase is observed. In order to achieve this phase diagrams of the systems are required (Figure 5- 1). It should also be noted that non-stoichiometric monocarbide phases are prevalent in both the Nb-C and Ta-C systems. This, as detailed in chapter 1, can drastically affect the properties of the compound (e.g. superconductivity).

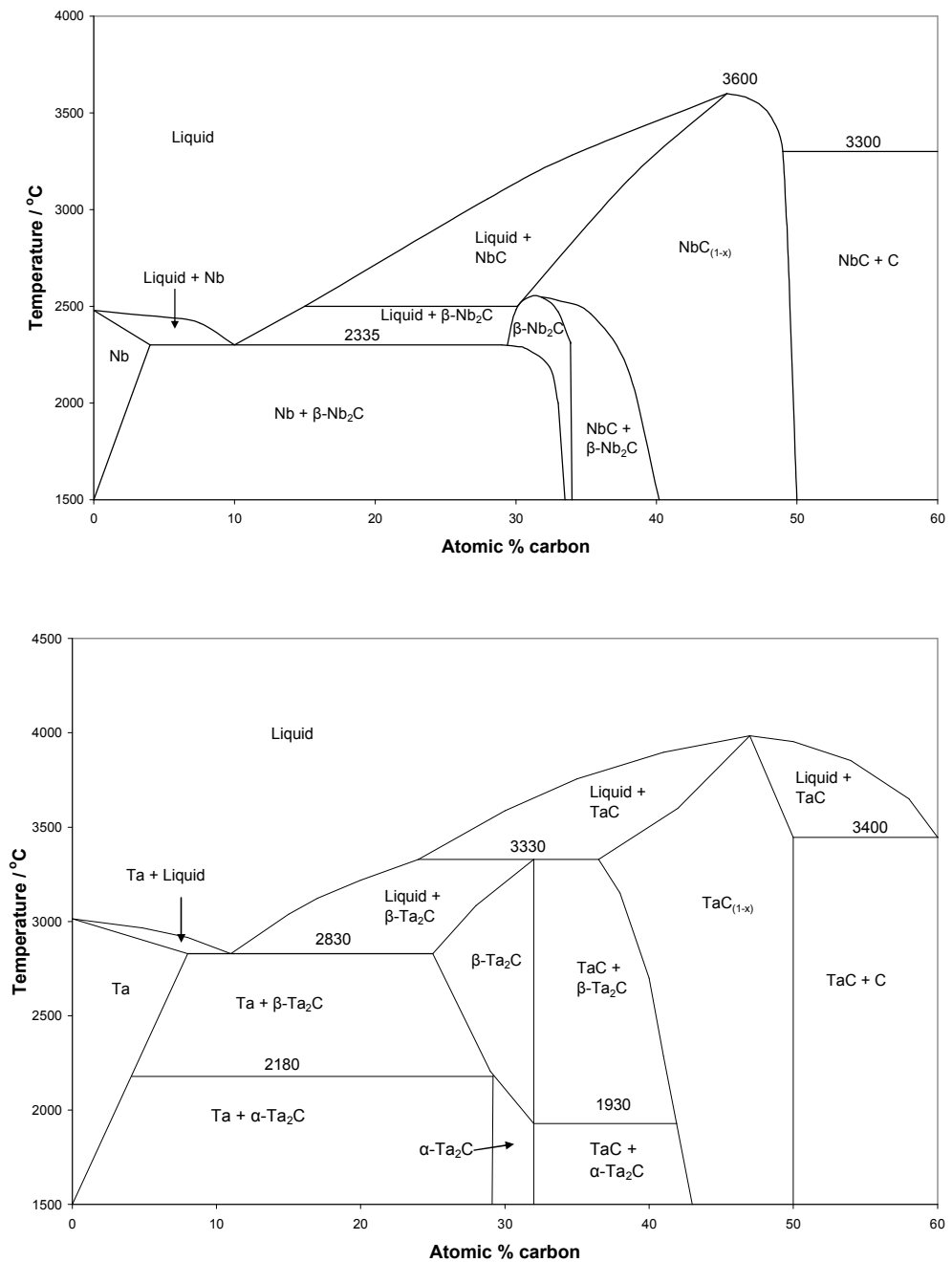
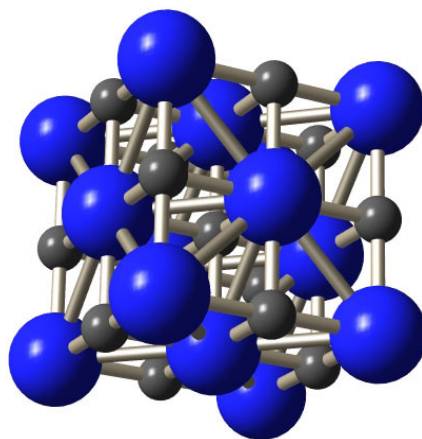


Figure 5- 1: Phase diagrams for Nb-C (top) and Ta-C (bottom) systems.<sup>1,3</sup>

With the correct stoichiometry to afford the desired phase, the phase diagrams indicate that synthesis is possible, without contamination from Nb<sub>2</sub>C or Ta<sub>2</sub>C, from 1500 °C to in excess of 3000 °C. In fact Pierson has extrapolated the phase diagrams to 1000 °C, indicating no additional phases between this temperature and 1500 °C.<sup>1</sup> However, despite the simplicity of the phase diagram, a more detailed look at each system is warranted; in particular the structure of the phases and specific synthetic routes to the carbide.

In the Nb-C system, Nb<sub>2</sub>C boasts a rhombohedral structure ( $\beta$ -Nb<sub>2</sub>C) with space group P3m1 above 1200 °C,<sup>4</sup> however, below this temperature Nb<sub>2</sub>C exists in an orthorhombic form ( $\alpha$ -Nb<sub>2</sub>C) with space group Pna2<sub>1</sub>.<sup>5</sup> The Ta-C system, similarly to Nb-C, contains two known structures for Ta<sub>2</sub>C; rhombohedral below ~2100 °C, with space group P3m1,<sup>6</sup> and hexagonal above this temperature, with space group P6<sub>3</sub>/mmc.<sup>7</sup> In both systems the monocarbides, NbC and TaC, are known to have only one structure, cubic, and belong to space group Fm $\bar{3}$ m with respective lattice parameters  $a = 4.4686 \text{ \AA}$ <sup>8</sup> and  $a = 4.4562 \text{ \AA}$  for the stoichiometric 1:1 carbide (Figure 5- 2).<sup>9</sup>



**Figure 5- 2: Structure of NbC and TaC. The grey atoms represent C and the blue atoms represent the metal Nb/Ta.**

Both NbC and TaC are known to exhibit superconductivity, however, the reported superconducting transition temperatures ( $T_c$ ) vary by a factor of *ca* 2 and 10 respectively in the literature with increasing C non-stoichiometry bringing about a rapid reduction in  $T_c$ .<sup>10, 11</sup> In fact, for a concentration of *ca* 15 % C vacancies, superconductivity is lost in the materials.<sup>10</sup> Giorgi et al. examined the variation in  $T_c$  with C stoichiometry indicating maximum values of 9.7 K for TaC<sub>0.99(1)</sub> and 11.1 K for NbC<sub>0.977(2)</sub> and loss of a transition at stoichiometries of TaC<sub>0.75(1)</sub> and NbC<sub>0.79(1)</sub> respectively.<sup>11</sup> With reference to these results it is possible to infer accurately as to the C stoichiometry of the material with respect to the  $T_c$  observed. Therefore, through the use of magnetic measurements (section 2.3.5.2), it is possible to determine C occupancy.

Conventionally the synthesis of both NbC and TaC is performed via the reduction of the oxide M<sub>2</sub>O<sub>5</sub> (where M represent Nb or Ta) using C, at temperatures around 1700 °C under flowing H<sub>2</sub>.<sup>2, 12</sup> This is a two stage process with the reduction happening prior to the direct synthesis of the metal with C to form the mono-carbide. In both cases the carbide can also be manufactured by means of the metal hydride, with C, under a vacuum. If a coating is required, processes such as Chemical Vapour Deposition (CVD), reactive evaporation or sputtering are used.

Unfortunately, the conventional synthesis requires high temperatures and long reaction times (~ 6 h), although, synthesis has been achieved from the oxide at temperatures as low as 1250 °C in only 1 h for TaC and 2 h for NbC in closed vessels under Ar gas.<sup>13</sup> Another synthetic route which has been used to

synthesise these two carbides is solid state metathesis (SSM).<sup>14, 15</sup> Relying on the chemical exchange of the reacting partners,  $\text{Al}_4\text{C}_3$  and  $\text{CaC}_2$  were both used to produce NbC and TaC from  $\text{NbCl}_5$  and  $\text{TaCl}_5$  respectively. Temperatures of 1000 °C and 350 °C were required for successful synthesis using  $\text{Al}_4\text{C}_3$  and  $\text{CaC}_2$  respectively, with reactions times of 1-2 h and less than 30 s reported in each case. However, in spite of these fast reaction times, a wide crystallite size distribution was observed for both NbC and TaC.<sup>6</sup>

The discussion so far has concentrated solely on synthesis using a conventional furnace, however, limited work has been carried out in the area of microwave synthesis of TaC (discussed further in section 1.4.2).<sup>16</sup> Using a microwave furnace, TaC was successfully synthesised from the oxide,  $\text{Ta}_2\text{O}_5$ , at 1500 °C within 1 h, although 100 % purity was never observed.<sup>16</sup> The limiting factor seemed to be the slow ramping of the microwave power from 500 W to 5 kW to avoid thermal shock of the reaction crucible during the experiment. Interestingly Hassine also noted that longer heating rates led to a larger carbide particle size.

### **5.1.1 Ternary carbides, Nb-Ta-C**

In contrast to the binary carbide systems, little work has been reported on the microwave synthesis of the ternary Nb-Ta-C system. Both Ta and Nb atoms are similar in atomic radius which allows for the ease in formation of this ternary system. In fact, nearly all mono-carbides form complete solid solutions with one another due to the relative similarity in the atomic size of the metal (Table 5- 1).

Element	<i>C</i>	<i>Nb</i>	<i>Mo</i>	<i>Ta</i>	<i>W</i>
Atomic Radius / Å	0.78	1.456	1.386	1.457	1.394

**Table 5- 1: atomic radii of elements discussed in this thesis.<sup>2</sup>**

As might be expected, the phase diagram for the ternary transition metal carbides are very complex in terms of temperature and composition. Although the majority of these carbides have been investigated, to date only partial studies, over limited ranges, have been carried out.<sup>17</sup>

$Nb_{1-x}Ta_xC$ , akin to NbC and TaC, retain the rock salt structure of the end members with the cell volume increasing linearly with  $x$ . These ternary compounds also exhibit superconductivity, however, the relationship between  $T_c$  and metal stoichiometry is apparently non-linear.<sup>18</sup> This results in a complex relationship between the structure and the superconducting transition ( $T_c$ ) which is still yet to be fully explained. Given these  $T_c$  results were also collected more than 4 decades ago, it is possible that they are not entirely accurate with respect to correlation with stoichiometry.

Synthesis of ternary solid solutions can be achieved through direct heating of the relevant monocarbides at high temperature or by heating stoichiometric amounts of the two metals required along with C.<sup>1</sup> Using this latter method, it is also possible to obtain the metals via reduction of the relevant metal oxides prior to forming the carbide. However, using the former procedure, one can guarantee a high purity of the ternary carbide, which has not appeared to be possible using the other methods.

## 5.2 EXPERIMENTAL: SYNTHESIS OF Nb-C, Ta-C, Nb-Ta-C

Investigations associated with the group V carbides were primarily concerned with the synthesis of the desired material. With successful synthesis of the group VI carbides WC (chapter 3) and Mo<sub>2</sub>C (chapter 4), much of the understanding gained could be applied to the formation of carbides within a different group. Group V was also ideal for the expansion of the carbide study from binary to ternary materials due to the known similarities in atomic size between Ta and Nb. Table 5- 2 summarises all the experiments discussed in this chapter.

Experiment	Applicator	Reaction	Purpose
1	DMO	$\text{Nb} + \text{C} \rightarrow \text{NbC}$	Synthesis of the desired carbide, TaC or NbC
2		$\text{Nb}_2\text{O}_5 + 7\text{C} \rightarrow 2\text{NbC} + 5\text{CO}$	
3		$\text{Ta} + \text{C} \rightarrow \text{TaC}$	
4		$\text{Ta}_2\text{O}_5 + 7\text{C} \rightarrow 2\text{TaC} + 5\text{CO}$	
5	Single mode cavity	$\text{Nb} + \text{C} \rightarrow \text{NbC}$	Synthesis and study of Ta-C and Nb-C reaction profiles. PND investigations.
6		$\text{Ta} + \text{C} \rightarrow \text{TaC}$	
7		$\text{Nb} + \text{C} \rightarrow \text{NbC}$	Study of mixing times versus phase formation
8		$1-x\text{Nb} + x\text{Ta} + \text{C} \rightarrow \text{Nb}_{1-x}\text{Ta}_x\text{C}$	Synthesis of various solid solutions and their study using PND

**Table 5- 2: Summary of all experiments carried out on the Ta-C, Nb-C and Ta-Nb-C systems.**

The Group V carbides, despite existing as both the mono- and bi-carbides, are relatively straight forward to form. The phase diagrams, present in section 5.1, indicate the mono-carbides NbC and TaC are formed within a large temperature range providing the stoichiometry of the metal and C are correct. Therefore it seems unlikely that any impurities, in the form of Nb<sub>2</sub>C and Ta<sub>2</sub>C respectively, will be observed. This is easily confirmed through the use of Powder X-ray Diffraction (PXD) (section 2.3.1) which is a standard characterisation test. Analysis first requires the sample pellet to be powdered and then loaded onto a glass slide. Samples were typically scanned for 20 min, between 0 ° and 80 ° 2θ, with a finite number of samples scanned for 12 h so that structural refinement could be carried out (section 2.3.3).

As well as PXD, a number of other characterisation methods were used in the investigation of the Group V carbides. These include dielectric property measurements (section 2.1.2), where no more than 0.5 g of sample was inserted into the cavity and five measurements taken so an average value could be obtained; SEM (section 2.3.6), EDX (section 2.3.6.1), XRF, CHN analysis (section 2.3.8) and thermal analysis (section 2.3.9) were also performed. A final important analytical tool used was the SQUID machine which allowed magnetic measurements to be taken of any given sample (section 2.3.5.2). This provided a method for both confirming the existence of the desired phase and estimating the C occupancy based on the superconducting transition temperature ( $T_c$ ) observed. Samples were typically scanned between 1.8 and 300 K with a magnetic field of 10 Oe. Data collection was concentrated around the suspected  $T_c$  of the material; between 1.8 and 20 K, so accurate results could be obtained.

All experiments discussed in this section (1-8) were performed using the experimental procedure outlined in section 2.2. This involved the sample being imbedded in graphite (acting as a susceptor) which was situated within a 10 mm quartz tube. In all cases stoichiometric amounts of the starting materials to give rise to the desired product were ground together prior to the pressing of pellets. 2 g pellets were used in the attempted synthesis of the carbide from the elemental powders and 1 g pellets in the case of the oxide precursors, resulting in similar pellet volumes for the equivalent metal and oxide reactions. Within the Domestic Microwave Oven (DMO), all work was carried out at 800 W. For the single mode cavity experiments the Sairem microwave generator was set to 3 kW. After the desired heating time samples were removed from the cavity and left to cool prior to characterisation.

The principal aim of the DMO experiments was the synthesis of the relevant carbide (1-4). The initial success with WC and Mo<sub>2</sub>C meant little preliminary experimentation was required allowing for precise and rapid synthesis of the desired phases. Experiments in the single mode cavity, on the other hand, were more complex (5-8). By this stage, synthesis was no longer the primary concern, superseded by the desire to further understand the reactions. PND was used to examine the final TaC and NbC phases (5, 6) enabling detailed structural refinement and analysis of the C stoichiometry (section 2.3.2). This could then be related directly to the T<sub>c</sub> collected from magnetic measurements. The reaction profile for both NbC and TaC synthesis, from the metal powder and C, was also studied in the 3-15 kW single mode cavity (5, 6). Using the experimental technique described above, samples were

heated for specific times between 5 and 30 s, at 5 s intervals. *In-situ* temperature measurements were taken throughout the experiment (described in detail in chapter 3) which, combined with *ex-situ* PXD and dielectric property data, allowed the study of the reaction profile. This resulted in the observation of a direction relationship between temperature, phase fraction and loss tangent, as observed for other carbide systems.

The final set of experiments to be carried out for the binary systems (7) ran concurrently with the investigation into the NbC reaction profile (5). The intimate mixing of reactants is vital in solid state reactions if a pure phase of the desired product is to be afforded. For this reason it was deemed important to investigate this variable further with reaction profiles mapped for a 3 series of pellets where the samples had been ground for 20, 10 and 0 min respectively.

The relative success with the binary systems led to the investigation into the more complex ternary compounds of the solid solution series Nb-Ta-C. A series of experiments were run in the single mode cavity (8) in which the attempted synthesis of 3 solid solution members was carried out; Nb<sub>0.8</sub>Ta<sub>0.2</sub>C, Nb<sub>0.5</sub>Ta<sub>0.5</sub>C and Nb<sub>0.2</sub>Ta<sub>0.8</sub>C. The experimental setup was as described previously (section 2.2) and the samples were irradiated for a variety of times, all at 3 kW applied power, with samples characterised post-reaction using PXD. Subsequent characterisation using PND and magnetic measurements was then married up alongside results for NbC and TaC with a view to investigating the trend in unit cell and T<sub>c</sub> across the Nb-Ta-C series.

## 5.3 RESULTS AND DISCUSSION: SYNTHESIS OF NbC AND TaC USING A DOMESTIC MICROWAVE OVEN (DMO)

### 5.3.1 NbC synthesis

The synthesis of NbC was investigated using both the metal powder, Nb (1), and the oxide precursor (Nb<sub>2</sub>O<sub>5</sub>) (2):



Using the experimental procedure described in section 2.2.1, the ideal heating time to afford NbC was investigated; all at 800 W applied power and starting with 30 min of microwave heating. Post-reaction, PXD was used to determine the phases present in any given sample and, subject to the result, the experimental parameters were adjusted accordingly.

Reaction (1) resulted in the successful synthesis of NbC in 30 min and, with refinement of the experimental procedure, it was possible to obtain a pure phase of NbC in 20 min. Reaction times of less than 20 min resulted in a mixture of the starting materials, Nb and C, and the carbide NbC. Subsequent structure refinement against the collected PXD data for the sample heated for 20 min, using the Rietveld method (GSAS and EXPGUI, section 2.3.3),<sup>19, 20</sup> resulted in the profile plot observed in Figure 5- 3. Table 5- 3 comprises selected crystallographic parameters post-refinement.

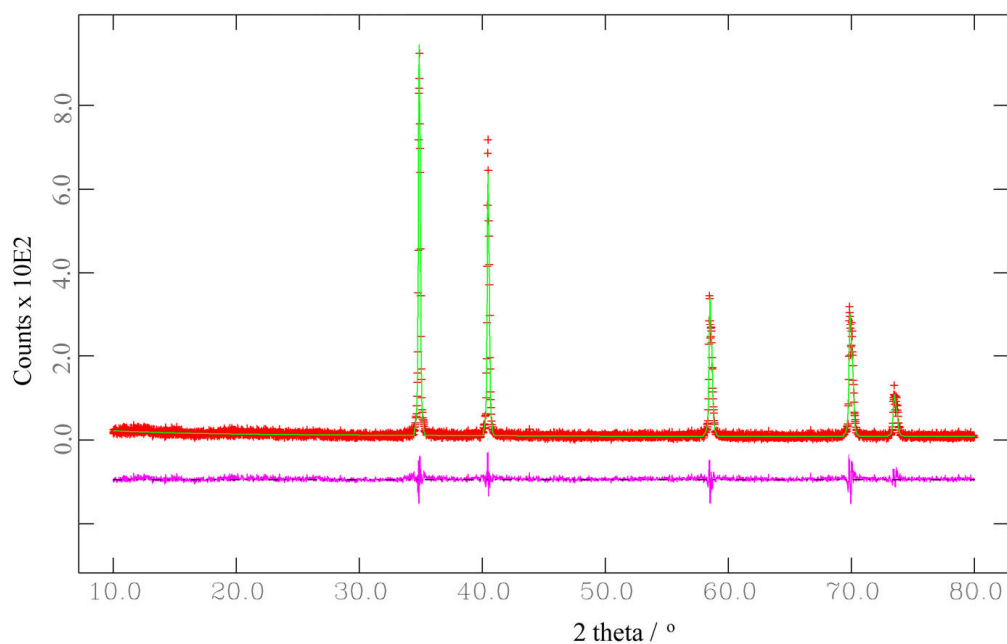


**Figure 5- 3: Observed (plusses), calculated and difference profile plot for the Rietveld refinement against PXD data for NbC produced in 20 min at 800 W in a DMO. Tick marks denote NbC diffraction peaks.**

Empirical formula	NbC
Crystal system, Space group	Cubic, $Fm\bar{3}m$
Unit cell formula weight, $M_w$	104.917
$a$ -parameter, $\text{Å}$	4.4639(2)
Unit cell volume, $\text{Å}^3$	88.953(2)
$Z$ , Calculated density, $\rho_x / \text{g cm}^{-3}$	1, 7.834
Observations, parameters	3500, 16
$R_p$ , $R_{wp}$ , $\chi^2$	0.0579, 0.0858, 1.373
Interatomic distance: Nb-C, $\text{Å}$	2.2320(1)
Interatomic distance: Nb-Nb, $\text{Å}$	3.1565(1)

**Table 5- 3: PXD crystallographic and bond information for NbC synthesised in 20 min at 800 W in a DMO.**

Lattice parameters are in good agreement with those studied previously, a difference of  $0.005 \text{ \AA}$ .<sup>8</sup> The pure-phase monocarbide was also confirmed using EDX, resulting in a Nb:C ratio of 1.0:0.97(1) with no other elements observed. Magnetic measurements confirmed the existence of only one superconducting phase with a superconducting transition temperature ( $T_c$ ) of 11.04(6) K (Figure 5- 4). This value alludes to only a slight C non-stoichiometry within the carbide, existing towards the upper range of the superconducting transition temperatures reported for NbC. In fact, This value, according to Giorgi et al.,<sup>11</sup> would imply an Nb:C ratio of around 1.0:0.975(2) which concurs with the ratio observed using EDX.

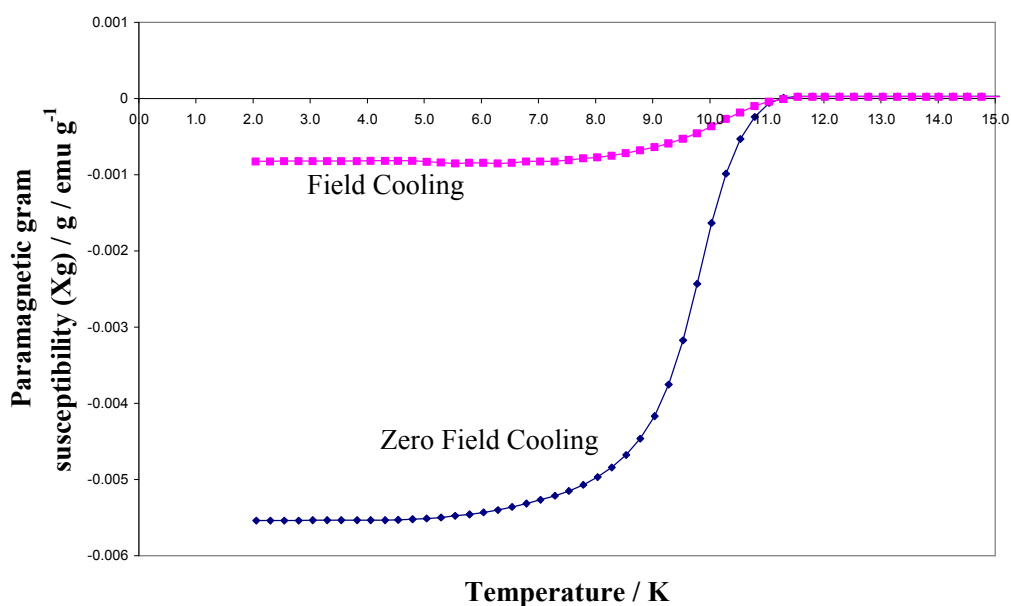


**Figure 5- 4: Plot of mass susceptibility,  $\chi_g$ , against temperature, for superconducting NbC synthesised in 20 min at 800 W in a DMO, showing a  $T_c$  onset at 11.04(6) K.**

Formation of NbC from the oxide also met with success (2). It was feared that pellets comprised of Nb<sub>2</sub>O<sub>5</sub> and C may fracture during the reaction,

as observed for work carried out in the single mode for previously studied carbides (WC and Mo<sub>2</sub>C). However, no occurrence of fracture was noted, perhaps due to the slower temperature rise and longer heating times, the evolution of CO/CO<sub>2</sub> gas caused only a slight “bloating” of the pellet. Ultimately successful synthesis of NbC was achieved in 30 min and, after further investigation, the experiment was refined to afford NbC in only 2 min heating time. For reactions times less than 2 min, PXD revealed a mixture of small amounts of Nb<sub>2</sub>O<sub>5</sub>, the partially reduced oxide NbO<sub>2</sub> and NbC. In fact, it seems that initial reduction of Nb<sub>2</sub>O<sub>5</sub> to NbO<sub>2</sub> is fairly rapid with further reduction of this intermediate oxide, alongside the formation of NbC, occurring much more slowly. The lack of Nb observed by PXD suggests any reduction prior to carbide formation is spontaneous once the dioxide is formed. It is likely the reaction proceeds as follows:



In further analysis of this reaction, TGA and mass spectrometry (section 2.3.9) were used to confirm the reduction of Nb<sub>2</sub>O<sub>5</sub> (under a conventional heating regime). Stoichiometric amounts of Nb<sub>2</sub>O<sub>5</sub> and C, to afford NbC, were ground together and placed into an alumina crucible. The crucible, under an argon atmosphere, was then heated to 1400 °C at 10 °C/min. Figure 5- 5 contains the resultant TGA data and a typical mass spectrograph for the reduction of Nb<sub>2</sub>O<sub>5</sub> (taken specifically at 1150 °C), indicating the evolution of predominantly CO alongside small amounts of CO<sub>2</sub>. Other peaks are due to the Argon carrier gas.

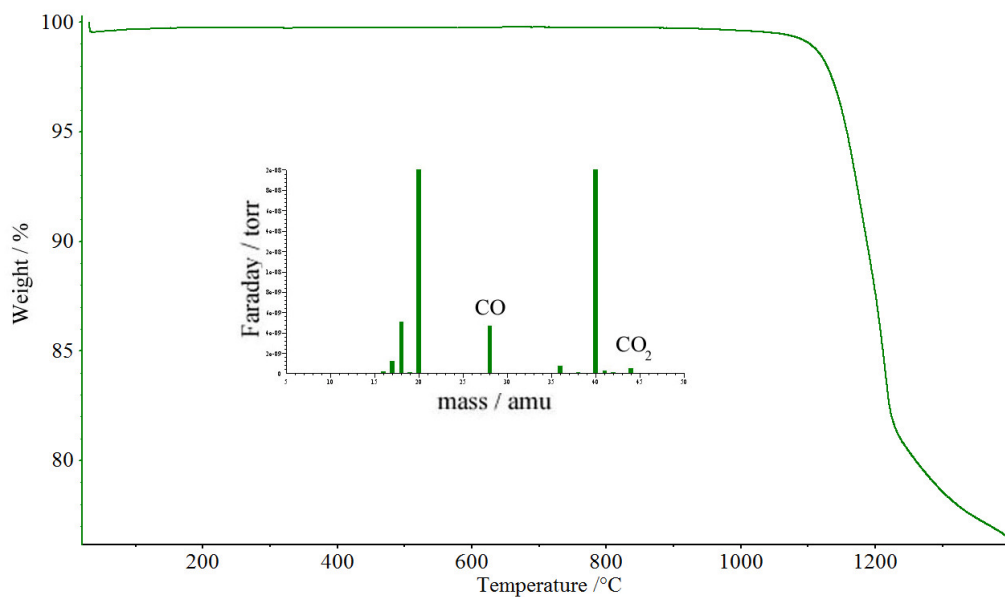


**Figure 5- 5: TGA for Nb<sub>2</sub>O<sub>5</sub> + C sample under argon. Mass spectrograph represents typical result during the reduction of the oxide (above 1080 °C).**

Two immediate observations are apparent from Figure 5- 5, the reduction of Nb<sub>2</sub>O<sub>5</sub> begins at around 1100 °C and from this point weight loss is rapid. Interestingly this indicates that temperatures in excess of 1000 °C must be occurring rapidly within the sample if complete synthesis of NbC is possible in 2 min in the DMO. However, unfortunately this cannot be confirmed as *in-situ* temperature measurements were not possible with the DMO setup. Also the TGA corroborates observations from PXD, indicating that, once the desired reaction temperature is reached, reduction of Nb<sub>2</sub>O<sub>5</sub> occurs rapidly. A weight loss of ~20 % is observed between 1100 and 1200 °C with the reduction beginning to plateau at this latter temperature. Complete reduction of Nb<sub>2</sub>O<sub>5</sub> to NbO<sub>2</sub> results in ~10 % weight loss, therefore within this temperature range reduction of the dioxide must also be taking place to account for the increased weight loss, all be it slower than the initial rapid reduction of Nb<sub>2</sub>O<sub>5</sub> to NbO<sub>2</sub>, as shown by PXD. Given complete reduction to the metal would result in

around ~40 % weight loss, by 1200 °C oxide must still exist, most likely only NbO<sub>2</sub> which could explain the gradient change observed in the TGA.

The NbC product was confirmed by Rietveld refinement against the PXD data collected for the sample heated for 2 min at 800 W in the DMO. The resultant profile is displayed in Figure 5- 6 with Table 5- 4 comprising selected crystallographic parameters post-refinement. Lattice parameters are in good agreement with those studied previously.<sup>8</sup> Magnetic measurements indicated a T<sub>c</sub> of 11.1(1) K, suggesting formation of NbC<sub>0.977</sub> as reported by Giorgi et al.,<sup>11</sup> with EDX confirming this ratio (1.0:0.97(1) for Nb:C).

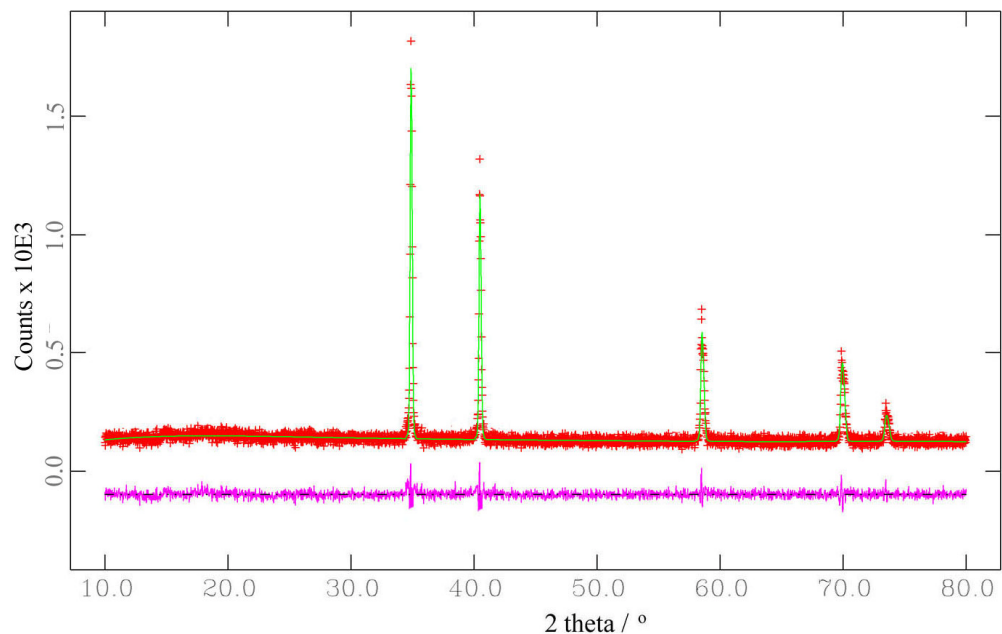


**Figure 5- 6: Observed (plusses), calculated and difference profile plot for the Rietveld refinement against PXD data for NbC produced in 2 min at 800 W in a DMO from the oxide, Nb<sub>2</sub>O<sub>5</sub>. Tick marks denote NbC diffraction peaks.**

Empirical formula	NbC
Crystal system, Space group	Cubic, $Fm\bar{3}m$
Unit cell formula weight, $M_w$	104.917
$a, c$ -parameter, Å	4.4635(2)
Unit cell volume, Å <sup>3</sup>	88.928(3)
Z, Calculated density, $\rho_x / \text{g cm}^{-3}$	1, 7.836
Observations, parameters	3500, 12
$R_p, R_{wp}, \chi^2$	0.0750, 0.0951, 1.337
Interatomic distance: Nb-C, Å	2.2318(1)
Interatomic distance: Nb-Nb, Å	3.1562(1)

**Table 5- 4: PXD crystallographic and bond information for NbC synthesised in 2 min at 800 W in a DMO.**

DMO experiments resulted in the successful synthesis of NbC from both the metal (Nb) and the oxide (Nb<sub>2</sub>O<sub>5</sub>). However, the reaction times were remarkably different. A total of 20 min was required for Nb plus C with only 2 min required for the oxide reaction. Despite the mass differences of the reactant mixtures, the pellet volumes were similar for both samples. With this in mind, one might have assumed that the oxide reaction would take longer as the reduction of the oxide must occur prior to the formation of any carbide. Clearly, however, this is not the case. Shimada et al. suggests that this reduced reaction time is due to CO evolved during the reaction aiding in oxide reduction.<sup>13</sup> Through experiments involving sealed and un-sealed reactions, it was noticed that a sealed system, thus inducing an increase in CO partial pressure, in fact resulted in a reduced and not a prolonged reaction time. One might consider that with more CO present the formation of NbC would be

discouraged, given the suspected reaction pathway described above, however, this is obviously not the case. Alternatively, it could be possible that CO is involved in the reduction process, thus covering the sample facilitates the reaction:<sup>13</sup>



Although this could be feasible, reactions reported in this chapter were all carried out in an open system, allowing the easy escape of CO gas. TGA using an open system, all be it with a gas flow, did indicate CO was the major gas evolved (not CO<sub>2</sub>). It is possible that small amounts of CO are, in fact, trapped within the pellet resulting in the bloated effect, or perhaps in the graphite susceptor. This would allow CO to participate in the reduction of the oxide; however, it is unlikely enough is present to make a marked difference.

A second option is that the dielectric properties of the reactants may differ. If the oxide presented a higher loss tangent than the metal (although both report high electrical conductivities) it would interact more rapidly with microwave radiation, resulting in a higher heating rate. In both cases, however, a susceptor was required to initiate the reaction, casting doubt on the favourable dielectric properties of the metal precursors. Analysis, using dielectric property measurements (performed as per section 2.1.2), confirmed this hypothesis, showing that both the metal (Nb) and the oxide (Nb<sub>2</sub>O<sub>5</sub>) possessed negligible loss tangents (0.01 and 0.017 respectively). It appears, therefore, that perhaps the rapid synthesis time associated with the metal oxide

could be due to the facilitated reduction via CO, however, this requires further investigation.

### 5.3.2 TaC synthesis

Synthesis of TaC was approached from two starting materials, the metal, Ta (**3**), and the oxide, Ta<sub>2</sub>O<sub>5</sub> (**4**):



Using the experimental procedure described in section 2.2.1, a series of experiments were carried out to determine the ideal heating time to manufacture TaC. With initial heating times of 30 min at 800 W, PXD post-reaction revealed a pure phase of TaC for synthesis from the metal (*equation vii*). After further investigation this heating time was refined to 20 min. Reaction times of less than 20 min resulted in a mixture of reactants, Ta and C, alongside the carbide TaC. The pure-phase TaC was subsequently refined using the Rietveld method (GSAS and EXPGUI, section 2.3.3)<sup>19, 20</sup> which resulted in the profile plot observed in Figure 5- 7. Table 5- 5 lists selected crystallographic parameters post-refinement.

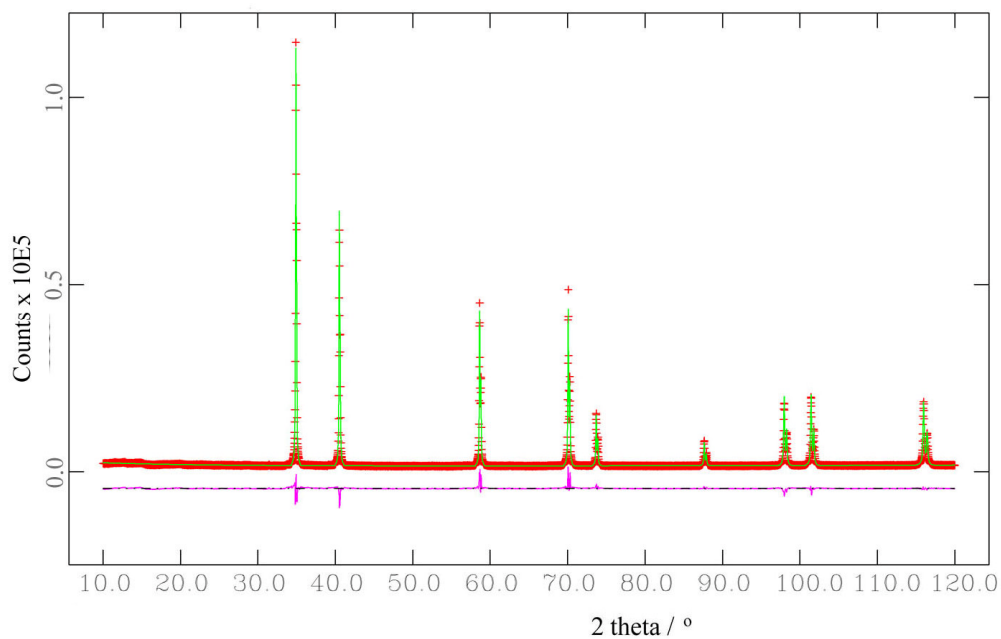


**Figure 5- 7: Observed (plusses), calculated and difference profile plot for the Rietveld refinement against PXD data for TaC produced in 20 min at 800 W in a DMO. Tick marks denote TaC diffraction peaks.**

Empirical formula	TaC
Crystal system, Space group	Cubic, $Fm\bar{3}m$
Unit cell formula weight, $M_w$	192.959
$a$ , $c$ -parameter, $\text{Å}$	4.45157(2)
Unit cell volume, $\text{Å}^3$	88.215(2)
$Z$ , Calculated density, $\rho_x / \text{g cm}^{-3}$	1, 14.643
Observations, parameters	5500, 19
$R_p$ , $R_{wp}$ , $\chi^2$	0.0483, 0.0641, 9.687
Interatomic distance: Ta-C, $\text{Å}$	2.2258(1)
Interatomic distance: Ta-Ta, $\text{Å}$	3.1477(1)

**Table 5- 5: PXD crystallographic and bond information for TaC synthesised in 20 min at 800 W in a DMO.**

Lattice parameters are in good agreement with those studied previously.<sup>9</sup> EDX confirmed the existence of only Ta and C, indicating a Ta:C ratio of 1.0:0.98(1). TGA under oxygen (Q600 TA instruments, sample heated at 2 °/min from 25 °C to 1000 °C) was also used to confirm the existence of TaC, revealing only a weight gain corresponding to the oxidation of the carbide at 600 °C (to Ta<sub>2</sub>O<sub>5</sub>, confirmed by PXD). Magnetic measurements of the TaC sample revealed a superconducting transition temperature ( $T_c$ ) of 9.78(8) K (Figure 5- 9), which lies towards the upper limit reported for this carbide.<sup>11</sup> Compositional variations, investigated by Giorgi et al., suggest that this  $T_c$  is associated with a Ta:C ratio of 1.0:0.987 which coincides with the values reported from EDX. As observed for the synthesis of NbC, magnetic measurements have offered both a way of confirming the formation of the desired phase, but also a method of inferring the C stoichiometry in the material.

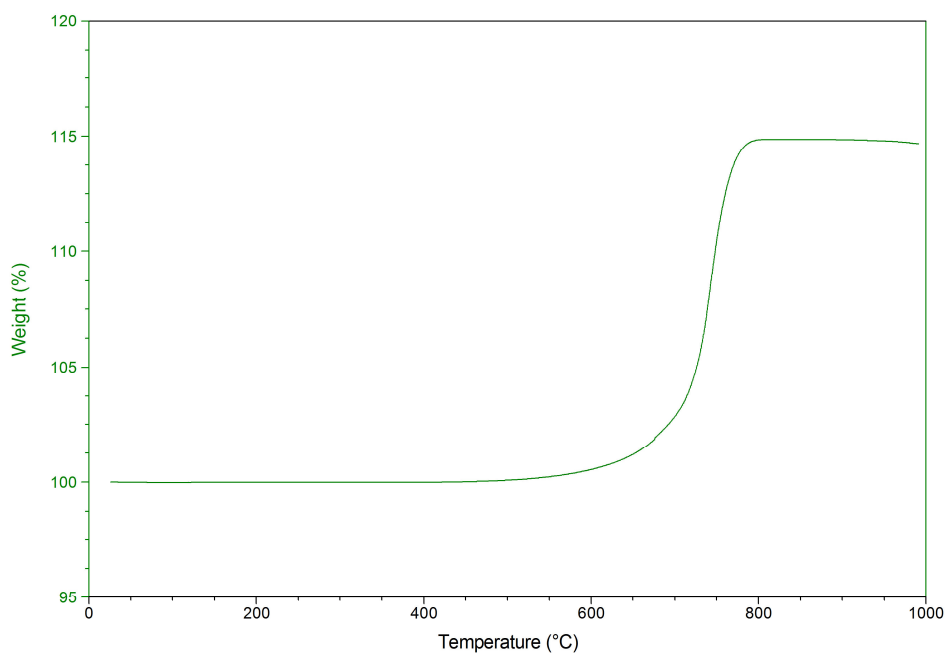


**Figure 5- 8: TGA plot indicating the oxidation of TaC beginning at 600 °C.**

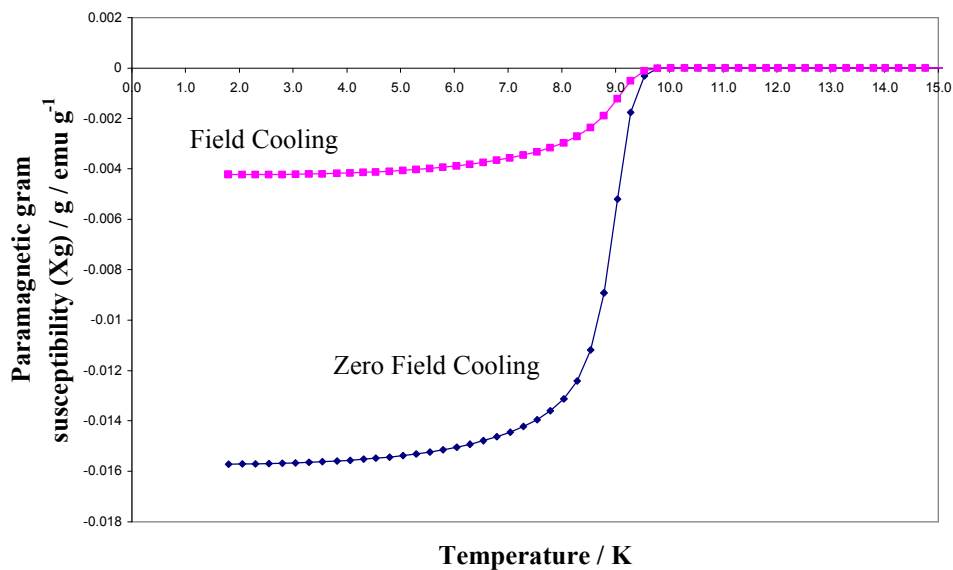


**Figure 5- 9: Plot of mass susceptibility,  $\chi_g$ , against temperature, for superconducting TaC synthesised in 20 min at 800 W in a DMO, showing a  $T_c$  onset at 9.78(8) K.**

Experiments concerning the formation of TaC from the oxide (4), Ta<sub>2</sub>O<sub>5</sub>, were carried out in a similar fashion to carbide synthesis from the metal. Following an identical preparation procedure, save for the different reactants, samples were initially heated at 800 W in the DMO for 30 min. Gas evolution, in the form of CO/CO<sub>2</sub>, caused the pellets to become slightly bloated and often brittle, however, no pellet fracturing was ever observed. Within the 30 min timescale successful synthesis of TaC was achieved and, through further investigation, this was reduced to only 5 min. Subsequent Rietveld refinement of PXD data collected for this sample resulted in the profile plot observed in Figure 5- 10. Table 5- 6 is comprised of selected crystallographic parameters post-refinement.

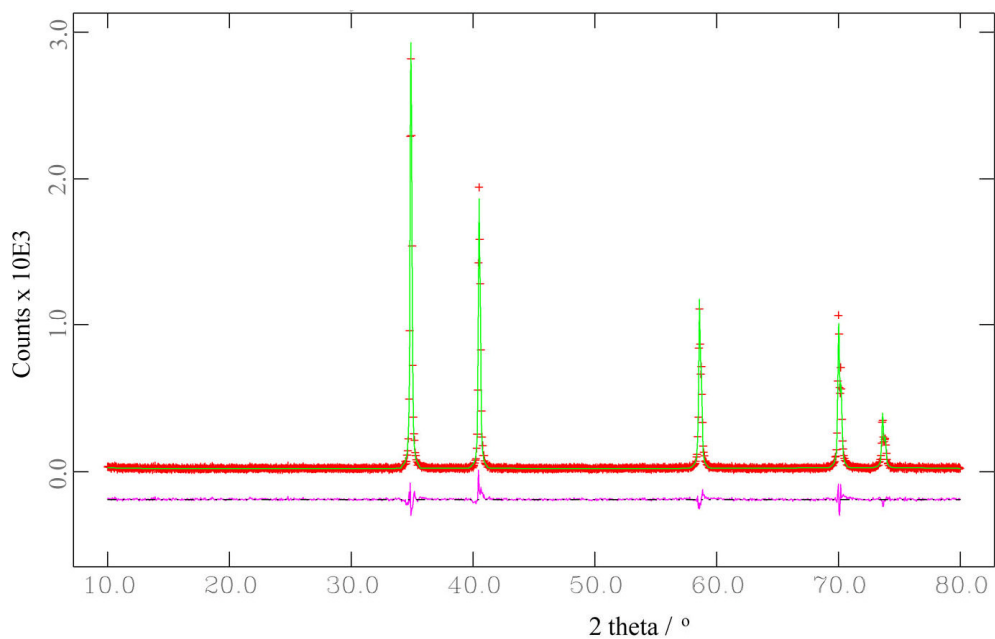


**Figure 5- 10: Observed (plusses), calculated and difference profile plot for the Rietveld refinement against PXD data for TaC produced in 5 min at 800 W in a DMO from the oxide, Ta<sub>2</sub>O<sub>5</sub>. Tick marks denote TaC diffraction peaks.**

Empirical formula	TaC
Crystal system, Space group	Cubic, Fm $\bar{3}$ m
Unit cell formula weight, M <sub>w</sub>	192.959
<i>a</i> , <i>c</i> -parameter, Å	4.4537(1)
Unit cell volume, Å <sup>3</sup>	88.345(4)
Z, Calculated density, ρ <sub>x</sub> / g cm <sup>-3</sup>	1, 14.508
Observations, parameters	1401, 14
R <sub>p</sub> , R <sub>wp</sub> , χ <sup>2</sup>	0.0477, 0.0631, 1.353
Interatomic distance: Ta-C, Å	2.2269(1)
Interatomic distance: Ta-Ta, Å	3.1493(1)

**Table 5- 6: PXD crystallographic and bond information for TaC synthesised in 5 min at 800 W in a DMO.**

Figure 5- 10 indicates the existence of a pure phase of TaC synthesised in 5 min from the metal oxide with lattice parameters in good agreement with those studied previously.<sup>9</sup> A Ta:C ratio of 1.0:0.97(1) was indicated via EDX which agrees, within error, with the metal to C ratio suggested by Giorgi et al. for TaC with a reported  $T_c$  of 9.53(8) K (collected via SQUID magnetometry).<sup>11</sup>

On investigation of reactions sub 5 min, a mixture of Ta<sub>2</sub>O<sub>5</sub> and TaC was observed and, unlike the synthesis of NbC from Nb<sub>2</sub>O<sub>5</sub>, no intermediate oxide was present. It appears the synthesis of TaC occurs directly from the reduction of the oxide and as soon as Ta exists it immediately forms the carbide. However, on further analysis of the PXD data collected from these incomplete reactions, phases of Ta<sub>2</sub>O<sub>5</sub> were found to exist. Below 1360 °C, Ta<sub>2</sub>O<sub>5</sub> is known to exist as an orthorhombic structure,  $\beta$ -Ta<sub>2</sub>O<sub>5</sub>, with space group Pmm2. For the high temperature form,  $\alpha$ -Ta<sub>2</sub>O<sub>5</sub>, the literature reports many possible structures which include tetragonal, monoclinic, triclinic, orthorhombic and hexagonal.<sup>21, 22, 23</sup> It is now widely accepted that tetragonal form is the most common crystal system observed,<sup>23</sup> with space group I4<sub>1</sub>/amd, however, authors still report the existence of the monoclinic phase, space group C2/c, and the orthorhombic phase,  $\beta$ -Ta<sub>2</sub>O<sub>5</sub>.<sup>23</sup> Further examination of the PXD data collected for the incomplete reactions indicates, in fact, the existence of three Ta<sub>2</sub>O<sub>5</sub> phases; orthorhombic, tetragonal and monoclinic. It appears that, after cooling to room temperature, two high temperature phases exist in addition to the low temperature phase. However, despite the presence of these multiple phases, all ultimately reduce to the metal, allowing the formation of the carbide, TaC, in 5 min.

Much of the controversy surrounding high temperature forms of Ta<sub>2</sub>O<sub>5</sub> seems associated with inaccurate measurements of phases at elevated temperatures. Often data are collected on cooling which can result in multiple phases being present, particular as  $\alpha$ -Ta<sub>2</sub>O<sub>5</sub> is known to reversibly return to  $\beta$ -Ta<sub>2</sub>O<sub>5</sub>, albeit slowly.<sup>2</sup> This may, in fact, explain why, on examination, PXD indicates multiple Ta<sub>2</sub>O<sub>5</sub> phases present for incomplete reactions. Due to the rapid cooling associated with many microwave experiments, it is therefore possible to isolate the kinetically stable high temperature polymorphs. This can result in the observation of multiple Ta<sub>2</sub>O<sub>5</sub> structures (see appendix) which is also noted in the laser radiation experiment carried out by Liu et al. in which rapid cooling is possible when the laser heating is complete.<sup>23</sup>

Finally, it is worth discussing the different reaction times for the metal and metal oxide experiments. Similar to investigations into NbC synthesis, the metal oxide resulted in a much faster reaction time than the metal. Although not complete in 2 min, as observed for Nb<sub>2</sub>O<sub>5</sub>, TaC was formed in only 5 min compared to 20 min for Ta plus C. It is still unclear as to why this is the case, with the experiment warranting further investigation, however, once again it seems that CO production may facilitate the formation of TaC despite the reactions carried out open to the atmosphere.

## 5.4 RESULTS AND DISCUSSION: SYNTHESIS OF NbC, TaC AND THE Ta-Nb-C SOLID SOLUTION SERIES USING A SINGLE MODE CAVITY

The single mode cavity was expected to offer faster reaction times as well as a more reproducible reaction. Unlike multimode applicators, a sample could be placed in a known location within the cavity and the system tuned to provide the most effective heating from the single standing wave (discussed in more detail in section 2.1.2). Through the use of this cavity, an in depth study of the reaction profile was undertaken for NbC and TaC, in addition to the successful synthesis of the carbides on an ultra rapid timescale. In addition, Ta-Nb-C solid solutions were investigated with specific interest in the comparison of the relationship between superconducting  $T_c$  and unit cell volume across the series. In order to obtain precise structural information, along with C stoichiometry information, PND was carried out on samples across the series. This also allowed correlation of the superconducting transition temperatures with the metal to C ratio.

### 5.4.1 Reaction profile investigations for NbC and TaC

With the achievement of successful synthesis of NbC and TaC from both the metal and metal oxide precursors, the next stage was to develop an understanding of the reaction process. For this, a series of experiments were run in order to generate a reaction profile for the carbide synthesis (**5, 6**):



The trends between *in-situ* temperature measurements and ex-situ PXD and dielectric property measurements were then analysed in an effort to further understand the reaction process. Both profiles will be discussed together as trends are similar. In fact, the data bear a great deal of resemblance to the study of WC and Mo<sub>2</sub>C within the single mode cavity (section 3.4.1 and 4.4.1.2 respectively).

Pellets were prepared according to the experimental procedure discussed in section 2.2.1, with stoichiometric amounts of Nb/Ta and C ground together to afford the desired carbide. A series of 2 g pellets were then heated, in turn, for a given amount of time between 5 and 30 s within the single mode cavity at a power input of 3 kW. Multiple repeats were carried out at each time. Characterisation post-reaction, using PXD, revealed the phases present after each reaction time which ultimately indicated a complete reaction had occurred within 20 s for reaction (5) and 15 s for reaction (6) (Figure 5- 11). These results were subsequently reinforced by XRF and EDX analysis (Table 5- 7), indicating the presence of no other elements, with observed M:C ratios (M = metal) corroborating those suggested by Giorgi et al.<sup>11</sup> given the relevant T<sub>c</sub>'s observed for NbC and TaC (Table 5- 7 and Figure 5- 12).

<b>Carbide</b>	<b>XRF M:C ratio</b>	<b>EDX M:C ratio</b>	<b>Sample T<sub>c</sub> / K</b>
NbC	1.00:0.97(1)	1.00:0.97(1)	11.29(6)
TaC	1.00:0.97(1)	1.00:0.97(1)	9.13(8)

**Table 5- 7: XRF, EDX and T<sub>c</sub> data for NbC and TaC carbides synthesised in 20 s and 15 s respectively in the single mode cavity at 3 kW.**

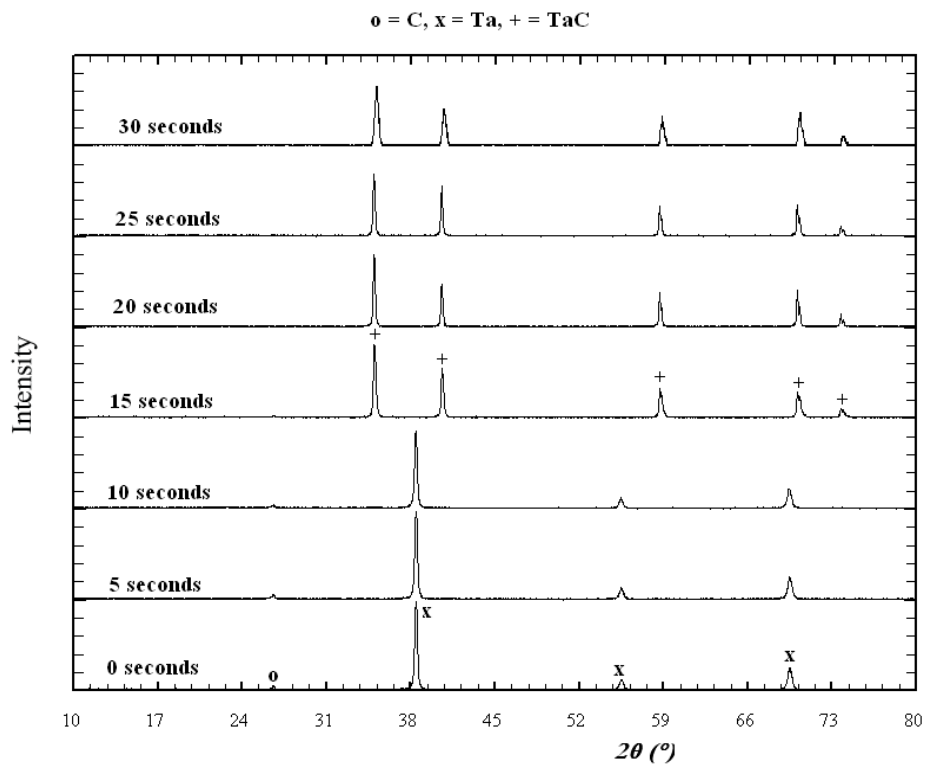
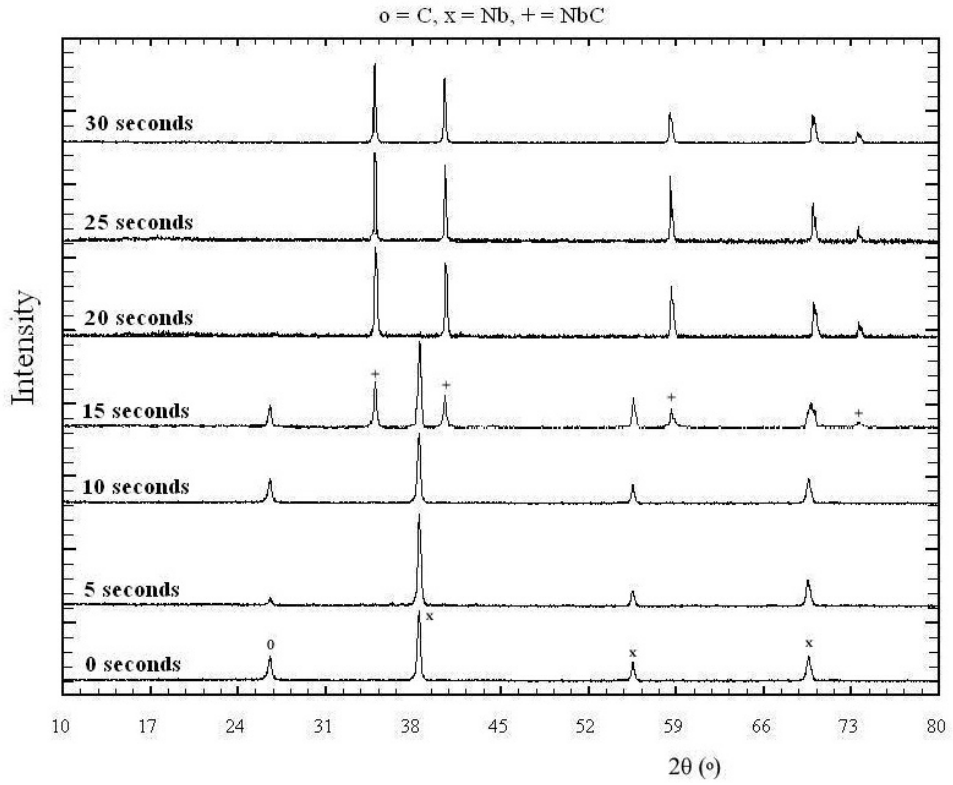


**Figure 5- 11: PXD patterns taken *ex-situ* from the Nb + C reaction (top), and the Ta + C reaction (bottom). Both were performed at 3 kW.**

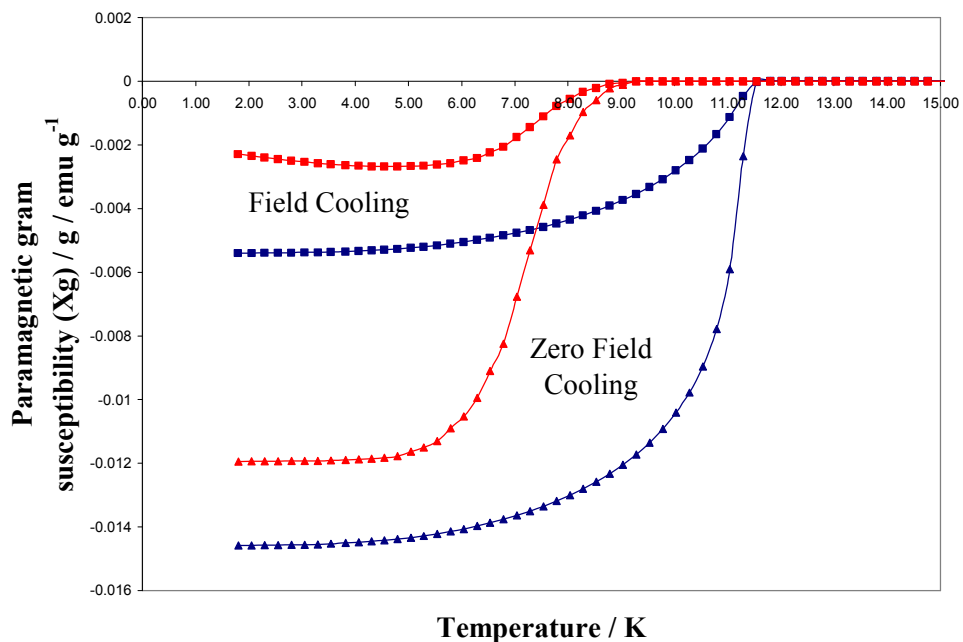


**Figure 5- 12: Plot of mass susceptibility,  $\chi_g$ , against temperature, for NbC, with a  $T_c$  onset at 11.29(6) K, synthesised in 20 s at 3 kW (blue lines); and TaC, with a  $T_c$  onset at 9.13(8) K, synthesised in 15 s at 3 kW (red lines).**

**Both reactions were carried out in a single mode cavity.**

The pure phases of NbC and TaC were further studied using Powder Neutron Diffraction (PND), which also confirmed single phase carbide formation. These results are discussed later in section 5.4.2 due to their relevance in the study of the Ta-Nb-C solid solution series.

In addition to *ex-situ* PXD, post-reaction, *ex-situ* dielectric property measurements were also taken at 293 K using the cavity perturbation technique (section 2.1.2). The resultant data, along with phase fraction information collected from PXD (Figure 5- 11) and temperature data from *in-situ* optical pyrometer measurements during the reactions, were then correlated resulting in the plots in Figure 5- 13 and Figure 5- 14 for NbC and TaC respectively. The

lines present on these reaction profiles act only as a visual guide to ensure the trend is apparent, but values are not absolute due to known change in dielectric properties with temperature.<sup>24</sup>

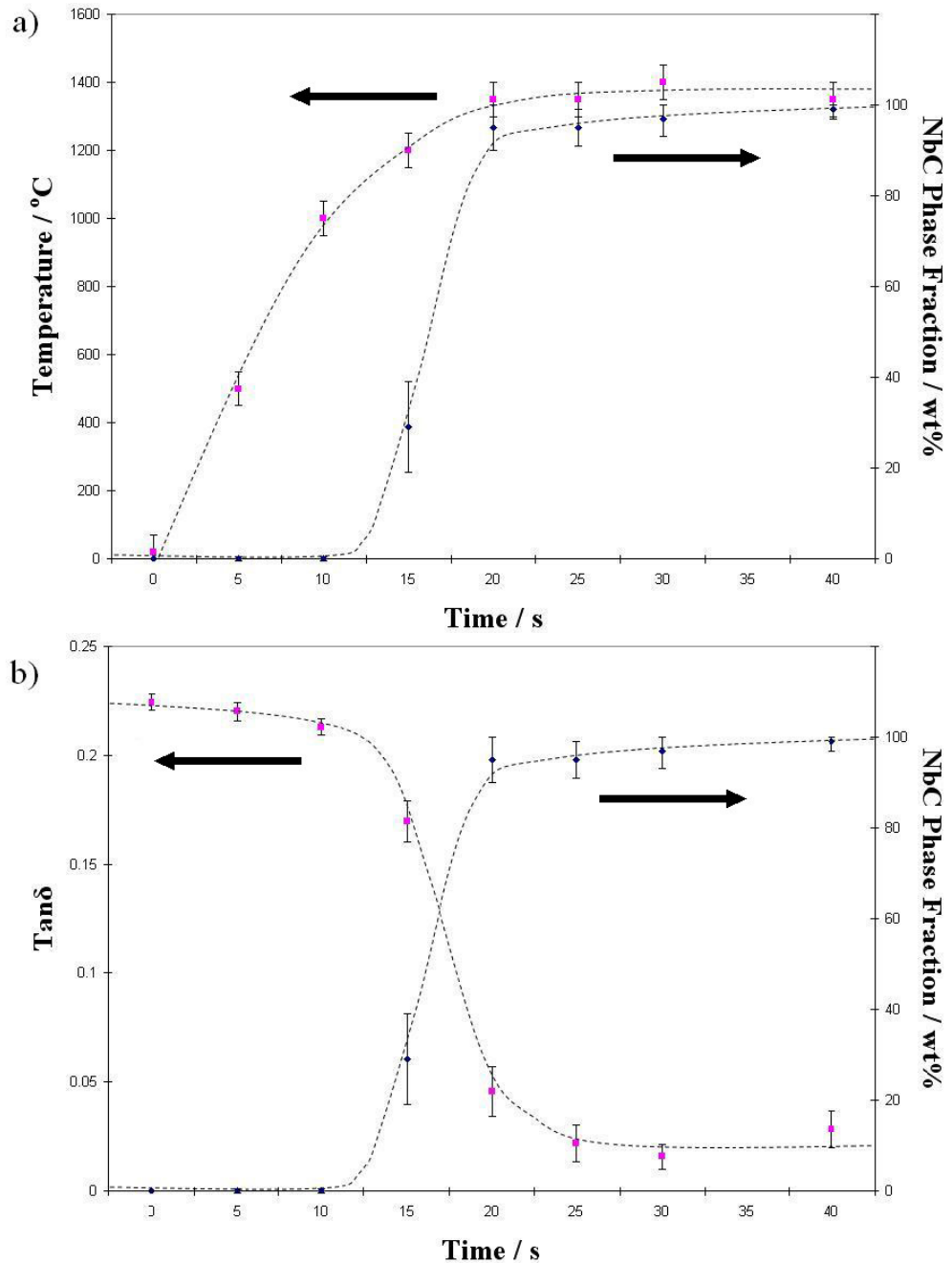


**Figure 5- 13: Plot of the Nb-C system phase fraction vs. reaction time (single mode cavity, 3 kW) superimposed with (a) reaction temperature and (b) tan  $\delta$  data.**

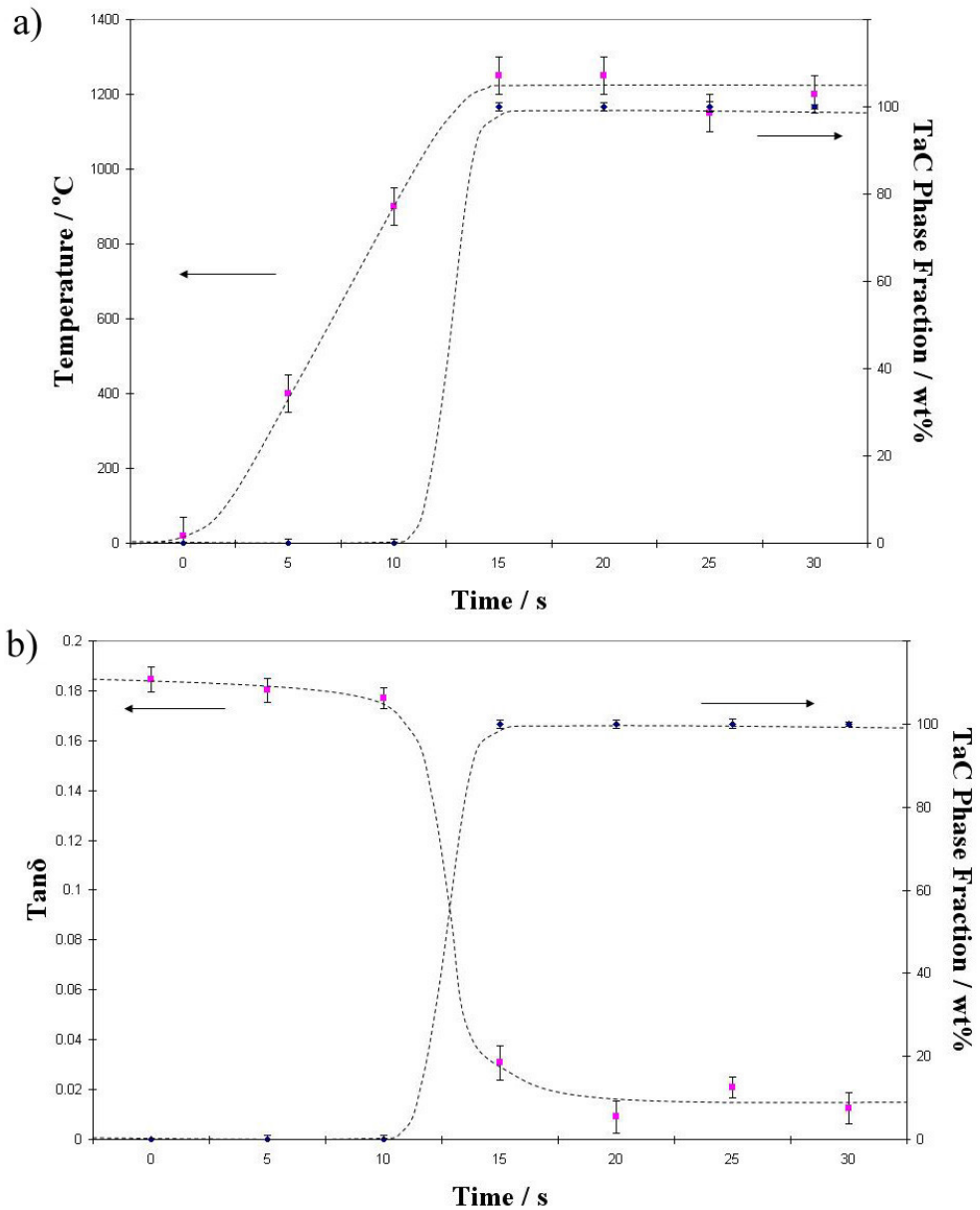


**Figure 5- 14: Plot of the Ta-C system phase fraction vs. reaction time (single mode cavity, 3 kW) superimposed with (a) reaction temperature and (b) tan  $\delta$  data.**

For both carbides (Figure 5- 13 and Figure 5- 14), formation of the product is negligible below 10 s, however, after this point it evolves rapidly, with very high purities reached for NbC in a further 10 s (20 s total) and only 5 s in the case of TaC (15 s total). The initial temperature rise in both systems is

rapid with (5) reaching  $\sim 1000$  °C in 10 s at which point the carbide phase formation begins. The temperature then continues to rise until NbC formation is complete, reaching  $\sim 1350$  °C after 20 s. At this point, after the vast majority of the product has been formed, the temperature plateaus until the experiment is terminated. This same pattern is observed for the Ta-C system (6), but with a temperature of  $\sim 900$  °C observed in 10 s and a plateau temperature of  $\sim 1200$  °C after 15 s. Hence, in both cases, rapid synthesis of NbC and TaC was achieved faster than the conventional method, but also at a lower temperature and in an open system (i.e. without a vacuum or cover gas). The temperature plateau effect also results in a self-terminating reaction, avoiding the often clear thermal runaway associated with microwave heating due to the observed increase in loss tangent with temperature.

The temperature vs. time profile is mirrored by the change in loss tangent,  $\tan\delta$ , ( $\tan\delta = \epsilon'' / \epsilon'$  where  $\epsilon'$  is the dielectric constant and  $\epsilon''$  is the dielectric loss) which in both cases decays rapidly as the product is formed (Figure 5- 13 and Figure 5- 14). The decay occurs as the highly conductive graphite starting material reacts with the metal (whose conductivity also reduces with temperature) to form the product. Although the values for  $\tan\delta$  are relative given that the measurements are taken *ex-situ* and the dielectric properties are temperature-dependent, the change in loss tangent with time is very pronounced. Ultimately, the reactions self-terminate on formation of the carbides (with lower values of  $\tan\delta$ ). Ideally, these could be confirmed using *in-situ* dielectric property measurements under synthesis conditions, however, this is beyond the capability of the current equipment.

Analogous self terminating reactions with similar loss tangent / phase fraction vs. time relationships were observed in the W-C and Mo-C systems (discussed in chapters 3 and 4 respectively). Common to all these M-C systems is a critical temperature at which product formation is initiated. Once reached, the formation of the carbides is subsequently extremely rapid, resulting in phase-pure products. This leads one to believe that the dielectric properties of the reactants are improved as temperature increases (in part due to the decreasing electrical conductivity with temperature for metals and the increasing conductivity (perpendicular to the planes) for graphite with temperature) to a point where the microwave interaction is optimum and product formation begins. Prior to this time point (critical initiation temperature) the majority of the irradiation is absorbed by the graphite powder susceptor (which is the major contributor to raising the reaction temperature via the dielectric loss and conduction).

#### ***5.4.1.1 Reactant mixing study; Nb + C***

The importance of the intimate mixing of reactants is paramount for solid state synthesis. Owing to the difficulty in mixing of solids, particularly those with varying particle sizes, the need for a homogeneous mixture is vital if the desired phase is to be formed without the existence of impurities, often in the form of un-reacted starting materials. Although perfect homogeneity is never reached, binary systems offer optimum mixing due to only two phases being initially present, with increasing phase numbers resulting in a more complex system. This complexity requires longer mixing times for increased

homogeneity, although this can often result in particle separation if large differences exist between particle sizes and/or densities. Instead of a homogeneous sample one is left with discrete regions of each reactant.

In order to investigate the mixing effect on carbide synthesis, a series of experiments were run for the Nb-C system (7). Reaction profiles were mapped for all reaction series, as discussed in section 5.4.1, but the sample pellets were prepared differently. Previously, all samples had been prepared by weighing out stoichiometric amounts of Nb and C, to afford NbC, and then ground for a continuous 10 min using a pestle and mortar. All samples were then pelleted under pressure for a further 10 min. For this series of experiments, the sample pelleting remained the same along with the quantity of sample used, but the grinding times were varied. In addition to the results already obtained for the Nb-C system (Figure 5- 13), 2 further series of experiments were run:

- a) Nb + C were ground together for 2 min prior to being pelleted.
- b) The reactants were not ground at all with one powder poured onto the other during the pelleting process.

Subsequent analysis of the data (discussed below) revealed a definite trend between grinding time and NbC phase formation, despite SEM showing no real difference in the sample homogeneities (Figure 5- 15).

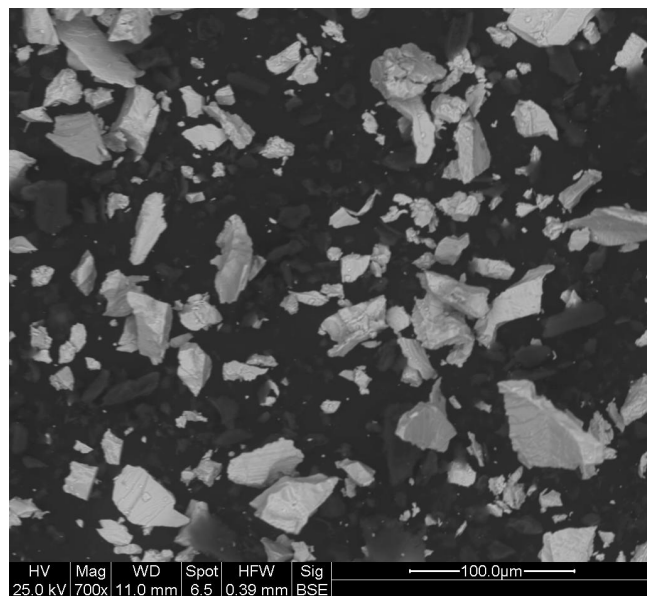
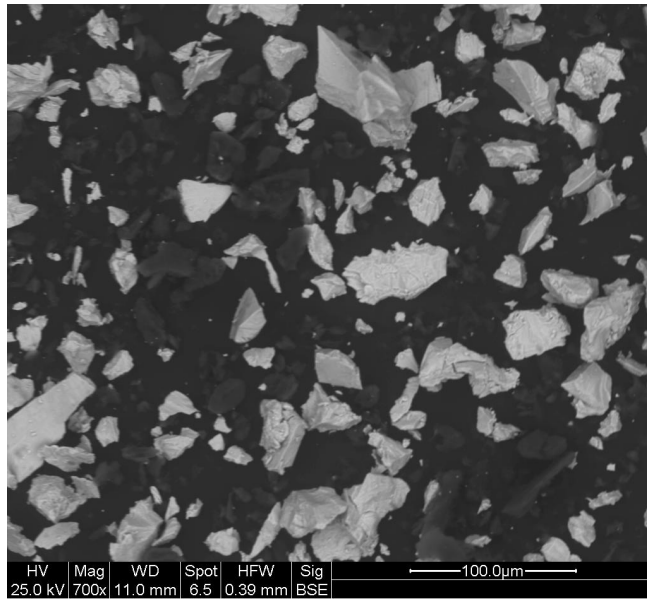


**Figure 5- 15: SEM images of Nb (light grey objects) + C (dark grey objects) powders, ground for 10 min (top); and ground for 2 min (bottom).**

For the samples ground for 10 min and 2 min no appreciable difference can be observed using SEM, with small discrete areas of Nb and C present in both cases. For the samples which were not ground at all an obvious difference was apparent with the mixing being practically non-existent. This dissimilarity mirrors itself in the dielectric measurement results (Figure 5- 16 and Figure 5-

17). The data collected for (b), which can be seen in Figure 5- 16, indicates no change in the loss tangent throughout the experiment. The loss tangent remains at 0.25 – 0.3, values associated with the starting mixture Nb + C, fluctuating only slightly across the 30 s reaction time. Analysis of PXD (see appendix), as suspected given these results, revealed the presence of only the metal and graphite, despite an observed pellet temperature in excess of 1200 °C. Interestingly the temperature increases steadily throughout the experiment, the rate of increase slowing only slightly at high temperature.

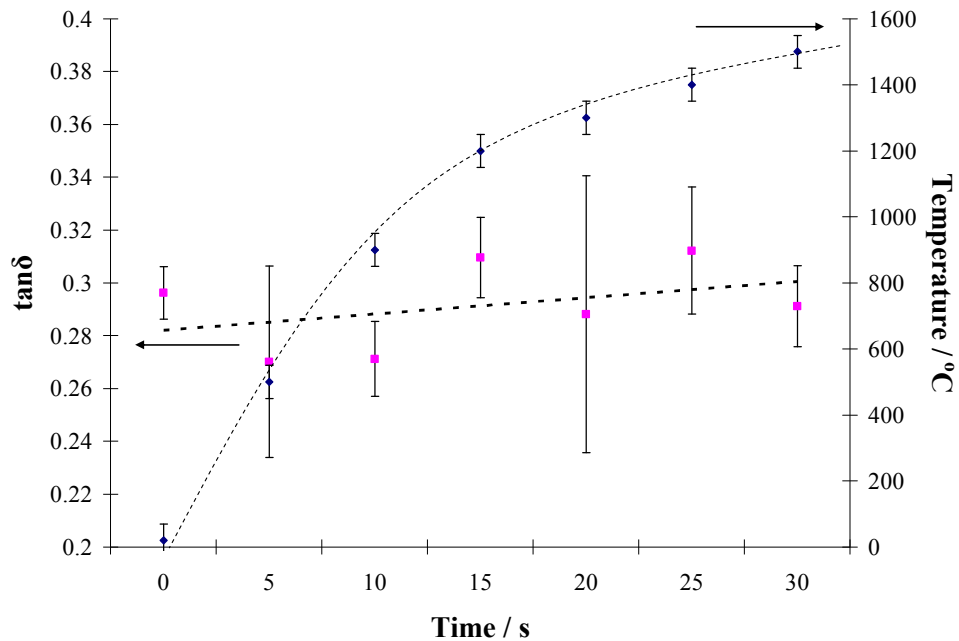


**Figure 5- 16: Plot of the Nb-C system  $\tan \delta$  data vs. temperature against reaction time (single mode cavity, 3 kW). Nb + C powder shaken together briefly (~2 s) prior to experiment.**

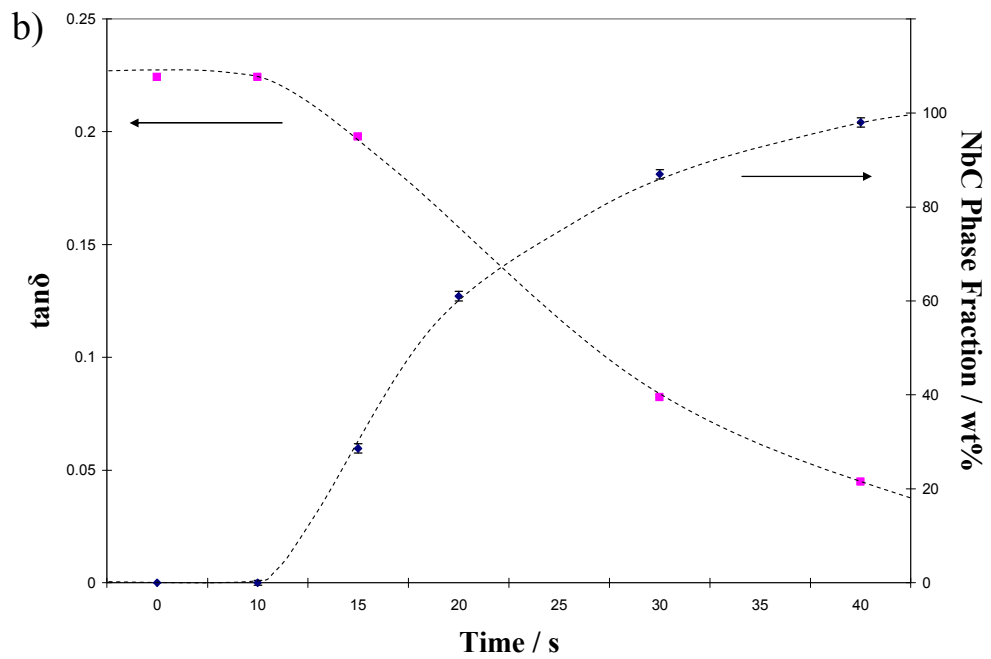
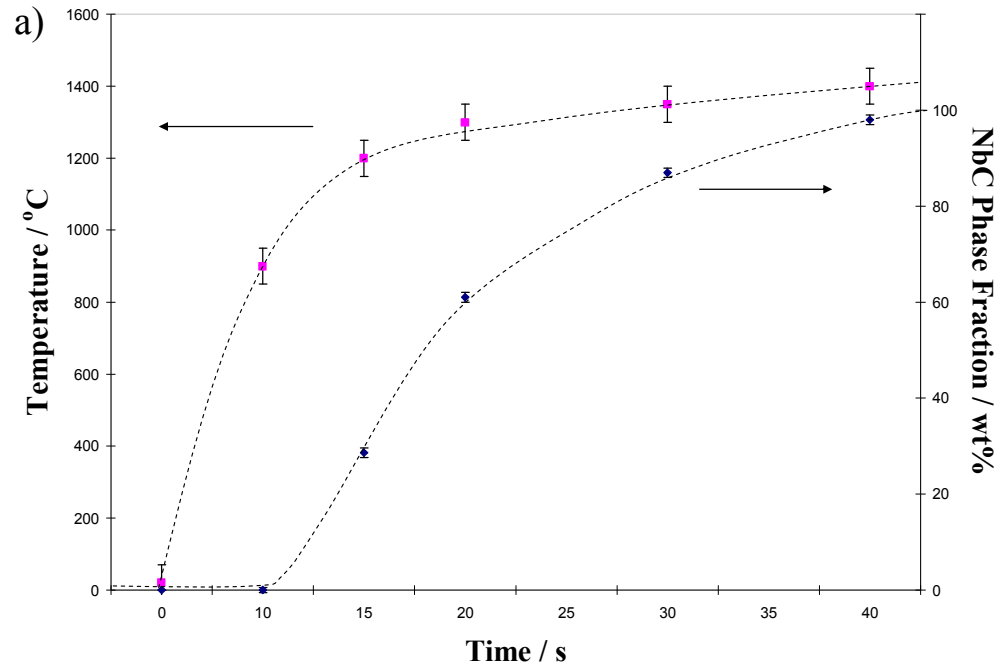


**Figure 5- 17: Plot of the Nb-C system phase fraction vs. reaction time (single mode cavity, 3 kW) superimposed with (a) reaction temperature and (b)  $\tan \delta$  data. Nb + C powder ground for 2 min prior to experiment.**

For the reaction in which the samples were ground for 2 min, (a), the recognisable reaction profile trend is observed (Figure 5- 17), however, there is a visible difference compared to the previously discussed results in section 5.4.1 (Figure 5- 13). Formation of the carbide still begins at 10 s, with a reaction temperature of  $\sim 900$  °C, however a further 30 s were required before a high purity of NbC was obtained ( $\sim 98$  %). During this period, the rate of increase of the temperature slowed, however no plateau was ever reached due to the slow formation of the carbide. In fact, the reaction time of 40 s is twice as long as the 20 s observed for the samples ground for 10 min and still a pure phase of NbC is not observed (Figure 5- 18).

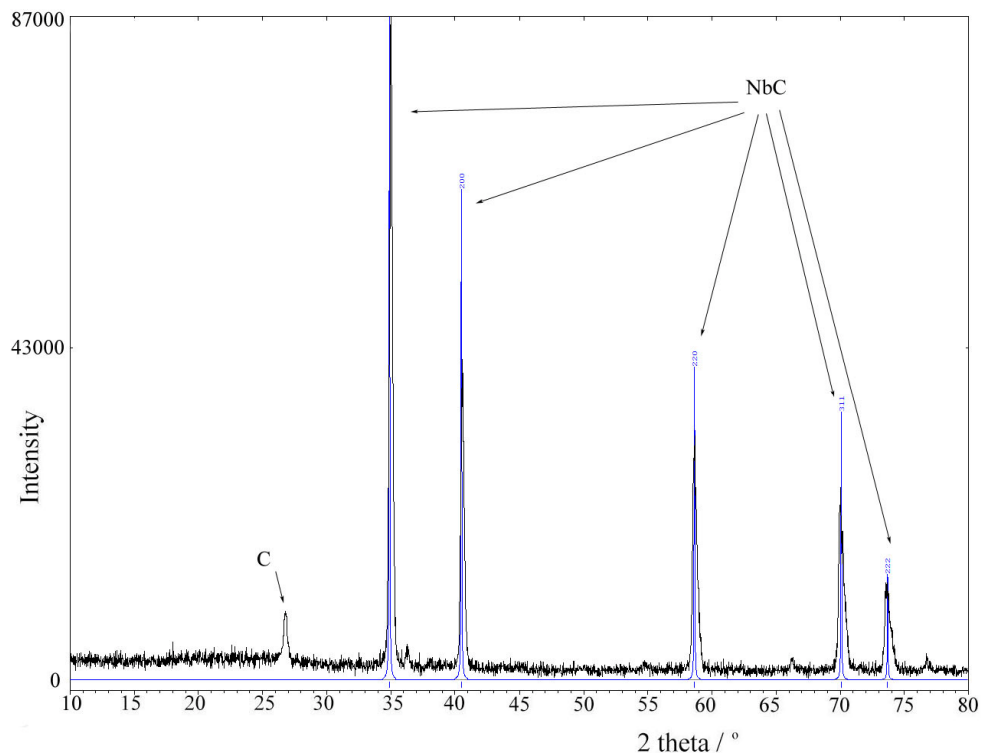


**Figure 5- 18: PXD plot of NbC synthesised in 40 s at 3 kW in the single mode cavity. Unlabelled peaks relate to Nb, still present in the final product along with C.**

The associated change in loss tangent and NbC formation is apparent, with  $\tan \delta$  decaying away as the carbide is formed. Despite the shallower trend lines observed, due to the slower formation of the carbide, the profile mirrors that seen in Figure 5- 17. Initially the loss tangent is high, owing to the presence of graphite and metal in the reaction mixture, but as the carbide is formed the loss tangent decreases towards that associated with NbC. However, a plateau is never observed; probably due to the high purity of NbC only being reached at 40 s. Reactions were not continued beyond this time due to problems with vessel breakage and melting of the quartz tubing, but one might predict such a plateau to exist given a longer heating time.

It certainly appears, as one might expect, that mixing has a direct effect on the microwave solid state reaction. Given these results, it is possible that with intimate mixing, perhaps using a more aggressive mill, the reaction time may be reduced even further.

#### **5.4.2 Nb-Ta-C solid solution series investigation through PND and magnetic measurements**

In this study, the solid solution Nb-Ta-C has been investigated (8). As discussed earlier (section 5.1.1), the similarity in atomic size between these two metals makes them ideal candidates ternary carbide synthesis.  $\text{Nb}_{1-x}\text{Ta}_x\text{C}$  retains the normal rock salt structure of the end members and, although the cell volume increases linearly with  $x$ , the relationship between  $T_c$  and metal stoichiometry is apparently non-linear.<sup>18</sup> Through the successful synthesis of a series of  $\text{Nb}_{1-x}\text{Ta}_x\text{C}$  carbides, this claim was investigated using PND and

magnetic measurements. PND allows the precise determination of the C stoichiometry in the carbide; something PXD is incapable of achieving due to the relationship between diffraction intensity and atomic number. The metal:carbon ratio can be compared to the data collected from XRF and EDX, but a direct comparison with the resultant superconducting transition temperatures collected via SQUID magnetic measurements is also possible.

The synthesis of the ternary carbides was carried out in similar fashion to the previously produced end members of the  $Nb_{1-x}Ta_xC$  series; NbC and TaC. Three ternary carbide compositions were investigated;  $Nb_{0.8}Ta_{0.2}C$ ,  $Nb_{0.5}Ta_{0.5}C$  and  $Nb_{0.2}Ta_{0.8}C$ , with stoichiometric amounts of Nb, Ta and C ground together to afford the desired products. The experimental procedure, outlined in section 2.2.2, was then used to synthesise the carbides in the single mode cavity. An applied power of 3 kW was used, with a number of heating times investigated. Ultimately, it was discovered that 20 s was required to achieve successful synthesis of all three ternary carbides. This was confirmed by PXD and reinforced using XRF, which show the presence of only Nb, Ta and C along with their ratios. Magnetic measurements revealed only one superconducting phase for each sample, associated with the ternary carbide. These results are summarised in Table 5- 8.

<b>Compound</b>	<b>Nb:Ta:C from XRF</b>	<b>T<sub>c</sub> / K</b>
$Nb_{0.8}Ta_{0.2}C$	0.80(1):0.20(1):0.97(1)	10.15(5)
$Nb_{0.5}Ta_{0.5}C$	0.50(1):0.50(1):0.96(1)	9.64(5)
$Nb_{0.2}Ta_{0.8}C$	0.20(1):0.80(1):0.97(1)	9.20(5)

**Table 5- 8: Selected data for Nb-Ta-C compounds.**

Figure 5- 19 shows the data obtained from magnetic measurements. Two plots are present, one showing both the field cooling and zero field cooling (top); and the second, which presents only a close up of the zero field cooling for the ease of viewing the  $T_c$  onsets (bottom).

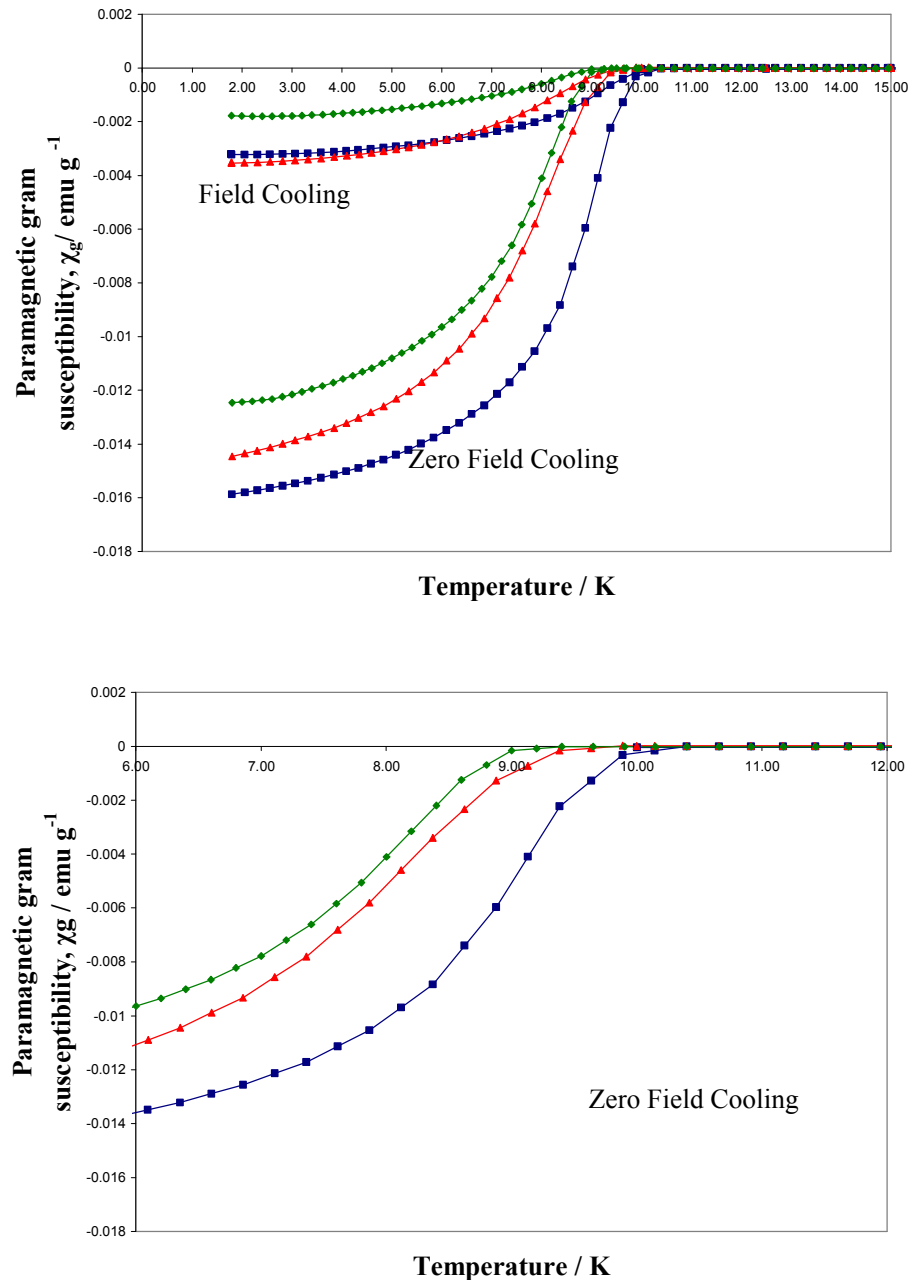


**Figure 5- 19: Plots of mass susceptibility,  $\chi_g$ , against temperature, for  $\text{Nb}_{0.8}\text{Ta}_{0.2}\text{C}$  (blue lines),  $\text{Nb}_{0.5}\text{Ta}_{0.5}\text{C}$  (red lines) and  $\text{Nb}_{0.2}\text{Ta}_{0.8}\text{C}$  (green lines), indicating  $T_c$  onsets of 10.15, 9.64 and 9.20 respectively.**

PND data were collected on D1A at the ILL in Grenoble (section 2.3.2.1). D1A operates with fixed scan times over a specified  $2\theta$  range, with multiple scans taken to increase the resolution of the diffraction pattern. The resultant pattern looks similar to PXD with  $2\theta$  plotted against intensity.

All three ternary carbides were investigated using PND, along with the  $\text{Nb}_{1-x}\text{Ta}_x\text{C}$  end members NbC and TaC. Approximately 2 g of a given sample was loaded into a 5mm diameter vanadium canister which was then attached to the diffractometer. The sample was scanned, between 0 and  $158^\circ$  in  $2\theta$  at a wavelength of  $1.39 \text{ \AA}$  with a step size of  $0.1^\circ$ , and data collected for 4 h. Rietveld refinement (section 2.3.3) against the data was performed using the General Structure Analysis System (GSAS)<sup>25</sup> through the windows based EXPGUI interface.<sup>26</sup> Structures were refined starting with those proposed in the literature (Table 5- 9); beginning with the background coefficients, followed by the cell parameters, atomic positions, profile parameters and isotropic temperature factors. Finally the C occupancy was refined.

Sample	Proposed Structure (Cubic, $\text{Fm}\bar{3}\text{m}$ )	Author
NbC	NbC	Will <sup>8</sup>
$\text{Nb}_{0.8}\text{Ta}_{0.2}\text{C}$	NbTaC <sub>2</sub>	Nowotny <sup>27</sup>
$\text{Nb}_{0.5}\text{Ta}_{0.5}\text{C}$		
$\text{Nb}_{0.2}\text{Ta}_{0.8}\text{C}$		
TaC	TaC	Fries <sup>9</sup>

**Table 5- 9: Structures proposed for the  $\text{Nb}_{1-x}\text{Ta}_x\text{C}$  samples synthesised and their respective authors.**

Resultant profile plots for the end members, NbC and TaC, can be seen in Figure 5- 20. Figure 5- 21 contains the profile plots for the 3 ternary carbides; Nb<sub>0.8</sub>Ta<sub>0.2</sub>C, Nb<sub>0.5</sub>Ta<sub>0.5</sub>C and Nb<sub>0.2</sub>Ta<sub>0.8</sub>C. Table 5- 10 comprises selected crystallographic parameters post-refinement for all 5 carbides.

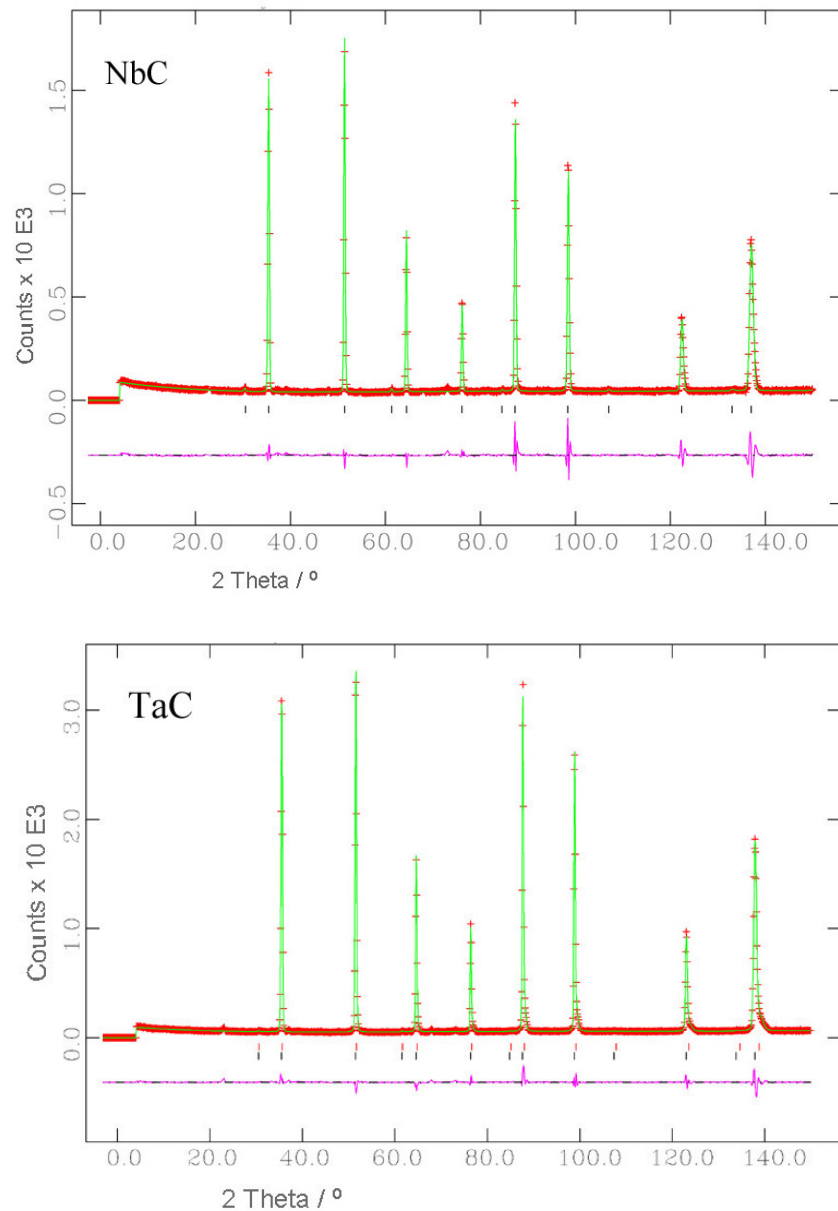


**Figure 5- 20: Observed (plusses), calculated (solid line) and difference (below) profile plot for the Rietveld refinement against PND data for NbC (synthesised in 20 s) and TaC (synthesised in 15 s); both undergone at 3 kW in a single mode cavity. Tick marks denote sample reflection positions.**

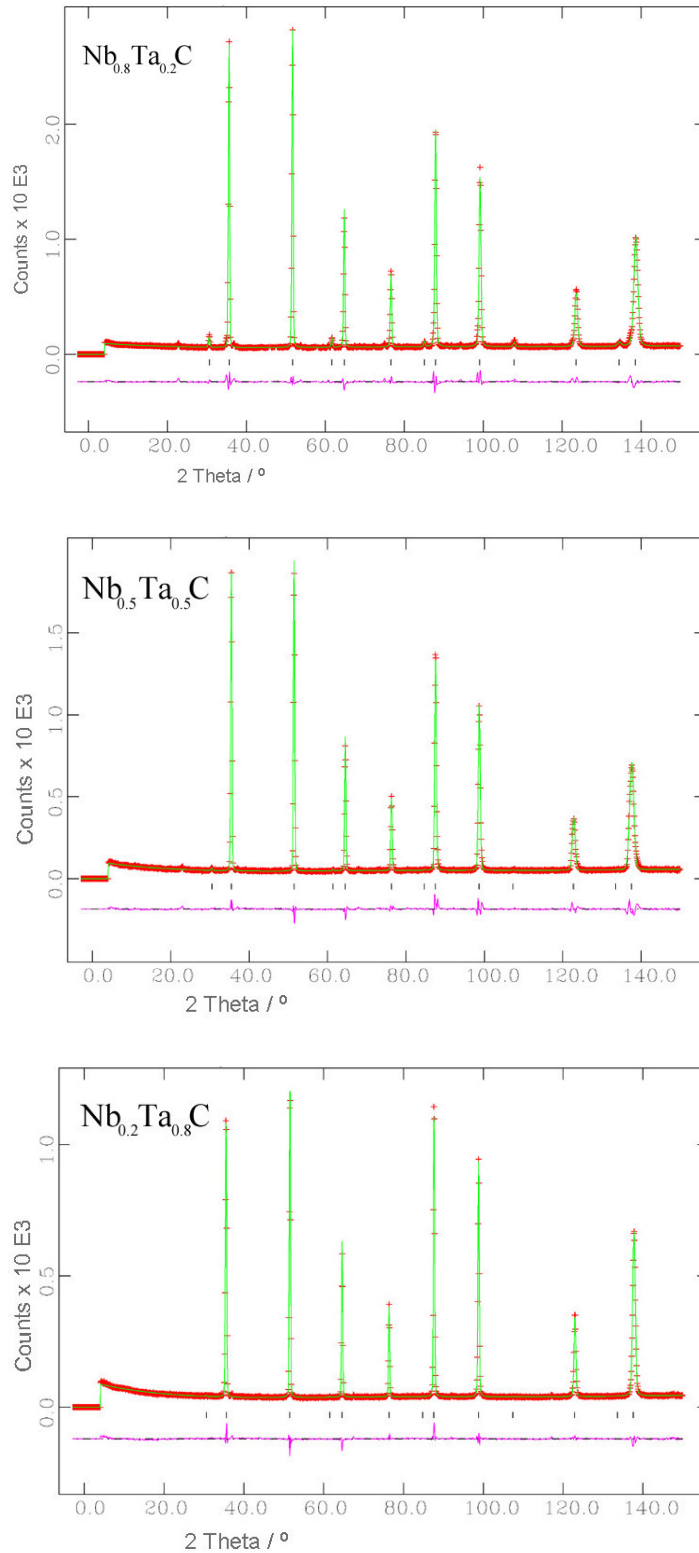


**Figure 5- 21: Observed (plusses), calculated (solid line) and difference (below) profile plot for the Rietveld refinement against PND data for  $\text{Nb}_{0.8}\text{Ta}_{0.2}\text{C}$ ,  $\text{Nb}_{0.5}\text{Ta}_{0.5}\text{C}$  and  $\text{Nb}_{0.2}\text{Ta}_{0.8}\text{C}$  (synthesised in 20 s at 3 kW in a single mode cavity). Tick marks denote sample reflection positions.**

Sample	NbC	Nb <sub>0.8</sub> Ta <sub>0.2</sub> C	Nb <sub>0.5</sub> Ta <sub>0.5</sub> C	Nb <sub>0.2</sub> Ta <sub>0.8</sub> C	TaC <sup>a</sup>
Crystal system	Cubic				
Space group	<i>Fm3m</i> (No. 225)				
Z	1				
M	104.92	122.53	148.93	175.35	192.96
$a$ -parameter, Å	4.46366(5)	4.45900(2)	4.45573(1)	4.45435(7)	4.45157(2), 4.450003(3)
Unit cell volume, Å <sup>3</sup>	88.935(9)	88.662(2)	88.462(8)	88.380(4)	88.215(3), 88.198(2)
Calculated density, $\rho_x$ / g cm <sup>-3</sup>	8.568	13.410	15.765	15.863	17.212, 16.558
(Nb,Ta) (0, 0, 0) occupancy	1.00:0.00	0.80:0.20	0.50:0.50	0.20:0.80	0.00:1.00, 0.00 :1.00
$U_{iso}$ / Å <sup>2</sup>	0.0038(2)	0.0034(2)	0.0037(5)	0.0028(5)	0.0008(2), 0.00607(2)
C ( $\frac{1}{2}$ , $\frac{1}{2}$ , $\frac{1}{2}$ ) occupancy	0.978(1)	0.981(2)	0.971(1)	0.975(1)	0.980(1), 0.975(1)
$U_{iso}$ / Å <sup>2</sup>	0.0038(2)	0.0035(3)	0.0017(6)	0.0017(5)	0.00806(2), 0.00760(1)
Observations, parameters	1459, 19	1459, 19	1459, 19	1459, 19	1459, 27
$R_p$ , $R_{wp}$ , $\chi^2$	0.0689, 0.0870, 6.502	0.0425, 0.0707, 5.896	0.0492, 0.0703, 4.114	0.0364, 0.0468, 2.745	0.0445, 0.0592, 4.210
Interatomic distance: (Nb,Ta)-C / Å	2.2318(1)	2.2295(1)	2.2279(1)	2.2272(1)	2.2258(1), 2.2250(1)
Interatomic Distance: (Nb,Ta)-(Nb,Ta) / Å	3.1563(1)	3.1530(1)	3.1507(1)	3.1497(1)	3.1477(1), 3.1467(1)

**Table 5- 10: Selected crystallographic data for Ta-Nb-C solid solutions from PND. <sup>a</sup> TaC was refined as two TaC<sub>1-x</sub> phases. The PND sample was composed of two different 2 g sample batches combined, hence the subtle discrepancy in carbon content between phases (2.79(2):1 phase ratio).**

Successful refinements were carried out across the Nb-Ta-C solid solution series. The cell parameters for the binary carbides are in excellent agreement with those reported for NbC<sub>1-x</sub> and TaC<sub>1-x</sub> compounds of equivalent stoichiometry.<sup>4, 8, 9</sup> The revealed C non-stoichiometry corroborates the metal:carbon ratios suggested by EDX and XRF (discussed in section 5.4.1). These C vacancies are also present in the ternary carbides; an occupancy of between 0.97 and 0.98 in all cases which agrees with the previously discussed XRF results. Cell parameters for these ternary carbides lie in between the end members with an increase in unit cell volume observed with Nb content. The T<sub>c</sub> for these materials also follows this trend, with the mixed metal carbides situated between NbC and TaC. Both the unit cell parameters and T<sub>c</sub> onset values are presented in Figure 5- 22.

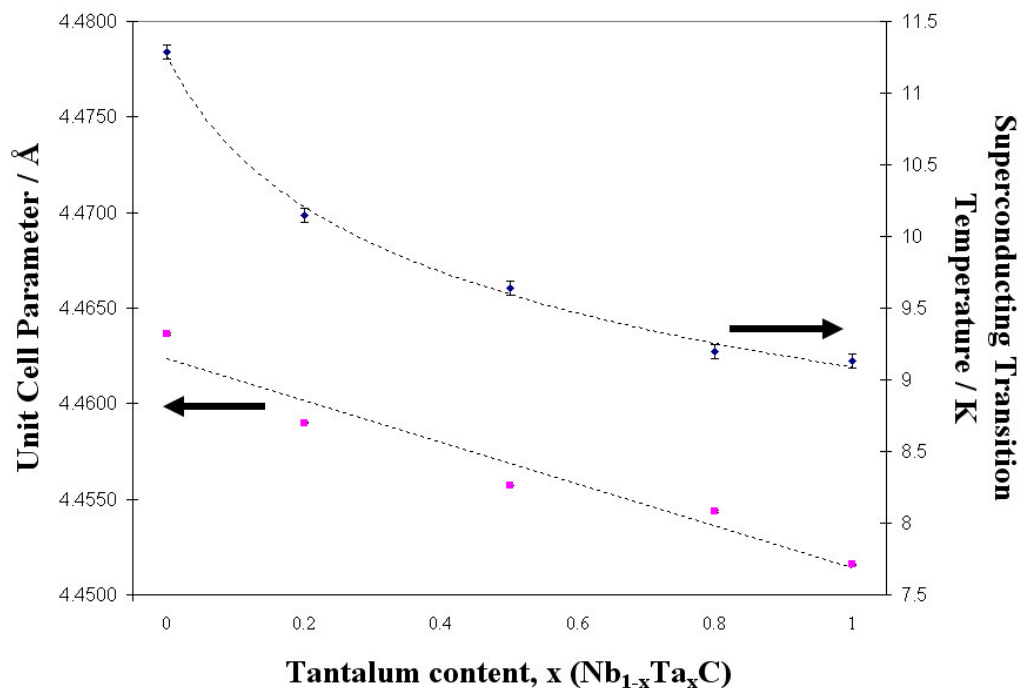


**Figure 5- 22: Plot of T<sub>c</sub> and lattice parameter *a* vs. *x* across the Nb<sub>1-x</sub>Ta<sub>x</sub>C solid solution (Trend lines act only as a guide to the eye).**

The change in cell parameter across the solid solution follows Vegard's law with a decrease in cell parameter,  $a$ , from NbC to TaC. Slight deviation from linearity might be explained by the small fluctuations from the idealised 1:1 metal:carbon stoichiometry (the lattice parameter for  $\text{NbC}_{1-x}$ , for example, varies non-linearly with  $x$ ).<sup>4</sup>

$T_c$ , on the other hand, presents a non-linear relationship with  $x$ , but unlike previous literature studies,<sup>18</sup> the  $T_c$  reaches a maximum at  $x=0$  and a minimum at  $x=1$ . Given the C stoichiometries of the carbides studied, and that a linear relationship between  $T_c$  and  $x$  exists for the interstitial nitrides  $\text{Hf}_{1-x}\text{Zr}_x\text{N}$ ,<sup>28</sup> it seems probable that the negative deviation from linearity for  $T_c$  versus  $x$ , observed for the  $\text{Nb}_{1-x}\text{Ta}_x\text{C}$  series, is a direct consequence of C non-stoichiometry. This is further reinforced by the fact that  $T_c$  declines with  $x$  in the Nb-C and Ta-C binary systems.<sup>11</sup>  $T_c$  onsets observed in materials from the DMO experiments reinforce this, indicating differing values associated with varying C occupancy (section 5.3). Therefore it seems likely that, contrary to previous hypotheses,<sup>18</sup>  $T_c$  is a linear function of the cell volume in 1:1 carbides and the electrons per unit volume arguments applied to intermetallics hold for the Nb-Ta-C system. In fact, an approximately linear relationship in  $T_c$  versus cell volume exists across the series investigated (Figure 5- 23). This further reinforces the expected linear relationship, signifying the direct relationship between  $T_c$  and cell volume despite the slight C non-stoichiometry observed in the carbides.

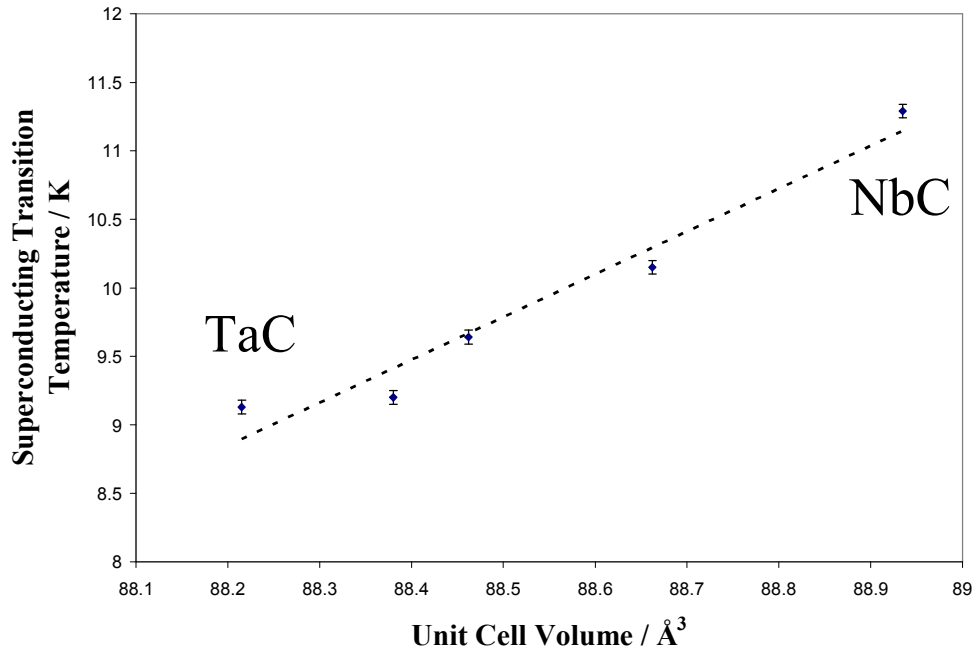


**Figure 5- 23: A plot indicating the approximate linear relationship between unit cell volume and  $T_c$  across the Nb-TaC solid solution series.**

## 5.5 CONCLUSIONS

The study of the binary carbides NbC and TaC, resulted in successful synthesis in both multimode (DMO) and single mode applicators. Within the DMO this was achieved from the metal and metal oxide precursors, with reaction times of 20 min required for the former, and 5 min for TaC and 2 min for NbC for the latter. The dramatic decrease in reaction time for the metal oxide experiments is still not fully understood, but a number of plausible suggestions exist. The possibility of enhanced loss for the oxide compared to the metal may explain the rapid reaction time, although investigation of this hypothesis revealed no such enhancement (e.g. a loss tangent of 0.017 for Nb<sub>2</sub>O<sub>5</sub>). In fact, both the metal and metal oxide boast negligible loss tangents, indicating a poor interaction with the microwave field.

An alternative suggestion centres on the argument that CO, produced during the reduction of the metal oxide, aids the further reduction of the oxide, thus encouraging the formation of the carbide. Although this has been demonstrated by Shimada et al.,<sup>13</sup> a closed system is required which traps the CO produced and allows it to participate in the reduction process. Reactions discussed in this chapter were all carried out in open systems with the CO allowed to escape on formation. It is possible however, that some of the CO is trapped in the graphite susceptor or within the pellet itself, but is unlikely enough exists to make an appreciable difference to the reduction of the metal oxide. Therefore, in the experiments discussed here, it is doubtful either the dielectric properties of the metal oxide or CO assisted reduction contribute to the decreased reaction time; an explanation for this is still elusive.

Synthesis undergone in the single mode cavity resulted in an expected reduction in reaction time compared to the DMO. Within 20 s, formation of NbC was achieved and for TaC a timescale of only 15 s was required. An investigation into reactant mixing revealed a strong correlation between reaction time and homogeneity showing the necessity for intimate mixing if efficient reactions are desired. It also suggests that the carbon component couples more readily to the microwave energy than the metal and in order for successful synthesis of the carbide, the particles must be intimately mixed in order for the formation of the desired material to begin.

Profile plots for both Nb-C and Ta-C systems showed similar trends, with carbide formation beginning at 10 s coinciding with a reaction temperature of  $\sim 1000$  °C. A temperature plateau was then observed associated

with the high purity production of the carbide, resulting in a self-terminating reaction. Examination of the loss tangent across the reaction profile revealed a decrease; mirroring the increase in carbide phase fraction. This trend, along with the others observed for both NbC and TaC are very similar to those observed in the W-C and Mo-C systems.

In all cases, regardless of applicator type, the carbide produced deviated slightly from the ideal 1:1 metal:carbon ratio due to the presence of C non-stoichiometry. In fact, this was apparent throughout all the carbides discussed in this chapter, including the ternary carbides investigated. C occupancy was confirmed using a variety of characterisation techniques; EDX, XRF and PND. All revealed similar metal:carbon ratios and, when compared to the  $T_c$  onsets obtained for the samples, agreed with the stoichiometries suggested by Giorgi et al. during his investigation of carbide superconductivity and C non-stoichiometry.<sup>11</sup> For example, Giorgi suggests a  $T_c$  onset of 11.1 K for NbC<sub>0.977</sub> with observations reported in this thesis suggesting a  $T_c$  onset of 11.29 K for a similar C non-stoichiometry, NbC<sub>0.978(1)</sub>. This C occupancy, obtained using PND, also matches closely to XRF and EDX predictions for the sample of NbC<sub>0.97(1)</sub>. In fact, this study, combined with work published by Giorgi, verifies the non-linear trend between  $T_c$  and C occupancy. This, in turn, explains the non-linear trend in  $T_c$  onset observed in the investigation of the Nb-Ta-C solid solution series. In this series successful synthesis of three ternary carbides, Nb<sub>0.8</sub>Ta<sub>0.2</sub>C, Nb<sub>0.5</sub>Ta<sub>0.5</sub>C and Nb<sub>0.2</sub>Ta<sub>0.8</sub>C, was achieved in 20 s in the single mode cavity at 3 kW. A linear trend in the cell parameter, following Vegard's law, was observed with only slight deviation due to variation in the C

stoichiometry of each material. Slight deficiency in C occupancy does not to affect the cell volume drastically, allowing a linear trend to still be possible. However, contrary to this, the  $T_c$  onset is affected greatly with a small variation in C stoichiometry. For this reason, as verified by the monocarbide investigations, a non-linear trend is apparent for the  $T_c$  onset along the series.

## 5.6 REFERENCES

- 
- <sup>1</sup> E. K. Storms, *The Refractory Carbides*, 1<sup>st</sup> Edition, Academic Press, New York, 1967.
- <sup>2</sup> H. O. Pierson, *Handbook of Refractory Carbides and Nitrides*, 1<sup>st</sup> Edition, Noyes, Park Ridge NJ, 1960.
- <sup>3</sup> L. E. Toth, *Transition Metal Carbides and Nitrides*, 1<sup>st</sup> edition, Academic Press, New York and London, 1971.
- <sup>4</sup> E. K. Storms and N. H. Krikorian, *J. Phys. Chem.*, 1959, **63**, 1747.
- <sup>5</sup> K. Yvon, H. Nowotny and R. Kieffer, *Monatshefte fuer Chemie*, 1967, 98, 34.
- <sup>6</sup> F. Lissner and T. Schleid, *Zeitschrift fuer Kristallographie*, 2001, 216, 329.
- <sup>7</sup> E. Rudy, C. E. Brukl and S. Windisch, *J. Am. Ceram. Soc.*, 1968, **51**, 239.
- <sup>8</sup> G. Will and R. Platzbecker, *Zeitschrift fuer Anorganische und Allgemeine Chemie*, 2001, **627**, 2207.
- <sup>9</sup> R. J. Fries and L. A. Wahman, *J. Am. Ceram. Soc.*, 1967, **50**, 475.
- <sup>10</sup> K. Schwarz and N. Rösch, *J. Phys. C: Solid State Phys.*, 1976, **9**, 433.
- <sup>11</sup> A. L. Giorgi, E. G. Szklarz, E. K. Storms, A. L. Bowman and B. T. Matthias, *Phys. Rev.*, 1962, **125**, 837.
- <sup>12</sup> T. Ya. Kosolapova, *Carbides: Properties, Production and Applications*, 1<sup>st</sup> Edition, Plenum Press, New York, 1971.
- <sup>13</sup> S. Shimada, T. Koyama, K. Kodaira and T. Mastushita, *J. Mater. Sci.*, 1983, **18**, 1291.
- <sup>14</sup> A. M. Nartowski, I. P. Parkin, M. MacKenzie, A. J. Craven and I. MacLeod, *J. Mater. Chem.*, 1999, **9**, 1275.

- 
- <sup>15</sup> A. M. Nartowski, I. P. Parkin, M. MacKenzie and A. J. Craven, *J. Mater. Chem.*, 2001, **11**, 3116.
- <sup>16</sup> N. A. Hassine, J. G. P. Binner and T. E. Cross, *Int. J. Refractory Metals & Hard Mater.*, 1995, **13**, 353.
- <sup>17</sup> G. Brauer and R. Lesser, *Z. Metallk.*, 1959, **50**, 8.
- <sup>18</sup> M. Wells, M. Pickus, K. Kennedy and V. Zackay, *Phys. Rev. Lett.*, 1964, **12**, 536.
- <sup>19</sup> A. C. Larson and R.B. Von Dreele, "The General Structure Analysis System", Los Alamos National Laboratories, Report LAUR086748, LANL, Los Alamos, N. M., USA, 1999.
- <sup>20</sup> B. H. Toby, *J. Appl. Crystallogr.*, 2001, **34**, 210.
- <sup>21</sup> N. P. Bansal, *J. Mater. Sci.*, 1994, **29**, 5065.
- <sup>22</sup> H. S. Hong and K. S. Lee, *J. Alloys and Compounds*, 2003, **360**, 198.
- <sup>23</sup> X. Q. Liu, X. D. Han, Z. Zhang, L. F. Ji and Y. J. Jiang, *Acta Mater.*, 2006, **55**, 2385.
- <sup>24</sup> D. J. Brooks, R. E. Douthwaite and L. J. Gillie, *Chem. Comm.*, 2005, **38**, 4857.
- <sup>25</sup> A. C. Larson and R. B. von Dreele, "*The General Structure Analysis System*", 2000, Los Alamos National Laboratories: Los Alamos, NM.
- <sup>26</sup> B. H. Toby, *J. Appl. Crystallogr.*, 2001, **34**, 210.
- <sup>27</sup> H. Nowotny and R. Kieffer, *Chemica Scripta*, 1988, **28**, 25.
- <sup>28</sup> A. L. Giorgi and E. G. Szklarz, *Bull. Am. Phys. Soc.*, 1962, **7**, 176.

## 6: GENERAL SUMMARY AND FURTHER WORK

The work described in this thesis covers investigations into the synthesis and reaction study of the transition metal carbides; specifically W-C, Mo-C, Ta-C, Nb-C and Nb-Ta-C systems. The research was approached from two distinct directions, although inevitably these crossed over: the development of a general experimental procedure to afford the desired materials and the in depth study of the resultant reactions.

Initial understanding of the microwave synthesis of solid state materials meant a great deal of experimentation was required to obtain a general idea of synthesis times and requirements. Through a series of systematic investigations an understanding of susceptors (used to initiate reactions by increasing the initial temperature), reaction vessels, sample locations and mode positions was obtained, resulting in the successful development of the experimental procedure. Originally established in the DMO, slight modifications were carried out for suitable use in a single mode cavity.

The final experimental procedure consisted of a 10 mm quartz (silica) tube (sealed at one end), containing the sample pellet imbedded in graphite powder (acting as a susceptor), being supported by silica flour within a beaker for DMO experiments and a larger quartz tube in the case of single mode cavity work. The silica flour acted as both a support and retainer of heat, thus maintaining the high reaction temperatures required for carbide synthesis. The quartz tubing, used as a reaction vessel, is microwave transparent and so allows

the applied power to reach the susceptor and pellet with minimal energy loss. The susceptor (graphite) was required after initial investigation revealed no heating of the metal and carbon reaction mixture. Graphite, capable of absorbing the microwave radiation and raising the reaction temperature, was used to help initiate carbide formation. Dielectric studies of W + C indicated the improved loss tangent at higher temperatures, demonstrating the requirement for a susceptor to reach this temperature, at which point the sample itself absorbs microwave energy with increased efficiency. However, careful use of the susceptor was required. Too much would not allow sufficient microwave energy to penetrate to the sample and too little would not provide adequate heat to raise the initial reaction temperature. The whole reaction vessel remained open to the atmosphere after extensive investigations revealed only minute amounts of surface metal oxide (< 5 nm depth) appearing after a given experiment (investigated for Mo<sub>2</sub>C synthesis from the metal). In fact, XPS was required to observe this with argon etching removing all traces of the oxide (MoO<sub>3</sub>).

Successful synthesis of the carbide was also dependent on applied microwave power, sample volume and reactant mixing. It became apparent, as for all solid state reactions, that mixing is of paramount importance for efficient reactions to take place. Poor mixing of the reactants can result in double the expected reaction time, as observed for NbC, and in extreme cases no product formation at all. Sample volume, as expected, also increases the reaction time to afford the pure carbide, providing all other variables are kept constant. This is certainly important when considering industrial scale up processes for carbide synthesis.

Applied power/greater power density is also an important factor, resulting in more rapid product formation. However, cavity type also plays an important role in reaction time, with single mode cavities proving much more efficient in both reaction reproducibility and synthesis time. This is the result of precise tuning of the sample to better match the system and, given power density is proportional to the electric field strength squared, achieve greater power density at the sample position. It should also be noted, however, that too much power can be detrimental, resulting in vessel fracturing and experimental safety issues.

Ultimately the successful experimental procedure resulted in complete synthesis in both the DMO and single mode cavity (Table 6- 1). Complete success was achieved for reactions involving the metal precursor, however, it transpired that work concerned with the metal oxide was more complex. Experiments concerning the metal oxide often resulted in pellet fracturing due to rapid CO/CO<sub>2</sub> gas evolution during the reaction. This was confirmed as resulting from the rapid temperature rise associated with the early stages of the reaction and thus the experimental procedure was re-examined. Resultant dielectric property and TGA studies of the MoO<sub>3</sub> oxide indicated the exact temperature at which reduction of the oxide occurred and the associated improvement of the loss tangent. Using lower powers (0 – 1 kW) the synthesis of Mo<sub>2</sub>C was achieved by controlling the power input during the oxide reduction stage of the process. This, to a degree, controlled the temperature rise and thus the gas evolved. This novel route allowed the successful synthesis of the carbide, all be it in slightly longer reaction times, in a single step process and without any pellet fracturing occurring.

Applicator	Carbide	Metal Precursor	Oxide Precursor
DMO	TaC	20 min	5 min
	NbC	20 min	2 min
	WC <sup>1</sup>	30 min	-
	Mo <sub>2</sub> C <sup>2</sup>	90 s	90 s
Single Mode Cavity	TaC	15 s	-
	NbC	20 s	-
	WC <sup>1</sup>	40 s	-
	Mo <sub>2</sub> C <sup>2</sup>	10 s	130 s
	Nb <sub>0.8</sub> Ta <sub>0.2</sub> C	20 s	-
	Nb <sub>0.5</sub> Ta <sub>0.5</sub> C	20 s	-
	Nb <sub>0.2</sub> Ta <sub>0.8</sub> C	20 s	-

**Table 6- 1: Reaction time information for all carbides investigated.**

A number of characterisation methods were used to investigate the materials produced, whether in phase identification or the properties of specific carbides. One of the most important of these techniques was Powder Neutron Diffraction (PND) which was able to confirm the formation of all the products, particularly in the case of Mo<sub>2</sub>C where PXD could not differentiate between the orthorhombic and hexagonal phase. PND also accurately identified carbon non-stoichiometry in all the carbides. This was particularly important when matching the resultant T<sub>c</sub> onsets, reported by Giorgi et al.,<sup>3</sup> with the samples. The carbon occupancy data were also able to establish reasoning for the non-linear relationship for the T<sub>c</sub> onset observed in the Nb-Ta-C solid solution

series, knowing the onset does not decrease linearly with carbon occupancy,<sup>3</sup> despite the linear trend for the cell parameters.

Although important, synthesis of the carbides was not the primary concern for much of this thesis. In order to build on the understanding of the formation of these refractory carbides, the reaction profile, formed from the specific metal powder, was mapped in the single mode cavity for each system. It was quickly apparent that a direct relationship existed between carbide phase fraction, reaction temperature and the sample loss tangent. In all cases a specific reaction temperature was required for formation of the carbide to begin, at which point the loss tangent was observed to decay away as the carbide was formed. This specific point could be manipulated through the use of excess C in the reaction mixture. The high loss tangent of graphite enabled desired temperatures to be reached faster by the inclusion of excess amounts, resulting in carbide formation beginning earlier than for a 1:1 metal:carbon ratio. Regardless of the quantity of C used, when a high purity of the carbide was reached the temperature was observed to plateau, resulting in a self terminating reaction. In all cases the successful synthesis of the carbide at 3 kW in a single mode cavity, to a high purity, was achieved in less than 30 s. This compares very favourably to conventional synthetic methods with, for example, WC taking 2 h to synthesise for the same volume.<sup>4</sup>

To develop a further understanding of the reaction, *in-situ* characterisation methods were investigated for WC. Through the use of high speed photography and thermal imaging, results obtained through other

methods were reinforced (such as temperature data) and the reaction was observed to initiate at the expected 5 s. It was also possible to observe localised heating at the surface of the pellet, alluding to a possible reaction mechanism, with perhaps these very hot areas suggesting much higher reaction temperatures than the average values observed through the optical pyrometer.

The work reported in this thesis has laid a foundation for the rapid microwave synthesis of the transition metal carbides, as well as developing the understanding of microwave heating in the solid state. The future, however, lies in the two distinct areas. Firstly, the design and construction of a single mode applicator, which can effectively heat loads on a continuous basis, should be investigated. This is vital if industrial scale up of this process is ever to be considered. Secondly, the use of *in-situ* characterisation and monitoring techniques should be utilised, with a view to controlling the manufacturing process (i.e. through the monitoring of dielectric properties and temperature) and further investigating the reactions as they proceed. Perhaps through the use of high speed photography and infrared spectroscopy, individual grains can be observed which may provide additional mechanistic information.

With regard to specific materials reported on in this thesis, additional work on the controlled manufacture of carbides from the metal oxide precursors should be considered. Given the relative late success with this work, further investigation is required to establish a reproducible and effective synthesis method through the control of the reaction temperature by varying the applied microwave power. Synthesis of the binary carbides proved to be

very successful with limited work on ternary systems following a similar trend. It would seem, therefore, that further investigation into these latter systems and perhaps more complicated multi-metal carbides could yield positive results.

In conclusion, much of the work published in this thesis adds considerably to both the understanding of solid state microwave heating and in the development of an efficient manufacturing method for transition metal carbides. The contributions can be defined as follows:

- The development of a reproducible process for the successful synthesis of transition metal carbides in unprecedented timescales.
- The understanding of reaction profiles for the formation of numerous carbides, indicating strong relationships between dielectric properties, carbide phase fraction and temperature. These relationships allow a degree of control over the reaction and also confirm the process to be self terminating.
- *In-situ* techniques, along with reaction profile investigations, have suggested possible reaction mechanisms (conduction/interfacial polarisation). Rapid and localised heating was observed, possibly suggesting local temperatures much higher than recorded, which may account for the rapid product formation.

## 6.1 REFERENCES

---

- <sup>1</sup> S. R. Vallance, S. Kingman and D. H. Gregory, *Adv. Mater.*, 2007, **19**, 138.
- <sup>2</sup> S. R. Vallance, S. Kingman and D. H. Gregory, *Chem. Commun.*, 2007, **7**, 742.
- <sup>3</sup> A. L. Giorgi, E. G. Szklarz, E. K. Storms, A. L. Bowman and B. T. Matthias, *Phys. Rev.*, 1962, **125**, 837.
- <sup>4</sup> T. Ya. Kosolapova, *Carbides: Properties, Production and Applications*, 1<sup>st</sup> Edition, Plenum Press, New York, 1971.

## 7: APPENDICES

All supplementary data can be found on the accompanying CD. The three instrument files for PXD and PND analysis can be found in the root directory on the CD.

### CHAPTER 3:

Relevant thesis section	Description	Location on CD
Section 3.3	Indexing of WC synthesised in the DMO in 30 min (Figure 3- 3).	Indexing_WC_30_DMO.txt
	PXD of WC synthesised in the DMO in 20 min	WC_20_DMO.raw
	PXD of W <sub>2</sub> C (synthesised in the DMO)	W2C_DMO.raw
Section 3.4	PXD patterns for all data concerned with WC synthesis versus cavity type and power (Figure 3- 5).	WC power comparison folder (18 files)
Section 3.4.1	EXPGUI file for WC PXD refinement (synthesised in the single mode cavity).	E53P6-1.exp
	PXD patterns and dielectric data for all samples concerned with WC reaction profile	Reaction profile study (75 files)
Section 3.4.1.1	EXPGUI file for WC PND refinement (synthesised in the single mode cavity).	WC_PND_SM.exp
Section 3.4.2	PXD patterns for all data concerned with WC synthesis vs. excess C experiments.	WC versus excess C folder (26 files)
Section 3.4.4	Video footage pertaining to the high speed photography and thermal imaging experiments	WC_high_speed.avi WC_thermal.avi
Section 3.4.5	Mass spectrometry and TGA data for WO <sub>3</sub> + C	Mass spectrometry and TGA for WO <sub>3</sub> folder (6 files)

## CHAPTER 4:

Relevant thesis section	Description	Location on CD
Section 4.3.1	EXPGUI files for Mo <sub>2</sub> C PXD refinements (synthesised in the DMO).	E19P1_hex.exp E19P1_ORTHO.exp
Section 4.3.2	EXPGUI files for Mo <sub>2</sub> C PND refinements (synthesised in the DMO).	Mo <sub>2</sub> C PBCN folder (78 files) Mo <sub>2</sub> C P63MMC folder (43 files)
Section 4.4.1	PXD patterns for all samples concerned with Mo <sub>2</sub> C reaction profile	Mo <sub>2</sub> C reaction profile folder (60 items)
	EXPGUI file for Mo <sub>2</sub> C PXD refinement (synthesised in the single mode cavity).	E58ON.exp
Section 4.4.1.1	EXPGUI files for Mo <sub>2</sub> C PND refinements (synthesised in the single mode cavity).	C50763PBCN.exp C50763P63MMC.exp
Section 4.4.1.2	Dielectric data for all samples concerned with Mo <sub>2</sub> C reaction profile	dielectric data.xls
Section 4.5.1.2	EXPGUI file for Mo <sub>2</sub> C PXD refinement (synthesised in the DMO from MoO <sub>3</sub> ).	E30P6-PBCN.exp
Section 4.5.2	EXPGUI file for Mo <sub>2</sub> C PXD refinement (synthesised in the single mode cavity from MoO <sub>3</sub> ).	E48P2.exp
Section 4.5.2.1	Mass spectrometry and TGA data for MoO <sub>3</sub> + C	Mass spectrometry and TGA for MoO <sub>3</sub> folder (13 files)
Section 4.5.2.2	EXPGUI file for Mo <sub>2</sub> C PND refinement (synthesised in the single mode cavity from MoO <sub>3</sub> ).	C50761.exp

## CHAPTER 5:

Relevant thesis section	Description	Location on CD
Section 5.3.1	EXPGUI file for NbC PXD refinement (DMO synthesis)	E66P4.exp
	EXPGUI file for NbC PXD refinement (synthesised in the DMO from Nb <sub>2</sub> O <sub>5</sub> ).	E70P5.exp
	Mass spectrometry and TGA data for Nb <sub>2</sub> O <sub>5</sub> + C	MS and TGA for Nb <sub>2</sub> O <sub>5</sub> folder (6 files)
Section 5.3.2	EXPGUI file for TaC PXD refinement (DMO synthesis).	E54ON.exp
	EXPGUI file for TaC PXD refinement (synthesised in the DMO from Ta <sub>2</sub> O <sub>5</sub> ).	E51P1.exp
	PXD pattern of intermediate Ta <sub>2</sub> O <sub>5</sub> to TaC reaction	Ta oxide intermediate.jpg
Section 5.4.1	PXD patterns and dielectric data for all samples concerned with NbC reaction profile	NbC reaction profile study folder (33 files)
	PXD patterns and dielectric data for all samples concerned with TaC reaction profile	TaC reaction profile study folder (40 files)
Section 5.4.1.1	PXD patterns and dielectric data for all samples concerned with Nb + C reactant mixing study	Nb + C mixing study folder (20 files)
Section 5.4.2	EXPGUI file for NbC PND refinements (synthesised in the single mode cavity).	NbC folder (104 files)
	EXPGUI file for TaC PND refinements (synthesised in the single mode cavity).	TaC folder (266 files)
	EXPGUI file for Nb <sub>0.8</sub> Ta <sub>0.2</sub> C PND refinements (synthesised in the single mode cavity).	Nb0.8 folder (39 files)
	EXPGUI file for Nb <sub>0.5</sub> Ta <sub>0.5</sub> C PND refinements (synthesised in the single mode cavity).	Nb0.5 folder (71 files)
	EXPGUI file for Nb <sub>0.2</sub> Ta <sub>0.8</sub> C PND refinements (synthesised in the single mode cavity).	Nb0.2 folder (211 files)

